AN EXPERIMENTAL INVESTIGATION OF A HEAT PUMP DRYER USED FOR DRYING OF WHEAT

Ph. D. THESIS

in

Mechanical Engineering
University of Gaziantep

by

Mustafa ÖZBEY
March, 2004

Approval of the Graduate School of Natural and Applied Sciences

Prof. Dr. Bülent GÖNÜL
Director

I certify that this thesis satisfies all the requirements as a thesis for the degree of Doctor of Philosophy.

Prof. Dr. Melda ÇARPINLIOĞLU
Head of Department

This is to certify that we have read this thesis and that in our opinion it is fully adequate, in scope and quality, as a thesis for the degree of Doctor of Philosophy.

Assoc. Prof. Dr. M. Sait SÖYLEMEZ
Supervisor

Examining Committee Members

Prof. Dr. Ömer T. GÖKSEL (Chairman)

Prof. Dr. Kadir AYDIN

Prof. Dr. Ali Rıza TEKİN

Prof. Dr. Melda ÇARPINLIOĞLU

Assoc. Prof. Dr. M. Sait SÖYLEMEZ

ABSTRACT

AN EXPERIMENTAL INVESTIGATION OF A HEAT PUMP DRYER USED FOR DRYING OF WHEAT

ÖZBEY, Mustafa
Ph. D. in Mechanical Engineering
Supervisor: Assoc. Prof. Dr. M. Sait SÖYLEMEZ

March 2004, 166 pages

In this study, a fluidized bed type heat pump dryer was designed and constructed for drying granular wheat particles. The system consisted of two main units: fluidized bed dryer as air circuit and the heat pump unit as refrigerant circuit.

In this thesis, the introduction of heat pump to fluidized bed type dryer, and the effects of swirling flow field in the bed, drying medium, on the wheat drying were experimentally investigated. Experiments were performed to investigate the effects of various system operating conditions and parameters on the performance of the system. These investigated operating parameters are the air mass flow rate, temperature of the air flow and swirl number of the flow field in the bed. Also, the various air circuit configurations including recycle of the exhaust air flow discharging from the bed into the ambient or evaporator or again the bed were investigated in order to test their effects on the system performance and efficiency.

In order to investigate the system performance, in this experimental study, the measured parameters were: mass flow rate of air passing through the bed; dry and wet bulb air temperatures at inlet and outlet sides of the dryer bed and evaporator of the heat pump; dry and wet bulb temperatures and the absolute pressure of the ambient air; temperatures of the refrigerant working in the heat pump at the inlet and outlet sides of the compressor, condenser, evaporator and expansion valve; the gage pressures of the refrigerant at the inlet and outlet sides of the compressor and expansion valve; power consumed by the compressor, centrifugal fan and electrical heater; axial and tangential velocity components of air flow in the bed and the static pressures at upstream and downstream sections of the bed. In order to evaluate the system performance, the calculated parameters were: moisture extraction rate, MER; specific moisture extraction rate, SMER; dryer efficiency, DE; coefficient of performance, COP, and swirl number, S.

Among the tested configurations, the configuration 6 which has a closed cycle has the highest MER, SMER, DE and the second highest COP. Thus, the configuration 6 is recommended as the best configuration.

Higher mass flow rates in the bed result in higher MER, but lower SMER and DE when higher air flow temperature in the bed result in higher MER and DE and lower SMER.

The swirling flow which has a swirl number in the range of 0.2-0.85 in the bed increased the MER of the dryer by 5-25 per cent and the SMER by 12-28 per cent and the DE up to 38 per cent.

When the cost rate of heat pump is compared with that of the direct electrical energy, it is observed that the heat pump is more economical device at the range of about 110 percent than the direct electrical heating.

Keywords: Heat pump dryer, fluidized bed dryer, wheat drying, swirling flow

ÖZ

BUĞDAY KURUTMAK İÇİN KULLANILAN ISI POMPALI BİR KURUTUCUNUN DENEYSEL İNCELENMESİ

ÖZBEY, Mustafa
Doktora tezi: Makine Mühendisliği Bölümü
Tez yöneticisi: Doç. Dr. M. Sait SÖYLEMEZ
Mart 2004, 166 sayfa

Bu çalışmada tanecikli bir malzeme olan buğdayı kurutmak için akışkan yataklı tip ısı pompalı kurutucu sistemi tasarlandı ve kuruldu. Sistem iki temel üniteden oluşmaktadır: hava devresi olarak kurutma ünitesi ve soğutucu akışkan devresi olarak ısı pompası ünitesi.

Bu tezde akışkan yataklı tip kurutma sistemine ısı pompasının bağlanması ve kurutma ortamı içindeki dönel akımın buğday kurutma üzerine olan etkileri deneysel olarak incelendi. Deneyler farklı sistem çalışma şartları ve parametrelerinin sistem performansı üzerine olan etkilerini incelemek için yapıldı. Bu incelenen değişkenler kurutma ortamı içindeki kütlesel hava akım miktarı, hava akım sıcaklığı ve kurutma ortamı içindeki akım alanının girdap sayısı. Ayrıca, kurutma ortamından çıkan sıcak ve nemli havanın dış ortama veya evaporator üzerine veya tekrar kurutma ortamı içine transfer edilmesini içeren farklı konfigurasyonlarının sistem performansı ve verimi üzerine olan etkilerini test etmek için incelendi.

Sistem performansını incelemek için, bu deneysel çalışmada ölçülen parametreler: kurutma ortamından geçen havanın kütlesel akım miktarı; kurutucunun kurutma ortamı ve ısı pompasının genleşme eşanjörü giriş ve çıkışlarında kuru ve nemli hava sıcaklıkları; çalışılan laboratuvar ortamındaki havanın kuru ve nemli

sıcaklıkları ve mutlak basıncı; ısı pompası ünitesinde çalışan soğutucu akışkanın kompresör, yoğuşma ve genleşme eşanjörlerinin ve genleşme valfinin giriş ve çıkış sıcaklıkları; kompresör ve genleşme valfi giriş ve çıkışlarında soğutucu akışkanın basıncı; kompresör, santrifüj fan ve elektrik ısıtıcısı tarafından harcanan güç; kurutma ortamı içinde havanın eksenel ve teğetsel hız bileşenleri ve kurutma ortamı öncesi ve sonrasında statik basınç. Sistem performansını değerlendirmek için ise hesaplanan değerler: nem çekme oranı, MER; belirli nem çekme oranı, SMER; kurutucu verimi, DE; performans katsayısı, COP, ve akım girdap sayısı, S.

Test edilen konfigurasyonlar arasında kısmi kapalı bir devre olan 6 nolu konfigurasyonun en yüksek performans ve verime sahip olduğu görüldü.

Kurutma ortamı içindeki kütlesel hava akım miktarının artırılması MER'i artırıyor, SMER'i ve DE'yi ise düşürüyor. Diğer taraftan kurutma ortamı içindeki hava akım sıcaklığının artırılması MER'i ve DE'yi artırıyor, SMER'i ise düşürüyor.

Kurutma ortamı içinde 0.2-0.85 aralığında girdap sayısına sahip dönel akım MER'i yüzde 5-25 aralığında, SMER'i yüzde 12-28 aralığında ve DE'yi yüzde 38'e kadar artırıyor.

Isı pompası ve elektrik enerjilerinin maliyetleri kıyaslandığında, ısı pompasının rezistanslı ısıtmadan yüzde 110 oranında daha ekonomik olduğu görülmüştür.

Anahtar kelimeler: Isı pompalı kurutucu, akışkan yataklı kurutucu, buğday kurutma, dönel akım

ACKNOWLEDGEMENTS

This study would have never been completed without continuous moral support, encouragement, understanding and patience of my wife, İlknur, and life delight, tightly dependence to life, completeness and enhancement role on my family happiness presented by my daughter, Ecenur, and therefore my very special thanks are due to them.

I would like to express my gratitude to Prof. Dr. Ömer T. GÖKSEL, Prof. Dr. Melda ÇARPINLIOĞLU and Assoc. Prof. Dr. M. Sait SÖYLEMEZ for their comments, suggestions and support.

I would like to express my sincere thanks to Research Fund of the University of Gaziantep for the research project supported under the code no: MF 01.07

I would like to express my sincere thanks to my friend Research Assistant Mr. Önder KAŞKA for valuable technical support during the experimental study.

Lastly, I wish to offer my thanks to the technical personnel of the Mechanical Engineering Department; especially Mr. Mehmet TAŞDEMİR, Mr. İbrahim KORKMAZ, Mr. Ömer SAVCI, Mr. Seyit BOSTANCIERİ and Mr. Akif PEKMEZ for their valuable help in the construction of the experimental set-up.

TABLE OF CONTENTS

ABSTRACT	ii
ÖZ	iv
ACKNOWLEDGEMENTS	vi
LIST OF TABLES	x
LIST OF FIGURES	xi
NOMENCLATURE	xvi
CHAPTER 1	
INTRODUCTION	1
CHAPTER 2	
LITERATURE SURVEY	7
2.1 INTRODUCTION	7
2.2 WORKS ON HEAT PUMP DRYERS	7
2.2.1 Introduction	7
2.2.2 Factors influencing HPD performance	10
2.2.3 Previous studies on heat pump dryers	14
2.3 WORKS ON FLUIDIZED BED DRYING	20
2.3.1 Introduction	20
2.3.2 Previous studies on the fluidized bed dryers	22
2.4 WORKS ON SWIRLING FLOW	32
2.4.1 Introduction	32
2.4.2 Previous studies on the swirling flow	35
2.5 CONCLUSION	40
CHAPTER 3	
EXPERIMENTAL SET-UP AND MEASUREMENT TECHNIQUES	42
3.1 INTRODUCTION	42
3.2 CONSTRUCTION OF THE EXPERIMENTAL SET-UP	42
3.2.1 Centrifugal Fan	45
3.2.2 Settling tank	45
3.2.3 Swirl generator	48
3.2.4 Electrical heater	50

3.2.5 Compressor 51
3.2.6 Condenser and evaporator 52
3.2.7 Expansion Valve 53
3.2.8 Axial fan 54
3.2.9 Working fluid in heat pump unit 54
3.3 MEASUREMENT DEVICES AND ITS TECHNIQUES 55
3.3.1 Pressure measurement gages 55
3.3.2 Pressure probes and wall static pressure tapings 56
3.3.3 Manometers 59
3.3.4 Temperature measurement 60
3.3.4.1 Thermocouple Configurations 60
3.3.4.2 Dry Bulb Temperature Measurement 61
3.3.4.3 Wet Bulb Temperature measurement 62
3.3.5 Hilton Data Logger 65
3.4 DRYER AIR CIRCUIT CONFIGURATIONS TESTED 66
3.5 TEST MATERIAL 69
CHAPTER 4
EXPERIMENTAL PROCEDURE AND EVALUATION OF DATA 71
4.1 INTRODUCTION 71
4.2 EXPERIMENTAL PROCEDURE 72
4.3 EVALUATION OF DATA 76
4.3.1 Mass transfer calculations 76
4.3.2 Heat transfer calculations and data evaluations 79
4.4 UNCERTAINTY ANALYSIS 84
CHAPTER 5
EXPERIMENTAL RESULTS 89
5.1 INTRODUCTION 89
5.2 THE RESULTS OF DRYING EXPERIMENTS FOR DRYER CONFIGURATIONS 89
5.3 THE EFFECTS OF DRY BULB TEMPERATURE IN THE DRYING MEDIUM FOR DRYING THE WHEAT GRAINS 105
5.4 THE EFFECTS OF AIR MASS FLOW RATE IN THE BED FOR DRYING WHEAT GRAINS 118

5.5 THE EXPERIMENTAL INVESTIGATIONS OF THE FLOW FIELD DEVELOPMENT IN THE BED 131

5.6 THE EFFECTS OF SWIRLING FLOW FIELD IN THE BED ON DRYING OF WHEAT GRAINS 135

5.7 COST ANALYSIS 145

5.8 CONCLUSION 147

CHAPTER 6

SUGGESTIONS FOR FUTURE WORK 151

APPENDIX 1 152

APPENDIX 2 153

REFERENCES 154

LIST OF TABLES

Table 3.1 The swirl generator configurations, dimensions and codes 50

Table 4.1 The conditions for configuration experiments 73

Table 4.2 The conditions for air dry bulb temperature, bed temperature, experiments 73

Table 4.3 The conditions for air mass flow rate experiments for the configuration 1 73

Table 4.4 The conditions for air mass flow rate experiments for the configuration 6 74

Table 4.5 The obtained swirl numbers for the tested swirl generators at tested Reynolds numbers 75

Table 4.6 The conditions for the drying experiments with the swirling flow field 76

Table 5.1 The MER value intervals for the configurations 95

Table 5.2 The consumed power magnitudes by the fan and the compressor 99

Table 5.3 The dry bulb and wet bulb ambient temperatures and humidity ratio magnitudes at days that configuration drying tests were done 103

Table 5.4 Cost rate analysis for some petroleum products 147

LIST OF FIGURES

Figure 2.1 Pressure-enthalpy diagram of an ideal vapor compression heat pump cycle 8
Figure 2.2a A schematically diagram of an open type heat pump dryer configuration 9
Figure 2.2b The ideal air circuit of a dryer in the psychrometric chart 10
Figure 2.3 HPD configurations 13
Figure 2.4 Schematic representation of the fluidized bed theory 20
Figure 2.5a Four different regions of gas fluidization 21
Figure 2.5b The relation between the gas velocity and the pressure drop in the bed 21
Figure 3.1 The experimental set-up 46
Figure 3.2 The axial guide vane type swirl generator construction view 49
Figure 3.3 The construction view of the electrical heater 51
Figure 3.4 The construction of condenser and evaporator 53
Figure 3.5 Construction of the three-tube pressure probe 57
Figure 3.6 Dry and wet bulb temperature probes and connections 63-64
Figure 3.7 Junction connections to the data logger 65
Figure 3.8 Heat pump dryer configurations 68
Figure 4.1 The schematic representation of measurement stations 80
Figure 5.2.1 The variation T_{db} and T_{wb} at inlet and outlet sides of the bed with time for the configuration 1 91
Figure 5.2.2 The variation T_{db} and T_{wb} at inlet and outlet sides of the bed with time for the configuration 2 92
Figure 5.2.3 The variation T_{db} and T_{wb} at inlet and outlet sides of the bed with time for the configuration 3 92
Figure 5.2.4 The variation T_{db} and T_{wb} at inlet and outlet sides of the bed with time for the configuration 4 93

Figure 5.2.5 The variation T_{db} and T_{wb} at inlet and outlet sides of the bed with time for the configuration 5 93
Figure 5.2.6 The variation T_{db} and T_{wb} at inlet and outlet sides of the bed with time for the configuration 6 94
Figure 5.2.7 The variation of MER with time for all configurations 97
Figure 5.2.8 The mean MER values for all configurations 97
Figure 5.2.9 The mean SMER values for all configurations 100
Figure 5.2.10 The COP values for all configurations 101
Figure 5.2.11 The variation of DE with drying time for all configurations 103
Figure 5.2.12 The mean DE values for all configurations 104
Figure 5.2.13 The variation of static pressure in the longitudinal direction of the bed for all configurations 104
Figure 5.3.1 The variation T_{db} and T_{wb} at inlet and outlet sides of the bed with time at mean T_b=40°C in the bed for the configuration 1 107
Figure 5.3.2 The variation T_{db} and T_{wb} at inlet and outlet sides of the bed with time at mean T_b=50°C in the bed for the configuration 1 107
Figure 5.3.3 The variation T_{db} and T_{wb} at inlet and outlet sides of the bed with time at mean T_b=60°C in the bed for the configuration 1 108
Figure 5.3.4 The variation T_{db} and T_{wb} at inlet and outlet sides of the bed with time at mean T_b=70°C in the bed for the configuration 1 108
Figure 5.3.5 The variation T_{db} and T_{wb} at inlet and outlet sides of the bed with time at mean T_b=40°C in the bed for the configuration 6 109
Figure 5.3.6 The variation T_{db} and T_{wb} at inlet and outlet sides of the bed with time at mean T_b=50°C in the bed for the configuration 6 109
Figure 5.3.7 The variation T_{db} and T_{wb} at inlet and outlet sides of the bed with time at mean T_b=60°C in the bed for the configuration 6 110
Figure 5.3.8 The variation T_{db} and T_{wb} at inlet and outlet sides of the bed with time at mean T_b=70°C in the bed for the configuration 6 110
Figure 5.3.9 The variation of difference between T_{db} at inlet and outlet sides of the bed with time at the m_a=0.231kg/s in the bed for different T_b in the bed for the configuration 1 111
Figure 5.3.10 The variation of difference between T_{db} at inlet and outlet sides of the bed with time at the m_a=0.231kg/s in the bed for different T_b in the bed for the configuration 6 111

Figure 5.3.11 The variation of difference between T_{wb} at inlet and outlet sides of the bed with time at the m_a=0.231kg/s for different T_b in the bed for the configuration 1 112
Figure 5.3.12 The variation of difference between T_{wb} at inlet and outlet sides of the bed with time at the m_a=0.231kg/s for different T_b in the bed for the configuration 6 112
Figure 5.3.13 The variation of MER with time at m_a=0.231kg/s for the different T_{db} in the bed for the configuration 1 114
Figure 5.3.14 The variation of MER with time at m_a=0.231kg/s for the different T_{db} in the bed for the configuration 6 114
Figure 5.3.15 The variation of MER with T_b in the bed for the configurations 1 and 6 115
Figure 5.3.16 The variation of SMER with T_b in the bed for the configurations 1 and 6 116
Figure 5.3.17 The variation of mean DE with the T_b in the bed at m_a=0.231kg/s for the configurations 1 and 6 117
Figure 5.4.1 The variation T_{db} and T_{wb} at inlet and outlet sides of the bed with time at m_a=0.1kg/s in the bed for the configuration 1 120
Figure 5.4.2 The variation T_{db} and T_{wb} at inlet and outlet sides of the bed with time at m_a=0.165kg/s in the bed for the configuration 1 120
Figure 5.4.3 The variation T_{db} and T_{wb} at inlet and outlet sides of the bed with time at m_a=0.231kg/s in the bed for the configuration 1 121
Figure 5.4.4 The variation T_{db} and T_{wb} at inlet and outlet sides of the bed with time at m_a=0.264kg/s in the bed for the configuration 1 121
Figure 5.4.5 The variation T_{db} and T_{wb} at inlet and outlet sides of the bed with time at m_a=0.1kg/s in the bed for the configuration 6 122
Figure 5.4.6 The variation T_{db} and T_{wb} at inlet and outlet sides of the bed with time at m_a=0.165kg/s in the bed for the configuration 6 122
Figure 5.4.7 The variation T_{db} and T_{wb} at inlet and outlet sides of the bed with time at m_a=0.2kg/s in the bed for the configuration 6 123
Figure 5.4.8 The variation T_{db} and T_{wb} at inlet and outlet sides of the bed with time at m_a=0.231kg/s in the bed for the configuration 6 123

Figure 5.4.9 The variation of difference between T_{db} at inlet and outlet sides of the bed with time at the T_b=50°C for different m_a in the bed for the configuration 1 124
Figure 5.4.10 The variation of difference between T_{db} at inlet and outlet sides of the bed with time at the T_b=50°C for different m_a in the bed for the configuration 6 124
Figure 5.4.11 The variation of difference between T_{wb} at inlet and outlet sides of the bed with time at the T_b=50°C for different m_a in the bed for the configuration 1 125
Figure 5.4.12 The variation of difference between T_{wb} at inlet and outlet sides of the bed with time at the T_b=50°C for different m_a in the bed for the configuration 6 125
Figure 5.4.13 The variation of MER with time at T_b=50°C in the bed for the different m_a in the bed for the configuration 1 127
Figure 5.4.14 The variation of MER with time at T_b=50°C in the bed for the different m_a in the bed for the configuration 6 127
Figure 5.4.15 The variation of mean MER with m_a at T_b=50°C in the bed for The configurations 1 and 6 128
Figure 5.4.16 The variation of mean SMER with m_a at T_b=50°C in the bed for the configurations 1 and 6 129
Figure 5.4.17 The variation of mean DE with the ma at T_b=50°C in the bed for the configurations 1 and 6 130
Figure 5.5.1 The axial air velocity distributions in the non-swirling and swirling flow fields in the bed 133
Figure 5.5.2 The tangential velocity distributions in the swirling flow field in the bed 133
Figure 5.5.3 The variation of swirl numbers, S, with the Re 134
Figure 5.6.1 The variation of T_{db} and T_{wb} at inlet and outlet sides of the bed in the swirling flow field with S=0.204 136
Figure 5.6.2 The variation of T_{db} and T_{wb} at inlet and outlet sides of the bed in the swirling flow field with S=0.25 137

Figure 5.6.3 The variation of T_{db} and T_{wb} at inlet and outlet sides of the bed in the swirling flow field with S=0.38 137
Figure 5.6.4 The variation of T_{db} and T_{wb} at inlet and outlet sides of the bed in the swirling flow field with S=0.425 138
Figure 5.6.5 The variation of T_{db} and T_{wb} at inlet and outlet sides of the bed in the swirling flow field with S=0.637 138
Figure 5.6.6 The variation of T_{db} and T_{wb} at inlet and outlet sides of the bed in the swirling flow field with S=0.67 139
Figure 5.6.7 The variation of T_{db} and T_{wb} at inlet and outlet sides of the bed in the swirling flow field with S=0.85 139
Figure 5.6.8 The variation of T_{db} differences between the inlet and outlet sides of the bed for non-swirling and swirling flow fields with drying time 140
Figure 5.6.9 The variation of T_{wb} differences between the inlet and outlet sides of the bed for non-swirling and swirling flow fields with drying time 140
Figure 5.6.10 The variation of MER with drying time for swirling and non-swirling flow fields in the bed 141
Figure 5.6.11 The variation of MER with S 142
Figure 5.6.12 The variation of SMER with S 143
Figure 5.6.13 The variation of DE with drying time for the swirling and the non-swirling flow fields in the bed 144
Figure 5.6.14 The variation of DE with S 145

NOMENCLATURE

A	: cross sectional area, m^2
b_1	: guide vane width on the hub, m
b_2	: guide vane width at the tip, m
c_p	: specific heat at constant pressure, J/kg K
C	: STP coefficient for alcohol, dimensionless
C	: condenser
CF	: contact factor, dimensionless
CO	: compressor
COP	: coefficient of performance, dimensionless
d	: diameter, m
D	: moisture diffusion coefficient, m^2/s
D	: dryer
DE	: dryer efficiency, dimensionless
E	: evaporator
EV	: expansion valve
f	: friction factor, dimensionless
F	: force, N
h	: specific enthalpy, kj/kg
h	: head in inclined tube of manometer, mm
H	: head, m
HPD	: heat pump dryer
g	: gravity acceleration, m/s^2
k	: thermal conductivity of wheat,
L	: bed height, m
m	: mass, kg
$\dot{m}$	: mass flow rate, kg/s
M	: moisture content, kg water/kg dry particle
MER	: moisture extraction rate, kg water/h
n	: number of blades

Nu : Nusselt number, dimensionless

q : specific heat transfer rate, kj/kg

$\dot{Q}$: heat transfer rate, kW

Q : volume flow rate, m^3/s

P : pressure, Pa

Pr : Prandtl number, dimensionless

r : local radius, m

R : pipe radius, m

Re : Reynolds number, dimensionless

RH : relative humidity, per cent

S : swirl number

SMER : specific moisture extraction rate, kg water/kWh

t : time, s

T : temperature, ^{o}C

u : axial velocity component, m/s

V : mean flow velocity, m/s

w : humidity ratio, kg water vapor/kg dry air

w : specific work, kj/kg

W : weight, N

$\dot{W}$: power, kW

WH : waste heat supply

v : tangential velocity component, m/s

x : axial distance, m

y : the distance from the wall in the bed, m

Greek Letters

α : manometer tube angle, degree

ν : kinematic viscosity, m^2/s

μ : dynamic viscosity, kg/m s

ρ : density, kg/m^3

Γ : swirl intensity, dimensionless

θ : camber angle, deg

γ : stagger angle, deg

Δ : difference

Σ : total

ε : porosity

Φ : spherecity, dimensionless

Subscripts

a : air

al : alcohol

amb : ambient

b : bed

comp : compressor

cond : condenser

db : dry bulb

di : dryer inlet

do : dryer outlet

H : high

L : low

mf : minimum fluidization

p : particle

r : refrigerant

s : saturated

s : static

t : total

v : vapor

w : water

wb : wet bulb

1,2,3…: measurement stations

CHAPTER 1

INTRODUCTION

Drying is a highly energy intensive process which is a common unit operation in many process and chemical industries and agriculture. Especially in agriculture, the drying of grain has frequently continued to be a headache for the farmers.

The process of drying includes the movement of water through the interior of the grain and the loss of water vapor from the grain surface in other words; this treatment is based on the principle of removal of moisture or liquid from a wet solid by bringing this moisture into a gaseous state. The loss of water vapor from the grain surface depends on the difference between the vapor pressure of the drying air and the vapor pressure of the water in the grain. The latter depends on the moisture content and the grain temperature. If the vapor pressure of the drying air is less than that of the water in the grain, the grain will loose moisture, that is, it will dry. In most drying operations, water is the liquid evaporated and air is the drying medium. Heat, necessary for evaporation, is supplied to the particles of the material and moisture vapor is removed from the material into the drying medium.

In many practical applications, drying is a process which requires high energy input because of latent heat of water evaporation and relatively low energy efficiency of industrial dryers. Traditional methods of drying involve the direct combustion of fossil fuels together with controlled ventilation and the direct solar drying. Such methods are obviously inefficient, major consumers of energy. That is, the expensive energy is depleted only to produce low grade heat for drying, and their efficiencies never exceeds 20% as mentioned in the previously available literature. By Bahu [73], it was reported that in manufacturing process where drying is required; the cost of drying can approach to 60-70 per cent of the total cost. The increase on fuel costs has decreased the manufacture of artificial drying machinery. Thus, it is the single most important challenge of the drying industry to maximize the rate of moisture removal with minimum energy. This saw interest revive in the heat pump as well as its potential for fuel saving. Artificial drying can give a certain amount of immunity to the weather, and is potentially attractive, therefore, provided that its cost is not too great. As well as for agricultural purposes, heat pumps as drying machines were seen to have other applications. In Germany, heat pumps have been used widely in timber drying, malt drying and baking industry, in Norway to produce dried fish and in France for drying plaster blocks for the construction industry. In the conventional dryers, humid and high temperature air from the dryer is vented to the atmosphere, which results in the loss of both the sensible and latent heat of vaporization of its moisture content. On the other hand, the direct solar drying highly depends on the climatic conditions and is impossible to achieve without severe losses to product quality and quantity due to the radiation exposed to the direct sun lights.

In order to increase the efficiency of drying in conventional dryers, the incorporation of a heat pump to a dryer can be operated. Heat pumps are devices which use an energy input to take thermal energy from a low temperature source and move it to a thermal sink at a higher temperature than the source. That is, heat pump is an equipment that moves heat from one place to another. Owing to their ability of delivering more energy as heat than they in fact consume as input work, many applications have been found for vapor compression heat pumps. They have also heat recovery feature to reduce energy consumption of the process. The application of heat pumps for drying has received continuous attention since it possesses two-fold beneficial characteristics. Through the evaporator, the heat pump recuperates sensible and latent heat from the dryer exhaust, hence the energy is recovered. Condensation occurring at the evaporator reduces the humidity of the working air, thus increasing the effectiveness of product drying. Therefore, the heat pump dryer can accelerate the drying process. The use of heat pump systems can significantly enhance the energy efficiency of conventional hot air dryers. The heat pump application in drying process has two advantages: to control the drying environment for product's quality and to reduce energy consumption. For food drying industries the heat pump dryers give also clean process air for drying. Although heat pumps have been used extensively in industry for many years, their use for drying has been limited.

Physical processes that use fluidized bed include drying, mixing, granulation, coating, heating and cooling. In a fluidized bed, particles confined to a vertical column are suspended by a sufficiently strong upward volumetric flux of fluid. In some circumstances the fluid flows uniformly through a bed of particles of constant concentration.

One of the most important applications of the fluidized bed is to the drying of solids. Fluidized bed is currently used commercially for drying such materials as granular materials, cereals, polymers, chemicals, pharmaceuticals, fertilizers and crystalline products, and minerals.

As we know the drying is essentially a process of simultaneously heat and mass transfer. In fluidized bed drying the process is carried out in a fluidized bed by drying medium Heat is transferred by convection from the surroundings to the particle surfaces, and from there, by conduction, further into the particle. Moisture is transported in the opposite direction as a liquid or vapor; on the surface it evaporates and passes on by convection to the surroundings.

Compared with other drying techniques, fluidized bed drying offers many advantages. High heat and mass transfer rates between the gas and particles are possible because of good contact or large contact area between particles and gas, good and rapid mixing of solids, nearly uniform moisture content distribution throughout the bed and closely controllable temperature in the bed and ease in transport and handling of particles. The thermal efficiency of these dryers is relatively high. It requires less drying time due to high rates of heat and mass transfer and provides for a wide choice in the drying time of the material. The absence of moving parts, other than the feeding and discharge devices, leads to reliable operation and low maintenance and also simple in construction and of relatively low capital equipment cost. The technique offers ease in operation adaptability to automation and the fluidity of particles provides and excellent condition for handling and for combining with several processes such as mixing, classification, and cooling. On the other hand, the disadvantages include high pressure drop, attrition of the solids and erosion of the containing surfaces. Although researchers on fluidized bed drying has not made much progress in recent years.

The economic benefits of energy and material savings have prompted and received greatest attention in order to increase convective heat transfer rates in the process equipment. Enhancement of convective heat transfer may be achieved by numerous techniques. One of these techniques is swirl flow devices. Swirl flow devices are designed to impart a rotational motion about an axis parallel to the flow direction to the bulk flow. That is, swirl flow is the descriptive term for a fluid flow in which the tangential component of the main stream velocity is a significant contribution to the resultant velocity. In addition, the swirling flow is a typical complex flow that affected by streamline curvature and flow skewness in addition to adverse and favorable pressure gradients. The presence of swirl introduces some favorable changes to the flow, such as increasing the flow paths, increasing energy dissipated by friction and introducing an angular acceleration to the fluid flow.

Swirl flows are found in nature, such as tornadoes, and are utilized in a very wide range of applications, such as cyclone separators, heat transfer tubes, spraying machines, heat exchangers, gasoline and diesel engines, gas turbines, combustion chambers and many other practical heating devices.

Swirl flow can be generally generated by turbulators, typical inserts, such as coiled wires, twisted tapes, helical vanes and spiral fins inserting into the pipe, helical grooves and roughness in the inner surface of the pipe, rotating boundary, coiled tubes, tangential entry of the fluid into a pipe, pipe entry swirl generators such as axial and radial guided vanes and propellers, etc. In all cases of swirling flow the heat transfer rates are increased at the expense of increased pumping power.

For all purposes, in this experimental study a fluidized bed type heat pump assisted dryer was designed and constructed to dry granular materials such as wheat. The concept of our study consists of mainly three parts: heat pump unit for obtaining the hot air flow in drying chamber, fluidized bed dryer unit in which the materials to be dry can be sufficiently contact with the hot air flow and swirling flow for increasing the convective heat transfer rate between the hot air flow and the particles to be dry in the drying medium. On the other hand, the experimental set up consists of mainly two units or circuits: heat pump unit as refrigerant circuit and fluidized bed dryer as air circuit.

In this thesis, the effects of the introduction of heat pump to a fluidized bed dryer, different heat pump configurations, the air temperature in drying medium, mass flow rates of air in drying medium and swirling flow in the drying medium on the drying performance of dryer were experimentally investigated and discussed according to the drying rate or moisture extraction rate, specific moisture extraction rate, dryer efficiency of the system and heat pump performance and the swirling flow field in the drying medium of the dryer.

The main innovations in this thesis can be collected under two main titles:

• the introduction of heat pump to a fluidized bed type dryer

• the effects of swirling flow field in the drying medium of the fluidized bed dryer on the drying of granular particles

In this study, a heat pump assisted fluidized bed dryer which the swirl flow can be generated in its bed was designed, constructed and experimentally investigated. The purpose of introducing a heat pump in a dryer is to achieve lower cost of heat energy necessary for drying as compared with the conventional systems.

Practically, this is conditioned by the followings:

- The different system configurations were tested. That is, the energy loss in the system is minimized while the energy at the dryer exhaust is recycled within the system which has different configurations
- The available waste heat was used
- The swirl generator was used to generate the swirling flow in the drying medium in order to increase the heat transfer rate between the air and the particles to be dry.

Previously there were many theoretical and/or experimental studies separately on heat pump systems and fluidized bed type systems and swirling flows. But, there were no cited experimental study on the introduction of heat pump system to fluidized bed dryer which swirling flow is obtained in its bed. That is, the combination of these concepts has not been investigated in any previous study. Therefore, my thesis is exposing a new drying system including the combination of these concepts, heat pump, fluidized bed and swirling flow.

As a result, the heat pump assisted dryer planned to be studied is to be a system which is an energy efficient device with the control of the moisture and temperature of the process air as well as heat recovery and waste heat and swirling flow. The heat pump assisted fluidized bed type dryer which has also the swirling flow field in its drying medium was experimentally studied in order to test its performance on drying of wet wheat particles. It is also believed that the heat pump assisted dryer offers products of better quality with clean process air and with less energy consumption. And also, it is purposed that this heat pump assisted dryer gives an answer to necessity of farmers or producers of our region for drying especially wheat.

In the second chapter of this thesis, an extensive available literature survey on the theoretical and experimental studies about the heat pump dryers and fluidized bed dryers and swirling flow fields that previously investigated by many researchers are separately presented.

The third chapter is devoted to the design and construction of experimental set-up and measurement devices and their techniques conducted.

In chapter four, the method of experiments, calculations performed on the measured data and uncertainty analysis of measured and calculated data are presented.

The experimental results on the performance of heat pump assisted fluidized bed dryer are discussed to determine the influence of operating parameters on the system performance in chapter five. The cost analysis is also presented in this chapter.

The estimated future studies on heat pump dryers are listed in chapter six.

The experimental study presented in this thesis was financially supported by the Research Fund of the University of Gaziantep under the project code of MF 01.07.

CHAPTER 2

LITERATURE SURVEY

2.1 INTRODUCTION

This chapter consists of a summary of the related literature on the heat pump dryer systems, fluidized bed dryers and swirling flow. The previously conducted theoretical and experimental studies of these concepts on the system performance are analyzed. Some theoretical considerations related with these concepts as factors or parameters affecting the system performance are also presented.

2.2 WORKS ON HEAT PUMP DRYERS

2.2.1 Introduction

The heat pump assisted dryer, HPD, that was studied in this thesis consists of two working fluid circuits, one of these is refrigerant circuit in the heat pump, and the other is drying air circuit. Drying air entering the drying chamber is heated up by the condenser, which is a component of the heat pump.

The heat pump assisted dryer is mainly consists of two parts, heat pump and drying unit. The main components of the heat pump consist of a compressor, condenser, evaporator and an expansion valve. In a vapor compression heat pump, heat transfer is achieved through the phase change of the working fluid in the evaporator and the condenser. Heat pumps deliver more energy as heat than they in fact consume as input work.

The working fluid in the evaporator, refrigerant, absorbs heat from low temperature heat source and vaporizes at a lower temperature and pressure. Then, this superheated vapor is compressed by the compressor to the condenser at a higher pressure and temperature. It condenses in the condenser by releasing heat to the air stream entering the drying chamber. The refrigerant exits from the condenser, usually as a sub-cooled liquid or a mixture of liquid and vapor. Next, the refrigerant passes through an expansion valve, flow regulating device. So, the refrigerant pressure drops. The drop in pressure is accompanied by a drop in temperature such that the refrigerant leaves the expansion valve and enters the evaporator as usually a sub-cooled liquid or a mixture of liquid and vapor with a low vapor quality. This cycle similarly continues, and the pressure-enthalpy diagram of an ideal cycle on the saturation lines of the refrigerant is theoretically shown in Figure 2.1.

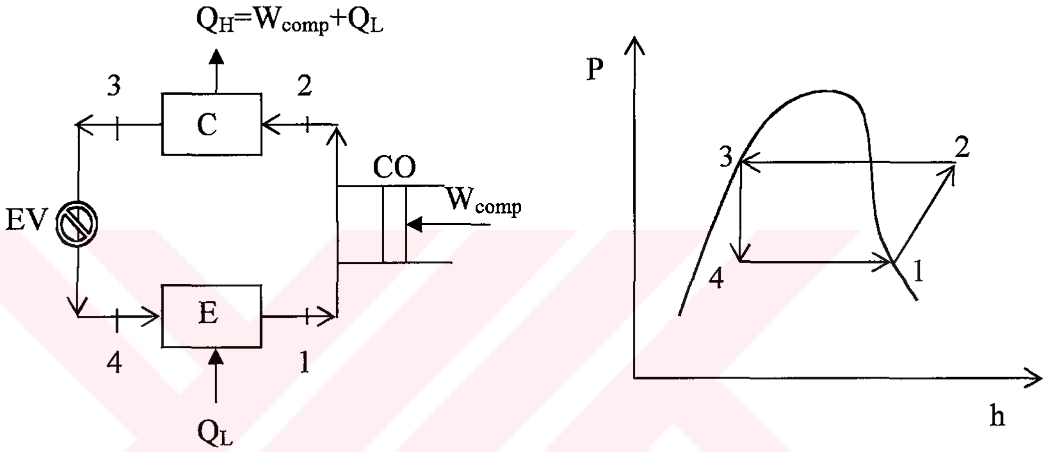

Figure 2.1 Pressure-enthalpy diagram of an ideal vapor compression heat pump cycle

The application of heat pumps for drying has received continuous attention since it possesses two-fold beneficial characteristics. Through the evaporator, the heat pump recuperates sensible and latent heat from the dryer exhaust, hence the energy is recovered. Condensation occurring at the evaporator reduces the humidity of the working air, thus increasing the effectiveness of product drying. It is therefore anticipated that the heat pump dryer can accelerate the drying process and use energy more efficiently. On the other hand, the heat pumps coupled with a dryer is a complex system since all the components are independent. Any change in one component will inevitably influence the others. Furthermore, a heat pump dryer is also a very complicated system because of the interaction between the working fluids, refrigerant in heat pump and air in dryer. Working air in the drying circuit interacts with the refrigerant in the heat pump circuit through the heat and mass transfer in the condenser and the evaporator in some situations. Ideally, the compressor isentropically compresses the working fluid refrigerant in the heat pump as vapor leaving from the evaporator at low pressure to the high pressure (process 1-2, compression) as shown in the Figure 2.1. Mechanical work which supplied by the compressor is added into the refrigerant, hence the compression process obtained by the compressor increases the enthalpy of refrigerant corresponding to its pressure and temperature and the refrigerant at superheated vapor state is obtained at the exit of the compressor and at inlet of the condenser. The compression is normally a polytropic process rather than isentropic one since the reversible adiabatic condition is not practically achievable. The superheated vapor refrigerant rejects heat at the condenser and becomes a saturated liquid (process 2-3, condensation) before isenthalpically expanding through the expansion valve (process 3-4, expansion). The low pressure refrigerant vaporizes in the evaporator (process 4-1, evaporation) by drawing heat from the surroundings, normally ambient air. If the heat pump is coupled with a dryer as illustrated in Figure 2.2a, the states of the process air on the psychrometric chart are ideally shown in Figure 2.2b.

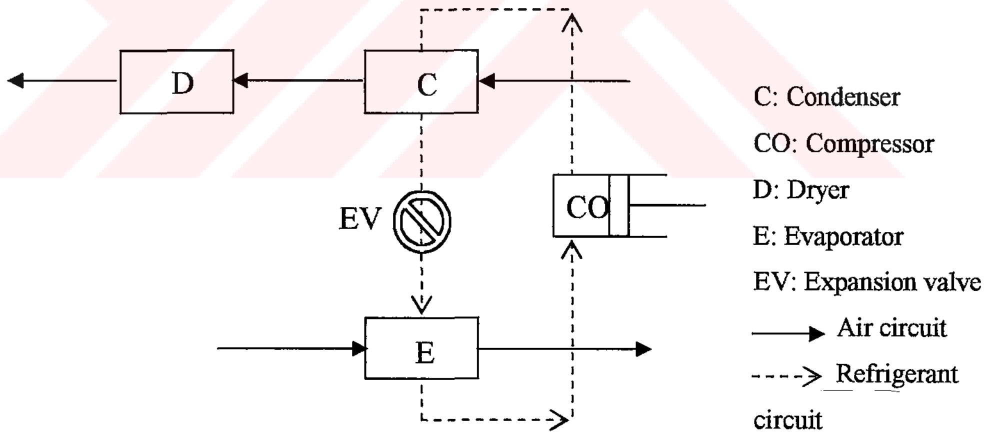

Figure 2.2a A schematically diagram of an open type heat pump dryer configuration

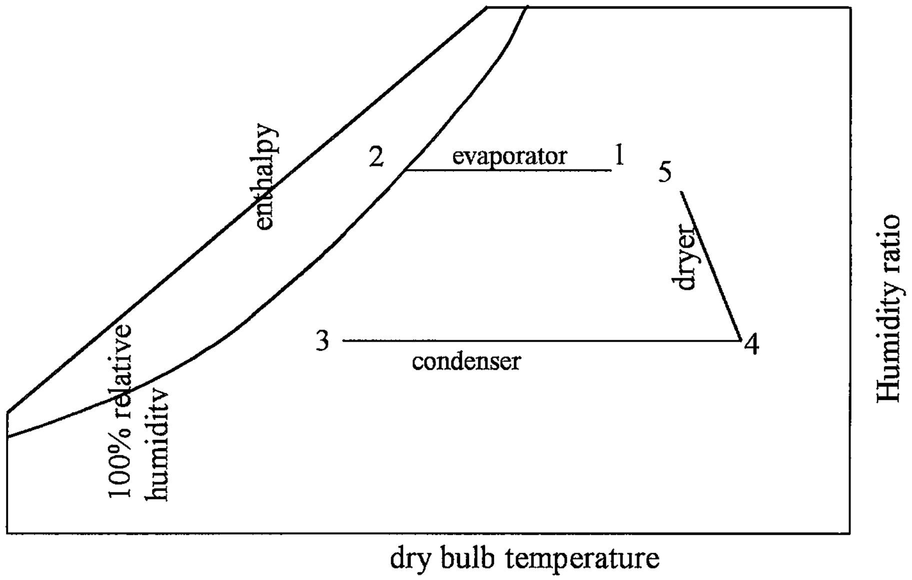

Figure 2.2b The ideal air circuit of a dryer in the psychrometric chart

The ambient air at condition 1 enters the evaporator. Its temperature is lowered and becomes saturated air which has 100% relative humidity at the evaporator exit (stage 2 in Figure 2.2b). That is, the air is dehumidified by cooling below its dew point temperature while it passes through the evaporator. The air at low temperature (stage 3) is passed through the condenser and its temperature rises by the heat released from the refrigerant side in the condenser, and then the air which has a higher temperature enters the dryer at stage 4, and then air absorbs moisture from a product as it flows through the drying chamber. As shown in the Figure 2.2b, the degree of dehumidification in the evaporator depends on the evaporator temperature. The temperature of the process air entering the dryer is limited by the condensing temperature of the heat pump working fluid. Obviously, a low evaporating temperature and a high condensing temperature are required for the effective dehumidification and high temperature of the process air, respectively.

2.2.2 Factors influencing HPD performance

In the drying process, the increased temperature enhances heat transfer rate into the drying materials which consequently raises the internal vapor pressure and increases the moisture diffusion rate from the drying materials. To assess the dryer performance, generally three parameters are employed in the available literature: the coefficient of performance, COP, the moisture extraction rate, MER, and the specific moisture extraction rate, SMER.

The MER and SMER are the performance parameters for drying application. The MER is equivalent to drying rate and it is defined as the mass of moisture removed from product per unit time as given by the following equation in units of g water/s,

$$MER = \dot{m}_a (w_{do} - w_{di}) * 1000 \qquad (2.1)$$

where

$\dot{m}$: mass flow rate of air, kg/s

w: humidity ratio, kg water/kg dry air

and subscripts do and di designate the dryer outlet and dryer inlet, respectively

On the other hand, the SMER is also a typical performance parameter defined as the mass of moisture removed from product per consumed total power in the system per unit time, in other words, the MER per consumed power in the system as given by the following equation in the unit of g water/kWs,

$$SMER = \frac{MER}{W_t} \qquad (2.2)$$

where

W_t: total power consumed by the dryer, compressor and centrifugal fan, kW

The performance of the heat pump is determined by using the COP which defined as the ratio of heat rejected at the condenser to the work used by the compressor and it is formulized in the following relation,

$$COP = \frac{Q_{cond}}{W_{comp}} \qquad (2.3)$$

Although the MER defines the dry product throughput rate, drying rate, or the drying capacity of the dryer and the COP is a useful performance indicator of the heat pump, the SMER is the only performance parameter taking into account of both dryer and heat pump. The SMER reflects on how efficient the energy usage is and defines the effectiveness of the energy used in the drying process.

As another performance parameter, the dryer efficiency, DE, of a dryer is defined as the ratio of the difference in the moisture content of air entering and leaving the dryer to that between the entering air and the air leaving the dryer at fully saturated condition as given in the following equation,

$$DE = \frac{w_{do} - w_{di}}{w_{s,do} - w_{di}} \tag{2.4}$$

where subscript s designates the saturated state

The DE can also be defined as the ratio of the actual moisture removal over the maximum possible moisture removal at a particular condition of the dryer. At the same time, the contact factor, CF, is used instead the DE in some available literature.

The factors affecting the performance of HPD are:

- ambient air characteristics, its relative humidity and temperature
- HPD configurations
- air mass flow rates
- compressor speed, and also its type and size
- bypass air ratio
- working refrigerant in heat pump
- sizes and types of the heat exchangers
- direction of air flowing across the dryer and the configuration of the dryer

The HPD configurations studied in the available literature are shown in Figure 2.3. In configuration A, open cycle 1 shown in Figure 2.3a, the ambient air is drawn in the evaporator. The moisture condensation occurs at the evaporator since the temperature of the process air passing through the evaporator is below the dew point. The dehumidified air leaving its moisture in the evaporator enters into the condenser after it leaves from the evaporator. Then the air temperature of airflow increases when it passes through the condenser by releasing heat from the refrigerant side in the condenser. Finally, the hot air leaving from the condenser enters the dryer and then discharges into the ambient. Therefore, this system is known as the dehumidifying HPD and an open cycle.

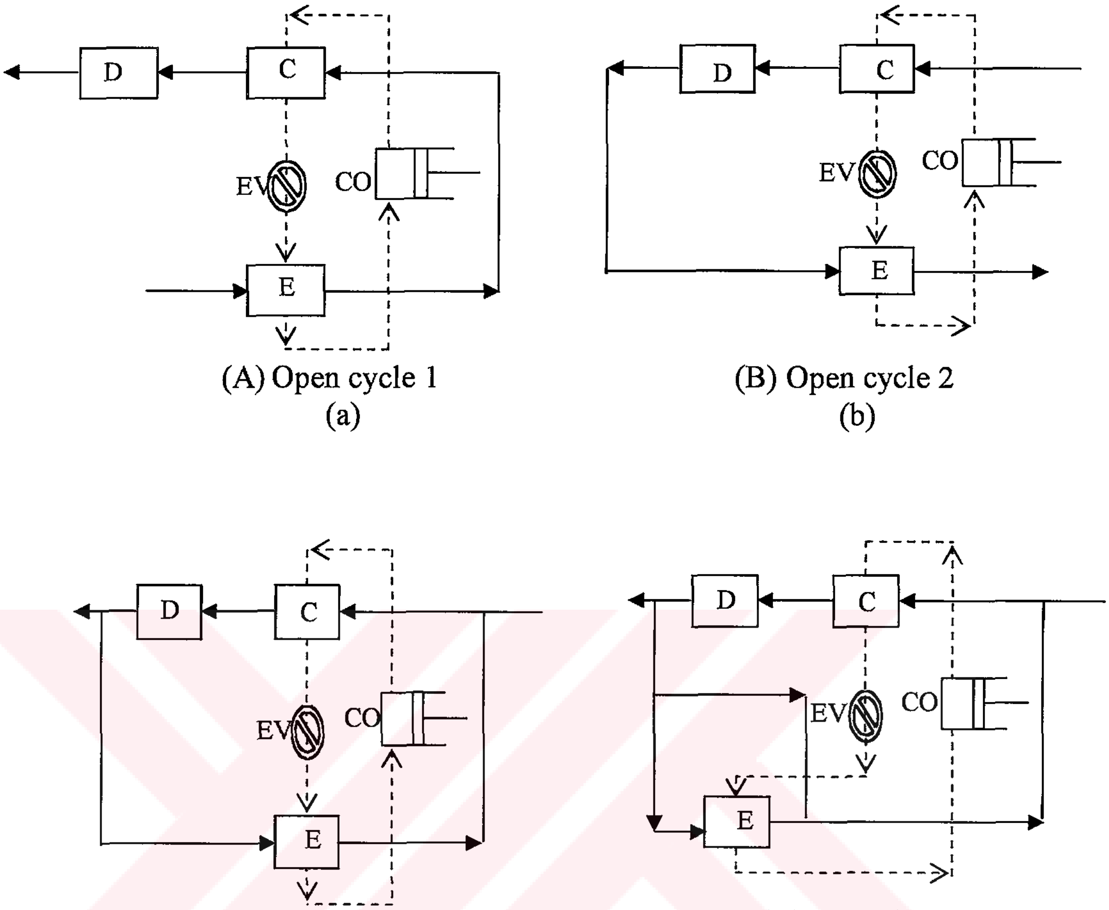

(A) Open cycle 1 (a)

(B) Open cycle 2 (b)

(C) Closed cycle 1 (c)

(D) Closed cycle 2 (d)

Figure 2.3 HPD configurations

C: Condenser	——	air circuit
CO: Compressor	- - - - -	refrigerant circuit
D: Dryer		
E: Evaporator		
EV: Expansion valve		

In configuration B, open cycle 2 shown in Figure 2.3b, the moisture in the working air is not extracted prior to entering the dryer. The moist air leaving the dryer passes through the evaporator, and then discharges into the ambient air. The working air is hotter than that of the configuration A, because the dehumidified air leaving from evaporator is not passed through the condenser, instead it discharges into the ambient. At the same time, the ambient air passes through the condenser and then through the dryer. In this case, the air leaving from the dryer relatively moist and hot, this enhances the heat recovery by the evaporator. In the configuration B condenser sensibly heats up the ambient air without moisture extraction in the evaporator which recovers both sensible and latent heat. Working air in the configuration B is, therefore, hotter but contains more moisture compared to that of configuration A.

The schematic diagram of configuration C is shown in Figure 2.3c. It is a partially close cycle with a partially discharged air and fresh air intake before and after the evaporator, respectively. That is, the hot and moist air leaving from the dryer is partially discharged into the ambient and the other partition is passed through the evaporator and the dehumidified air in the evaporator is passed through the condenser by mixing with the ambient air. Configuration D, which shown in Figure 2.3d, is a modification of C where a bypass passage across the evaporator is added. A closed cycle dryer recirculates moisture-laden air, but with a higher air temperature, there should be a greater moisture carrying capacity.

2.2.3 Previous studies on heat pump dryers

Toal et al. [19,20] experimentally investigated the feasibility of using a heat pump as an alternative to other forms of drying where low temperature drying of a substance. Toal et al. [19,20] concluded that the heat pump is a more efficient mechanism for drying than pure resistive heating. He also investigated optimum conditions of air flow velocity, air temperature, and condenser and evaporator temperature within the HPD and several different types of cycles and dryers. So, he showed that raising the air temperature greatly increases the moisture carrying capacity of that air, but also raises the refrigerant temperature within the heat pump, reducing the dehumidifying effect of the evaporator and he also showed that how the maximum moisture carrying capability of air increases exponentially within temperature over the range 20-50°C. The results also showed that the open cycle dryer takes up to three times as long to reach a similar moisture content as the corresponding closed cycle, and the worst performance was that of the open cycle dryer B. As a result he noticed that the significant improvements over conventional drying methods were obtained by using lower temperature drying by heat pump mainly as dehumidifier.

Prasertsan et al. [3-9] investigated theoretically and experimentally the factors influencing HPD performance, the ambient conditions, moisture extraction rate, MER, specific moisture extraction rate, SMER, coefficient of performance, COP, recirculation air ratio, RAR, evaporator bypass air ratio, BAR, dryer efficiency, DE, and product throughput. They investigated the performance of the heat pump dryer by simulating models of heat pump dryer components. The thermodynamically finite difference method was employed in the simulation to examine the state of the working fluids and heat and mass transfer by divided the condenser and evaporator into several infinitesimal elements in their theoretical studies [5,7,8]. They experimentally investigated on the performance of a batch type HPD designed to be operated in four configurations, two open systems and two partially closed systems as shown in Figure 2.3, in order to verify the results obtained by computer simulation. The experimental results have successfully verified the HPD models developed in their models. It was noticed that, among the four HPD configurations, configuration A had the worst performance because the air entered the dryer at low temperature. Although the specific humidity of the working air of configuration A was low due to the pre-dehumidification, the relative humidity might be high because of its low temperature. Thus, the drying ability of the air was limited. Moreover, in comparison to the other configurations, the air entering evaporator of configuration A was at lower enthalpy. Therefore, the energy related performance, SMER, was poor. Furthermore, the condition of the dryer inlet air affects the product drying rate or MER. The configuration B performed better than A in the SMER, and also both open systems, A and B, considerably depended on the ambient temperature was high, the SMER was apparently high, in spite of high specific humidity. In the configuration C, it is shown that the higher RAR is, the lower SMER is achieved and tends to be at lower temperature and in the configuration D, bypass air facilitates the moisture condensation over the evaporator coil and enhances the dehumidifying capability because more latent heat is transferred at the evaporator. The SMER values in configuration D generally are in the same range as found in the configuration C. Although the highest MER was obtained in the testing of configuration D, it does not imply that configuration D is the most effective HPD because the dryer loads and ambient conditions of every test might not be identical.

Therefore, results were not comparable. They concluded that SMER and MER are the weak functions of ambient temperature, RAR increases with increasing MER, BAR has negligible effect on the system performance, the more the BAR is, the less the SMER, however, the MER slightly increases with the BAR and as the BAR increases the compressor power increases due to increase of pressure ratio of the system, and MER and SMER increases linearly with DE. They also concluded that the system can be completely open or particularly close, that is HPD system cannot be completely close, and the close cycle configuration either with or without evaporator bypass air is not appropriate for the high drying rate process. Instead, the open cycle B where the air simply passes through a series of condenser, dryer and evaporator as shown in Figure 2.3 seems to be the best configuration since it gives the highest SMER and MER. They found that the operating conditions for optimum MER and SMER are not necessarily identical, that is he noticed that the condition giving maximum SMER does not correspond to the condition for maximum MER or COP and the system operating with high humidity air entering the evaporator always gives high SMER. And he also attracts attention that the mode of HPD operation is very complicated since there are many factors effecting the performance of HPD and the interaction between these factors, and it can be stressed that the system that is appreciably successful in one country or for one dryer type does not necessarily warrant the success for the others.

The performance of a dehumidifying R114 compression heat pump with auxiliary heat input before the condenser and before the evaporator was also experimentally studied while maintaining evaporating temperature constant. In both cases, the considering temperature increased with heat input. A decrease in COP values with increasing heat input was also observed in both cases. When heat was input before the condenser, the dehumidification rate increased initially and then started to fall with increasing heat input. A continuous fall in dehumidification rate was observed with increasing heat input before the evaporator. This is attributed to ineffective use of evaporator area caused by increased superheat.

In the theoretical study of Zylla et al. [21], the simplification of the HPD model required many assumptions which might not be true, for example the COP was assumed as high as 10.57 times of the Carnot cycle. In addition, temperature difference between the outlet and heat exchanger surface (condenser and evaporator) was assumed at 5°C.

Simulation based on energy balance at each component of vapor compression heat pumps was reported by Almedia et al. [11] in 1990. In this study the heat was used to preheat the air stream before it enters the drying chamber. He assumed constant heat transfer coefficients based on the arithmetic overall temperature difference in the condenser and evaporator despite the fact of phase change of the refrigerant and condensation of water on the evaporator, and polytropic process for the compressor in modeling the heat pump. The main conclusions which can be drawn from the results are that higher mass flow rates imply lower specific power consumption, SPC. However, air mass flow rate is increased so does the pressure drop across the condenser and drying chamber, and the overall power consumption would certainly be affected. It was noticed that heat pump proved to be more efficient than conventional heating system at any operating condition.

Pendyala et al. [14] modeled the HPD by considering the heat transfer and simultaneous heat and mass transfer zones. Simulation proposed by Pendyala et al. took into account of refrigerant phase change and water vapor condensation on the heat exchangers, evaporator and condenser, but ignored pressure drop in the system. He modeled the heat exchangers by writing the enthalpy balance for differential lengths considering the various zones on the air and refrigerant sides and the compressor by considering the polytropic compression. This model has been used for simulating an existing system using R11 working refrigerant to study the effect of approach velocity of air to the evaporator and of the suction superheat on the SEC of the HPD. Also, the performance of an HPD operated using R11 and R12 as working refrigerants in the heat pump was experimentally studied by Pendyala et al. [15]. The system performance was evaluated by using the parameters: coefficient of performance, COP, and the specific power consumption, SEC, defined as the energy supplied for unit weight of the moisture removed. They experimentally concluded that the COP and SEC values obtained using R11 were 3.5 and 3500kj/kg, respectively, and the corresponding values of R12 were 2.5 and 1800kj/kg while it was operated at 65°C using R11 and 55°C using R12. In spite of the lower COP for R12, the corresponding SEC values were better because the system could be operated without any additional electrical heating with R12. They also showed that an optimum approach air velocity to the evaporator of 1.4m/s gave the lowest SEC values of R12 as the working refrigerant fluid in the heat pump.

Baines and Carrington [25] presented a simulation analysis of closed Rankine cycle HPD in which the air recirculation ratio within the drying chamber is high. The simulation results illustrated the need for the dryer control strategy to take advantage of the performance characteristics of the HPD. Also, this study had emphasized the use of second law analysis reported earlier by Carrington and Baines [26] to provide a physical understanding of the factors controlling the efficiency of the system by investigated the loss mechanisms in the HPD. The avoidable and unavoidable loss processes in heat pump dryers were identified and compared with those in conventional heat and vent dryers in theoretical study done by Carrington and Baines [26] in 1988.

Carrington and Bannister [12] presented an empirical model based on laboratory measurements made on a prototype heat pump dryer with R134a. This model was set up by coupling the sub-models using energy and mass balances. In this study also lumped components models for the principal elements of a heat pump dehumidifier using R134a and a scroll compressor had been developed on the basis of the their experimental measurements. The model was used to illustrate the potential for increasing the energy efficiency and capacity of the dehumidifier by resizing the heat exchangers and air flows.

The continuous cross flow heat pump assisted dryer model theoretically and experimentally studied by Jolly et al. [16] and Jia et al. [17] took account of detailed heat and mass transfer phenomena taking place in each component in the system which included the pressure drop for many different system configurations shown in the Figure 2.3. The simulations showed that there has been some misunderstanding reported in the previous literature. In particular, the results show that the evaporator air bypass ratio is not as critical as previously indicated by Baines and Carrington [25]. While their results show that bypassing around the evaporator can increase the SMER almost three timed and that the maximum SMER is very sensitive to the BAR. Jolly et al. [16] and Jia et al. [17] also showed that bypassing warm air around the evaporator can improve the SMER or the system performance by about 20%. The reason is that in Carrington's and other author's models they did not take account of heat and mass transfer in the evaporator and condenser. They assumed a constant temperature difference between the air and refrigerant at the exit of the coils. Jolly et al. [16] and Jia et al. [17] also showed that the highest COP give the highest SMER and that the optimum dryer can be achieved by maximizing the SMER. Baines and

Carrington [25] also pointed out that this conclusion, whereas the simulation and experimental results of Tai et al. [22,23] showed that a HPD can be optimized by maximizing the COP of the heat pump. Jolly also showed that bypassing air to the condenser inlet is much better than bypassing air to the condenser exit for both open and closed systems and also investigated that the effect of the compressor speed., the heat transfer areas of the evaporator and condenser, and the total air mass flow rate on the performance of the system. At the same time, he made the comparison of the open and closed cycle HPD and showed that the open system is more sensitive to ambient air conditions than the closed type, and suggested that closed type HPD should operate in winter and the open type in summer. The same suggestion was done by Prasertsan et al. [5,7,8], and at the same time he noticed that this should not always be true but would depend on the ambient humidity, type of dryer and dryer efficiency as well.

Chou et al. [10] developed a simple mathematical model of a HPD by using the first law and psychometric equations to simulate the steady state system by assuming the COP of eight. The concept of contact factor was used in the mathematical model to describe the heat and mass (moisture) transfer process between the product and the drying medium. The simulation was limited to the air side only, no effect of the refrigerant was taken into account. Results indicated that the SMER and SPC are strongly influenced by the CF of the dryer. The CF of the dryer is sensitive only to the relative humidity and velocity of air entering the dryer. Also, a performance chart to guide the selection of the HPD components was proposed in their study [10].

Clements et al. [18] experimentally investigated the performance of a prototype heat pump assisted continuous conveyer type dryer by using wetted foam rubber as the test material being dried. This dryer had achieved an average SMER of about 2kg/kWh. In addition, the following conclusions that have satisfactory agreement with the simulated results by Jolly [16] and Jia et al. [17] were drawn for this dryer investigated:

a) A high relative humidity of the air entering the evaporator is very important to the successful design of a heat pump assisted dryer.

b) The BAR is not as critical as some previous literature has indicated (Baines and Carrington [25]).

c) A higher compressor speed corresponds to a lower SMER for the dryer investigated; however, the product throughput is increased.

It is obvious that many various simulations used different assumptions, and a lot of these away from the expense of accuracy. Moreover, many experimental investigations were done at different operating conditions. Therefore, the results of both theoretical and experimental studies are in different or even contradictive conclusions.

2.3 WORKS ON FLUIDIZED BED DRYING

2.3.1 Introduction

In a fluidized bed, particles confined to a vertical column are suspended by a sufficiently strong upward volumetric flux of fluid. In some circumstances the fluid flows uniformly through a bed of particles of constant concentration. As we know the drying is essentially a process of simultaneously heat and mass transfer. It is defined as the process of the removal of moisture or liquid from a wet solid by bringing this moisture into a gaseous state. In most drying operations, water is the liquid evaporated and air is the drying medium. Heat, necessary for evaporation, is supplied to the particles of the material and moisture vapor is removed from the material into the drying medium. In fluidized bed drying the process is carried out in a bed by drying medium as shown in Figure 2.4. Heat is transferred by

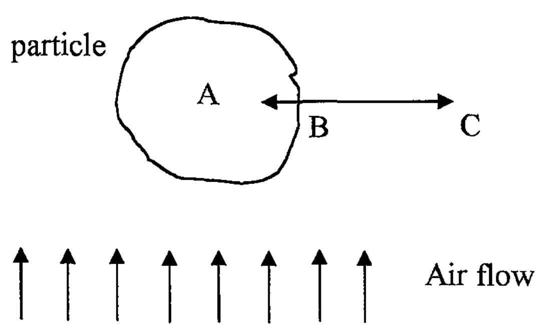

Figure 2.4 Schematic representation of the fluidized bed theory

convection from the surroundings (C) to the particle surfaces (B), and from there, by conduction, further into the particle (A). Moisture is transported in the opposite direction as a liquid or vapor; on the surface of the particle it evaporates and passes on by convection to the surroundings.

Figure 2.5.a illustrates schematically a typical fluidized bed classification. An idealized plot of the pressure drop across the bed, ΔP_b, versus gas velocity, u, is shown in Figure 2.5.b.

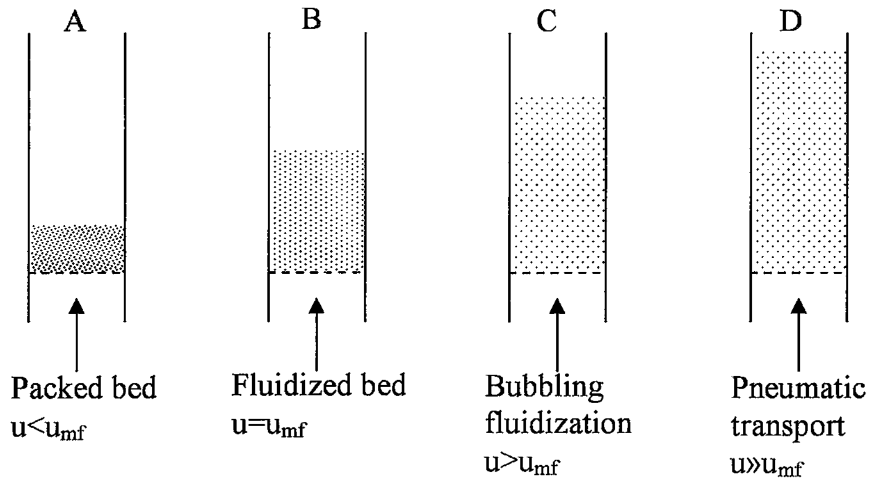

Figure 2.5a Four different regions of gas fluidization

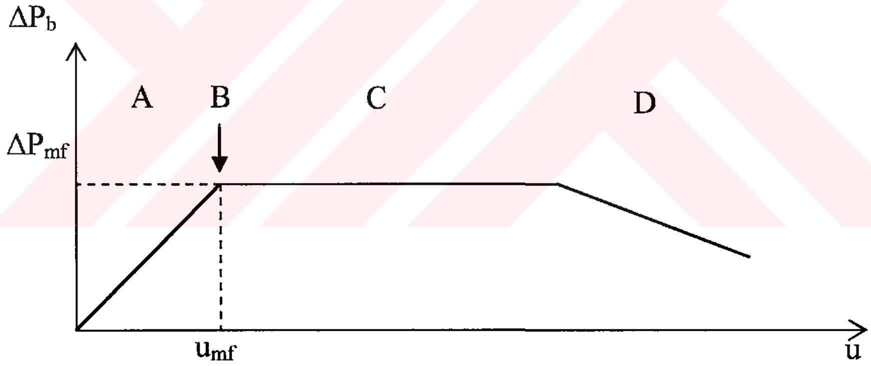

Figure 2.5b The relation between the gas velocity and the pressure drop in the bed

In fluidized bed, as the upward fluid velocity is increased, the pressure drop across the particle layer, ΔP_b, increases linearly (for large and dense particles, however the relationship is parabolic) as shown in Figure 2.5b. At a certain gas velocity, the pressure drop across the bed reaches the equivalent to the weight of the particles in the bed per unit area of the bed, ΔP_{mf}. When the fluid velocity in the bed reached to the point B shown in Figure 2.5b, all particles are suspended in the upward flowing gas or starts expanding in height while the pressure drop levels off and no longer increases as the fluid velocity is increased. At this point the upward force exerted by the fluid on the particles is sufficient to balance the net weight of the particles and the particles begin to separate from each other and float in the fluid. The layer of particles is now incipiently fluidized and particle mixing takes place in the bed. The gas velocity at this point where the bed just begin to fluidize is called as the minimum fluidization velocity, u_{mf} . When the gas velocity increased further above u_{mf}, any additional fluidizing gas passes through the particle layer as bubbles, ΔP_b remains constant at ΔP_{mf}. When the gas velocity is smaller than the minimum fluidization velocity, $u<u_{mf}$, the bed is called as the fixed or packed bed. The velocity which the first particle is carried out of the bed is called as the terminal velocity, u_t. When the fluid velocity is greater than or equal to minimum fluidization velocity and it is less than the terminal velocity, $u_{mf} \leq u < u_t$, the bed forms a fluidized bed. At the other case, when the fluid velocity is greater than or equal to terminal velocity, $u \geq u_t$, much larger than the minimum fluidization velocity, the particles is pneumatically transported towards discharge side of the bed, and the bed mobilizes.

Fluidized drying of granular products of solids can be batchwise or continuous. Batch operation is preferred for small scale production and for heat sensitive materials. The process conditions are easily selected in batch drying, and the product is of uniform quality due to homogeneity of the bed at any instant during its operation. In continuous fluidized drying, the product from the dryer under steady state operation corresponds in its properties to the material within the dryer due to high degree of solids mixing.

Fluidized bed dryers are widely used in a number of industry sectors to dry finely divided 50-5000μm particulate materials and are normally of circular or square cross-section and contain relatively deep 250-450mm beds of particles.

2.3.2 Previous studies on the fluidized bed dryers

Geldart [99,100] observed the nature of particles fluidizing. He categorized his observations by particle diameter versus the relative density difference between the fluid phase and the solid particles. Geldart [99,100] identified four regions in which the fluidization character can be distinctly defined.

Group A particles fluidize smoothly and have a range particle size typically 20-200μm. When fluidized by air at ambient conditions, this group particles give a region of non-bubbling fluidization beginning at minimum fluidization velocity, followed by bubbling fluidization as fluidizing velocity increases. Geldart [99,100] observed that group A particles has maximum bubble size is less than 10cm and bubbles spit and coalesce frequently through the bed and also gross circulation of solids occurs.

Group B particles, the most common and typically 200-800μm, give only bubbling fluidization under these conditions. These are made of coarser particles, sand-like, than group A particles and more dense. Unlike group A particles, group B particles form bubbles as soon as the gas velocity exceeds minimum fluidization velocity. Geldart [99,100] also observed that group B particles have bubble sizes independent of the particle size and have gross circulation.

Group C particles, typically less than 20μm, are very fine and are difficult to fluidize and tend to rise as a slug of solids and tend to be cohesive.

Group D particles are very large than 1000μm and dense particles. This group particles is difficult to fluidize as very high gas velocities are needed. Geldart [99,100] observed that this group particles forms bubbles which coalesce rapidly and grow large and this group particles can be spouted from the top of the bed easily.

One of the primary works in fluidized bed drying is that of Vanecek et al. [91]. They proposed a design procedure for fluidized bed dryers based on the total heat and mass balance of the whole drying apparatus. They considered the bed as a homogeneous system, i. e. no bubbles and their interactions in the bed. Simmonds et al. [92] experimentally investigated drying of granular product in a circulation dryer and found that the rate of drying was independent of air velocity in the range of 1.64m/s to 8.74m/s. He also concluded that the majority of the drying of wheat does not occur in the constant rate period, but only in the falling rate period. The rate of drying was proportional to the free moisture content of the grain, while the grain temperature was related to the moisture content at any certain stage in the drying process. Hoebink and Rietema [69,70] described mass transfer from the solids to a rising bubble with the assumption of no diffusion limitations inside the solids. Two contributions were conducted for: the mass transfer from the dense phase across the cloud boundary and the mass transfer from the solids passing the cloud during the rise of the bubble. A similar model also was presented for the heat exchange between the bed and the rising bubbles. The model which takes into account the action of bubbles, considers only the situation that moisture transport between particles and gas can be described with a single and constant overall mass transfer coefficient.

Later, they modified the model to include a variable mass transfer because of diffusion inside the solid particles which are dried in a fluidized bed can not be neglected. The concept of a constant mass transfer coefficient is no longer adequate to describe the moisture transport of solids which are dried in a fluidized bed. However, mass transfer was considered to be fast in the dense phase, and equilibrium between the solid particles and interstitial gas was assumed.

Plancz [68] proposed a mathematical model for continuous fluidized bed drying by employing a three phase model representing a dilute (bubble) phase, interstitial gas phase and solid phase, inside the bed. The bubble phase was assumed to be in plug flow while the interstitial gas and the solids were assumed to be perfectly mixed. Using a simplified lumped model for single solid particle, the heat and mass transfer between the interstitial gas and solid phase as well as the heat transfer between the solid phase and particles were modeled. Numerical computation based on this model was done to study the effects of the process parameters as particle and bubble-size, gas velocity, inlet gas temperature and residence time, on the moisture content of the solid outlet. His model may contribute to the better understanding as well as quantitative describing of the continuous drying process in fluidized bed. It can be also employed for simulation and dimensioning of dryer equipments. However, the lumped model for solid particles is not realistic.

Uçkan and Ülkü [93] studied the effects of air temperature and velocity on the drying rate of corn in a batch fluidized bed, and developed a model based on diffusion theory. They assumed that the drying air left the bed in mass and a thermal equilibrium with the grain, and ignored the presence of bubbles and their interactions with other phases and observed the strong effect of gas temperature on drying rate.

Giner and Calvelo [51] used the kinetic parameters obtained from the thin-layer drying experiments for wheat based on internal control transfer and absence of temperature gradients inside the kernels. The drying operation in a batch fluidized bed was modeled by assuming a perfect mixing of solids. They, however, did not consider the presence of bubbles inside the bed and assumed thermal equilibrium. Predictions of the model showed that drying times could be decreased about four fold by raising the air temperature from 40°C to 70°C. In this theoretical study, grain wheat kernels were assimilated to ellipsoids having average dimensions of 3.2mmx1.6mmx1.4mm and average volume of the grains was determined as $3.16 \times 10^{-2} cm^3$ and density as $1380 kg/m^3$. Chandran et al. [49] presented a kinetic model for constant and falling rate periods and compared their results with the experimental data obtained using drying of sand and zeolit (ion exchange resin) in a batch system. They found that when these materials were subjected to batch drying, they exhibited both constant rate and falling rate periods. The drying rate was enhanced in the constant rate period with an increase in temperature and flow rate of the heating medium, and was reduced with an increase in the particle size and bed height. Chandran et al. [49] also compared the performance of a batch system with a continuous system. They also found that for a certain drying time, batch operations gave lower average moisture content. The difference in the average moisture content of the product, for a certain drying time, in the falling rate period was large and this difference increases as the moisture content approaches the equilibrium moisture content. Abid et al. [65] performed an experimental and theoretical analysis on the mechanism of heat and mass transfer during the drying of corn kernels in a fluidized bed containing particles. It was found that, as with wheat, the humidity and velocity of the gas had only a small effect on the rate of drying. Therefore, there was no drying in the constant rate period. They recorded the temperature of the grain during drying and reported that the temperature of the product quickly reached that of the surroundings. Hence, the supply of heat to the particles was not a mechanism limiting drying. Their theoretical analysis based on irreversible thermodynamics, and accounted for the transfer of water by diffusion under the influence of concentration gradient of the moisture, and by thermo-diffusion under the influence of temperature gradient in his theoretical investigation. They found the external conditions such as the humidity and velocity of the gas have only a small effect on the rate of drying.

Thomas and Varma [66] proposed a steady-state core model for drying kinetics of granular cellular materials, green pepper, black pepper and mustard and compared with the experimental data for batch and continuous fluidized bed drying investigated at different temperatures and flow rates of the heating medium, particle size and mass of solids. They indicated that inter-particle diffusion controls the drying process; the drying of these materials exhibits constant rate and falling rate periods for each material and the falling rate might be nonlinear depending on the nature of the material and the critical moisture content were found to depend on the velocity and temperature of the heating medium, as well as the particle size and mass of solids. They predicted the performance of the continuous fluidized bed drying from the kinetic data obtained, using a batch fluidized bed dryer and assuming ideal mixing of solids.

Sirinivasa et al. [72] presented a model for drying of solids in a batch fluidized bed considering the heat and mass transfer among the bubble, interstitial gas, and solid phases. However, they used a simplified model for mass and energy equation of interstitial gas and bubble phases. They also used the equilibrium assumption between gas and solid particles and particles are homogeneous in spherical shape and uniform in size during drying; all particles within the bed are at the same temperature and have the same moisture content at any instant during the drying process; the bubble size is uniform and does not depend on the location within the bed, and evaluated the effective diffusivity of the solid particles by matching the experimental data with the model.

Zahed et al. [94] presented a model with allowance for the diffusional moisture transport in the particles and for interstitial gas to particle mass transfer within the dense phase, as well as interphase exchange resistance between gas bubbles and the dense phase. They predicted the bed temperature and moisture content of the solids under various batch drying conditions. However, similar to Sirinivasa et al. [72], they neglected the unsteady term in the mass and energy equations for interstitial gas and bubble phases and also assumed thermal equilibrium model and constant bubble size.

Alvarez and Shene [95] estimated the overall heat transfer coefficient using drying data in the constant rate period. They reported much lower heat transfer coefficients than those reported in the literature. Theologos et al. [96] developed a model based on the two phase flow theory and the drying kinetics model of Maroulis et al. [97]. They predicted the pressure drop, bed void fraction, temperature distribution in the gas and solid phases, humidity ratio, and the overall particle moisture in the bed.

Van Ballegooijen et al. [98] developed a numerical model for the prediction of drying process in a fluidized bed dryer of materials with diffusion limited behavior. They compared the results of the numerical model with laboratory experiments for silica gel particles and found a large discrepancy.

A close examination of the previous modeling studies reveals that many assumptions were made to simplify the analysis of drying process. First, in almost all of the works, it was assumed that for all particle groups with different specifications, the hydrodynamics of the fluidized beds is identical and the two phase theory of fluidization can be used for the modeling purpose. Also, the bubble diameter and velocity were assumed to be constant along the bed height. These assumptions ignore the fact that the hydrodynamics of fluidized bed is dependent on particle specifications, and each particle group manifests its own behavior in the bed. It is known that while the two phase theory of fluidization is suitable for group A particles, it cannot be used for other particle groups without a significant error. Geldart [99,100] reported that application of two phase theory for group D particles, the group that is mainly used in the drying process, results in up to 50 per cent error in the bubble flow rate.

Second, in most of the works the variation of air temperature along the bed axis is neglected. A uniform temperature is assumed. Furthermore, the variation of air temperature with time is also neglected in order to obtain an analytic solution. The uniform temperature assumption for air is not reasonable, especially in the initial period of drying.

Third, in many of studies, the diffusion equations were not used in the conservative form. They were manipulated to take a simple form with a constant effective diffusion coefficient. This assumption may have a considerable adverse effect on the results, since the diffusion equation plays a fundamental role in the moisture content distribution inside the particle. However, Hajidavalloo and Hamdullahpur [45,46] used a diffusion equation in a most general and exact form satisfying the conservative properties of the materials, and avoided any simplification for the diffusion coefficient. They developed a comprehensive mathematical model to simulate the simultaneous unsteady heat and mass transfer processes in a batch bubbling fluidized bed drying of large particles. Although the model is applicable to a wide range of particles, sand and wheat were chosen as examples. The effects of particle moisture content and relative humidity of fluidizing gas on the fluidization behavior were investigated in their study [45]. The drying mechanism for the solid phase was considered in two stages: the falling rate and the constant rate. In the development of the model, the commonly used two phase theory was not used because of its insensitivity to the particle group used in the bed. A newly developed expression to determine the minimum fluidization velocity of wet particles was used and the model also considered their physical variation along the bed. Also, three phase model representing the interstitial gas phase, the bubble phase, and the solid phase were modeled separately to describe the thermal and hydrodynamic characteristics of the bed. This model was developed to simulate the moisture content and temperature variation as a function of time inside a fluidized bed dryer. The model also predicted the moisture content and temperature distribution within a solid particle without using and adjustable parameters to fit the experimental data. The results showed that the distributions of moisture and temperature inside the particle are highly dependent on mass and heat transfer Biot numbers. In the case of wheat particles, with a high mass transfer Biot number, there is a large gradient of moisture concentration contrary to temperature profile which is nearly flat due to small heat transfer Biot number. In the second part of their works [47], they experimentally investigated the drying of wheat to assess the validity of the mathematical model described in Part 1 [45,46] and test its accuracy. In the experiments, temperature at different elevations, humidity of the exit air, bed pressure drop, fluidization velocity and moisture content of particles at different times were measured. Each experiment was repeated at three inlet air temperatures: 40°C, 49.5°C, and 60°C. Results of the model predictions showed very good agreement with a large number of experimental data obtained in drying wheat. The agreement of model prediction and experimental data indicated that the model is fully predictable for drying of other materials in the fluidized bed with no restriction in the range of operational conditions such as the air temperature and the relative humidity. It was found that the drying of grain materials is usually controlled by internal mass transfer parameters. The inlet air temperature has an important effect on the magnitude of drying rate while the gas velocity and bed hold up do not show significant contribution to the drying rate. The effect of temperature is more critical than other parameters and could reduce the drying time substantially. It was also found that the gas temperature gradient along the bed is initially important when the moisture on the surface of particles is removed and after that period the temperature profile has only a small gradient in the bed. They also observed that analysis of the exhaust air humidity results shows that after a period of rapid increase of the gas humidity at the initial stage, it does not vary much for the rest of the drying period. The high humidity of gas at initial stage can be attributed to the fast removal of surface moisture of materials at the beginning of drying. After the removal of the surface moisture, the rest of the internal moisture cannot be removed easily because of the low-mass diffusivity coefficient of material, causing a rapid decrease in the relative humidity of the exhaust air. The low humidity of the exit gas can be considered as an advantage for air recycling. Since this exit gas has high enthalpy and low humidity, it can be reused in the drying process to reduce the amount of heating to the bed and consequently increase the thermal efficiency of the drying process. Also, they attracted attention that using the two phase theory of fluidization for groups B and D particles underestimates the drying rate of particles in the bed, therefore, it is not recommended for use the two phase theory in the modeling of these particle groups and Syahrul et al. [48] used an energy model to optimize the fluidized bed drying conditions of large wet particles, group D. They [48] exposed that energy efficiencies were found to be decreasing with increasing drying time, therefore, the shorter drying period results in the higher energy efficiency, and also energy efficiencies are higher at the beginning of the process than that at the final state in addition to the conclusions observed in the previous studies [45-47]. The initial moisture content of the bed materials can have an important effect on the drying rate depending on the physical properties of bed materials. Syahrul et al. [48] also studied on an energy analysis of a fluidized bed drying system to optimize drying characteristics for large wet particles using energy models. Three critical factors; the inlet air temperature, the fluidization velocity and the initial moisture contents of the material were studied to determine their effects on the overall energy efficiency. He used different experimental data sets for wheat taken from the literature as mentioned before. The results show that the energy efficiencies of the fluidized bed dryer decrease with increasing drying time and become the lowest at the end of the drying process. Therefore, the shorter drying period resulted in the higher energy efficiency. It was observed that the inlet air temperature has an important effect on energy efficiency for the material where the diffusion coefficient depends on both the temperature and the moisture content of the particle. Furthermore, the energy efficiencies showed higher values for particles with high initial moisture content while the effect of gas velocity varied depending on the material properties.

Hajidavalloo and Hamdullahpur [45] also investigated the minimum fluidization velocity experimentally and found it to be in the following relation,

$$\frac{1.75}{\varepsilon_{mf}^{3}\Phi}\mathrm{Re}_{mf}^{2}+\frac{150(1-\varepsilon_{mf})}{\varepsilon_{mf}^{3}\Phi^{2}}\mathrm{Re}_{mf}=\frac{d_p^{3}\rho(\rho_p-\rho)g}{\mu^{2}} \tag{2.5}$$

where Re_{mf} is the Reynolds number at minimum fluidization as

$$Re_{mf} = \frac{d_p u_{mf} \rho}{\mu},$$

He also found that the minimum fluidization velocity depends on the moisture content of particles, and increasing the moisture content increases the minimum fluidization velocity and suggests the following expressions to determine u_{mf} for wet wheat particles:

$$u_{mf} = 0.9813M_p + 0.9054 \qquad 0.1 \leq M_p \leq 0.4 \tag{2.6a}$$

$$u_{mf} = 0.1317\ln(M_p) + 1.4 \qquad 0.4 \leq M_p \leq 0.6 \tag{2.6b}$$

where M_p is the moisture content of grain on a dry basis, kg water/kg solid, and is calculated by dividing the weight of water by the weight of dry material.

$$M_p = \frac{W_w}{W_d} * 100 \qquad \text{or} \qquad M_p = \frac{W_b - W_d}{W_d}$$

where W is the weight, kg, and subscripts w, b and d are water, material before drying and dry material, respectively. The wheat kernel is approximately ellipsoidal in shape with a thread in the direction of longer diameter. In their study, however, for simplicity of the numerical solution the wheat kernel was assumed to be spherical with an average diameter of 3.66mm, density of 1215kg/m^3 and specific heat of 1790j/kg. The moisture diffusion coefficient of wheat, D, is given by Becker [56] as

$$D = \frac{1}{130.5} \exp\left(\frac{-6140}{T_p}\right) \tag{2.7}$$

where T_p: particle temperature, ^{o}C

and the thermal conductivity, k, and specific heat of wheat, c_p, correlations by Kazarian and Hall [57]

$$k = 0.1167 + 0.1318\left(\frac{M_p}{1+M_p}\right) \tag{2.8}$$

$$c_p = 1398.3 + 4090.2\left(\frac{M_p}{1+M_p}\right) \tag{2.9}$$

Baker [42] described the development and application of a computer code that enabled the drying time, thermal efficiency and energy consumption of well mixed fluidized bed dryers to be estimated from experimental drying curves. Baker et al. [43] extended the model to include the calculation of bed area and costing the equipment in 2000. The results indicated that, in all cases, both the bed area and energy consumption decreased with increasing bed temperature and the thermal efficiency of the dryer increases with increasing gas temperature and outlet moisture content and with decreasing heat loss under all condition. Their conclusions verified to results that found by Syahrul et al. [48]. Baker [42] also showed that the drying rate is independent of humidity for wheat, while, in the case of zerolit, the drying rate varies with humidity. In addition, heat recovery and exhaust air recycle modules had been developed and the effectiveness of recycling the exhaust air was again shown to depend on the drying characteristics of the solids in his study in 2000 [43]. However, heat recovery was seen to be more widely applicable. Baker's model was based on Reay and Allen's approach [76,77] to fluidized bed dryer design, as modified by McKenzie and Bahu [103], and consisted of a material model and an equipment model. The material model enabled isothermal bed batch drying curves to be transformed from one set of operating conditions to another. The analytical model formulated in his work [44] done in 2000 succeeds to developing and improved understanding of fluidized bed drying and largely explained the predictions obtained in Baker's simulations [42]. Baker's analytical equations can be applied only for solids that exhibit first order drying kinetics. Of the three materials studied by Reay and Alley [76,77], both zeolit and iron ore behaved in this manner, the drying rate is predominately gas film controlled. Wheat, in contrast exhibited non-linear falling rate drying kinetics, dominating internal resistance to moisture transport.

Keey [78] indicated that first order drying is observed with small highly hygroscopic particles; clearly, the zeolit and iron ore both fall into this category. He also suggested that materials such as wheat should exhibit similar behavior under conditions where the drying process is controlled by movement through a thin shell near the surface. In support of this contention, he quoted the results of experiments reported by Krischer and Kast [79] for the drying of a single layer of wheat grains. When the drying rates were very low, the drying curves showed prolonged linear second falling rate periods. The results of Reay and Allen [76,77] also support this observation. At 333K and 353K, their drying curves for wheat exhibited distinct curvature. However, at 313K, the curvature was very much reduced. Presumably, if experiments had been undertaken at even lower temperatures, linear drying curves would have been obtained. So that, they showed that the drying rate is independent of humidity for wheat while in the case of zeolit the drying rate varies with humidity.

The slugging behavior of large particles was investigated by Dimattia [106] for various particles, i. e. red spring wheat, long grain rice and whole peas. Slugging can be a common occurrence in a fluidized bed utilizing large particles, and involves piston like movement of the bed material. They investigated effect of bed height, gas velocity, initial moisture content and air temperature on drying rate. By Dimattia [106], it was found that 'wall slug' do not inhibit, or slow the drying rate of red spring wheat at tests performed to determine the effect of this phenomenon on the drying rate of red spring wheat, it is not necessary to operate the bed at a high u/u_{mf}. Fluidized bed drying retains very high effectiveness at low u/u_{mf}; consequently, it is a preferable alternative to traditional spouted bed dryers. Drying times are shortened, thus requiring less energy.

2.4 WORKS ON SWIRLING FLOW

2.4.1 Introduction

The reduction in the world's limited fuel resources and the ever increasing cost of energy over the recent years accelerated the research on the enhancement of heat transfer rates in many applications in order to particularly reduction in the energy usage.

Heat transfer enhancement may be achieved by numerous techniques. One of these techniques is to generate the swirling flow. Swirling flow can be generally generated by turbulators, typical inserts, such as coiled wires, twisted tapes, helical vanes and spiral fins inserting into the pipe; treated surfaces, rough surfaces, extended surfaces; rotating boundary, coiled tubes, tangential entry of the fluid into the duct; pipe entry swirl generators such as guided vanes and propellers.

Swirl flow devices or techniques are designed to impart a rotational notion about an axis parallel to the flow direction to the bulk flow. Swirl flow is the descriptive term for a fluid flow in which the tangential component of the main stream velocity is a significant contribution to the resultant velocity. Moreover, a swirling flow is a typical complex flow that is affected by streamline curvature and flow skewness in addition to adverse and favorable pressure gradients. In a swirling pipe flow there is an axial flow upon which the tangential velocity component is superimposed. Thus the streamlines are spiral in the downstream direction and the turbulent structures are subject to the mixed effects of centrifugal force due to the streamline curvature and flow skewness caused by the non-uniform spiral pitch in the flow. A knowledge of the flow behavior near walls is important for predictive purposes particularly as regards skin friction and heat transfer.

Swirl flows are found in nature, such as tornadoes, and are utilized in a very wide range of applications, such as cyclone separators, heat transfer tubes, spraying machines, heat exchangers, gasoline and diesel engines, gas turbines and many other practical heating and cooling devices.

Swirl flows may be classified into three groups depending upon characteristic velocity profiles: curved, rotating and vortex flow. These velocity profiles are different, depending upon the particular flow geometry and swirl generation methods. Curved flow is produced by a stationary boundary, causing a continual bending of the local velocity vector. Curved flows can be generated by inserting turbulators such as coiled wires, twisted tapes and helical vanes and fins inserting into the pipe, and by coiling the tube helically or by making helical grooves and roughness in the inner surface of the duct. Rotating flow is generated by a rotating boundary, either confining the flow as far a rotating tube or locally influencing the flow field as for a spinning body in a free stream. Vortex flow arises when a flow with some initial angular momentum is allowed to decay along the length of the tube. These type swirl flows decaying are generated by the use of tangential entry swirl generators such as guided vanes.

Guided vane swirl generators may be grouped into two types: radial guide vanes and axial guide vanes. Radial guided vane swirl generators are generally mounted between two discs, and the vanes are so constructed as to be adjustable to obtain the desired initial degree of swirl. Axial guide vane swirl generators consist of a set of vanes fixed at a certain angle to the axial direction of the duct, which give a swirling motion to the fluid. Generally, the vanes are mounted on a central hub, and they occupy space in an annular region between the hub and the inner surface of the duct.

It is well known that the swirling flow improves heat transfer coefficients in pipe flows at the expense of increased pumping power due to increasing the flow paths, increasing energy dissipated by friction and introducing an angular acceleration to the fluid flow. For a constant pumping power a comparison of swirl and straight flow indicated an improvement in heat transfer rate of at least 20 per cent with swirling flow.

In the investigations of swirling flows, the most useful development has been the concept of the swirl number, which adequately defines the local flow field. The swirl number, S, is defined as the ratio of the angular momentum flux to the axial momentum flux of the swirling flow as given in the following relation

$$S = \frac{\int_0^R uvr^2 dr}{R\int_0^R u^2 r dr} \tag{2.10}$$

where u: local axial velocity component of air, m/s

v: local tangential velocity component of air, m/s

r: local radius of the pipe, m

R: pipe radius, m

This concept was firstly used by Leuckel [128] in 1968 and later many researchers were used the swirl number to correlate the heat transfer coefficient and friction coefficient measurements for swirling flow in pipes.

2.4.2 Previous studies on the swirling flow

Many investigations have been experimentally and theoretically conducted to determine mainly the heat transfer characteristics in swirling flow generated with various techniques.

Smithberg and Landis [109], Junkhan et al. [110], Hong and Bergles [111], Lopina and Bergles [120] used the twisted tape type swirl generators for their experimental studies. In 1964, Smithberg and Landis [109] investigated the velocity distributions, friction losses and heat transfer characteristics for fully developed turbulent flow in tubes with twisted tape swirl generators. They [109] had also developed model for the prediction of heat transfer coefficient which involves an analogy type formulation in which assumed that an incompressible flow could be considered to consist of an axial flow with a superposed forced vortex flow and negligible secondary circulation effects. They [109] resulted the following principal conclusions: The velocity field is helicoidally and corresponds to a forced vortex in the core superposed on an essentially uniform axial flow; the Nusselt number could be increased markedly at a given Reynolds number; but there would be an even greater increase in the friction factor due to the flow mixing effects and the increase in the wetted surface. Then, Thorsen and Landis [121] presented an excellent extension of the earlier development of Smithberg and Landis [109] in 1964, and their semi-analytical prediction method appears to account for all their observed variations in heat transfer coefficient with the swirl flow of air subjected to large radial temperature gradients.

Junkhan et al. [110] presented an experimental study on three popular turbulator inserts for fire tube boilers in 1985. Turbulators used in their study are twisted tape type swirl generators. These were two commercial turbulators consisting of narrow, thin metal strips bent and twisted in zig-zag fashion to allow periodic contact with the tube wall, and one commercial turbulator consisting of a twisted strip with width slightly less than tube diameter. They [110] concluded that the first and second type turbulators displayed 135 and 175 percent increases in heat transfer coefficient at a Reynolds number of 10000, respectively. A third type turbulator provided a 65 percent increase in heat transfer coefficient. The friction factor increases accompanying these heat transfer coefficient increases were 1110, 1000 and 160 percent, respectively, for the same Reynolds number.

Lopina and Bergles [120] investigated experimentally the heat transfer and pressure drop characteristics of single phase water in swirling flow which was generated by tight fitting full length twisted tapes with twist ratios from 2.5 to 9.2 in tubular test section. They [120] also compared the heat transfer and friction data combined in a constant pumping power for swirl and straight flow, which indicated that improvement of 20 percent can readily be obtained with swirl flow.

Hong and Bergles [111], in 1976, experimentally investigated the heat transfer coefficients for laminar flow of water and ethylene glycol in an electrically heated metal tube with two-twisted tape inserts. By Hong and Bergles [111], the Nusselt number for fully developed flow was found to be a function of tape twist ratio, Reynolds number and Prandtl number. These Nusselt numbers were as much as nine times the empty tube constant property values, also, the friction factor was affected by tape twist only at high Reynolds number.

Sethumadhavan and Raja Rao [112], Kumar and Judd [113], Uttarwar and Raja Rao [114], Özbey [126] experimentally studied on turbulent flow heat transfer and fluid friction in swirling flow generated by helically wire coil inserted tubes.

Sethumadhavan and Raja Rao [112] investigated the helical wire coil inserts tightly fitted in tube varying pitch, helix angle and wire diameter. The friction and heat transfer results were correlated in terms of roughness Reynolds number, momentum transfer roughness function and heat transfer roughness function. An optimization of the heat transfer rate and also minimization of pumping power and heat exchanger frontal area to identify the most efficient tube within the matrix of data.

An experimental study of forced convection heat transfer and frictional power loss of water flowing in a vertical tube in which placed the coiled wire turbulence promoters of various pitch to tube diameter ratio of 1 to 5.5 was presented by Kumar and Judd [113] in 1970. They observed that the heat transfer could be increased considerably by as much as 280 percent, although the increased frictional power loss was much greater than the increased heat transfer.

An experimental study had been carried out on isothermal pressure drop and convective heat transfer to grade oil in laminar flow in one smooth tube and seven wire coil inserted tubes varying wire diameter and pitch of wire coil by Uttarwar and Raja Rao [114] in 1985. The performance of these wire coil inserts had been evaluated by two different criteria based on the objective of either maximizing heat transfer rate or minimizing exchanger size. The results indicated that an improvement as high as 350 percent was obtained in heat capacity and reduction in heat exchanger area of about 70 to 80 percent could be achieved using wire coil inserted tubes when compared with a smooth tube at constant pumping power. The heat transfer results by Uttarwar and Raja Rao [114] also indicated that Nusselt number was a function of the helix angle, Reynolds number and Prandtl number. In their study, an important feature had been also observed in the case of laminar flow heat transfer augmentation was that the net improvement in the heat transfer coefficient was much higher than that observed for turbulent flow heat transfer. This was clear from the fact that the earlier work of Sethumadhavan and Raja Rao [112] on wire coil inserted tubes for turbulent flow showed only 30 to 50 percent improvement in heat transfer coefficient as compared to the reported improvement of 350 percent for laminar flow heat transfer in wire coil inserted tubes.

Hay and West [116] experimentally studied on the local heat transfer coefficient at various downstream stations for air flowing through a pipe with a swirling motion produced by a single tangential inlet. The dimensions of the tangential inlet slot and the angle of tangency were varied and the augmentation of heat transfer was found to be a function of the swirl number and a correlation for this function is presented as

$$\frac{Nu}{Nu_{\infty}} = (S+1)^{1.75} \tag{2.11}$$

where, Nu: local Nusselt number

Nu_{∞}: Nusselt number for fully developed non-swirling turbulent flow in pipe

S: Swirl number

While the values of Nu_{∞} should be obtained from a relevant correlation for fully developed non-swirling turbulent flow, for example, the equation [116] given in the following relation would be used.

$$Nu_{\infty} = 0.023\, Re^{0.8}\, Pr^{0.3} \tag{2.12}$$

And also, an expression for the local swirl number in terms of pipe diameter and downstream distance was given in by Hay and West [116] for decaying turbulent swirl flow in circular pipe as

$$S = 1.72 \exp(-0.04\, x/D) \tag{2.13}$$

where x: axial downstream distance from the pipe inlet, m

D: pipe inside diameter, m

At some locations the augmentation could be as much as eight times the value for fully developed non-swirling turbulent flow.

Ito et al. [115] theoretically and experimentally studied on the decay process of turbulent swirling flow generated by tangential inlet in a circular pipe and on a method to estimate the tangential mean velocity distribution. In their study, they presented the following relationship between the swirl intensity and the tangential velocity

$$\Gamma = 2\pi r v \tag{2.14}$$

where Γ: swirl intensity, m^2/s

v: tangential velocity component, m/s

r: local radius of pipe, m

Algifri et al. [117] experimentally investigated the heat transfer coefficients for air measured along a heated pipe for decaying swirling flow generated by radial blade cascade, radial guided vane type swirl generator, and presented the conclusion that there was an augmentation of swirling flow heat transfer coefficient at inlet to the extent of 90 percent compared to that of fully developed non-swirling flow, however, this enhancement in the heat transfer comes down to 40 percent at 50 diameters distance from the pipe inlet.

Kitoh [119] performed an experimental investigation to understand the physics of turbulent swirling flow in a straight circular pipe. He [119] generated the decaying free vortex type swirl flow produced by a radial guide vane type swirl generator placed at the inlet side of a long straight circular pipe. Kitoh [119] observed the results that the swirling component decays downstream as a result of wall friction and the swirl intensity, defined as a non-dimensional angular momentum flux, decays exponentially. The velocity distributions are continuously changing as they approach fully developed parallel flow. The structure of the tangential velocity profile which has a significant influence on the swirling flow structure was classified into three regions: core, annular and wall regions. The core region is characterized by a forced vortex motion, because, the centrifugal stabilizing effect becomes important, and the flow was dependent upon the upstream conditions. In the annular region, the skewness of the velocity vector was noticeable and highly anisotropic. The tangential velocity was expressed as a sum of free and forced vortex motion. In the wall region the skewness of the flow becomes weak due to only the centrifugal destabilizing effect appears.

In 1997, Özbey [126] performed an experimental study on the enhancement of heat transfer and the flow structure in the swirling turbulent pipe flow generated by the helically coiled wire turbulators. In this experimental study, the used helically coiled wires had different dimensions of wire diameter, pitch, number of coils and helix angle and the experiments had been conducted at various Reynolds number in the range of 30000-90000 and at constant wall temperature of 90°C at the inlet side of the test section in which the turbulator inserted. He [126] concluded that the heat transfer rates on the pipe wall increased in the range of 16-32 percent with turbulators over those in the smooth pipe without turbulator. Furthermore, low axial and tangential velocities in the core region surrounded by high axial and tangential velocities in the annular region near the wall of the pipe were observed in the experiments. In other words, the axial and tangential velocity profiles showed a decrement in the central portion of the pipe while the maximum axial and tangential velocity magnitudes in the cross-section of the pipe were seen near the wall at a certain radial distance from the center of the pipe.

Yılmaz et al. [122] experimentally investigated the heat transfer and friction characteristics of a decaying swirl flow of air produced by a radial guide vane swirl generator in 1999. The vanes of the swirl generator, which have different angles of 15, 30, 45, 60 and 75°, were designed to be adjustable to obtain different swirl intensities. An augmentation of up to 98 percent in Nusselt number was obtained in the decaying swirl flow depending upon the Reynolds number, Prandtl number and the vane angle at a constant heat flux boundary condition. However, the increase in pressure drop with decaying swirl flow was much higher than the increase in Nusselt number at constant Reynolds number.

In 2002, Yılmaz et al. [123] performed a similar experimental study to their previous experimental study in 1999 [122]. Only difference was to be that they used the radial guide vane swirl generator which had spherical and conical deflecting elements in their work in 2002. An augmentation up to 150 percent in Nusselt number relative to that of the fully developed axial flow was obtained with a constant heat flux boundary condition, depending upon the vane angle, Reynolds number and type of the swirl generators.

Bali [124] numerically and experimentally studied on fluid flow characteristics in the swirling air flow produced by a propeller type, axial guide vane, type swirl generator in 1998. She concluded that axial velocity profile showed a decrement in the central portion of the pipe and a n increased axial velocity was seen near the wall; tangential velocity profiles had a maximum value and its location moved in radially with distance; the swirl number or intensity decreased exponentially with the axial distance; no reverse flow appeared because of the weakness of swirl.

In 1999, Bali and Ayhan [125] experimentally studied on heat transfer augmentation as continuous work of previous work performed by Bali [124] in 1998. Consequently, they [125] concluded that swirl generator which was inserted the inlet of the pipe increased pressure losses rather than the heat transfer enhancement. Although the Nusselt numbers increased at the rate of 12-58 percent in comparison of the smooth pipe, the pressure losses increased 4.5-5.4 times. The enhancement of heat transfer coefficients for the range of 7000-15000 Reynolds number was lower than that of higher Reynolds numbers.

2.5 CONCLUSION

As seen, it has been theoretically and experimentally investigated the operating parameters and performance of a fluidized bed and heat pump assisted fluidized bed dryers in order to dry various granular materials, especially wheat and zeolit. The effect of swirling flow field on the enhancement of heat transfer has also satisfactorily investigated for especially pipe flows by using various swirl generating techniques. There have been many theoretical and experimental investigations on separately fluidized bed drying with and without heat pump and enhancement of heat transfer rate by using various types of swirl generators or other swirl generating techniques. However, it has not been investigated on a fluidized bed drying by generating swirling flow field in its drying medium, bed, and on a fluidized bed type dryer which coupled with a heat pump in order to dry granular material wheat in the available literature.

This thesis will be fill this gap in the available literature because of it has the feature of combination of these three subjects, fluidized bed type dryer, heat pump assisted dryer and swirling flow field.

CHAPTER 3

EXPERIMENTAL SET-UP AND MEASUREMENT TECHNIQUES

3.1 INTRODUCTION

In this chapter of the thesis, the configuration of the experimental set-up, the construction of the parts, specifications of the components, measurement and control devices and the measurement techniques are presented.

3.2 CONSTRUCTION OF THE EXPERIMENTAL SET-UP

In this experimental study a fluidized bed type heat pump dryer, FBHPD, was designed and constructed. FBHPD mainly consists of three parts and two circuits: dryer unit as air circuit, heat pump unit as refrigerant circuit and control and measurement devices. A general arrangement of the laboratory scale FBHPD experimental set-up is shown in the Figure 3.1. The experimental set-up consists of the following basic parts as shown in the Figure 3.1.

A. Dryer unit

1. Centrifugal fan
2. Settling tank
3. Bed
4. Heater
5. Particle holder
6. Pipe system
7. Transition parts
8. Swirl generator
9. Insulation material

B. Heat pump unit
   1. Compressor
   2. Condenser
   3. Evaporator
   4. Expansion valve
   5. Axial flow fan
   6. Expansion tank
   7. Refrigerant filter
   8. Solenoid valve
   9. R-22 refrigerant fluid

C. Control and measurement devices
   1. Pitot tube
   2. Three-tube pressure probe
   3. Static pressure tapings
   4. Manometers
   5. Bourdon type pressure measurement gages
   6. Voltage and frequency control devices
   7. Pressure regulator
   8. 3-phase electrical power consumption meter
   9. Electrical power measurement device
   10. K-type thermocouples
   11. Data logger

As shown in Figure 3.1, air is supplied to the bed by a centrifugal fan driven by an electric motor controlled by an AC variable speed control unit. Air is suctioned from the atmosphere through a pvc pipe mounted at suction side of the centrifugal fan and firstly delivered into the settling tank. The suction pipe had length of 317cm and inner diameter of 20cm. After the settling tank, air flows through a condenser, which mounted in a conical convergent section. Another convergent section, which an electrical heater was placed in, was mounted downstream of the condenser section. The swirl generator section was placed downstream of the electrical heater section, and then the particle holder section consisting of a metal screen was mounted upstream of the bed. The metal screen had wire thickness of 0.45mm and the mesh size of 2mmx2.2mm. The bed was placed on the particle section and had two glass sections that had the dimensions of 170mmx300mmx2.5mm in order to observe the motion of particles in the bed. A convergent discharge part was mounted at the top of the bed in order to exhaust the air flow into the atmosphere. In order to obtain various dryer air circuit configurations, an aluminum flexible tube line which had 13cm inner diameter and 0.55mm wall thickness was used to connect the between bed exit and evaporator inlet, the bed exit and the suction pipe inlet, the evaporator exit and the suction pipe inlet. The bed and the other parts placed after the settling tank were made from smooth drawn steel tube and the outside walls of all these parts were also insulated by using 15mm thick grey insulation material.

In the heat pump circuit, the refrigerant working fluid, R22, in the evaporator absorbs low-grade heat from low temperature medium and vaporizes. Then the R22 leaving from the evaporator is suctioned and compressed by the compressor to the condenser that mounted in the first convergent section downstream of the settling tank as shown in Figure 3.1. After the R22 exits from the condenser by releasing heat to the air flow discharged by the centrifugal fan, it flows through the expansion tank, solenoid valve, filter and expansion valve, respectively. Finally, the R22 enters into the evaporator, and then again, the compressor suctions it. Therefore, the refrigerant circuit continues to flow in this cycle.

In the heat pump unit, the expansion tank, solenoid valve and the filter were used in order to increase the safety and the working life of the unit. The expansion tank was mounted at the exit line of the condenser in order to decrease the non-uniformity and to regulate the refrigerant flow in the unit. It had an approximately 5lt volume and a cylindrical configuration which had 16cm outer diameter and 25cm height. At any location after the expansion tank, the solenoid valve was mounted. It had an orifice with 10mm diameter. The refrigerant filter, dehydrator, was mounted at any location between the solenoid valve and the expansion valve. It filters the contaminants in the working refrigerant in the heat pump unit, so that, the quality of the refrigerant could be saved and its working life increases.

In the heat pump unit, all components, compressor, condenser, evaporator, expansion valve, expansion tank, solenoid valve and the filter, were mounted each other by soldering with the copper tubes which had a 1mm wall thickness, and by using rekor connections at some locations. The line between the solenoid valve and the expansion valve was mounted by using copper tube with 12.5mm outer diameter; and the line between the evaporator and the compressor by using copper tube with 16mm outer diameter; and the other lines were mounted by using the copper tubes with 9.6mm outer diameter. The line between the compressor and the condenser was insulated by using a 10mm thick black insulation material.

3.2.1 Centrifugal Fan

A horizontal shaft centrifugal fan, which capable of delivering 0.5m^3/s of air under a head of 200mm WC when running at 1400rpm, was used in order to supply air necessary to drying medium in the experimental set-up. It had an impeller that with 300mm outer and 240mm inner diameters and 16 forward curved blades. The fan was driven by 3hP, 1400rpm AC electric motor which controlled by an AC variable speed control unit. AC variable speed control unit adjusts the rotational speed of the fan by controlling the frequency of the input voltage coming to the electric motor. The rotational speed of the motor could be changed safely from 0 to 1400rpm via the AC variable speed control unit. Thus the air flow rate through the bed, drying medium, could be controlled at various amounts. The electrical power consumption of the fan was measured by an electrical power consumption counter in the unit of kWh.

3.2.2 Settling tank

A settling tank, which has a dimension of 90cmx90cmx90cm, was used in the experimental set-up. It had 15mm wall thickness and its material was chipboard. The settling tank was mounted at discharge side of the centrifugal fan by a flexible material in order to avoid vibrations caused by working centrifugal fan. The settling tank was used in order to remove the flow irregularities and the non-uniformity and to reduce the size of the eddies and fluctuations created in the air discharged by the centrifugal fan. Therefore, it is possible that a steady, axis-symmetric and homogeneous air flow is provided in the condenser and in the bed.

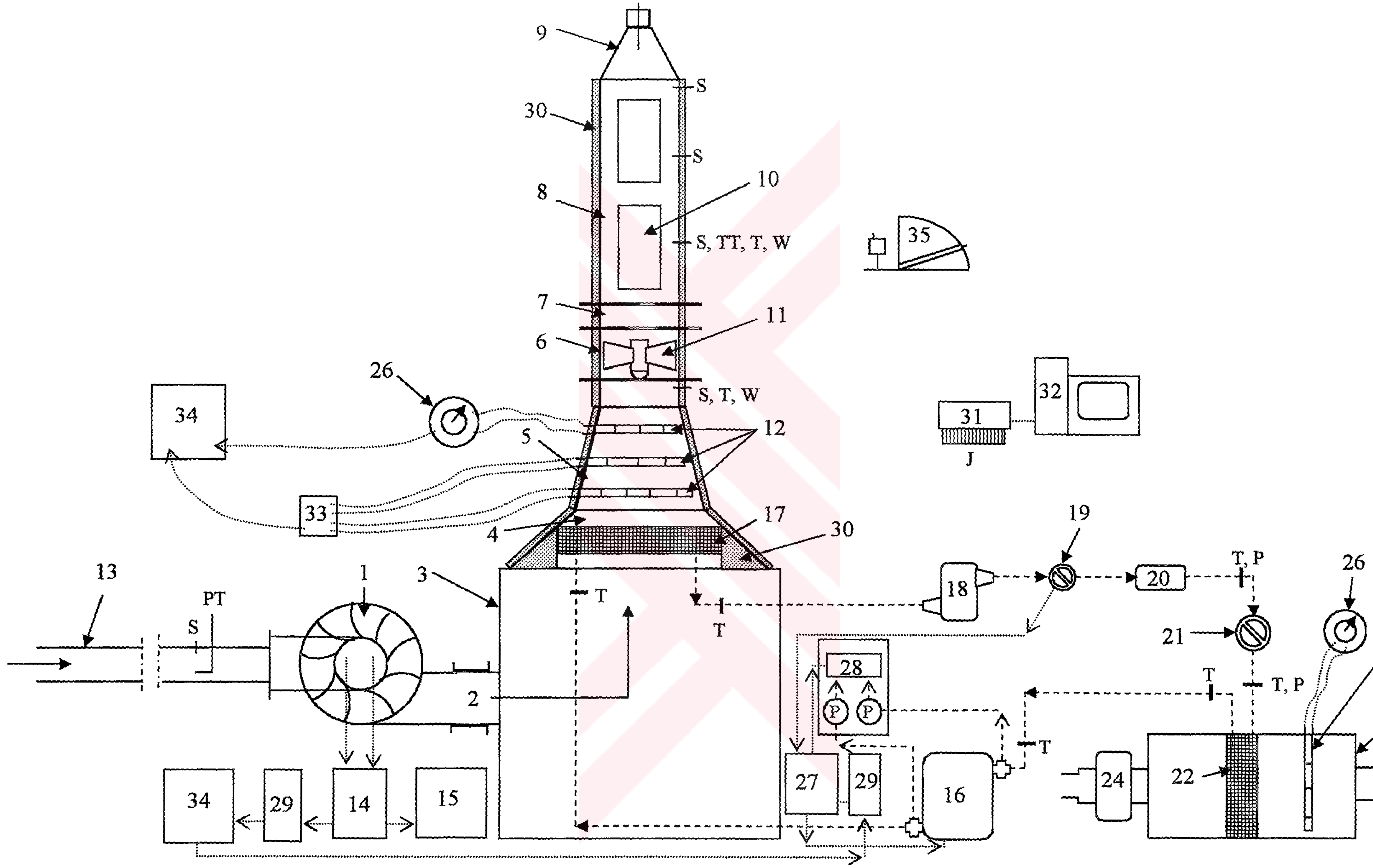

Figure 3.1 The experimental set-up

1. centrifugal fan
2. flexible connection
3. settling tank
4. first convergent section
5. second convergent section
6. swirl generator section
7. test material holder section
8. bed
9. top convergent discharge part
10. glass observation section
11. swirl generator
12. electrical heater resistances
13. suction pipe line
14. electrical board
15. variable speed control unit
16. compressor
17. condenser
18. expansion tank
19. solenoid valve
20. filter
21. expansion valve
22. evaporator
23. evaporator enclosure tank
24. axial fan
25. electrical heater resistance
26. voltage regulator device
27. compressor electrical board
28. dual pressure regulating device
29. 3-phase electrical power counter
30. insulation material
31. data logger
32. computer
33. power switch
34. electrical energy supply
35. manometers

P : gage pressure measurement stations

PT: pitot tube station

S : static pressure measurement stations

T : dry bulb temperature measurement stations

TP: 3-tube pressure probe station

TT: three-tube pressure probe station

W: wet bulb temperature measurement stations

⟶ air flow direction

- - - - - -► refrigerant flow direction

·········> cable connections

3.2.3 Swirl generator

In order to produce the swirling flow in the bed, an axial guide vane type swirl generator was used in the experimental set-up. The construction drawing of the swirl generator is given in the Figure 3.2. It was designed in the construction of vanes fixed at a certain angle called as the stagger angle. The stagger angle, γ, is defined as the angle between the chord line of the vane and the axial direction of flow as shown in Figure 3.2b.

The vanes were made with 1.5mm thick metal sheet and were mounted on a central hub shown in Figure 3.2c. They occupy space in an annular region between the hub and the wall of the duct. These guide vanes were constructed as changeable vanes that had different camber angle, θ, defined as the angle between the tangents at both tips of the vane and the mean camber line of the vane as shown in Figure 3.2b. Swirl generator had also a conical rounded deflecting element mounted front side of its central hub in order to decrease the air flow resistance, or pressure drop, causing by swirl generator.

The swirl generator had eight guide vanes at three different configurations as forward and backward curved vanes and radial vanes. The total 20 various swirl generators that have different configurations and dimensions were tested in flow field investigation experiments and their dimensions and designations are given in the Table 3.1. In order to call the tested swirl generators, a code system was used as an example F6030. In this code, as shown in the following code representation, the first letter gives the vane configuration type and the first two digit number gives the camber angle and the latter two digits number gives the stagger angle and the last two or three digits number, if it is used, defines the Reynolds number.

F603090

→ x1000 Reynolds number, Re=90000

→ stagger angle, γ=30°

→ camber angle, θ=60°

→ vane configuration; F: forward
B: backward
R: radial

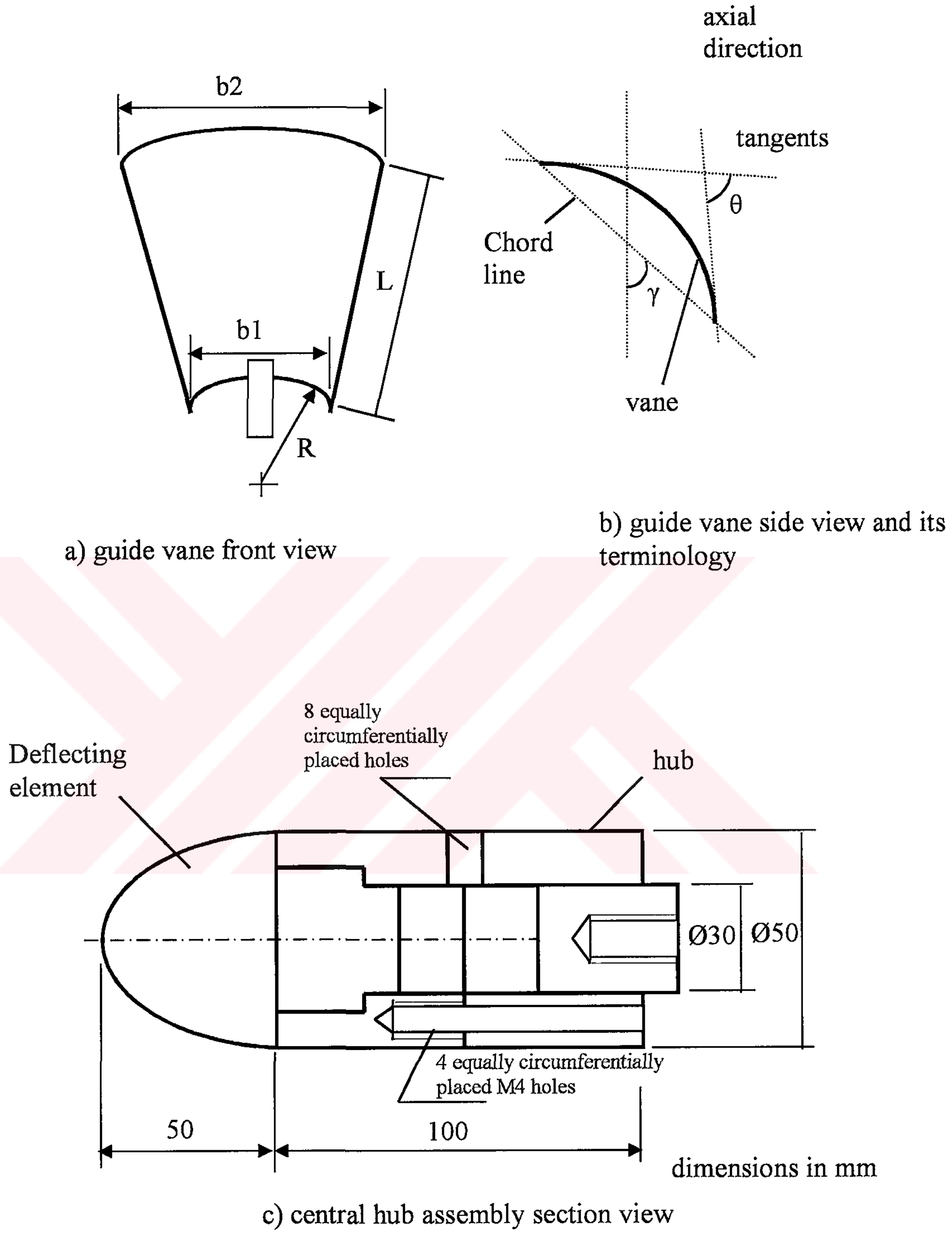

Figure 3.2 The axial guide vane type swirl generator construction view

Table 3.1 The swirl generator configurations, dimensions and codes.

dimensions and configurations	θ deg	γ deg	n	L cm	b1 cm	b2 cm	code
Forward	60	30	8	12	7	10	F6030
		45					F6045
		60					F6060
	90	30			9	14.5	F9030
		45					F9045
		60					F9060
		75					F9075
Backward	60	45			7	10	B6045
		60					B6060
Radial	180	30			10	16	R30
		45					R45
		60					R60
		75					R75

3.2.4 Electrical heater

An electrical heater, which rated of 7.5kW, was used to heat air flow entering into the bed in order to compare the performance of the heat pump dryer with the dryer that had the electrical heater supply. Heater consisted of three different rated resistances, which spirally coiled, and each had the rated power of 2.15kW, 2.65kW and 2.75kW. One of them, which were the rated power of 2.75kW, was connected to the voltage regulating device, devotrans, in order to vary the output voltage of the resistance. So that, the desired air flow temperature in the bed could be obtained. The resistances were mounted in the second convergent part placed at downstream section of the condenser section as shown in Figure 3.1, and dimensions of this convergent part was given in Figure 3.3

In order to test waste heat configuration, configuration type 2 shown in Figure, an electrical resistance rated of 2.2kW was mounted at an upstream section of the evaporator in the evaporator enclosure tank. It was rated by means of a voltage regulating device, devotrans, in order to obtain the power rated at the desired amounts.

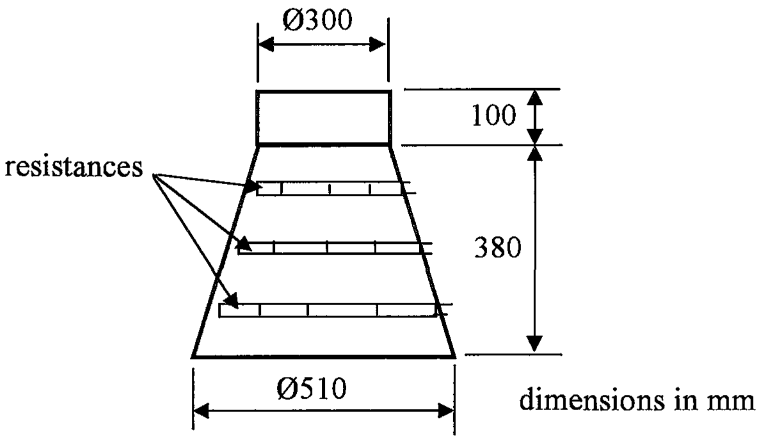

Figure 3.3 The construction view of the electrical heater

3.2.5 Compressor

A reciprocating compressor with two pistons was used in the heat pump unit of the experimental set-up. Its technical specifications are given in the following list:

1. Mark : L'unite Hermetique
2. Model number : TFH4531F
3. Type : Two pistons reciprocating
4. Working fluid : R22
5. Maximum allowable pressure : 25bar
6. Ambient temperature range : -35°C - +46°C
7. Rotation speed (50Hz) : 2900rpm
8. Volumetric flow rate (50Hz) : $9.8m^3/s$
9. Voltage/Phase/Frequency/Ampere : 400V/3/50Hz/5A

In order to obtain that the compressor works in the minimum and maximum allowable pressure range, a dual pressure control device called as generally presostat was used. It consisted of the presostat circuit and two pressure measurement gages; one of them had lower pressure range and the other had higher pressure range. If the compressor's suction and discharge pressures reach the minimum and maximum allowable pressure magnitudes when it is working, the presostat rejects and turn off the compressor by cutting off the electric circuit. Presostat had the lower pressure range of 0-7bar and the higher pressure range of 7-30bar, but for the compressor used in this study the presostat was adjusted at the lower pressure range of 1-3bar and the higher pressure of 25bar.

The electrical power consumption of the compressor was measured by an electrical power consumption counter in the unit of kWh. The counter was the Koehler marked.

3.2.6 Condenser and evaporator

A cross flow finned-tube heat exchangers were used as condenser and evaporator in the experimental set-up. They consisted of copper tubes and fins. The copper tubes had an external diameter of 9.6mm and a wall thickness of 0.3mm and had 315 external fins per meter made from 0.2mm thick aluminum sheet. The external dimensions of condenser were 0.4m length, 0.4m width and 0.12m deep, and it was constructed with four rows of tubes, consisting of 16 tubes each row, totally 64 copper tubes. The condenser was horizontally placed in a convergent part mounted at top of the settling tank and fitted into the convergent section with air flow normal to the tubes as shown in Figure 3.1.

The evaporator construction was similar to the condenser and used the same type of tubing. However, only 3 rows of tubes consisting of 16 tubes each row, totally 48 tubes, were used. The external dimensions of evaporator were 0.4m length, 0.4m width and 0.1m deep. The evaporator was vertically placed in its enclosure tank as shown in Figure. In addition, the evaporator was fitted into its enclosure with air flow normal to the tubes.

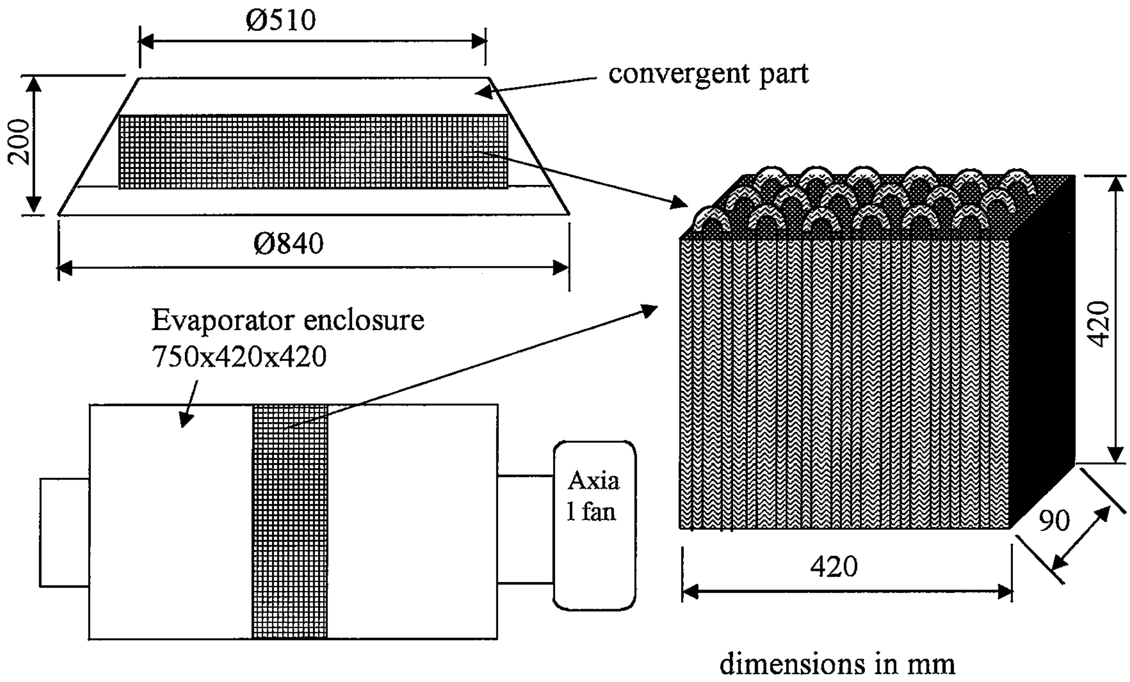

Figure 3.4 The construction of condenser and evaporator

3.2.7 Expansion Valve

A thermostatic expansion valve was used in the heat pump unit of the experimental set-up. The expansion valve is used in order to reduce the pressure of refrigerant fluid leaving from the condenser at high pressure and temperature as generally liquid and vapor mixture. After the expansion valve, the refrigerant fluid pressure and temperature reduce simultaneously. Therefore, the refrigerant fluid generally at the saturated mixture state at lower temperature and pressure is obtained at exit of the valve, and then it flows into the evaporator. Its technical specifications are given in the following list:

1. Mark	: Danfoss
2. Model number	: TXZ 68Z 3206
3. Working fluid	: R22
4. Working range	: -40°C - +10°C
5. Maximum allowable pressure	: 34bar

3.2.8 Axial fan

An axial flow type fan, which capable of delivering 800m^3/h of air under a head of 370Pa when running at 1100rpm, was used in order to supply air necessary to evaporator. The fan was driven by 80W rated DC electric motor. The axial fan suctioned the air flow over the evaporator placed in an enclosure tank and it was mounted at the discharge side of the evaporator enclosure.

3.2.9 Working fluid in heat pump unit

Closed cycle vapor compression type heat pumps require a working fluid. Traditionally, the most common working fluids for heat pumps have been R11, R12, R22 and R134a. Working fluids for heat pumps are classified as CFC, HCFC, HFC, mixtures and natural working fluids due to their chlorine content and chemical stability.

CFCs, chlorofluorocarbons, are harmful to the global environment due to both high ozone depletion potential and a global warming potential. This group includes the following refrigerants: R11, R12, R13, R113, R114, R115, R500, R502, R13B1, and their use in new plants is now banned although they are still permitted in existing plants. However, only purified, recycled, refrigerants from decommissioned and retrofitted plants are available. It is therefore expected that these refrigerants will become more and more expensive, and at some point will no longer be available.

HCF, hydrochlorofluorocarbons, working fluids also contain chlorine, but they have much lower ozone depletion potential than CFCs. HCFCs include R22, R401, R402, R403, R408 and R409. HCFCs are so-called transitional refrigerants, because they are alternative working fluids to CFCs and they have at least the same reliability and cost effectiveness with CFCs. Moreover, the energy efficiency of the systems with HCFCs should be maintained or be even higher in order to make heat pumps an interesting energy saving alternative.

HFCs, hydrofluorocarbons, can be considered long term alternative refrigerants. This means that they are chlorine free refrigerants such as R134a, R152a, R32, R125 and R507. since they do not contribute to ozone depletion, these are long term alternatives to R12, R22 and R502. However, they do still contribute to global warming special attention must be given to the use of lubricants. Mineral oils are non-miscible with these refrigerants. Normally only ester-based lubricant oils recommended by the refrigerant manufacturer should be used. Mineral oils residues must be completely removed during retrofitting.

A mixture consists of two or more pure working fluids. Mixtures represent an important possibility for replacement of CFCs, both for retrofit and new applications. However, these group refrigerants require equipment modification; moreover, they are less available due to higher cost.

Natural working fluids are substances, naturally existing in the world such as ammonia, hydrocarbons, water, and carbon dioxide. They generally have negligible global environmental drawbacks. They are therefore long term alternatives to the CFCs. However, some of the natural working fluids are flammable or toxic. Therefore, the safety implications of using such fluids may require specific system design and suitable operating and maintenance requirements. Due to these reasons this group refrigerants are not preferred in use. Due to these reasons, the R22 called as chlorodihluoromethane, which is included in the HCFC group, was used as working refrigerant fluid in heat pump unit in the experimental set-up, and it has the chemical formula of $CHClF_2$. Its physical properties are given in the following list:

1. Molecular mass : 86.48
2. Boiling point : -40.76°C
3. Freezing point : -160°C
4. Critical temperature : 96°C
5. Critical pressure : 4974kPa

3.3 MEASUREMENT DEVICES AND ITS TECHNIQUES

3.3.1 Pressure measurement gages

Bourdon type pressure measurement gages were used to measure the gage pressure of working refrigerant at four different stations in the heat pump unit. Totally four pressure gages were used; both of them had the lower pressure range of 0-8bar, 0-120psi, and the others had the higher pressure range of 0-35bar, 0-500psi. The pressure gages with the lower range were connected to the compressor suction side and the evaporator inlet or the expansion valve exit. The pressure gages with the higher range were connected to the compressor discharge side and the expansion valve inlet. The case of the gages had the 65mm diameter and they had the vertical configuration with bottom stem mounted to the surface of the measurement station. The gages with the lower pressure range had the grades at 0.1bar intervals; and the gages with the higher pressure range had the grades at 0.2 bar intervals. The gages were also calibrated or tested by means of a dead-weight tester and the pressure magnitudes that were read by gages were exactly same with the pressure magnitudes produced by the weights loaded in the dead weight tester.

3.3.2 Pressure probes and wall static pressure tapings

A L-shaped copper pitot tube of 2.2mm outer diameter and 1.1mm inner diameter together with a wall static pressure tapping drilled on the pipe wall at the line of the tip of pitot tube were used to measure the average velocity at the reference station on the suction pipe line shown in the Figure 3.1. This reference station was placed at the section that had the distance of 317cm from the inlet of the suction pipe. The pitot tube was traversed across the pipe cross-section with an accuracy of ±0.025mm by means of a traverse mechanism that had capable of traverse in the radial direction of the pipe.

The static pressures on the walls of the dryer ducts were measured by using the wall static pressure tapings. Its measurement stations are shown in the Figure 3.1. The wall static pressure tapings consist of three circumferential equally spaced holes drilled on the walls of the ducts. In order to measure the static pressure at a certain station, the average magnitude of static pressure measured by three tapings that spaced circumferential equally at that station was taken by four-way tube connections. However, only one tapping was used to measure the static pressure at the reference station in order to regulate the mass flow rate in the set up, because of the static pressure distribution across the pipe was constant.

A three-tube pressure probe constructed from copper tubes of 1.2mm outer diameter and 0.5mm inner diameter was used to measure the magnitude of axial and tangential velocity components and direction of air velocity and static pressure distribution in the swirling flow field in the bed. The three-tube pressure probe consisted of a forward facing pitot tube and two inclined side tubes which was formed with a half apex angle of 35°, its construction is shown in the Figure 3.5.

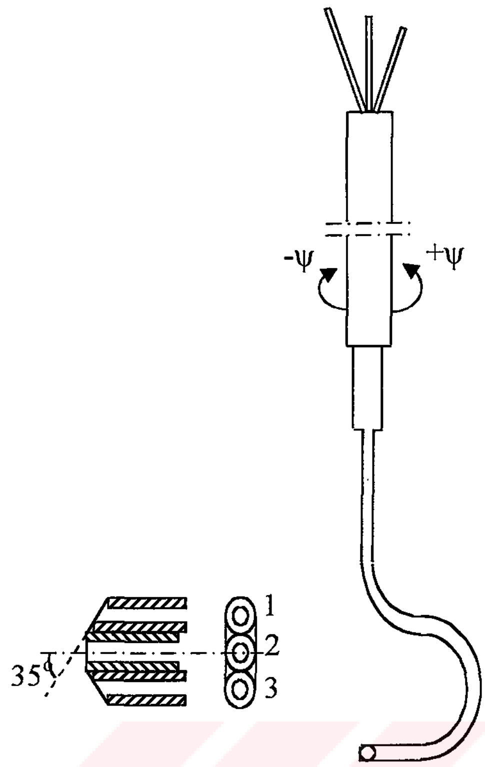

Figure 3.5 Construction of the three-tube pressure probe

The method of measurement with the three-tube pressure probe was based on the calibration of the probe which means the determination of the probe sensitivity to its rotational position through the calibration parameters [89] to measure the velocity and direction of flow and static pressure.

The probe calibration was made in axial, uniform and fully developed flow field in a pipe that had inner diameter of 10cm. In order to calibrate the three pressure probe, it was positioned at the centerline of the pipe and was rotated with 2° increments of yaw angle, ψ, to cover the range 45° at both clockwise and counterclockwise directions. The heads sensed by the probe were recorded at each yaw angle and the dimensionless calibration parameters F, Q and Z defined below were formed:

$$F = \frac{(H_1 - H_2)}{(H_3 - H_m)} \tag{3.1}$$

$$Q = \frac{(H_3 - H_m)}{V^2 / 2g} \tag{3.2}$$

$$Z = \frac{(H - H_3)}{(H_3 - H_m)} \tag{3.3}$$

where

$$\frac{V^2}{2g} = H - H_s \tag{3.4}$$

H is the head recorded at the center tube in axial probe position, ψ=0°. H_1, H_2 and H_3 are heads recorded at the side tubes, 1 and 2, and the center tube of the probe, 3, in any rotated position of the probe, respectively. H_m is defined as the mean head of the side tubes, $(H_1+H_2)/2$, and H_w is the head recorded from the wall static pressure tapping, and V is the local resultant flow velocity.

The calibration parameters F, Q and Z are non-dimensional ratios of the heads indicated by the tubes of the probe. The calibration was made at four different Reynolds number as 30000, 50000, 70000, 90000, and the calibration parameters were plotted as a function of the yaw angle, ψ. The calibration curves of F and Q obtained are shown in Figures at Appendix 1. These calibration curves were used for the calculation of mean flow parameters without rotating the probe at the measurement station in the bed in which had the swirling air flow. The relationships between calibration parameters and the probe position are used to determine the local values of the yaw angle, axial and tangential velocity components and static pressure. The calibration has no significant dependency on Reynolds number for covered speeds and the calibration parameters of F, Q and Z have also a linear variation with yaw angle in the range of 20° at both clockwise and counterclockwise directions as shown in the calibration curves at Appendix 1.

For the measurements of swirling flow in the bed, the three-tube pressure probe was traversed in the radial direction without rotating about its yaw plane and the heads of the tubes sensed by the tubes of the probe, H_1, H_2 and H_3, were recorded. The calibration parameter F was calculated from the Equation 3.1 by using the recorded heads. Ψ was determined by using the calibration curve for F in Figure 1 at Appendix 1.

The value of Q corresponding to the determined value of Ψ was determined from the calibration curve for Q in the Figure 2 at Appendix 1 and local resultant flow velocity and its axial and tangential components were calculated as follows respectively

$$V = \sqrt{\frac{2g(H_3 - H_m)}{Q}} \tag{3.5}$$

$$u = V * \text{Cos}\psi \tag{3.6}$$

$$v = V * \text{Sin}\psi \tag{3.7}$$

The measurement of the mean flow parameters by using the null-reading method was a difficult and rather time-consuming technique in which the probe is rotated at a measurement station until the same head is recorded by the side tubes of the probe for measuring the flow direction. The presented method of measurement with a three-tube pressure probe which is based on the probe calibration is much more practical eliminating the experimental difficulty in probe utilization with no loss in accuracy in the measured flow parameters [89]. Since the same magnitudes at measured parameters were obtained by probe calibration and null-reading method.

In order to traverse the three-tube pressure probe at the radial direction in the bed, a traverse mechanism that had capable of traverse in the radial direction with a vernier scale precision of ±0.025mm was used. However, in order to calibrate the probe, a traversing mechanism that had capable of the radial traverse and rotation of the probe in yaw plane was used.

3.3.3 Manometers

In order to take static pressure, flow velocity and its direction measurements were used by the well type inclined alcohol manometers. These measurement readings were reduced the standard STP conditions for alcohol used as manometer fluid by using the chart in Appendix 2. In order to determine the reduction coefficient from this chart, the ambient absolute pressure and the temperature in the laboratory in which worked were measured by using the barometer with mercury and a simple thermometer with mercury, respectively.

3.3.4 Temperature measurement

In the experimental study, the dry bulb and wet bulb temperatures of air flow, T_{db} and T_{wb}, working refrigerant in the heat pump unit and the ambient air in the labratory were measured at different stations in the experimental set-up. Dry bulb and wet bulb temperatures of air flow in the dryer unit at five stations and the dry bulb temperatures of the refrigerant in the heat pump unit at six stations that shown in Figure 3.1 were measured by using K-type thermocouples which consisted of nickel and aluminium dissimilar wires. All temperature measurement data were collected by means of a data logger connected to the serial port of the PC 133MHz computer.

3.3.4.1 Thermocouple Configurations

Thermocouples are pairs of wires, of dissimilar metals, connected to both ends. When two junctions are subjected to different temperatures, and electrical potential is set up between them, or if they carry a current from an external source, the two junctions will be different temperatures. When one of the junctions is maintained at a fixed temperature, such as melting ice the other junction may be used as thermometer.

Any convenient size of wire may be used for thermocouples, but a good electrical contact at the junctions and good insulation of the rest of the wire are important. Insulations may be enamel, plastic, silk, or cotton for low temperatures and asbestos, glass, porcelain, or other refractory materials for high temperatures.

The temperature of the hot junction, measuring junction, can be determined only by reference to cold junction, reference junction, of known temperature. A vacuum bottle filled with cracked ice and water is a good junction container, provided that there is enough ice. For non-copper couples, two cold junctions will be necessary if copper lead wires are desired. Although the ice point is the most common reference temperature, any constant temperature can be used, and for high temperature work the cold junctions are sometimes buried underground, deep enough so that the seasonal temperature change is negligible.

Another reference junction scheme uses an external source of controlled voltage instead of thermocouple sources. Mercury batteries or rectified alternating current is used with a bridge circuit and balanced so as to produce a voltage equivalent to that representing ice immersion of the original cold junction. Cold junction compensators may also be built into the indicating or recording instruments themselves. A technique is to provide software compensation in the data acquisition system. In this technique the temperature of the measurement junction(s) is/are measured with a RTD or thermistor and compensation provided with a build in microprocessor. Direct digital readout of temperature is then provided. With appropriate switching one use the same junction(s) for several types of thermocouples. Such compensation assumes a polynomial relation, and if the thermocouple wire and/or junctions do not conform to the NBS standard, then an error in measurement will result. To alleviate this difficulty, the junctions may be calibrated against known standard and known temperature.

3.3.4.2 Dry Bulb Temperature Measurement

Dry bulb temperature measurement in the air circuit was done by a thermocouple temperature probe which was constructed as shown in Figure 3.6a and 3.6b. It consisted of three parts; thermocouple, copper tube, and glue support. Glue support was used as insulator and connector for these two parts. The measuring junction of the thermocouples were made by twisting and by sensitivly soldering the tips of nickel and aluminium wires at a configuration as shown in Figure 3.6e. The copper tube of the probe had the dimensions of 3.2mm inside diameter, 4.6mm outside diameter, and 25cm length.

The dry bulb temperature measurement in the refrigerant circuit was done by K-type thermocouples by attached to the outer surface of the copper tube in which the refrigerant flows. The tip of the measuring junction of the thermocouple had the same configuration with that of the dry bulb thermocouples as shown in Figure 3.6e. However, in order to measure the temperature of the refrigerant flowing in copper tubes in the heat pump unit, the tips of the thermocouples were tightly attached to the outer surface of the copper tube by wramping with threadseal tape and covered by the black insulation material which had 15mm thickness as shown in Figure 3.6d.

For calibration of the probe; dry-bulb temperature of the air stream was measured with a calibrated mercury thermometer and a digital thermometer. These measured values were compared with the value measured by the Data Logger. All of these three results were approximately same.

3.3.4.3 Wet Bulb Temperature measurement

A probe was used to measure the wet bulb temperature in the air circuit. It was made from the copper tube which had the same dimensions with that of the dry bulb temperature probes. However, the copper tube consisted of two parts: one of them was the longer part and the other was the probe measuring tip which had the 15mm length. The probe measuring tip was attached with the glue by mounting with the flexible plastic tube to the longer part of the probe as shown in Figure 3.6c. These flexible plastic tube and glue support were also used to obtain the insulation between the longer part and the tip of the probe. The thermocouple was fitted into the probe and the tip of the thermocouple was sensitively soldered to the tip of the probe as shown in Figure 3.6c. The probe tip was also covered with a 40mm length cotton sleeve. Other end of the cotton sleeve was submerged into water to get wetness. For a thermocouple unit with wick feed a length of wick 0.5 to 1cm long, below the thermocouple junction, must be exposed to the air flow to minimize errors due to heat conduction from the water reservoir and also to ensure the feeding of water to the sleeve at about wet bulb temperature. Two small water containers which were connected by a flexible plastic tube that had 2.2mm outside and 1.1mm inside diameters with each others. Inside container was used for wetting the cotton sleeve; outside was used for adding make-up water. Also, a flexible tube was mounted top of the water reservoir in the duct and the other end of this flexible tube was opened to the atmosphere in order to obtain the same water levels in the both reservoirs as shown in Figure 3.6a.

For calibration of the probe; wet-bulb temperature of the air stream was measured with a calibrated mercury thermometer and a digital thermometer. These measured values were compared with the value measured by the Hilton Data Logger. All of these three results were approximately same with a maximum error of 10%.

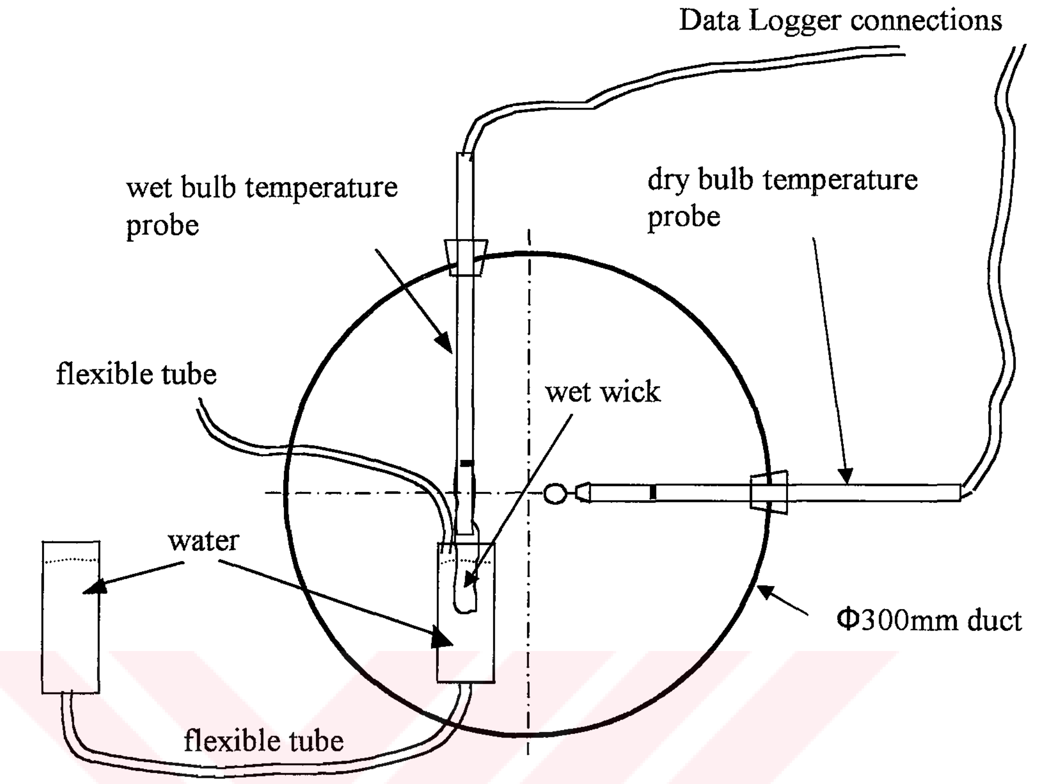

a) connections of temperature probes

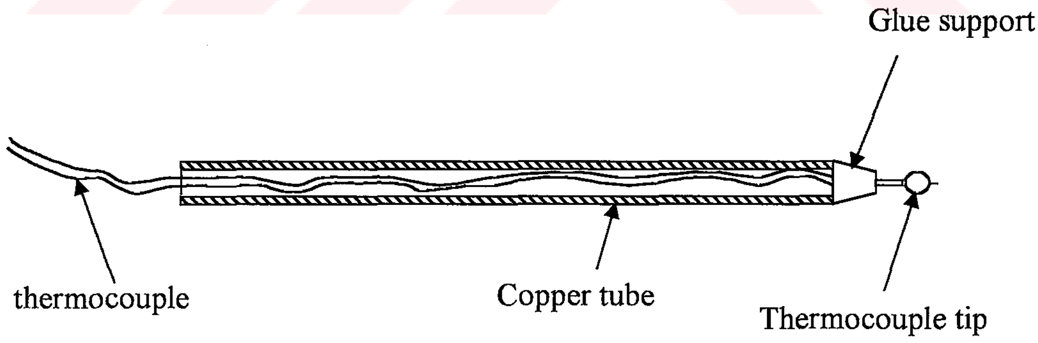

b) The construction of dry bulb temperature probe

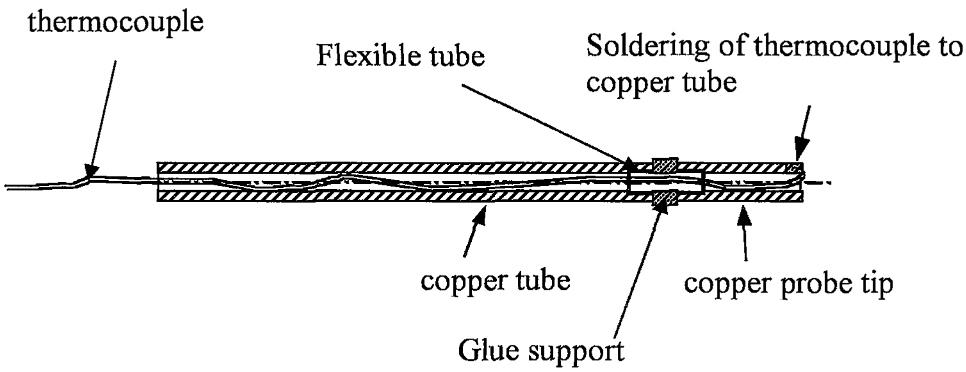

c) The construction of wet bulb temperature probe

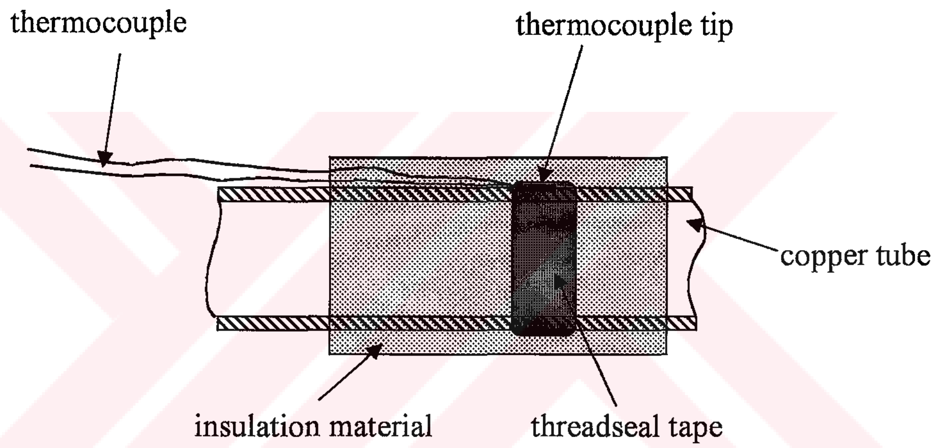

d) drybulb temperature measurement method in heat pump unit

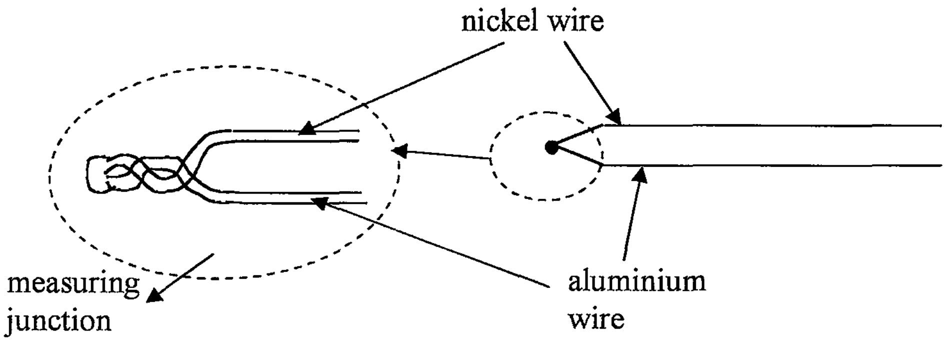

e) Thermocouple measuring junction configuration

Figure 3.6 Dry and wet bulb temperature probes and connections

3.3.5 Hilton Data Logger

The Hilton Data Logger is a microprocessor controlled computer interface that may be simply configured as a combined data logger and controller. The unit is designed to be operated on a computer serial link responding to simple (ASCII) alphanumeric commands and returning numeric data.

Up to 15 interfaces may be operated on single RS232 serial link with each being identified by its own ident number.

The Hilton Computer Interface is a multi-channel analogue and digital unit with both input and output capability. Commands and data are transferred via a 5 wire RS232 serial link using ASCII character strings sent and received by a controlling computer.

The controlling computer may be an PC or PC compatible running either the Hilton data logging software or any other software package designed to use the following command formats.

As the interface has its own on board computer or microprocessor and independent memory, it is possible to set up the system to return data from most standard transducers in the form required by the user or the user's software.

Up to 15 thermocouple inputs may be addressed and these connect to terminals labeled D1+D1-D2+D2-etc. Either type T or type K thermocouples may be used. On High Gain the maximum readable input voltage corresponds to approximately 500°C. On low Gain the corresponding maximum is approximately 1300°C.

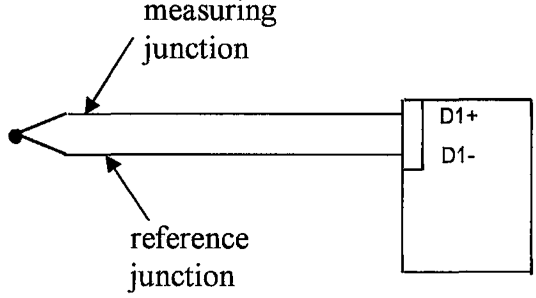

Figure 3.7 Junction connections to the data logger

The Hilton Data Logger used in the study has it own cold junction compensator. An execute program called as TALK.EXE allows single channels to be accessed and updated rapidly, useful when testing the response of a new sensor. Talk is also used to calibrate the cold junction compensator which effect 15 temperature channels equally.

3.4 DRYER AIR CIRCUIT CONFIGURATIONS TESTED

In this experimental study, six different heat pump dryer configurations were investigated. At these configurations, air flow circuits were only varied; the refrigerant circuit in the heat pump unit was constant cycle. The tested air circuit configurations are given in the Figure 3.8.

In the configuration 1, the air discharged by the centrifugal fan passes through the condenser and then through the bed of the dryer, and finally the hot and wet air discharges into the atmosphere as shown in Figure 3.8a. On the other hand, the ambient air passes through the evaporator and then again discharges into the ambient. This configuration was completely open cycle.

In order to investigate the effect of convection of waste heat on the evaporator and simultaneously on the performance of the heat pump, the configuration 2 was tested. It had the same air flow cycle with that of the configuration 1, however, an electrical resistance of 2kW rated power was used to heat the air flow entering the evaporator for simulating the any waste heat.

In configuration 3, the suctioned air flow from the ambient passes through the condenser and then through the bed of the dryer. The exhaust hot and wet air that discharged from the dryer passes through the evaporator and then discharges into the ambient as shown in Figure 3.8c. This configuration was the partially open system.

The configuration 4 was the same air cycle with that of the configuraion 3 except the air flow that exits from the dryer partially discharges into the ambient by passing across the evaporator and the other partition of the air flow passes through the evaporator and then again it discharges into the ambient as shown in Figure 3.8d. This bypass ratio was 50 per cent.

The ambient air passes through the evaporator and then discharged air flow from the evaporator passes through the condenser by mixing with the ambient air at inlet side of the suction pipe in the configuration 5 as shown in Figure 3.8e. This partially mixtured air flow firstly passes through the condenser and then through the dryer, and finally it discharges into the ambient. This partially mixture ratio of the ambient air with the air flow discharged from the evaporator was 50 per cent. This configuration was the partially open and partially closed cycle system.

In the configuration 6, as similar to that of the configuration 5, the air flow which discharged from the evaporator passes through the condenser and then through the dryer by partially mixing with the ambient air at the inlet side of the suction pipe. The exhaust hot and wet air flow which discharged from the dryer passes through the evaporator as shown in Figure 3.8f. As in the case of configuration 5, the partially mixture ratio of the ambient air with the air flow discharged from the evaporator was 50 per cent in the configuration 6.

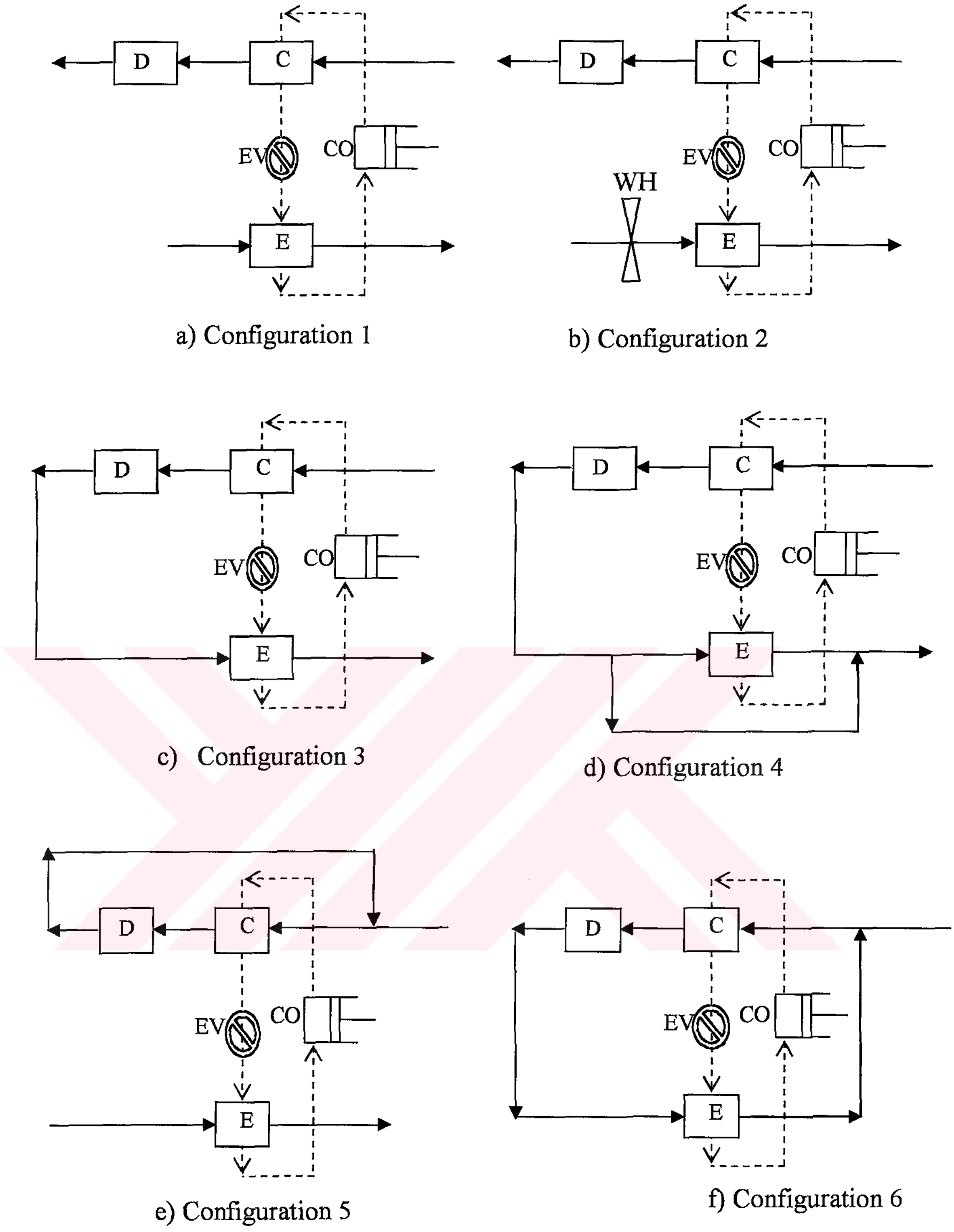

Figure 3.8 Heat pump dryer configurations

C: Condenser

CO: Compressor

D: Dryer

E: Evaporator

air circuit

refrigerant circuit

EV: Expansion valve

WH: Waste heat

3.5 TEST MATERIAL

In this experimental study, wheat particles as test material were used in order to dry in fluidized bed heat pump dryer. The wheat kernel is approximately ellipsoidal in shape with the average dimensions of 3.2mmx2.7mmx6.7mm. This measurement of dimension was done by measuring the dimensions of any selected 20 grains and it was taken the arithmetic average of these measurements. The density of wheat grains, which tested, was the 1255kg/m^3. The density measurement was done by weighting any selected 100 wheat grains, and they were put into the scaled glass tube in which the water existed at a certain level. Then, the water level difference was recorded. This water level difference measurement gives the total volume of 100 grains. The density of grains was determined by dividing the weight of grains to their volume. Wheat is one of the main agricultural products and has extensively application in drying systems. Wheat belongs to the hygroscopic materials group and has a very low mass diffusivity. In other words, wheat exhibits a dominating internal resistance to moisture transport. Wheat grains are classified as the D group particles, which cover the large particles that have the greater dimension than 1000μm [99]. The harvest of wheat with moisture of about 25 per cent requires artificial drying of the grains to obtain aqueous activities which inhibit both bacterial growth and spoilage reactions [51]. The moisture diffusion coefficient of wheat, D, is given by Becker [56] as

$$D = \frac{1}{130.5}\exp\left(\frac{-6140}{T_p}\right) \tag{3.8}$$

and the correlations of thermal conductivity and specific heat of wheat by Kazarian and Hall [57], respectively, as

$$k_t = 0.1167 + 0.1318\left(\frac{M_p}{1+M_p}\right) \tag{3.9}$$

$$c_p = 1398.3 + 4090.2\left(\frac{M_p}{1+M_p}\right) \tag{3.10}$$

Wheat with initial moisture of approximately 9 per cent (dry basis) was used in this experimental study. Samples were wetted to a moisture of about 60 per cent (dry basis) by adding the necessary amount of water and leaving them at ambient temperature, which about 28-30°C, for 24-48hr by occasional mixing of the grains.

CHAPTER 4

EXPERIMENTAL PROCEDURE AND EVALUATION OF DATA

4.1 INTRODUCTION

In this chapter of the thesis, the procedure of the experimental study and the calculations on the measured experimental parameters are discussed.

In the designed and constructed experimental set-up, the influence of several system and operating parameters on the performance of the system were investigated by measuring the dry bulb and wet bulb air temperatures at inlet and outlet sides of the dryer and the evaporator, the temperatures of the working refrigerant and the gage pressure at various sections in the heat pump unit and the power consumed by the compressor, centrifugal fan and the electrical resistances, and the air mass flow rate in the dryer and the axial and tangential flow velocity components of the air flow in the swirling flow field in the bed.

The performance of the fluidized bed heat pump dryer would be evaluated in terms of moisture extraction rate, MER, specific moisture extraction rate, SMER, coefficient of performance, COP, and the dryer efficiency, DE. The calculations of these performance parameters were also explained in this chapter of the thesis, and the definitions of these parameters are given in the section of 2.2.2 of Chapter 2.

The purpose of this study is to investigate the impact of varying some of these operating parameters on the performance of fluidized bed heat pump dryer. The results will be used to improve the understanding on the operation of fluidized bed dryers and the introduction of the heat pump to the fluidized bed dryer and optimization of the system performance by changing certain operating air circuit configurations, and the effects of swirling flow field on the drying performance and improvement of the system components and the drying characteristics of the wheat.

There are in fact so many parameters that influence the operation of fluidized bed heat pump dryer that is difficult to quantify their impact and the interactions on the system performance.

4.2 EXPERIMENTAL PROCEDURE

First of all, flow field investigations were done at 3 different Reynolds numbers, 50000, 90000, 125000, by testing 13 various swirl generators. Then, the drying experiments were done for 6 various air circuit configurations, 4 various air mass flow rates in the dryer, 4 various air temperatures in the bed and in the flow field which had 7 various swirl numbers.

Wheat grains were used as the drying material. 1000g dry wheat particles, which had the initial moisture of about 9 percent (dry basis), a shape similar ellipsoidal with the average dimensions of 3.2mmx2.7mmx6.7mm and the density of about 1255kg/m^3, were wetted to a moisture of about 60 per cent by adding the necessary amount of water and leaving them at ambient temperature, which was about 28-30°C, for 24-48h by occasional mixing of the grains. For all experimental sets, 1600g wetted wheat grains were put in the bed in order to test its drying process for all experimental sets.

Experimental study was done under the 4 main titles:

- Configuration experiments
- Air mass flow rate experiments
- Air dry bulb temperature, bed temperature, experiments
- Drying experiments with the swirling flow field

Configuration experiments were done at 6 different air circuit configurations, which are schematically shown in the Figure 3.8, and at a certain air mass flow rate and air dry bulb temperature in the bed and in the nonswirling flow field during the test period of 60min in order to see the effects of air circuit configuration types on the system performance for drying the wheat grains. The experimental conditions for the configuration experiments are shown in the Table 4.1.

Table 4.1 The conditions for configuration experiments

Configuration Experiments	Configuration code	m_a	T_b	S	m_p
	1	0.231kg/s	50°C	0	1600g
	2				
	3				
	4				
	5				
	6				

In order to see the effects of air dry bulb temperature through the bed, bed temperature, on the wheat drying process, the bed temperature experiments were done at 4 different bed temperatures and at a certain air mass flow rate through the bed and in the non-swirling flow field during the test period of 40min for 2 different configurations 1 and 6. The test conditions for the bed temperature experiments are given in the Table 4.2.

Table 4.2 The conditions for air dry bulb temperature, bed temperature, experiments

Bed temperature experiments	T_b	m_a	S	m_p	Configurations
	40 °C	0.231kg/s	0	1600g	1 and 6
	50 °C				
	60 °C				
	70 °C				

In order to see the effects of air mass flow rate through the bed on the wheat drying process, air mass flow rate experiments were done at 4 different air mass flow rates and at a certain air dry bulb temperature in the bed and in the non-swirling flow field and for 2 different configurations 1 and 6 during the test period of 40min. The conditions for the experiments that were done in order to see the effects of air mass flow rate through the bed are given in the Table 4.3 and the Table 4.4 for configuration 1 and 6, respectively.

Table 4.3 The conditions for air mass flow rate experiments for configuration 1

Air mass flow rate experiments	m_a	T_b	S	m_p	Configurations
	0.1kg/s	50°C	0	1600g	1
	0.165kg/s				
	0.231kg/s				
	0.264kg/s				

Table 4.4 The conditions for air mass flow rate experiments for configuration 6

	m_a	T_b	S	m_p	Configurations
Air mass flow rate experiments	0.1kg/s	50°C	0	1600g	6
	0.165kg/s				
	0.2kg/s				
	0.231kg/s				

For the experiments of air dry bulb temperature and air mass flow rate through the bed, configurations 1 and 6 were selected, because, configuration 1 is an open cycle and has the most simple configuration, on the other hand, configuration 6 is also a closed cycle and exposed the best performance results in the configuration experiments.

In order to see the effects of swirling flow field on the wheat drying process, firstly, the flow field were experimentally investigated by generating the swirling flow in the drying medium of the dryer, bed, by using an axial guide vane type swirl generator. For the flow field investigations, 13 different swirl generators which have the different configurations and dimensions; and the configuration types, dimensions and calling codes of the swirl generators tested are given in the Table 3.1; and the tested Reynolds numbers for the swirl generators and the swirl numbers which obtained by testing these swirl generators in the flow field investigation experiments are given in the Table 4.5. The construction drawing and dimensioning of the swirl generator are given in the Figure 3.2 and their code system is explained in the section of 3.2.3.

Table 4.5 The obtained swirl numbers for the tested swirl generators at tested Reynolds numbers

CONFIGURATIONS	SWIRL GENERATOR CODE	Re	S
FORWARD	F6030	50000	0.18
		90000	0.2
		125000	0.19
	F6045	50000	0.3
		90000	0.3
		125000	0.294
	F6060	50000	0.457
		90000	0.48
		125000	0.5
	F9030	50000	0.25
		90000	0.25
		125000	0.255
	F9045	50000	0.375
		90000	0.38
		125000	0.38
	F9060	50000	0.63
		90000	0.637
		125000	0.635
	F9075	50000	0.84
		90000	0.85
		125000	0.84
BACKWARD	B6045	50000	0.265
		90000	0.235
		125000	0.24
	B6060	50000	0.4
		90000	0.4
		125000	0.414
RADIAL	R30	50000	0.088
		90000	0.11
		125000	0.9
	R45	50000	0.2
		90000	0.204
		125000	0.202
	R60	50000	0.43
		90000	0.425
		125000	0.415
	R75	50000	0.66
		90000	0.67
		125000	0.665

Finally, the 7 different swirl generators were selected among the swirl generators which done their flow field investigations since they exposed different swirl numbers with each others in order to test the drying process with the swirling flow field. For the drying experiments with the swirling flow field, the tested swirl generators and their swirl numbers and experimental conditions are given in the Table 4.6. As shown from this table the drying experiments with the swirling flow field were done at a certain air dry bulb temperature and air mass flow rate through the bed and for 7 different swirling flow field and for configuration 1.

Table 4.6 The conditions for the drying experiments with the swirling flow field

	Swirl generator code tested	S	m_a	T_b	m_p	Configuration
Drying experiments with swirling flow field in the bed	R45	0.204	0.231kg/s	50 °C	1600g	1
	F9030	0.25				
	F9045	0.38				
	R60	0.425				
	F9060	0.637				
	R75	0.67				
	F9075	0.85				

4.3 EVALUATION OF DATA

4.3.1 Mass transfer calculations

At reference station on the suction line shown in the Figure 3.1, the average air velocity was measured in order to control or adjust the air mass flow rate or air flow velocity or Reynolds number in the dryer unit by using the pitot tube and wall taping together placed in the suction line of the centrifugal fan. The sensed total head by the pitot tube and the static head by the wall taping were measured by the well type inclined manometer in which filled the alcohol as the manometer fluid. The measured air flow velocity was determined as the following calculations

$$\frac{\rho_a}{2}u^2 = P_T - P_s = \rho_{al} g(H - H_s) \tag{4.1}$$

where

u: local axial flow velocity, m/s

ρ_a: air density, kg/m^3

ρ_{al}: alcohol density, kg/m^3

H: the vertical component of total head recorded in the inclined manometer leg, m

H_s: the vertical component of static head recorded in the inclined manometer leg, m

By subtracting u and reducing alcohol heads to STP conditions, the following relation is obtained,

$$u = \sqrt{2\frac{\rho_{al}}{\rho_a}\frac{(h - h_s)}{1000 * C}\text{Sin}\alpha} \tag{4.2}$$

where

C: coefficient of STP conditions for alcohol

α: the angle of the inclined tube of manometer, degree

h: the total alcohol head recorded in the inclined tube of the manometer, mm

h_s: the static alcohol head recorded in the inclined tube of the manometer, mm

The coefficient C was used to reduce the sensed alcohol heads by the manometer to the STP conditions by using the STP chart for alcohol in Appendix 2.

The axial velocity distribution was determined by traversing the pitot tube across the pipe cross-section at any three different rotational speeds of the fan. Then these determined velocity distributions were numerically integrated in order to calculate the volume flow rate of air as seen in the following relation

$$Q = 2\pi\int_o^R urdr \tag{4.3}$$

where

Q: volume flow rate of air, m^3/s

R: radius of the pipe, m

r: local radius of the pipe, m

The mean or average air flow velocity was calculated as

$$V = \frac{Q}{\frac{\pi}{4}D^2} \tag{4.4}$$

where

V: mean flow velocity of air, m/s

D: diameter of the pipe, m

The radial distance where the average flow velocity occurred was determined by withdrawing the location corresponding to the mean flow velocity magnitude from the velocity distribution chart, u versus r. The pitot tube was positioned at this location where the average flow velocity occurred. In order to obtain the desired mass flow rate of air or the Reynolds number in the dryer unit, the rotational speed of the fan was adjusted by the variable speed control unit until the sensed head in the manometer reached to the magnitude which gives the average flow velocity as seen in the following relation

$$(h - h_s) = \frac{1000 * C}{2 \mathrm{Sin}\alpha} \frac{\rho_a}{\rho_{al}} V^2 \tag{4.5}$$

Thus, the mass flow rate, $\dot{m}$, or mean flow velocity or the Reynolds number, Re, of the air flow in the dryer unit were regulated by calculating the desired amounts as

$$\dot{m} = \rho_a Q = \rho_a \frac{\pi}{4} D^2 V \tag{4.6}$$

$$\mathrm{Re} = \frac{VD}{\upsilon} \tag{4.7}$$

where

υ: kinematic viscosity of the air, m^2/s

In order to measure the axial and tangential air velocity components and its direction in the swirling flow field in the bed of the dryer, the measurement method was previously explained in the section 3.3.2. The swirl number, S, was determined by numerically integrating the distributions of axial and tangential velocity component across the cross section of the bed as seen in the following relation

$$S = \frac{\int_o^R uvr^2 dr}{R\int_o^R u^2 r dr} \tag{4.8}$$

where

S: swirl number, dimensionless

u: axial velocity component, m/s

v: tangential velocity component, m/s

r: local radius of the bed, m

R: radius of the bed, m

4.3.2 Heat transfer calculations and data evaluations

The dry bulb and wet bulb temperature measurements that made with thermocouples were read by means of the data logger unit. A software that written by Fortran 90 was used to reduce these data to Microsoft Excel format.

For the further calculations, the temperature measurements and their stations are designated as the following list and the locations of measurement stations are shown in the Figure 4.1

T_{db}: dry bulb temperature of air, °C

T_{wb}: wet bulb temperature of air, °C

T: temperature of refrigerant, °C

Subscripts

di: dryer inlet side

do: dryer outlet side

a: air

r: refrigerant

1, 2, 3...: measurement stations:

1: compressor inlet

2: compressor outlet or condenser inlet

3: condenser outlet

33: expansion valve inlet

4: expansion valve outlet or evaporator inlet

5: evaporator outlet

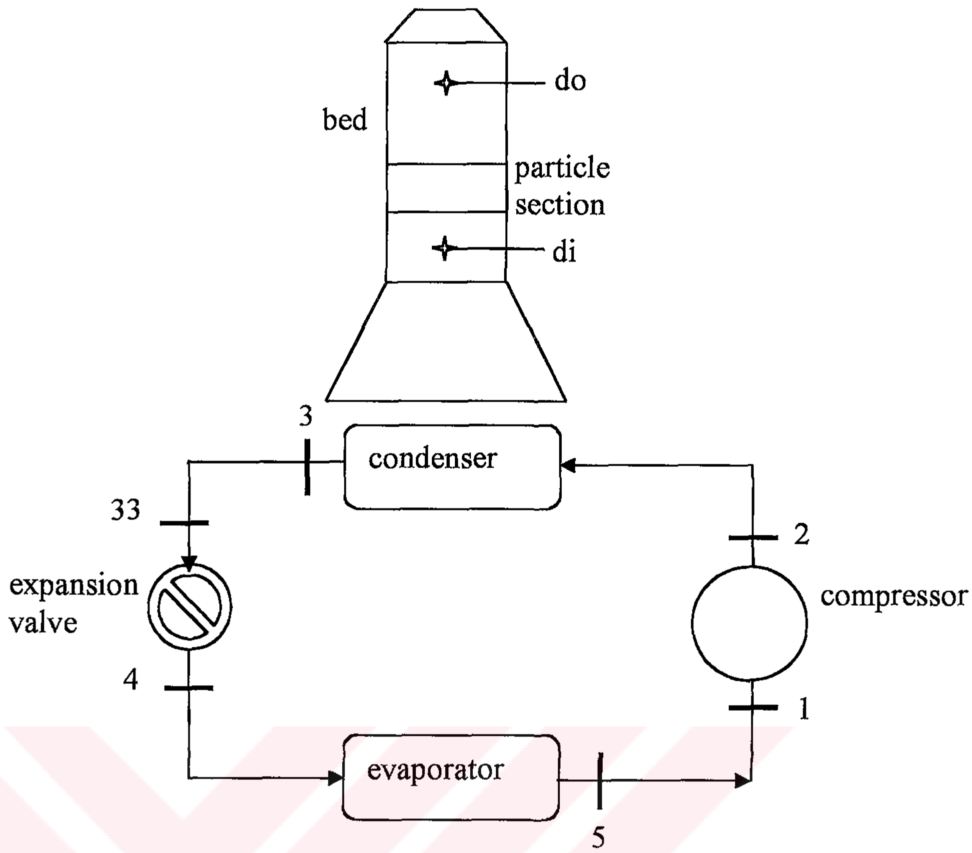

Figure 4.1 The schematic representation of measurement stations

As an example, $T_{db,di}$ designates the dry bulb temperature of air at inlet side of the bed, and $T_{r,4}$ designates the temperature of refrigerant at the exit side of the expansion valve or inlet side of the evaporator.

In addition to temperature measurements in the refrigerant circuit, the gage pressure measurements were done by using the bourdon type pressure gages. There is no any data reduction because of the gage pressure data were directly read from the scale of the gage in the unit of bar, kg/cm^2. In order to convert the pressure in the unit of bar to kPa, the following conversion was used as

$$100\text{kpa}=1\text{bar}=1\text{kg/cm}^2$$

The gage pressure measurements for the refrigerant circuit were done at the stations designated by the numbers of 1, 2, 33 and 4 in the heat pump unit as shown in the Figure 4.1. For the gage pressure measurements of the refrigerant in the heat pump unit and their stations, P designates the gage pressure of the refrigerant in kPa, and subscripts r and numbers designate the refrigerant and measurement stations. As an example, $P_{r,2}$ designates the gage pressure of the refrigerant in the heat pump unit at station 2, that is, the outlet side of the compressor.

For drying process, the moisture extraction rate, MER, or drying rate as another call, which indicates the product throughput rate or productivity of the dryer, was calculated as

$$MER = \dot{m}_a \left(w_{do} - w_{di}\right) * 1000 \qquad (4.9)$$

where

$\dot{m}$: mass flow rate of air in the dryer, kg/s

w: humidity ratio, which is also called as absolute or specific humidity, kg water/kg dry air

subscripts do and di designate the dryer outlet and dryer inlet, respectively

MER: moisture extraction rate, g water/s

In order to derive this relation, equation 4.9, the conservation of mass equation for the dry air and the water masses for the humidifier section in which placed the wet particles, between the stations of dryer inlet, di, and the dryer outlet, do, as shown in the Figure 4.1, reduces to

$$\text{dry air mass,} \qquad \dot{m}_{a,di} = \dot{m}_{a,do} = \dot{m}_a \qquad (4.10)$$

$$\text{water mass,} \qquad \dot{m}_{a,di}\, w_{di} + \dot{m}_w = \dot{m}_{a,do}\, w_{do} \qquad (4.11)$$

where subscript w designates the water

If the equation 4.11 is arranged for the water mass flow rate through the humidifying section or particle section as

$$\dot{m}_w = \dot{m}_a \left(w_{do} - w_{di}\right) \qquad (4.12)$$

$\dot{m}_w$ in the equation 4.12 can be called as MER.

In order to calculate MER values, the humidity ratio, w, of air was determined from ASHRAE standards [127] by using the measured dry bulb and wet bulb temperature data as

$$w = \frac{(2501 - 2.381T_{wb})w_s - (T_{db} - T_{wb})}{(2501 + 1.805T_{db} - 4.186T_{wb})} \tag{4.13}$$

where

w_s: the saturated humidity ratio at wet bulb temperature

In order to determine w_s, an equation was derived by using the linear regression method from the published data in the ASHRAE standards [127] as

$$w_s = 1 * 10^{-4} * \exp\left(3.572565 + 0.0782933T_{wb} - 0.000431823T^2{}_{wb} + 0.0000028735T^3{}_{wb}\right) \tag{4.14}$$

The heat transfer rate at the condenser for the refrigerant side per unit weight of refrigerant was calculated from

$$q_{r,cond} = (h_{r,3} - h_{r,2}) \tag{4.15}$$

where

$q_{r,cond}$: specific heat transfer rate at the condenser for the refrigerant side, kj/kg

h: the specific enthalpy, kj/kg

subscripts r designates the refrigerant, and subscripts 2 and 3 designate the inlet side and outlet sides of the condenser as shown in the Figure 4.1

The station 2 actually designates the exit side of the compressor, but since the distance between the compressor exit and the condenser inlet was short and this line was insulated, the heat transfer loss in this line was about 1°C, therefore, this loss was neglected and the station 2 at the compressor exit was simultaneously assumed as the station at the condenser inlet.

The enthalpy values of the working refrigerant, R22, in the heat pump were determined by using the EES software, Engineering Equation Solver-Academic version prepared by S. A. Klein and F. L. Alvarado and distributed by McGraw Hill Higher Education.

The work consumed by the compressor per unit weight of the refrigerant was calculated as

$$w_{comp} = \left(h_{r,2} - h_{r,1}\right) \tag{4.16}$$

where

w_{comp}: specific work consumed by the compressor, kj/kg

At the same time, the power consumed by the compressor and the centrifugal fan were measured by the electrical power meter in the unit of kWh. This measured data was divided by the working time period for the compressor and the centrifugal fan, so, the power consumed by the compressor and the centrifugal fan were obtained in the unit of kW.

The specific moisture extraction rate, SMER, which implies the energy efficiency in the drying process of the system was calculated from

$$SMER = \frac{MER}{\dot{W}_t} \tag{4.17}$$

where

SMER: specific moisture extraction rate, g water/kWs

$\dot{W}_t = \dot{W}_{comp} + \dot{W}_{fan}$: the total power consumed by the compressor and the centrifugal fan, kW

The performance of the heat pump was evaluated by the coefficient of performance, COP, calculated as

$$COP = \frac{q_{cond}}{w_{comp}} \tag{4.18}$$

The dryer efficiency, DE, was determined by using the following relation

$$DE = \frac{w_{do} - w_{di}}{w_{s,do} - w_{di}} \tag{4.19}$$

where subscript s designate the saturated

In this relation humidity ratios at inlet and outlet sides of the bed were determined by using the relations given in the Equations 4.13 and 4.14.

4.4 UNCERTAINTY ANALYSIS

Any experimental result involves some level of uncertainty that may originate from causes such as the lack of instrument accuracy, random variation in the measurands, approximations in data reduction relations, and competence of the people using the instruments. Eventually, the primary measurements must be combined to calculate a particular result that is desired. All these individual uncertainties in the primary measurements eventually translate into uncertainty in the final results. A more precise method of estimating error in experimental results is the uncertainty analysis. The method is based on a careful specification of the uncertainties in the various primary experimental measurements. For example, a certain temperature reading might be expressed as

$T=100^{o}C\pm1^{o}C$ or $T=100^{o}C\pm1$ percent

The plus or minus notation is used to designate the uncertainty, and this designation is stating the degree of accuracy with which researcher believes the measurement has been made. We may note that this specification is in itself uncertain because the experimenter is naturally uncertain about the accuracy of these measurements. A set of measurements is made in this thesis, and the uncertainty in each measurement is expressed with the same odds. These measurements are then used to calculate some desired result of the experiments. That is, these primary measurements are then used to estimate the uncertainty in the calculated results. It is important to note that the uncertainty be made by the experimenter based on the total laboratory experience.

The R is to be a result estimating data as a function of primary measured variables as the independent variables, x_1, x_2,…x_n. Thus,

$$R=f(xi),\ i=1,2,\ldots n$$

Let w_R be the uncertainty in the result and w_i be the uncertainties in the independent variables, and the uncertainty of the desired result may be estimated by

$$w_R = \left[\sum_{i=1}^{n} \left(w_{x_i} \frac{\partial R}{\partial x_i} \right)^2 \right]^{1/2} \qquad (4.20)$$

In this thesis, the flow velocity and pressure measurements in the air circuit of the system were done by using a type of manometer called a well manometer which has an uncertainty of reading scale of 1/10 mm. As the manometer fluid, the ethyl alcohol was used and its density is 820kg/m^3 with the uncertainty of ±1 percent.

The pressure and temperature measurements of the ambient air were done in days when the experiments were done with the uncertainties of ±0.15 percent and ±1°C, respectively. For the nominal values of ambient air pressure and temperature of 92600Pa and 27°C, respectively, the uncertainty of ambient air density are estimated as,

$$\rho = \frac{P}{RT} = 1.075 \mathrm{kg/m^3}$$

$$w_\rho = \left[\left(\frac{\partial \rho}{\partial P} w_P \right)^2 + \left(\frac{\partial \rho}{\partial T} w_T \right)^2 \right]^{1/2} = \left[\left(\frac{P}{RT} w_P \right)^2 + \left(-\frac{P}{RT^2} w_T \right)^2 \right]^{1/2}$$

$$w_\rho = 3.93 \mathrm{x} 10^{-3}$$

Thus, the density of ambient air was estimated with the uncertainty of ±0.365 percent.

The air flow velocities were calculated by using the pressure values measured by the manometers and their uncertainty are estimated as,

$$P_T - P_S = P_{dyn} = \frac{\rho}{2} u^2 \qquad (4.21)$$

If the dynamic pressures are converted the heads sensed by the manometer and the coefficient, C, which is used in order to reduce the alcohol heads to heads in the STP conditions, and the inclination of the manometer reading column are introduced into the Equation 4.21, the air flow velocity can be calculated by using the following relation,

$$u^2 = 2g\frac{\rho_{al}}{\rho}\frac{h}{1000C} \tag{4.22}$$

where

h: the vertical component of alcohol head sensed by the manometer in its inclined column in mm

ρ: density of air, kg/m^3

ρ_{al}: density of alcohol, kg/m^3

g: gravity acceleration, m/s2

C: the coefficient of STP condition

The coefficient, C, is determined from the chart in Appendix 2 by measuring the ambient air pressure and temperature and it has the uncertainty of ±0.4 percent, which is determined by the way similar with that of the ambient air density explained previously.

$$w_u = \left[\left(\frac{\partial u}{\partial \rho_{al}}w_{\rho_{al}}\right)^2 + \left(\frac{\partial u}{\partial \rho}w_{\rho}\right)^2 + \left(\frac{\partial u}{\partial h}w_h\right)^2 + \left(\frac{\partial u}{\partial C}w_C\right)^2\right]^{1/2}$$

$$\frac{\partial u}{\partial \rho_{al}} = \frac{1}{2}\left(2g\frac{h}{1000C\rho}\right)^{1/2}\rho_{al}^{-1/2}$$

$$\frac{\partial u}{\partial \rho} = -\frac{1}{2}\left(2g\rho_{al}\frac{h}{1000C}\right)^{1/2}\rho^{-3/2}$$

$$\frac{\partial u}{\partial h} = \frac{1}{2}\left(2g\frac{\rho_{al}}{1000C\rho}\right)^{1/2}h^{-1/2}$$

$$\frac{\partial u}{\partial C} = -\frac{1}{2}\left(2g\frac{h\rho_{al}}{1000\rho}\right)^{1/2}C^{-3/2}$$

for the nominal values and uncertainties of the independent variables are given as the followings,

ρ=1.075kg/m^3±0.365 percent

ρ_{al}=820kg/m^3±1 percent

C=1.036±0.4 percent

h=20mm±1mm in the inclined column of the manometer with the angle of 20°±1°. Thus, the uncertainty of the vertical component of h is the ±2.44 percent and its nominal value is 6.84mm and the nominal value of air flow velocity is calculated by using the Equation 4.22 as u=9.94m/s. Then,

w_u=0.1338

That is, the uncertainty of the local air flow velocity is estimated as ±1.35 percent.

The air mass flow rate is determined by using the relation given in the Equation 4.6. The cross-sectional area of the pipe or bed, A=πd^2/4 where d is the diameter of the pipe and d=20cm±0.1cm, thus, A=0.0314m^2±1.05 percent and the nominal value of the air mass flow rate is calculated as 0.231kg/s. The mean flow velocity of air is determined by taking the numerical integration of the flow velocity distribution, which has uncertainty of ±1.35 percent, in the pipe by traversing across its cross-section. The traversing mechanism has an uncertainty of the reading scale of 1/20mm, and the numerical integration of the local flow velocities results the uncertainty of about ±2 percent in the mean flow velocity. Thus, the total uncertainty in the determined mean flow velocity of the air is about ±1.42 percent. So, the uncertainty of the air mass flow rate is estimated by the similar way that used to determine that of the local air flow velocity, which explained previously, as

$$w_{\dot{m}} = \left[\left(\frac{\partial \dot{m}}{\partial \rho} w_\rho\right)^2 + \left(\frac{\partial \dot{m}}{\partial A} w_A\right)^2 + \left(\frac{\partial \dot{m}}{\partial V} w_V\right)^2\right]^{1/2}$$

$$w_{\dot{m}} = \left[(AVw_\rho)^2 + (\rho V w_A)^2 + (\rho A w_V)^2\right]^{1/2} = 2.778\text{x}10^{-3}$$

So, the uncertainty of the air mass flow rate is estimated as ±1.18 percent.

The swirl numbers have the uncertainty of ±4.6 percent since the numerical integration method was used to integrate the axial and tangential flow velocity distributions across the bed.

The pressures of refrigerant in the heat pump unit were measured by using the bourdon type pressure gages, which have the reading scale of 0-8kg/cm^2 to measure the lower pressures at outlet side of the expansion valve and the inlet side of the compressor, and 0-35kg/cm^2 to measure the higher pressures at outlet side of the compressor and the inlet side of the expansion valve. The pressure gages that have the lower measurement range had an uncertainty of reading scale of 1/10kg/cm^2, and the pressure gages that have the higher measurement limit had an uncertainty of reading scale of 1/5kg/cm^2. Also, these pressure gages were calibrated by using the dead-weight tester and it was observed that they had the measurement uncertainty of about ±2 percent.

The electrical energy consumed by the compressor, centrifugal fan and the electrical heater were measured by using the electric counter, which had the reading scale of 80 revolutions/kWh and the uncertainty of reading scale of 1/100 kWh.

The thermocouple probes that were used to measure the dry bulb and wet bulb temperatures in the dryer unit and the thermocouples that were used to measure the temperature of the refrigerant in the heat pump unit were calibrated by comparing their temperature measurements with that of the mercury thermometer standardized by ASTM. The measurement uncertainty of the thermocouples was estimated as ±0.5 percent and the data logger that was used to collect the temperature measurements in the dryer and meat pump units had the reading uncertainty of 1/100°C.

In the humidity ratio calculations the Equations 4.13 and 4.14 which were used in the humidity ratio calculations has the error margin of about ±2.7 percent with respect to ASHRAE standarts [127].

The uncertainty of enthalpies of working refrigerant, R22, in the heat pump, which were determined by using EES software, is estimated as ±1.3 percent.

The uncertainties of the calculated performance parameters, MER, SMER, COP and DE, were estimated to be ±2.9 percent for MER, ±4.3 percent for SMER, ±3.6 percent for COP and ±2.2 for DE by using the relation given in the Equation 4.20.

CHAPTER 5

EXPERIMENTAL RESULTS

5.1 INTRODUCTION

In this chapter of the thesis, the experimental results are presented by plotting measured and evaluated data, and these observed results are discussed. First of all, the results of the drying experiments which were done in order to investigate the effect of air circuit configurations of the dryer in order to dry wheat grains are presented. These tested configurations are shown schematically in the Figure 3.8. Then, the effects of air mass flow rate and air flow temperature in the bed on the dryer performance are experimentally investigated for the configurations 1 and 6, which are shown schematically in the Figure 3.8. Finally, the results of the swirling flow field experiments and the effects of the swirling flow field in the drying medium, bed, on the dryer performance are experimentally investigated.

5.2 THE RESULTS OF DRYING EXPERIMENTS FOR DRYER CONFIGURATIONS

The variation of measured dry bulb and wet bulb temperatures at inlet and outlet sides of the bed, that is, at the downstream and the upstream sections of the drying medium in which the wetted wheat grains were placed, with the drying time are given in the Figures 5.2.1-5.2.6 for six different air circuit configurations. For these configuration tests the dry bulb air flow temperature at the inlet side of the bed was at about 50°C, and the drying time period was 60min. This air flow temperature at the inlet side of the bed was satisfactorily hold constant within the range of ±2°C during the time period of 60min, that is its uncertainty was ±4 per cent; and the air mass flow rate in the bed was 0.231kg/s. The dry bulb and wet bulb air temperatures at inlet and outlet sides of the bed are not fairly varied with time as shown in the Figures 5.2.1-5.2.6. The variation of these temperatures with the time are about in the range of ±2°C except first drying time period of 15min because this period is necessary for the all system parts takes place to thermal equilibrium with the working fluids in the system. For all configurations, the dry bulb air temperatures at inlet and outlet sides of the bed are naturally greater than that of the wet bulb air temperatures for all configurations as shown in the Figures 5.2.1-5.2.6. As shown from the Figures 5.2.2 and the Figure 5.2.6, the dry bulb temperature magnitudes at outlet side of the bed are greater than that of the dry bulb temperatures at inlet side of the bed for configurations 2 and 6 during the drying time of 60min. For the configurations 1, 3 and 4, when the dry bulb temperature magnitudes at outlet sides of the bed are less than that of the inlet side of the bed in the first drying time period of about 15min, then, the dry bulb temperatures at outlet sides of the bed are greater than that of the inlet side of the bed as shown in the Figures 5.2.1, 5.2.3 and 5.2.4. The cause of these observed results is that the moisture is introduced into the bed, in which the wet wheat grains are placed, causes the additional heating at the outlet side of the bed. That is, because of the humidification process in the bed by introduced moisture, the dry bulb air temperatures at outlet side of the bed are greater than that of the dry bulb temperatures at inlet side of the bed, $T_{db,do}>T_{db,di}$. However, for the configuration 5, as shown in the Figure 5.2.5 T_{db} magnitudes at outlet side of the bed are less than that of the inlet side of the bed because of the exhaust wetted hot air flow leaving from the bed was reentered into the bed with recycling as schematically shown in the Figure 3.8e. The cause of this case is that the wetted air flow reentering the bed decreases the moisture extraction rate capacity of the air flow in the dryer, $w_{do}-w_{di}$.

The differences between the magnitudes of dry bulb temperatures at outlet and inlet sides of the bed, $T_{db,do}-T_{db,di}$, are in the range of about 0-3°C for the configurations 1, 2, 3, 4 and 6 as shown in the Figures 5.2.1-5.2.4 and 5.2.6. For the configuration 5, the dry bulb temperatures at outlet side of the bed is also less than the dry bulb temperatures at inlet side of the bed in the range of about 3-10°C, $T_{db,do}<T_{db,di}$, as shown in the Figure 5.2.5.

For all configurations, the magnitudes of wet bulb temperatures at outlet side of the bed are greater than that of the inlet side of the bed, $T_{wb,do}>T_{wb,di}$, as shown in the Figures 5.2.1-5.2.6. The differences between the magnitudes of wet bulb temperatures at outlet and inlet sides of the bed are in the range of about 1-4.5°C for all configurations as shown in the Figures 5.2.1-5.2.6. As similar with the results observed for the dry bulb temperature variations with the time, the variation of wet bulb temperatures with the drying time is approximately steady with the uncertainty of ±2°C in the drying time period of 60min except for the first period of about 15min, because this time period of 15min is necessary in order that the all system parts takes place thermal equilibrium with the working fluids in the system.

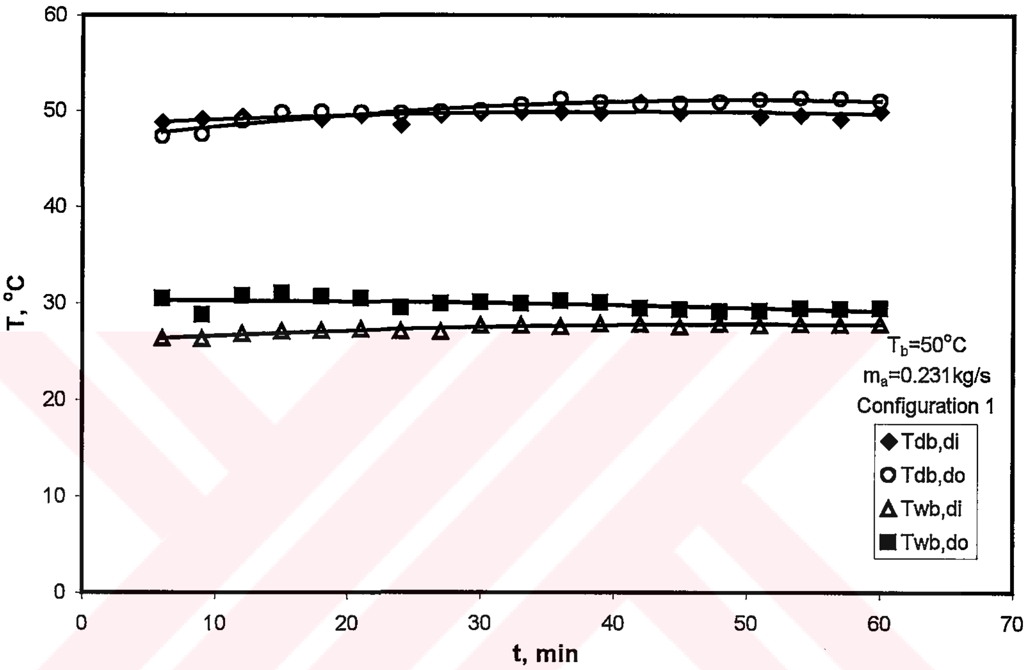

Figure 5.2.1 The variation T_{db} and T_{wb} at inlet and outlet sides of the bed with time for the configuration 1

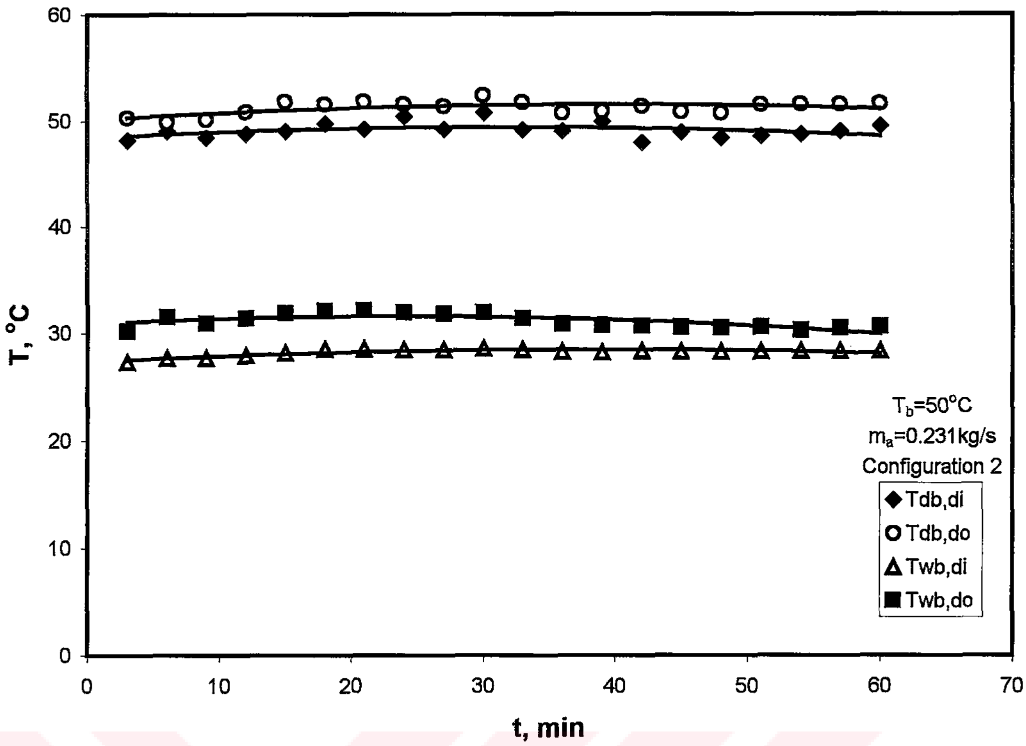

Figure 5.2.2 The variation T_{db} and T_{wb} at inlet and outlet sides of the bed with time for the configuration 2

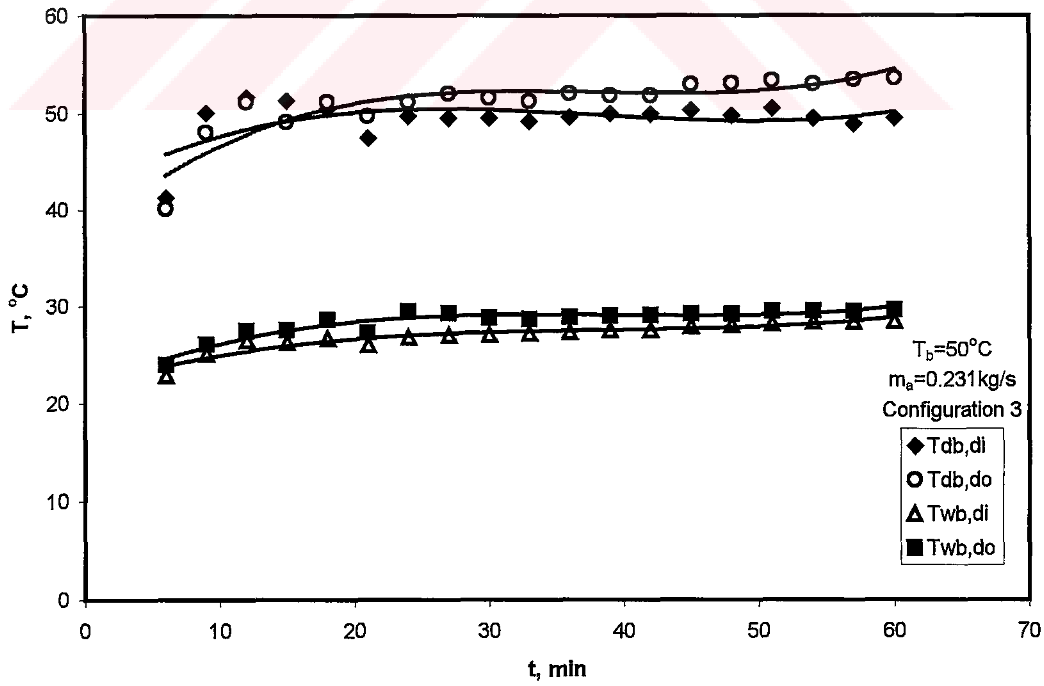

Figure 5.2.3 The variation T_{db} and T_{wb} at inlet and outlet sides of the bed with time for the configuration 3

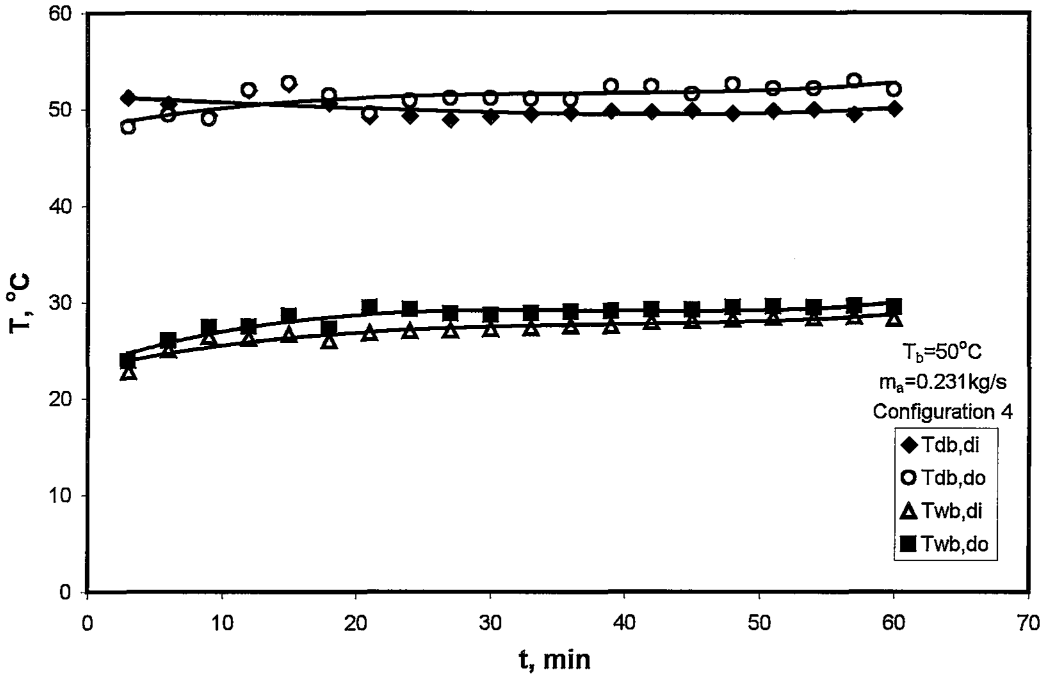

Figure 5.2.4 The variation T_{db} and T_{wb} at inlet and outlet sides of the bed with time for the configuration 4

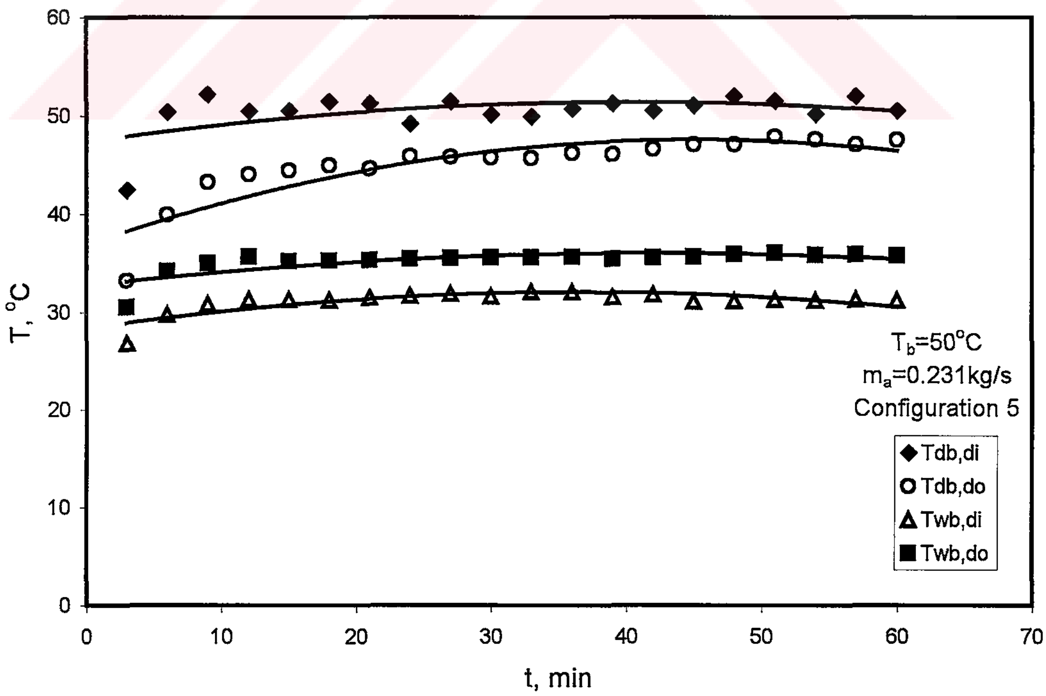

Figure 5.2.5 The variation T_{db} and T_{wb} at inlet and outlet sides of the bed with time for the configuration 5

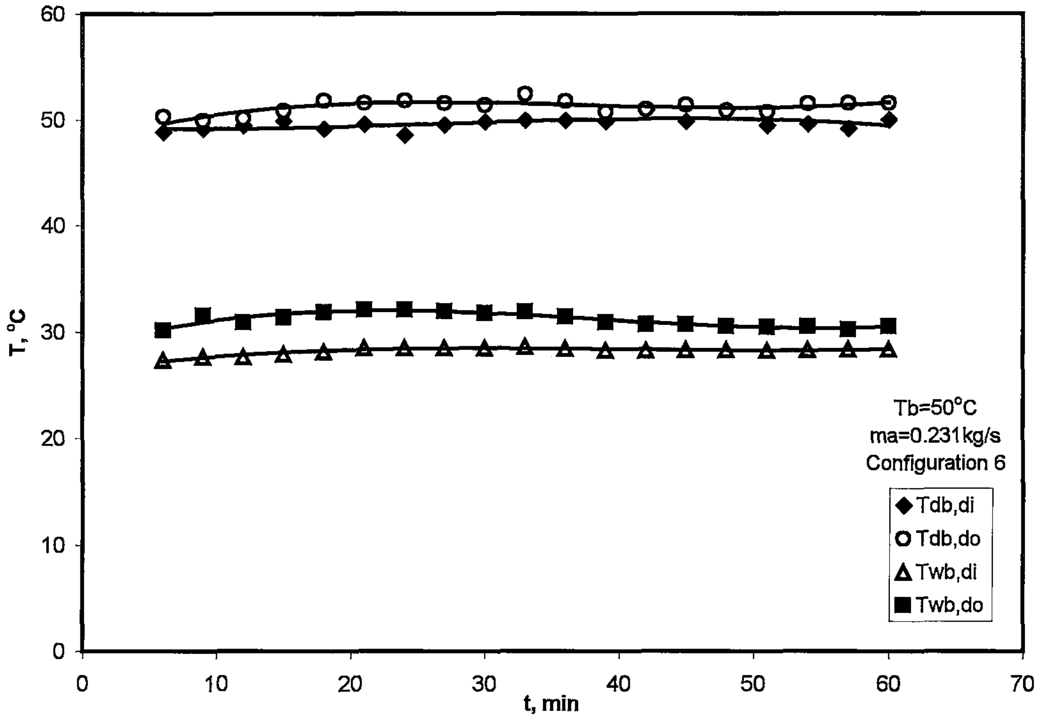

Figure 5.2.6 The variation T_{db} and T_{wb} at inlet and outlet sides of the bed with time for the configuration 6

The measured dry bulb and wet bulb temperatures at inlet and outlet sides of the bed were used to calculate the humidity ratios at these sections by using the equation 4.13 in order to determine the instant moisture extraction rates, MER, which formulized in the equation 4.9. The variation of MER values with the drying time is shown in the Figure 5.2.7 for the tested configurations. The MER values are decreasing with the drying time for all tested configurations as shown in the Figure 5.2.7. But, the variations of MER with respect to configurations are not clearly seen from this figure. The bands, which MER values are lying in, are given in the following table,

Table 5.1 The MER value intervals for the configurations

Configurations	MER value intervals, g water/s
1	0.06 – 0.27
2	0.05 – 0.23
3	0.035 – 0.275
4	0.04 – 0.27
5	0.06 – 0.16
6	0.12 – 0.245

These results do not give a net or clear opinion about the variation of instant MER with drying time for all tested configurations. Therefore, in order to see the mean values of MER, the arithmetic mean of the MER magnitudes are taken during the test period of 60min, and these magnitudes are compared with the MER magnitudes that measured by weighting the wheat grains before and after drying tests. The deviation of the mean MER values from the MER values determined by weighting is in the range of ±9%. The mean MER magnitudes for all configurations are shown in the Figure 5.2,8. The lowest MER is observed for the configuration 5 while the highest MER is observed for the configuration 6 as shown in the Figure 5.2.8. For the configuration 5, MER reduces since the wetted exhaust hot air flow leaving from the bed is recycled into the bed, that is, since the air flow in the bed that carrying more moisture reduces the own moisture extraction capacity, therefore, the moisture extraction rate, MER, magnitude is low when it is compared with that of the others. In the case that the wetted exhaust air flow discharged from the bed is transferred into the evaporator and then the discharged air flow from the evaporator is recycled into the bed for the configuration 6, the moisture extraction capacity of the air flow in the bed increases because of the exhaust wetted hot air flow discharged from the bed is leaving its moisture when it is passing through the evaporator and this dry air flow discharged from the evaporator is recycled into the bed. Therefore, the MER value for the configuration 6 is high when it is compared with that of the others.

The MER values are approximately same for the configurations 1 and 2 as shown in Figure 5.2,8 because of there is no any difference between their air circuit configurations, in both configurations the exhaust wetted air leaving from the bed is discharged into the ambient. Only difference between the configurations 1 and 2 was that the waste heat supply was used to heat air flow entering into the evaporator from the ambient for the configuration 2, but this case is not affecting the air circuit configuration and also MER values of them.

The MER values for the configurations 3 and 4 are in a moderate range, that is, they are greater than that of the configurations 1, 2 and 5 and less than that of the configuration 6 as shown in Figure 5.2.8. For the configurations 3 and 4, the exhaust wetted air flow discharged from the bed is transferred into the evaporator and then the air flow passing through the evaporator is discharging into the ambient. Only difference between them is that the exhaust wetted air leaving from the bed is partially transferred into the evaporator and the other partition of the wetted exhaust air leaving from the bed is re-discharged into the ambient without passing through the evaporator in the configuration 4, when the exhaust wetted hot air leaving from the bed passes completely through the evaporator in the configuration 3. This bypass air ratio was about 50 per cent for the configuration 4. In the configurations 3 and 4, the pipe line that mounted between the dryer exhaust section and the evaporator inlet section occurs the extra air flow resistance in the bed, that is, it causes the higher static pressures in the bed than that of the configurations 1 and 2 as shown in the Figure 5.2.13. Thus, MER values for the configurations 3 and 4 are higher than that of the configurations 1 and 2. On the other hand, the configuration 4 has the lower MER than that of the configuration 3 because of the bypass of about 50 per cent of the air flow discharged into the ambient without entering into the evaporator for the configuration 4 reduces the air flow resistance in the bed. When compared with that of the configuration 3 as seen from the Figure 5.2.13. In addition, any relation between the MER and the static pressures measured at the inlet and outlet sides of the bed are observed when the Figures 5.2.8 and 5.2.13 are compared with each other. For instance, the highest MER value is obtained at the highest static pressure magnitudes in the bed for the configuration 6 as shown in these figures.

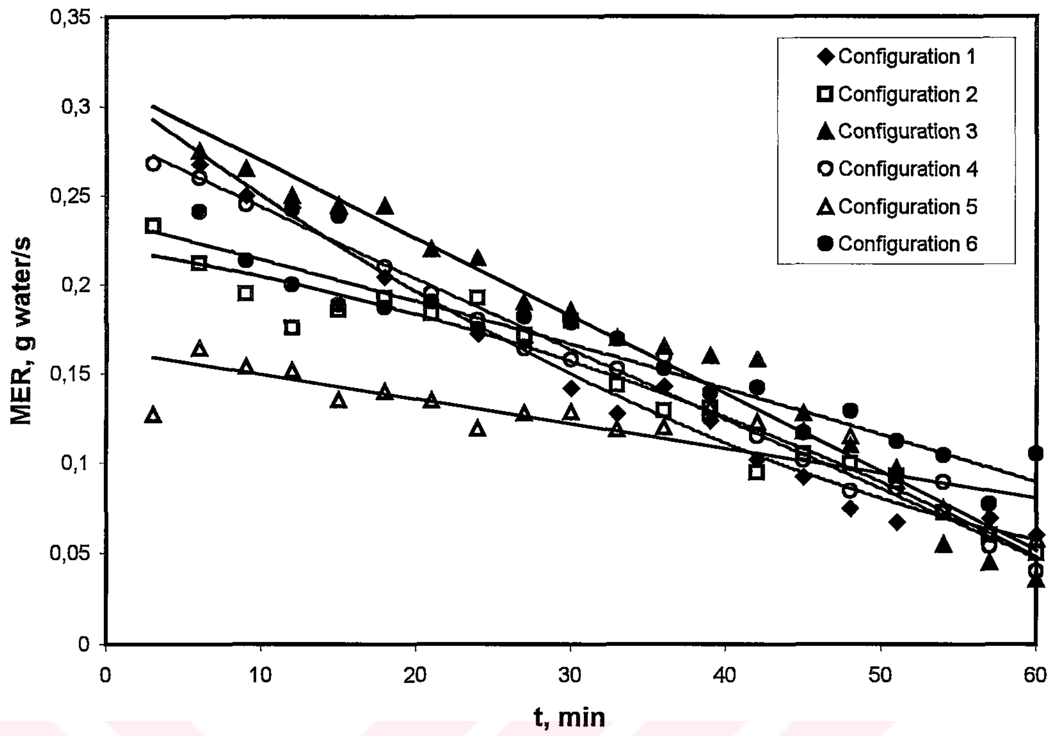

Figure 5.2.7 The variation of MER with time for all configurations

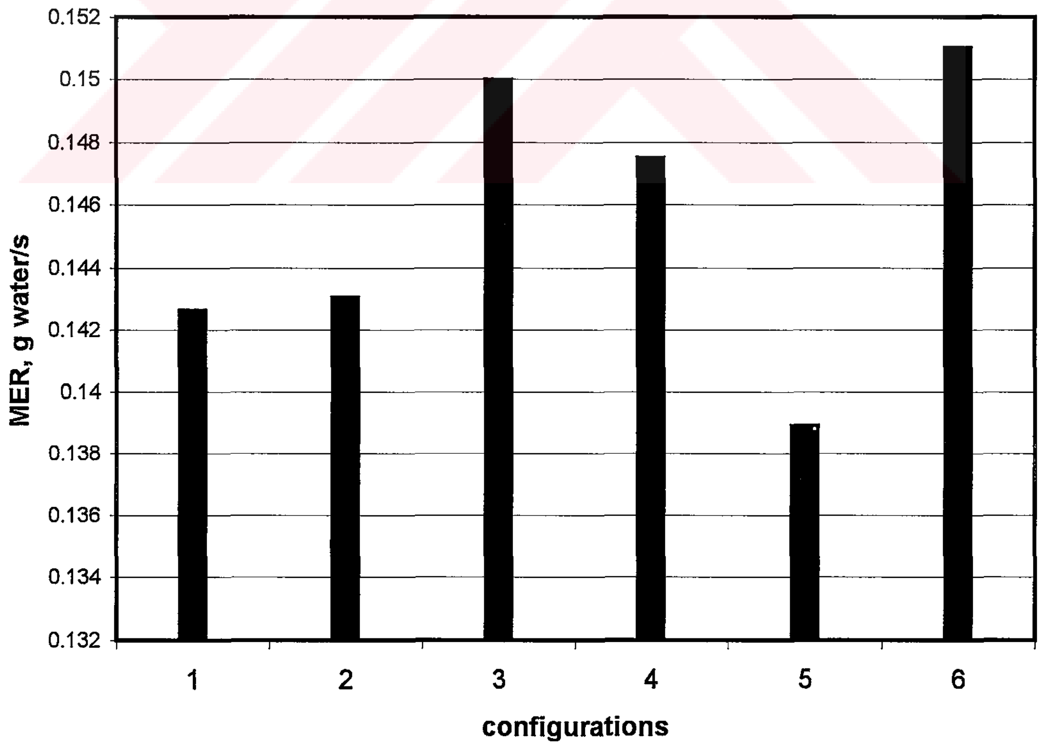

Figure 5.2.8 The mean MER values for all configurations

Figure 5.2.9 is showing the SMER amounts for the configurations. The SMER for the configuration 2 is higher than that of the configuration 1 because of the power consumed by the compressor for the configuration 2 is less than that of the configuration 1 as shown in the Table 5.2. However, the air circuit configuration for the configurations 1 and 2 are the same, the only difference between them is that the any waste heat supply rated of 2kW was used at upstream section of the evaporator in the configuration 2 as different from the configuration 1. The cause of this result is that the any waste heat usage at upstream section of the evaporator increases the dry bulb temperature of the air flow entering the evaporator and so evaporation temperature in the evaporator. In this case, the power consumed by the compressor decreases and this result causes the increase in SMER for the configuration 2 when that is compared with that of the configuration 1.

For the configurations 3 and 4, SMER values are greater than that of the configuration 1. Because the wetted exhaust hot air flow leaving from the bed or dryer is transferred into the evaporator and this wetted and hot air flow reduces the power consumed by the compressor by increasing the evaporation temperature in the evaporator for the configurations 3 and 4. On the other hand, when the SMER values of the configurations 3 and 4 are compared with each other, the SMER for the configuration 4 is greater than that of the configuration 3. However, the air circuit configurations for either are similar except the some partition of the discharged wetted hot air flow leaving from the dryer is bypassed into the ambient and the other partition of the discharged air flow from the dryer passes through the evaporator for the configuration 4 while the discharged wetted hot air flow leaving from the dryer is completely passes through the evaporator in the configuration 3. This bypass air ratio was about 50%. In this case, the bypass process reduces the consumed power by the fan for the configuration 4 in order to obtain the same amounts of air flow rate in the dryer for the configurations 3 and 4. As shown from the Figure 5.2.13, the generated static pressure magnitudes of air flow in the dryer for the configuration 4 is less than that of the configuration 3, because bypass process reduces the air flow resistance in the bed when the configurations 3 and 4 are compared with each other. Although, the MER for the configuration 3 is greater than that of the configuration 4, the SMER for the configuration 4 is greater than that of the configuration 3 since the power consumed by the fan for the configuration 3 is greater than that of the configuration 4 as shown in the Table 5.2.

The SMER for the configuration 5 is in the range between that of the configuration 1 and the configurations 2, 3, 4. The exhaust wetted hot air flow discharged from the bed is recycled into the bed in the configuration 5. This case reduces the moisture extraction capacity of air flow in the dryer, therefore, the configuration 5 has the lowest MER value as shown in the Figure 5.2.9, furthermore the consumed power by the fan reduces since the discharged air flow from the dryer is recycled into the dryer. As shown in the Table 5.2 the lowest consumed power of the fan is observed for the configuration 5 among the all tested configurations. Thus, the configuration 5 has the lower SMER than that of the configurations 2, 3 and 4. On the other hand, although the MER for the configuration 1 is greater than that of the configuration 5 as shown in the Figure 5.2.8, the SMER for the configuration 1 is less than that of the configuration 5 since the power consumed by the fan for the configuration 1 is greater than that of the configuration 5 in order to obtain the same amounts of air flow rate in the dryer. Also, the configuration 1 has the lowest SMER in spite of the MER for this configuration is not the lowest value. This case can be explained by the consumed power by the compressor for the configuration 1 are greater than that of the others as shown in the Table 5.2. Thus, it has the lowest SMER.

The configuration 6 has the highest SMER among the all tested configurations as shown in the Figure 5.2.9. In this configuration, the power consumed by the compressor reduces since the evaporation temperature in the evaporator increases by the wetted hot air flow discharged from the dryer is passed through the evaporator and the power consumed by the fan reduces because of the dry air passed through the evaporator is recycled into the bed. At the same time, it has the highest MER, therefore, the highest SMER is observed in the configuration 6.

Table 5.2 The consumed power magnitudes by the fan and the compressor

Configurations	W_{comp}, kWh	W_{fan}, kWh
1	2.05	1.45
2	1.8	1.45
3	1.63	1.81
4	1.61	1.63
5	2.04	1.25
6	1.63	1.6

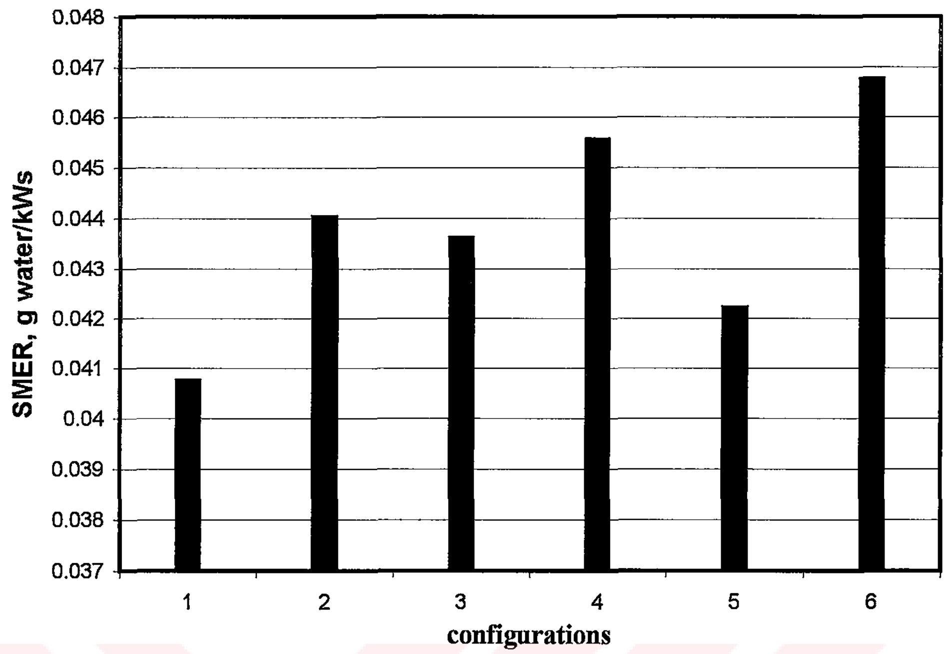

Figure 5.2.9 The mean SMER values for all configurations

Figure 5.2.10 shows the COP values of the heat pump unit for all configurations. One of the main effect which affecting the COP of the heat pump unit is the evaporation temperature in the evaporator and this effect is only related with the dry bulb and wet bulb temperatures of the air flow passing through the evaporator, and consequently its moisture content or humidity ratio. The air circuit configurations of the system affects the dry and wet bulb temperatures of the air flow passing through the evaporator. When the configuration 1 has the lowest COP value of 2.84, the configurations 3 and 6 have the highest COP values of 3.35 and 3.34, respectively; and the configuration 4 has the COP value of 3.23 near to that of the configurations 3 and 6. In the configuration 6 the wetted air flow passing through the evaporator is the same with that of the configuration 3. Thus, the COP values for the configurations 3 and 6 are approximately same. The hot exhaust air flow leaving from the bed, which carrying the highest moisture by taking from the wetted wheat grains in the bed, was passed through the evaporator in the configuration 3 and 6. Thus, the configurations 3 and 6 have the highest COP values. Because the wetted hot air passing through the evaporator increases the evaporation temperature in the evaporator. Since the bypassed air flow at the partition of about 50 percent into the ambient without entering through the evaporator little reduces its moisture transferred into the evaporator, therefore, the configuration 4 has little less COP than that of the configuration 3 and 6.

The any waste heat usage of 2kW rated at upstream section of the evaporator increases the dry bulb temperature of the air flow approaching the evaporator in the configuration 2. When the dry bulb temperature of the approaching air flow to the evaporator was about 27°C in the configuration 1, the dry bulb temperature of air flow approaching to the evaporator was about 37°C in the configuration 2 in which is used the waste heat at upstream section of the evaporator. This waste heat of 2kW rated or the occurred temperature difference of 10°C across the evaporator causes the increase in COP. Thus, the COP value of the configuration 2 is greater than that of the configuration 1 as shown in the Figure 5.2.10.

The configuration 5 has the second lowest COP value after that of the configuration 1. In either configurations, the wetted hot air flow leaving from the bed is not transferred into the evaporator, instead, it is discharged into the ambient in the configuration 1, and it is recycled into the bed in the configuration 5. Therefore, they have the lower COP values than the others. Because there is no any effect in order to reduce the power consumed by the compressor in the configurations 1 and 5, since the ambient air is passing through the evaporator in either configuration, 1 and 5.

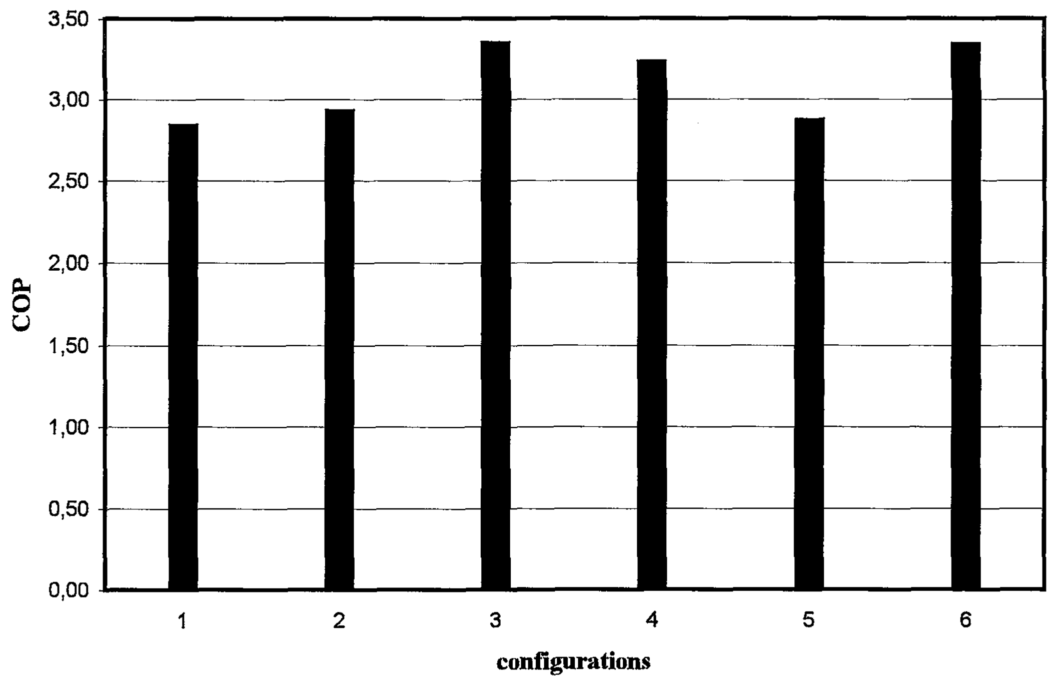

Figure 5.2.10 The COP values for all configurations

The dryer efficiency, DE, which is an another performance parameter for the dryer, gives in fact the moisture extraction capacity ratio for the dryer. The variation of DE with the drying time during the test period of 60min is given in the Figure 5.2.11. The DE values for all tested configurations are lying in the range between about 10-55 per cent as shown in the Figure 5.2.11, but the differences in DE values for the configurations are not clearly seen since the instant DE values have the fluctuations during the test period of 60min. Thus, the arithmetic mean of the DE values during the drying test is given in the Figure 5.2.12. As similar the results of the MER and SMER, the configuration 6 has the highest DE. On the other hand, the lowest DE is observed for the configuration 5. The main effect which is affecting the DE is the amount of moisture carried in the air flow entering the bed. The wetted air flow leaving from the bed is recycled into the bed, therefore, the moisture carrying capacity of the air flow in the dryer reduced, so the DE value for the configuration 5 is lower than that of the others. For the configuration 6, the wetted air flow leaving from the bed is transferred into the evaporator by leaving its moisture on the evaporator is recycled into the bed, so, the dry air entering the dryer increases own moisture carrying capacity, and thus the DE for the configuration 6 is higher than that of the others.

The configurations 3 and 4 have the lower DE than that of the configurations 1 and 2, however, for these configurations, 1, 2, 3 and 4, the ambient air is passed through the bed, that is, the moisture carrying capacity of the air passing through the dryer might be same with each other. But, the lower DE values observed in the configurations 3 and 4 when they are compared with that of the configurations 1 and 2. This case can be explained by the existent moisture content carried in the ambient air. When we observed the humidity ratio of the ambient air at the dates when the tests were done, the humidity ratios of the ambient air for the configurations were recorded in the following table

Table 5.3 The dry bulb and wet bulb ambient temperatures and humidity ratio magnitudes at days that configuration drying tests were done

Configurations	$T_{db,amb}$, °C	$T_{wb,amb}$, °C	w_{amb}, kg water/kg dry air
1	28.0	18.5	0.0093
2	29.0	19.5	0.0094
3	29.5	19.0	0.0103
4	29.7	20.0	0.0106
5	30.0	20.5	0.0116
6	29.5	20	0.0107

As a result of these, ambient humidity ratio measurements for the configuration 3 and 4 the ambient air have the higher humidity ratios than that of the configurations 1 and 2. Therefore, the configurations 3 and 4 have the lower DE values than that of the configurations 1 and 2.

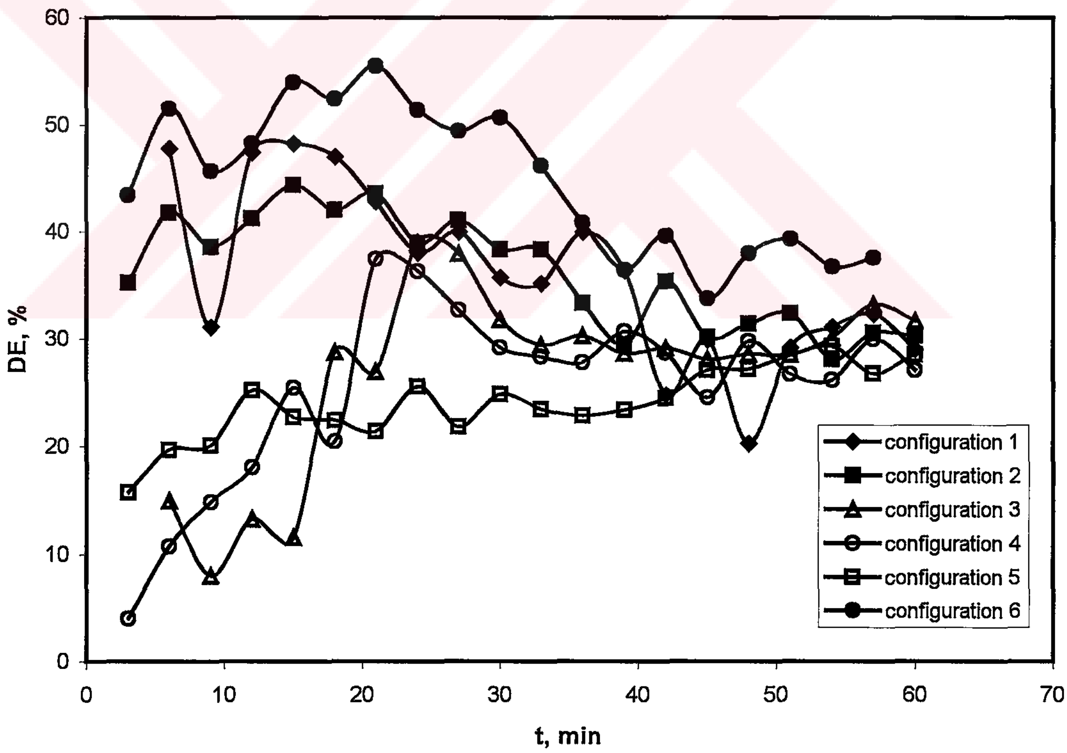

Figure 5.2.11 The variation of DE with drying time for all configurations

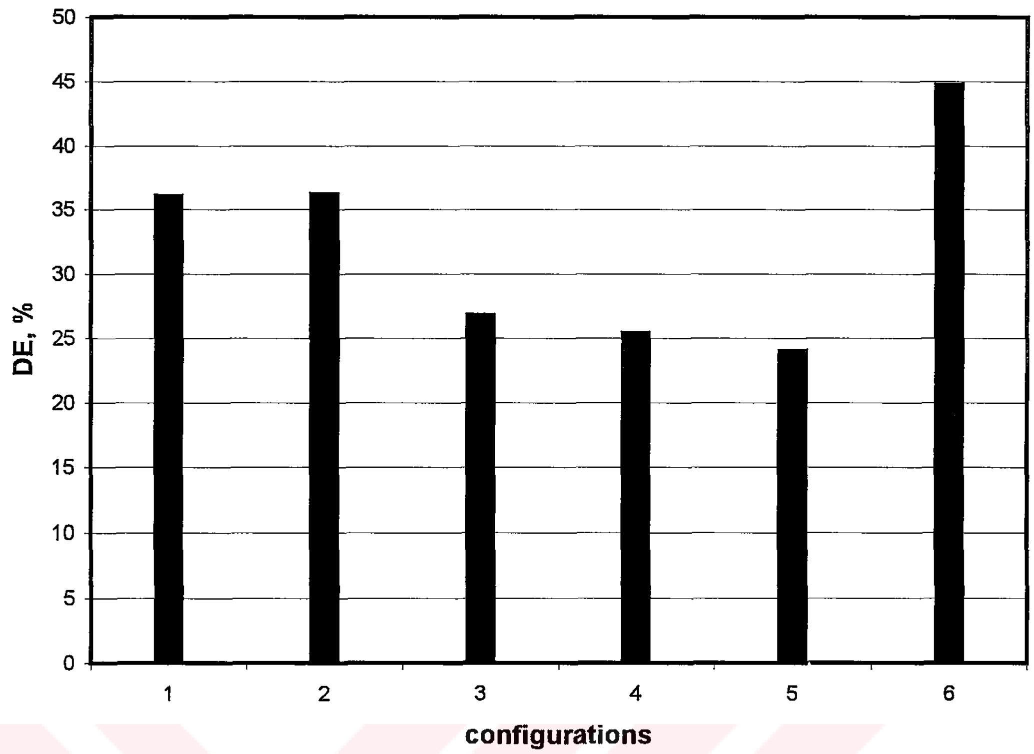

Figure 5.2.12 The mean DE values for all configurations

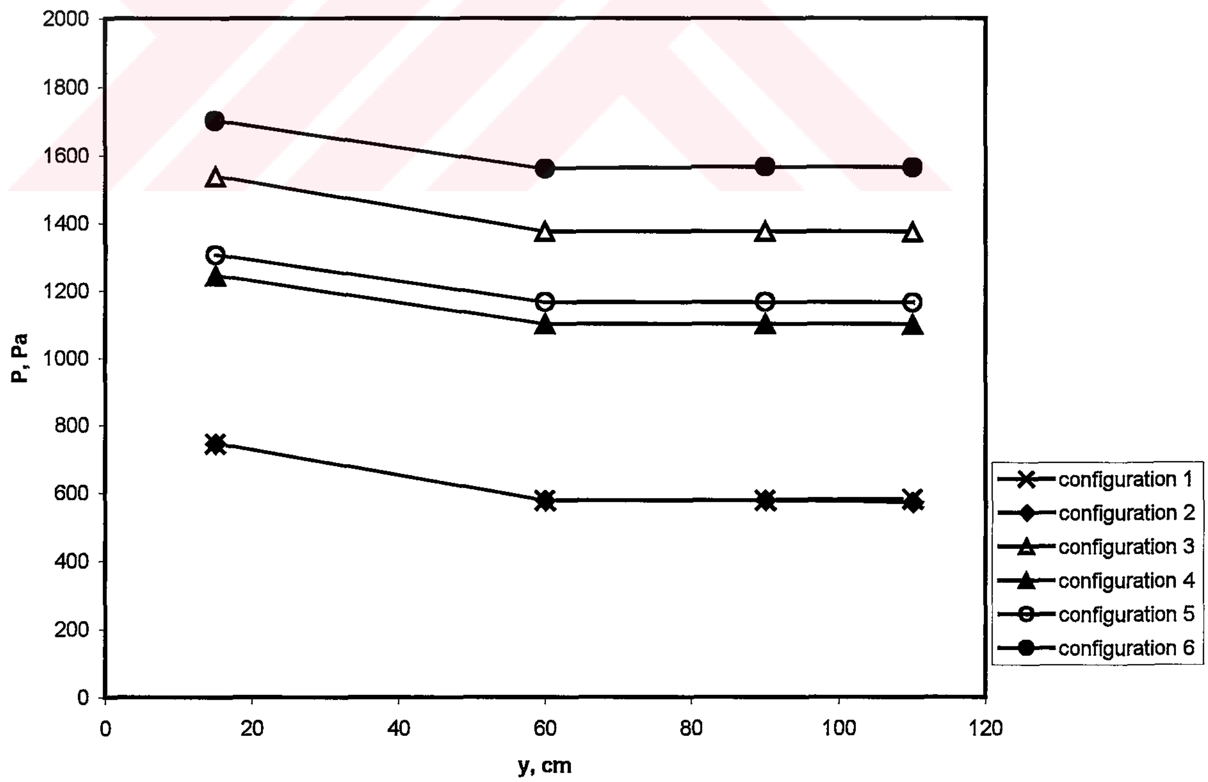

Figure 5.2.13 The variation of static pressure in the longitudinal direction of the bed for all configurations

5.3 THE EFFECTS OF DRY BULB TEMPERATURE IN THE DRYING MEDIUM FOR DRYING THE WHEAT GRAINS

In order to see the effect of dry bulb of temperature in the drying medium, bed temperature, for drying the wet wheat grains, the drying experiments at four different dry bulb temperatures, 40, 50, 60 and 70°C, in the bed and for two different configurations, 1 and 6, were done by using the electrical heater to heat the air flow entering into the bed. The variations of dry bulb and wet bulb temperatures at inlet and outlet sides of the bed with drying time are shown in the Figures 5.3.1-5.3.4 for the configuration 1 and in the Figures 5.3.5-5.3.8 for the configuration 6. The dry bulb temperatures at inlet and outlet sides of the bed are naturally greater than the wet bulb temperatures at inlet and outlet sides of the bed for either configuration 1 and 6 as shown in these figures. When the dry bulb temperatures at inlet side of the bed are remaining constant in a band between ±2°C of the nominal dry bulb temperature magnitudes at the inlet side of the bed for each sets, the dry bulb temperatures at outlet sides of the bed are gradually increasing with drying time during the test period of 40min. When the difference between the magnitudes of dry bulb temperatures at inlet and outlet sides of the bed is high at the beginning of the drying, this difference is gradually decreasing with the drying time. At the end of the drying test period of 40min, this difference is completely closed, that is, the dry bulb temperatures at outlet side of the bed are gradually increasing with the drying time and becomes near to the dry bulb temperatures at inlet side of the bed towards the end of the drying time for either configuration as shown in the Figures 5.3.1-5.3.8. This result is also more clearly observed from the Figure 5.3.9. Furthermore, the differences between the dry bulb temperatures at inlet and outlet sides of the bed are increasing with the increasing air dry bulb temperature in the bed for either configuration as shown in the Figures 5.3.9-5.3.10.

The wet bulb temperatures at outlet side of the bed are also greater than the wet bulb temperatures at inlet side of the bed for either configuration 1 and 6 during the drying test as shown in the Figures 5.3.1-5.3.8. The difference between the wet bulb temperatures at outlet and inlet sides of the bed is remaining about constant during the drying time for the configuration 1 as shown in the Figures 5.3.1-5.2.4. Because, the wet bulb temperatures at inlet and outlet sides of the bed are less gradually increasing with the drying time and the difference between the magnitudes of them are about constant in a band of 1.5°C during the drying test as shown from these figures for the configurations 1. Also, this result is clearly shown in the Figure 5.3.11. At the same time, as shown from this figure, the differences between the wet bulb temperatures at outlet and inlet sides of the bed are increasing with the increasing dry bulb temperature in the bed as similar to the results observed for the difference between the dry bulb temperatures at inlet and outlet sides of the bed shown in the Figure 5.3.9. For the configuration 6, when the wet bulb temperatures at outlet sides of the bed are remaining approximately constant during the test, the wet bulb temperatures at inlet side of the bed are gradually increasing with the drying time as shown in the Figures 5.3.5-5.3.8. Thus, the differences between the wet bulb temperatures at outlet and inlet sides of the bed are decreasing with the drying time for the configuration 6. This result can be clearly seen in the Figure 5.3.12. Furthermore, the differences between the wet bulb temperatures at outlet and inlet sides of the bed are increasing with the increasing bed temperature. When the differences between the wet bulb temperatures at outlet and inlet sides of the bed are higher at the beginning of the drying test, these differences are very less towards the end of the drying test, because of these differences are decreasing with the drying time for the configuration 6 as shown in the Figure 5.3.12.

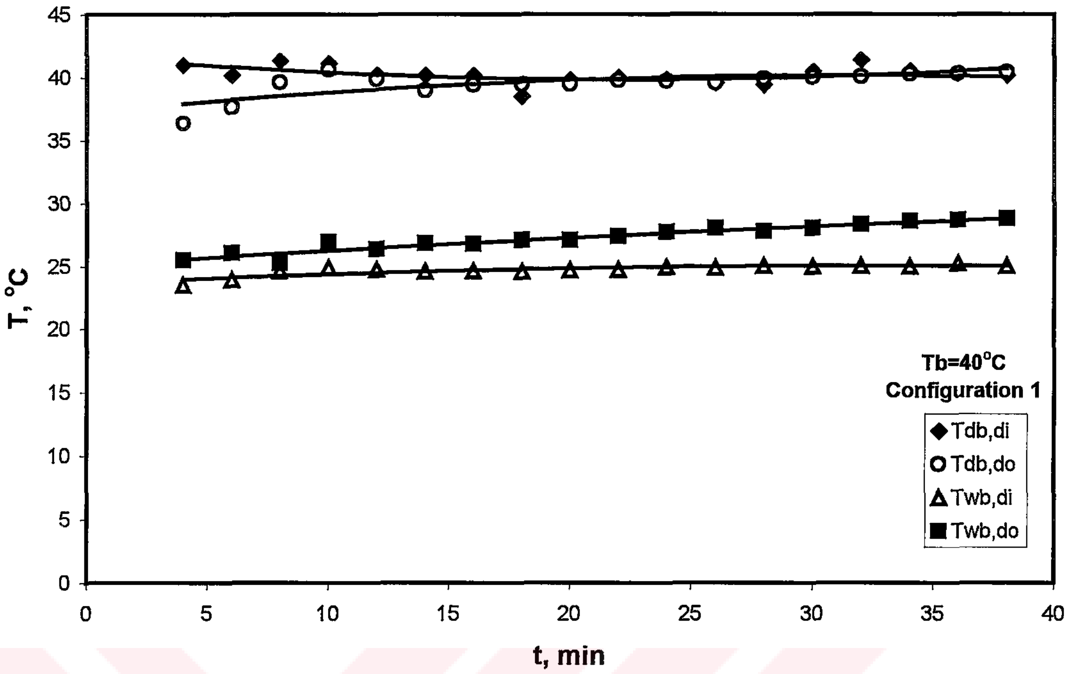

Figure 5.3.1 The variation T_{db} and T_{wb} at inlet and outlet sides of the bed with time at mean T_b=40°C in the bed for the configuration 1

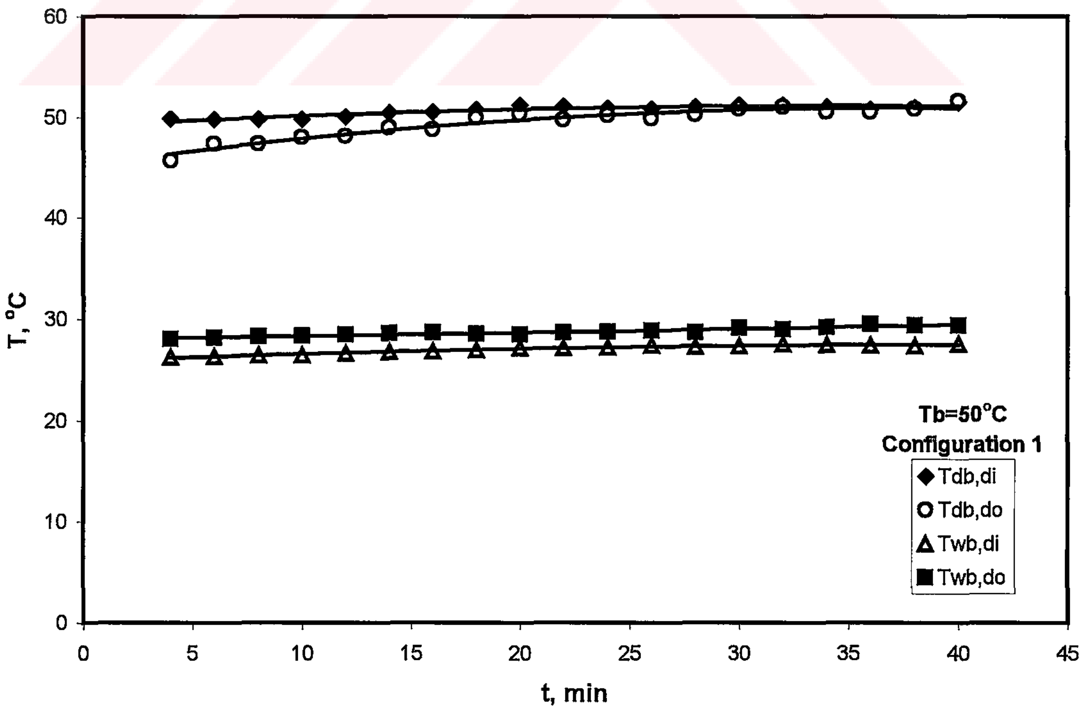

Figure 5.3.2 The variation T_{db} and T_{wb} at inlet and outlet sides of the bed with time at mean T_b=50°C in the bed for the configuration 1

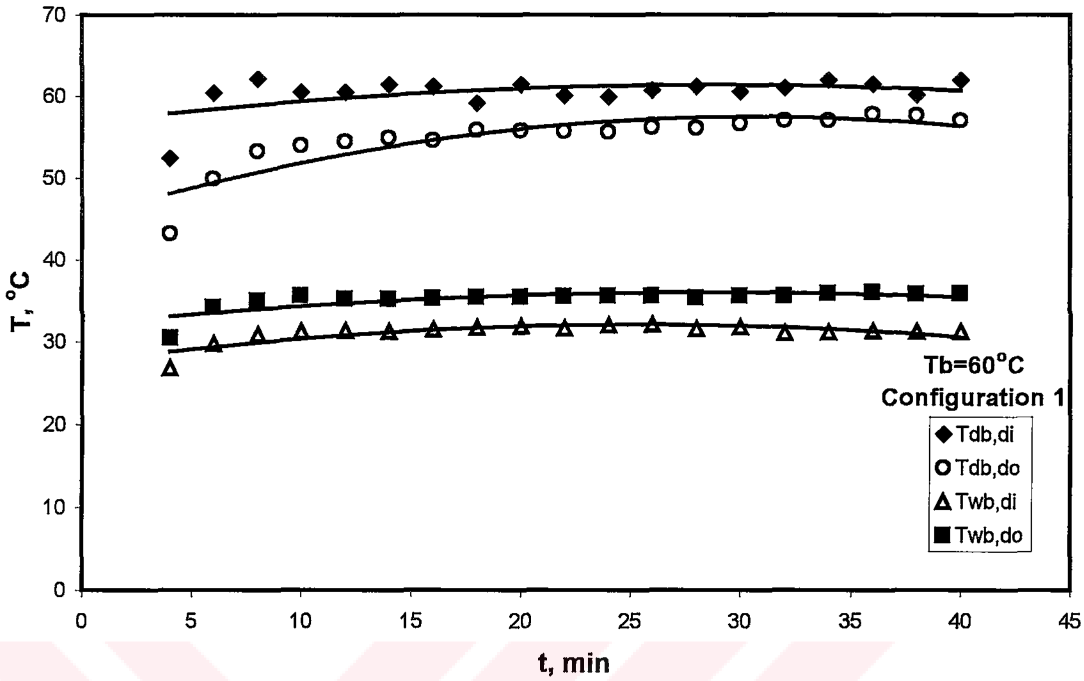

Figure 5.3.3 The variation T_{db} and T_{wb} at inlet and outlet sides of the bed with time at mean T_b=60°C in the bed for the configuration 1

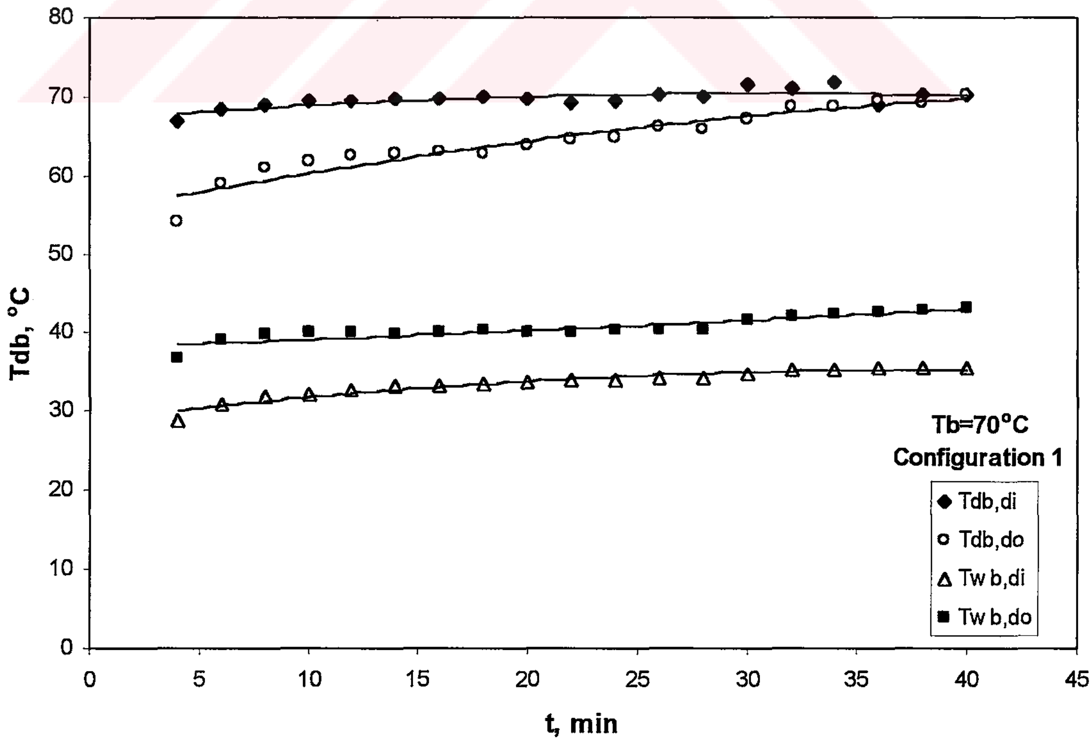

Figure 5.3.4 The variation T_{db} and T_{wb} at inlet and outlet sides of the bed with time at mean T_b=70°C in the bed for the configuration 1

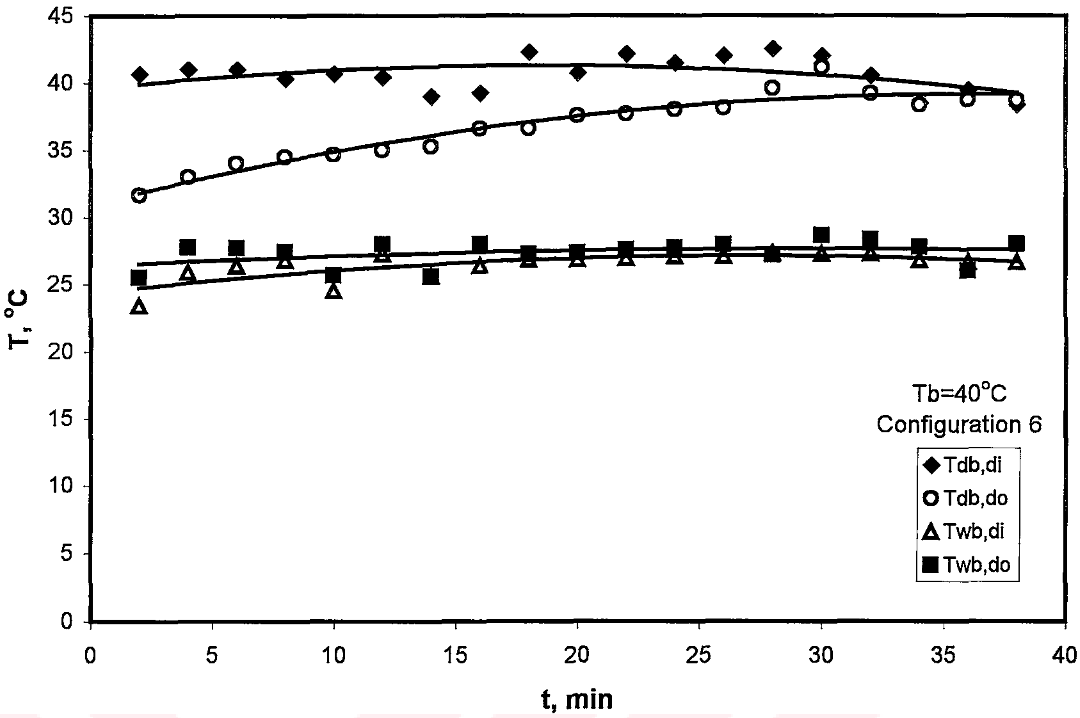

Figure 5.3.5 The variation T_{db} and T_{wb} at inlet and outlet sides of the bed with time at mean T_b=40°C in the bed for the configuration 6

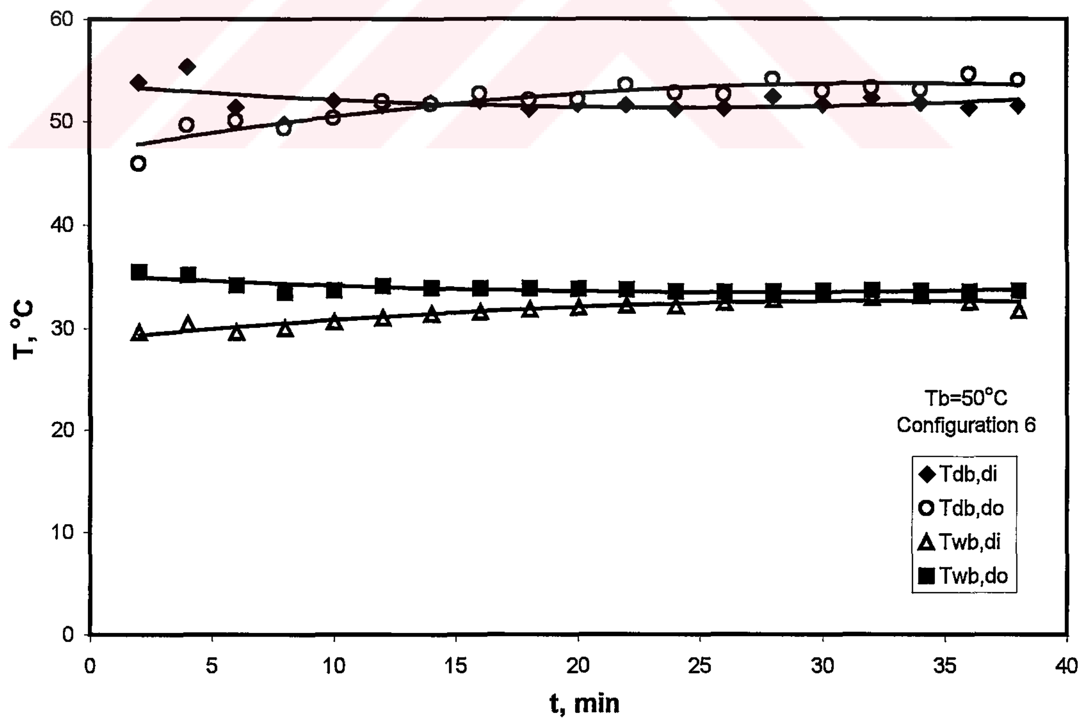

Figure 5.3.6 The variation T_{db} and T_{wb} at inlet and outlet sides of the bed with time at mean T_b=50°C in the bed for the configuration 6

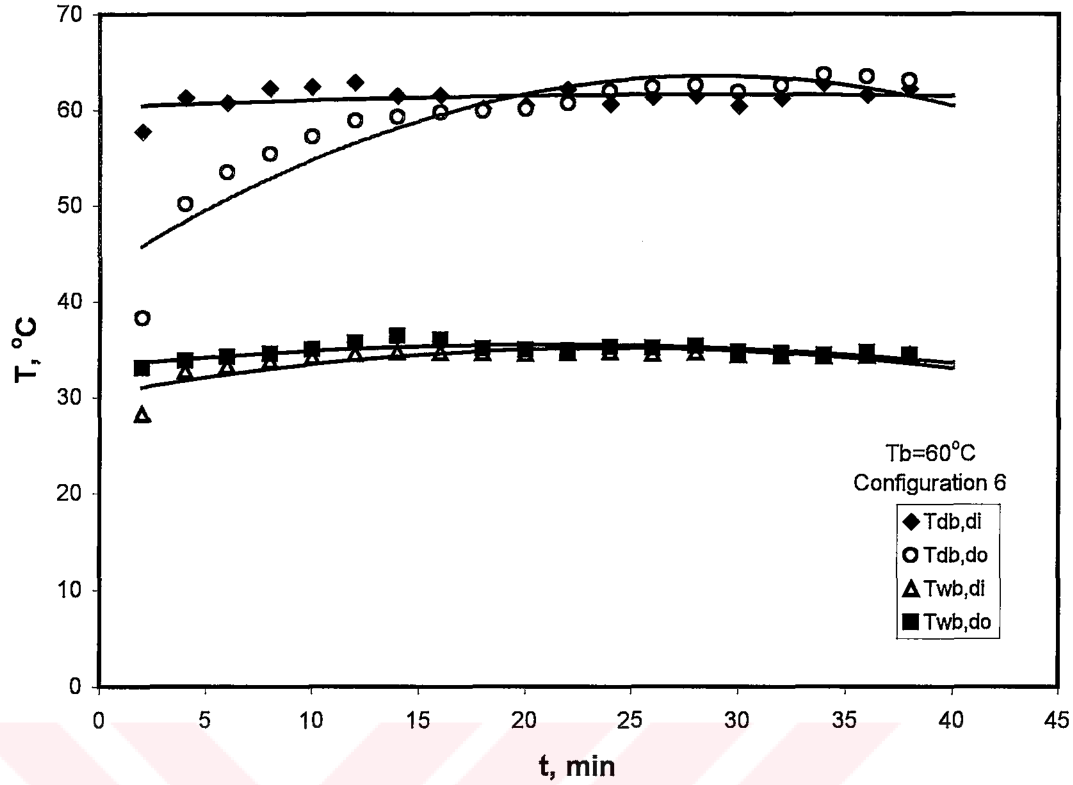

Figure 5.3.7 The variation T_{db} and T_{wb} at inlet and outlet sides of the bed with time at mean T_b=60°C in the bed for the configuration 6

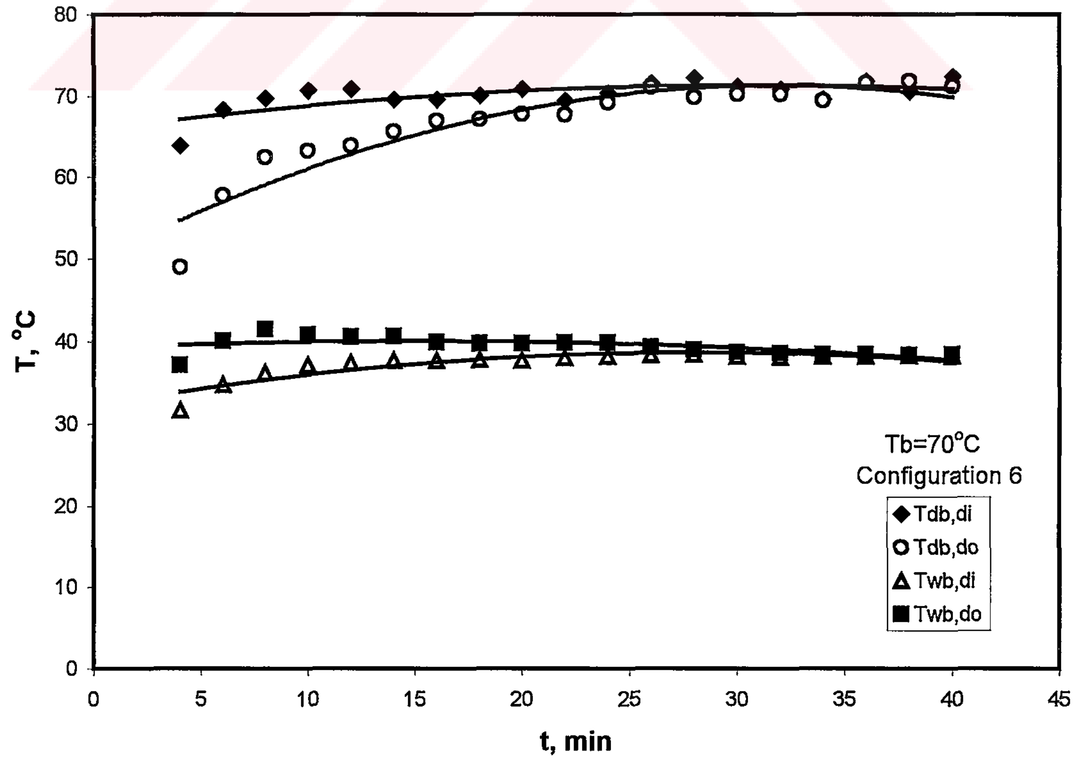

Figure 5.3.8 The variation T_{db} and T_{wb} at inlet and outlet sides of the bed with time at mean T_b=70°C in the bed for the configuration 6

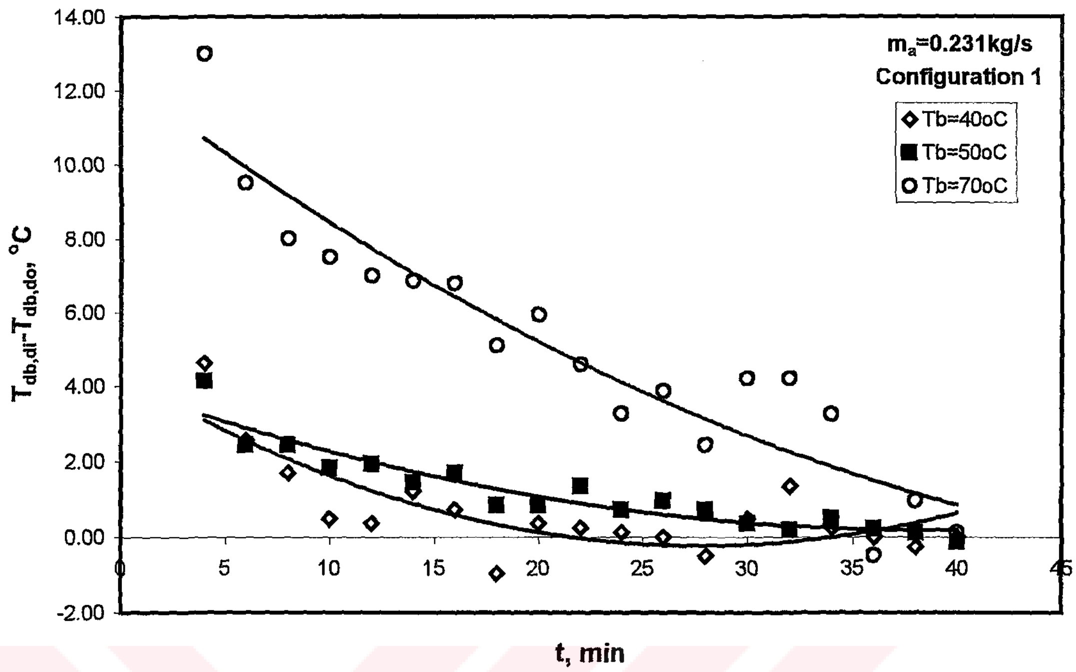

Figure 5.3.9 The variation of difference between T_{db} at inlet and outlet sides of the bed with time at the m_a=0.231kg/s in the bed for different T_b in the bed for the configuration 1

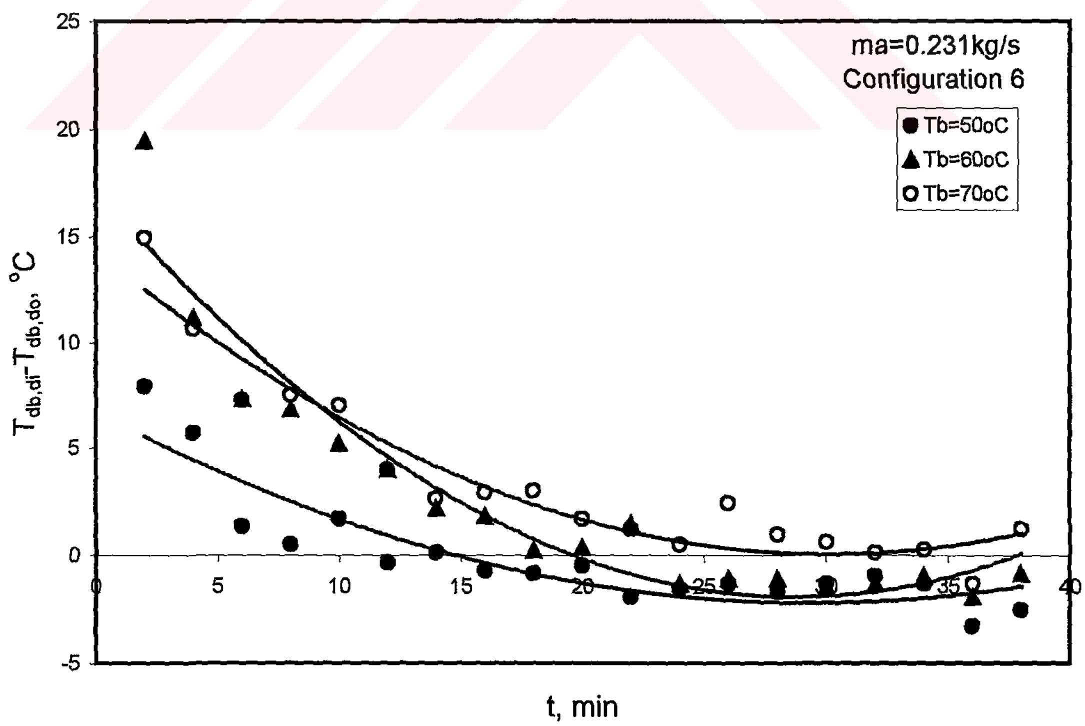

Figure 5.3.10 The variation of difference between T_{db} at inlet and outlet sides of the bed with time at the m_a=0.231kg/s in the bed for different T_b in the bed for the configuration 6

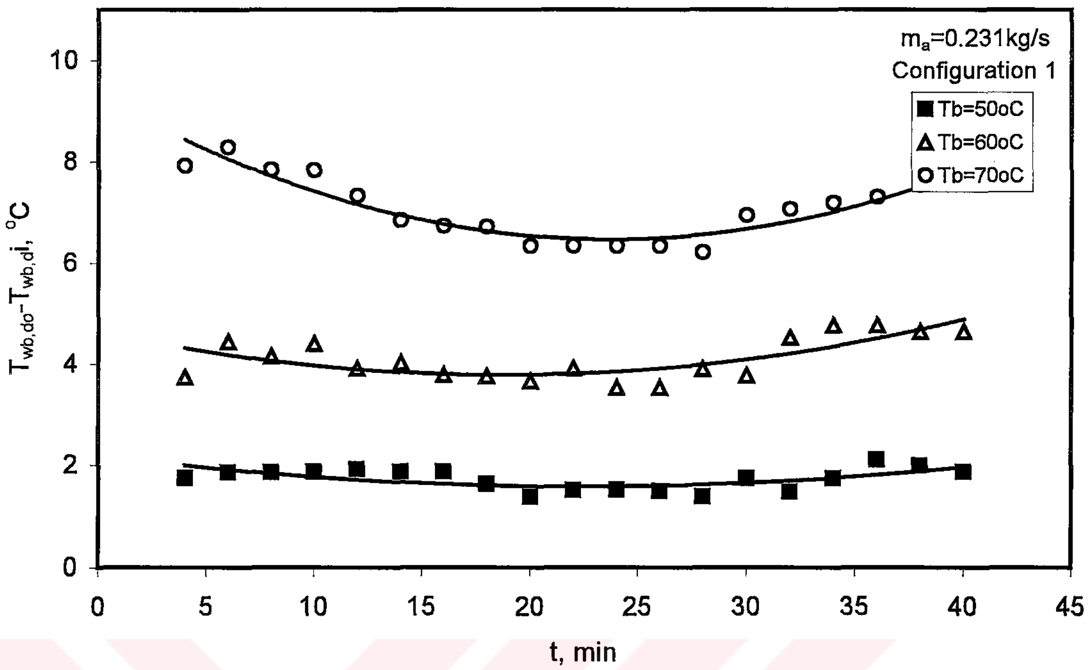

Figure 5.3.11 The variation of difference between T_{wb} at inlet and outlet sides of the bed with time at the m_a=0.231kg/s for different T_b in the bed for the configuration 1

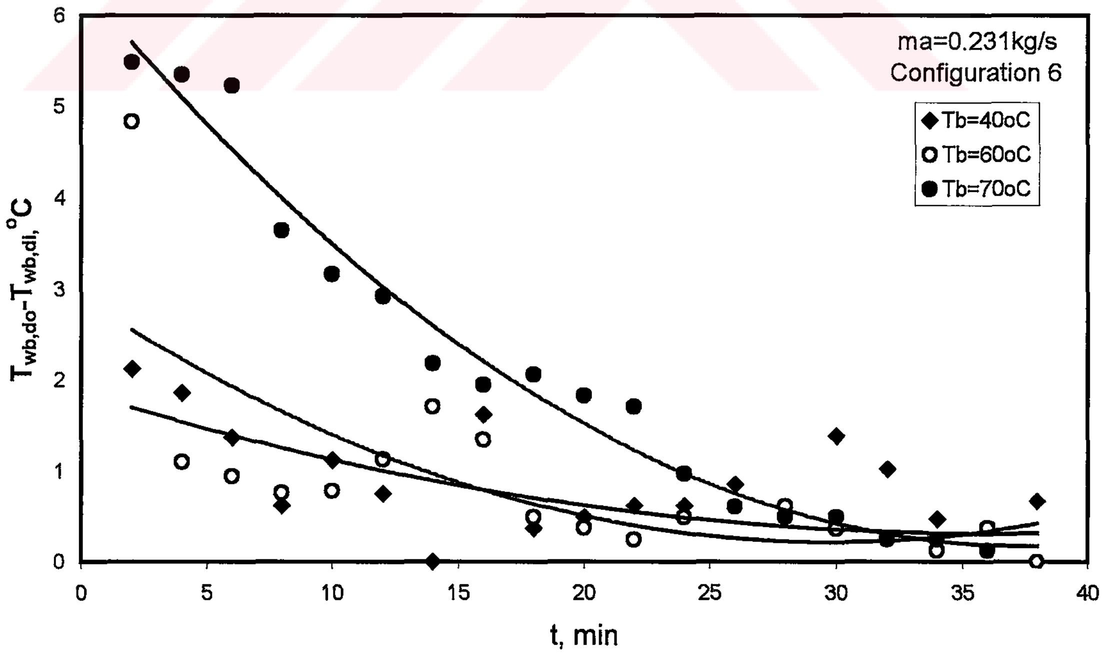

Figure 5.3.12 The variation of difference between T_{wb} at inlet and outlet sides of the bed with time at the m_a=0.231kg/s for different T_b in the bed for the configuration 6

In order to see the variation of MER with drying time, the variation of MER with drying time at four different air dry bulb temperatures, bed temperatures, 40, 50, 60 and 70°C, for two different configurations 1 and 6 and at air mass flow rate of 0.231kg/s in the bed are plotted in the Figure 5.3.13 for the configuration 1 and in the Figure 5.3.14 for the configuration 6. For all bed temperatures, the MER values are gradually decreasing with the drying time as shown in the Figure 5.3.13 for the configurations 1 and as shown in the Figure 5.3.14 for the configuration 6. At the same time, the higher air dry bulb temperatures in the bed result the higher MER values for the configurations 1 and 6 as shown in the Figures 5.3.13 and 5.3.14, respectively. In order to see more clearly the variation of MER with the bed temperatures, the mean MER values during the drying test period of 40min are plotted corresponding to the dry bulb temperatures at inlet side of the bed, bed temperature, in the Figure 5.3.15 for either configuration. The increase in mean MER values with the increasing bed temperature is clearly shown from the Figure 5.3.15 for either configuration 1 and 6. This increase in MER with the increasing bed temperature is also linear and the relation of variation of mean MER with the bed temperature is formulized as the following equations for the configurations 1 and 6 with the error margins of ±0.3 percent and ±0.7 percent , respectively,

$$MER=0.0038T_b-0.008 \quad \text{for the configuration 1} \tag{5.3.1}$$

and

$$MER=0.0039T_b+0.0109 \quad \text{for the configuration 6} \tag{5.3.2}$$

Also, the mean MER values for the configuration 6 are greater than that of the configuration 1 for all bed temperatures at the same air mass flow rate as shown in the Figure 5.3.15.

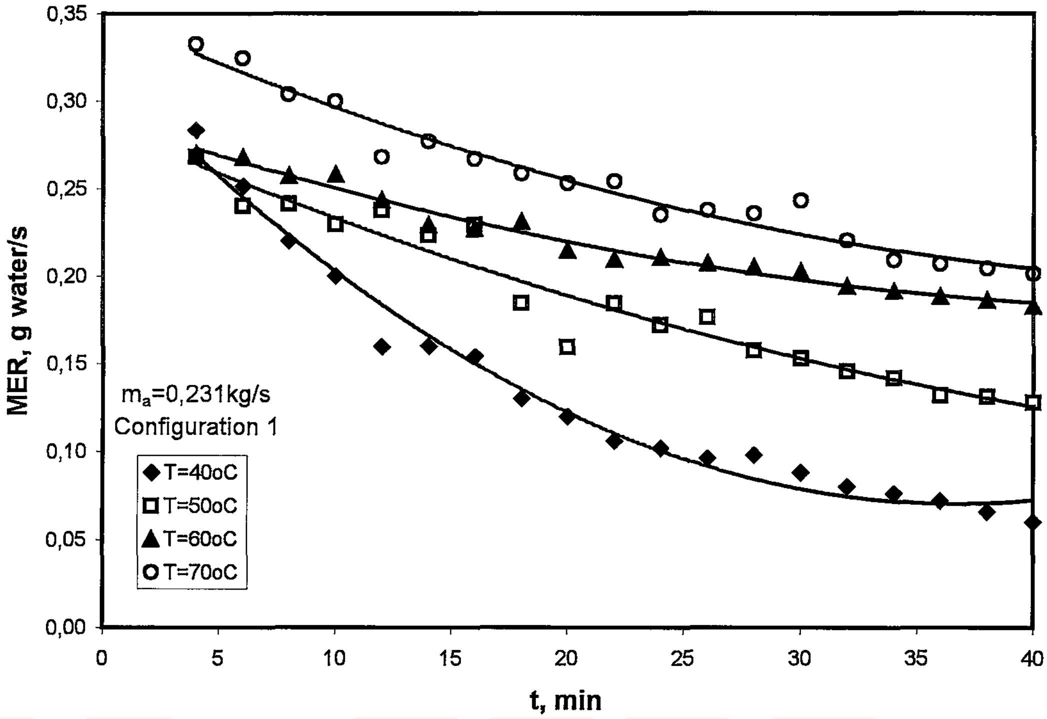

Figure 5.3.13 The variation of MER with time at m_a=0.231kg/s for the different T_{db} in the bed for the configuration 1

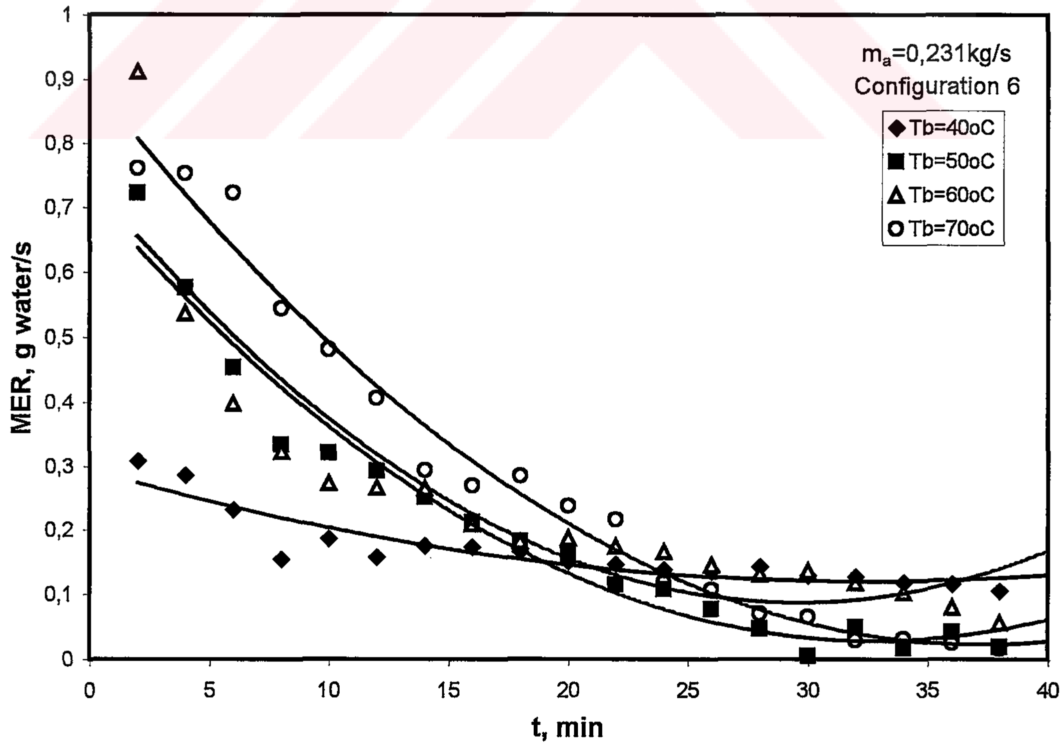

Figure 5.3.14 The variation of MER with time at m_a=0.231kg/s for the different T_{db} in the bed for the configuration 6

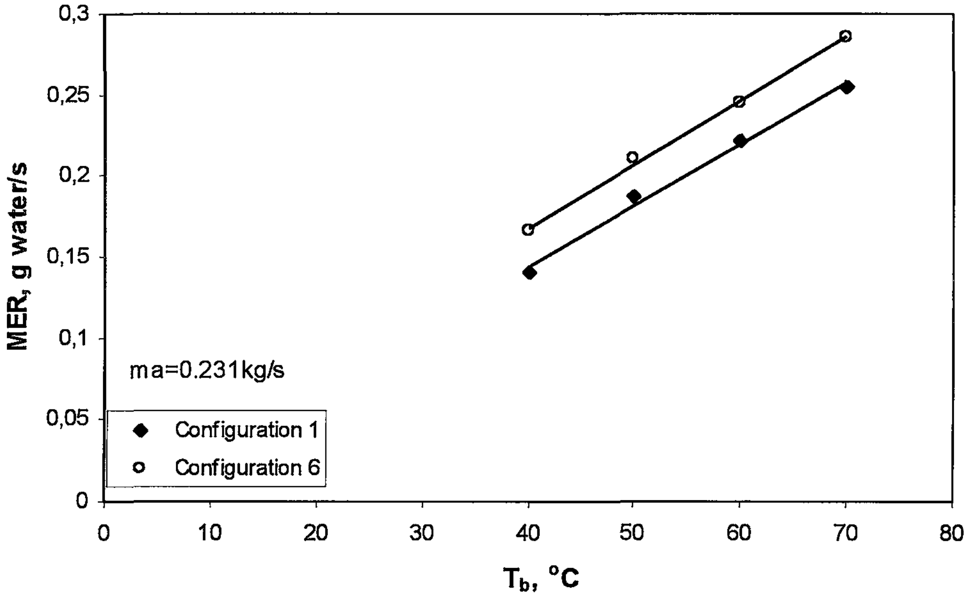

Figure 5.3.15 The variation of MER with T_b in the bed for the configurations 1 and 6

On the other hand, the variation of SMER with the bed temperatures are plotted in the Figure 5.3.16 for the configurations 1 and 6. The SMER is decreasing with the increasing bed temperature as shown in the Figure 5.3.16 for either configuration, because of the power consumed by the electrical heater are increasing in order to obtain the drying medium at higher temperatures and at the same air mass flow rate. Also, this decrease in the SMER with the increasing bed temperature is also linear and the relation between them is given in the following equations for the configurations 1 and 6 with the error margins of ±5 percent and ±3 percent, respectively,

$$SMER=-0.0003T_b+0.0514 \quad \text{for the configuration 1} \qquad (5.3.3)$$

and

$$SMER=-0.0002T_b+0.0541 \quad \text{for the configuration 6} \qquad (5.3.4)$$

Furthermore, the SMER values for the configuration 6 are higher than that of the configuration 1 as shown in the Figure 5.3.16.

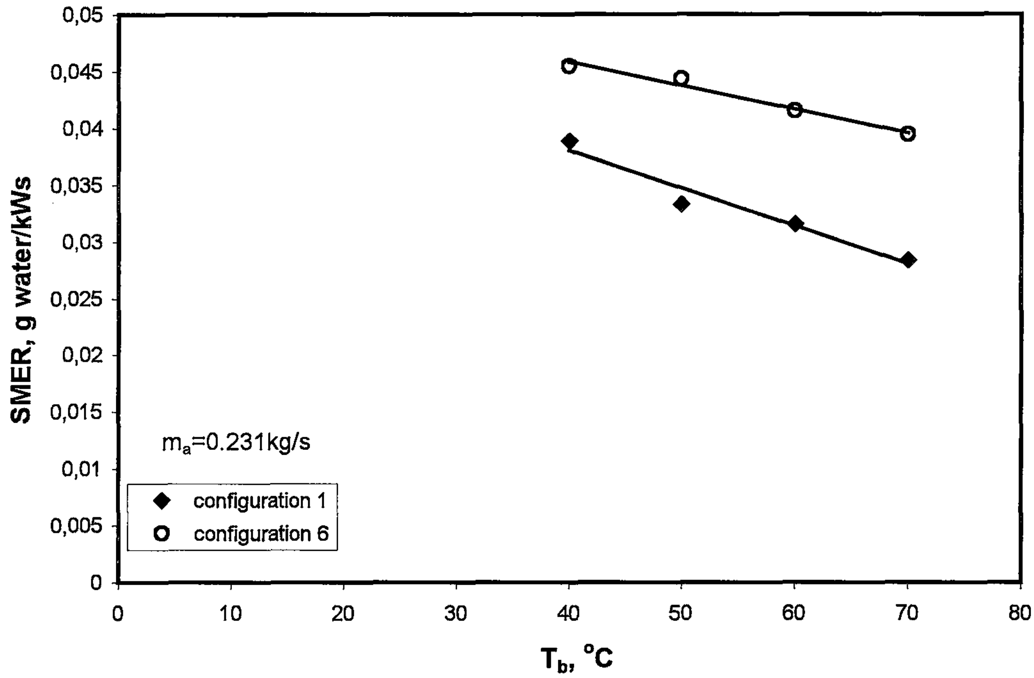

Figure 5.3.16 The variation of SMER with T_b in the bed for the configurations 1 and 6

In the Figure 5.3.17 the mean DE values during the drying test are plotted corresponding to the bed temperatures. The increase in DE with the increasing bed temperature is observed from this figure for either configuration. These increases in DE with the increasing bed temperature is also linear and this linear relation between them is given in the following equations for the configurations 1 and 6 with the error margins of ±1 percent and ±0.5 percent, respectively,

$$DE=0.534T_b+19.18 \quad \text{for the configuration 1} \tag{5.3.5}$$

and

$$DE=0.3367T_b+27.826 \quad \text{for the configuration 6} \tag{5.3.6}$$

When the DE values at the bed temperature of 40oC are about the same for the configurations 1 and 6, the increase in DE values with the bed temperature for the configuration 1 is higher than that of the configuration 6. That is, the difference between the DE values of the configurations 1 and 6 is increasing with the increasing bed temperature.

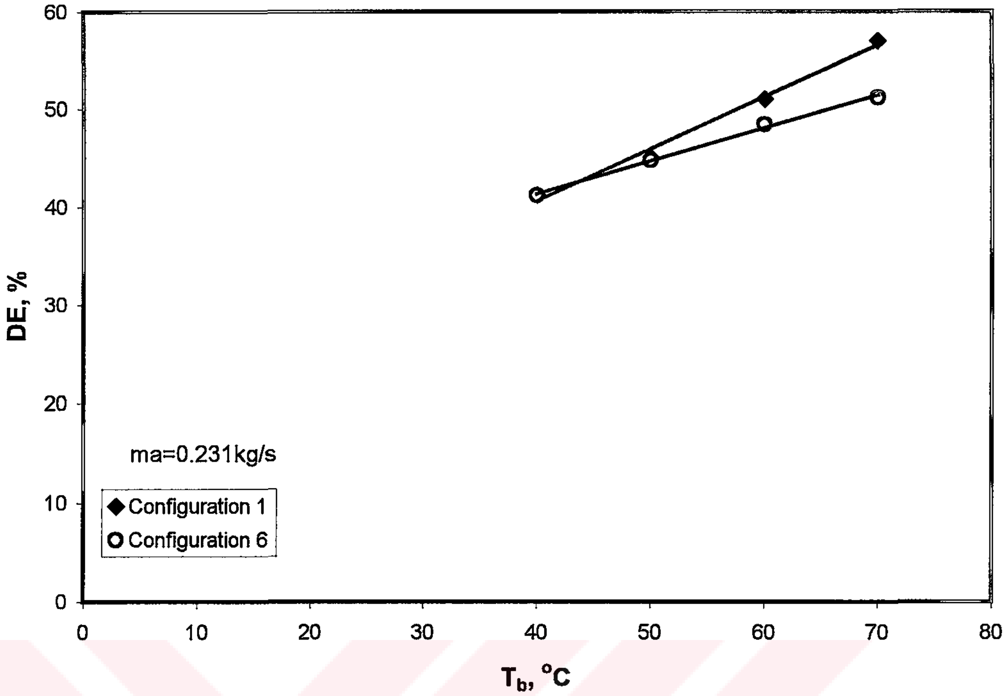

Figure 5.3.17 The variation of mean DE with the T_b in the bed at m_a=0.231kg/s for the configurations 1 and 6

5.4 THE EFFECTS OF AIR MASS FLOW RATE IN THE BED FOR DRYING WHEAT GRAINS

In order to see the effects of air mass flow rate in the bed for drying the wet wheat grains, the drying experiments were done at four different air mass flow rates of 0.1, 0.165, 0.231 and 0.264kg/s for the configuration 1 and at four different air mass flow rates of 0.1, 0.165, 0.2 and 0.231kg/s for the configuration 6 by using the electrical heater to heat the air flow entering into the bed at 50°C. The variation of air dry bulb and wet bulb temperatures at outlet and inlet sides of the bed with drying time during the test period of 40min are shown in the Figures 5.4.1-5.4.4 for the configuration 1 and in the Figures 5.4.5-5.4.8 for the configuration 6. From these figures, similar results are observed with that of the effects of bed temperature, which is explained in the previous section of 5.3.

The dry bulb temperatures at inlet and outlet sides of the bed are greater than the wet bulb temperatures at inlet and outlet sides of the bed during the test for either configuration, 1 and 6, as shown in the Figures 5.4.1-5.4.8. When the dry bulb temperatures at inlet side of the bed are remaining about constant at the range between ±2°C of 50°C, the dry bulb temperatures at outlet side of the bed are gradually increasing with the drying time for all tested air mass flow rates as shown in the Figures 5.4.1-5.4.8 for either configuration. While the differences between the dry bulb temperatures at inlet and outlet sides of the bed are high at the beginning of the drying test, these differences decrease towards the end of the test. The dry bulb temperatures at inlet side of the bed are greater than the dry bulb temperatures at outlet side of the bed for all tested air mass flow rates and for the configurations 1 during the test as shown in the Figures 5.4.1-5.4.4. The differences between the dry bulb temperatures at inlet and outlet sides of the bed are decreasing with the drying time especially for the configuration 1. On the other hand, for the configuration 6, the dry bulb temperatures at outlet sides of the bed are less than that of the inlet side of the bed, and the differences between the dry bulb temperatures at inlet and outlet sides of the bed are decreasing with the drying time and these differences are closing at the approximately half of the drying time, after that the dry bulb temperatures at outlet sides of the bed are greater than that of the inlet side of the bed for all tested air mass flow rates. At the same time, these results are clearly observed from the Figure 5.4.9 for the configuration 1 and from the Figure 5.4.10 for the configuration 6. Also, the differences between the dry bulb temperatures at inlet and outlet side of the bed are decreasing with the increasing air mass flow rates in the bed for the configurations 1 and 6 as shown in the Figures 5.4.9 and 5.4.10, respectively.

On the other hand, the wet bulb temperatures at inlet and outlet sides of the bed are less gradually increasing during the drying test and the difference between the wet bulb temperatures at inlet and outlet sides of the bed are remaining about constant with the drying time during the test period of 40min for the configuration 1 as shown in the Figures 5.4.1-5.4.4. This result is clearly observed from the Figure 5.4.11 for the configuration 1. In addition, the difference between the wet bulb temperatures at outlet and inlet sides of the bed are decreasing with the increasing air mass flow rates in the bed as shown in the Figure 5.4.11 for the configuration 1.

For the configuration 6, the wet bulb temperatures at outlet side of the bed are gradually increased at the first drying time of 15min for all tested air mass flow rates, and then they are about constant during the drying test while the wet bulb temperatures at inlet side of the bed are less gradually increasing with the drying time during the test for all tested air mass flow rates as shown in the Figures 5.4.5-5.4.8. The differences between the wet bulb temperatures at outlet and inlet sides of the bed are decreasing with the drying time, that is, when these differences are high at the beginning of the drying test, the differences between the wet bulb temperatures at outlet and inlet sides of the bed are closing toward the end of the drying test. This result is clearly observed from the Figure 5.4.12 for the configuration 6. From this figure, the differences between the wet bulb temperatures at outlet and inlet sides of the bed are decreasing with the drying time and at the same time the differences between them are increasing with the increasing air mass flow rate for the configuration 6.

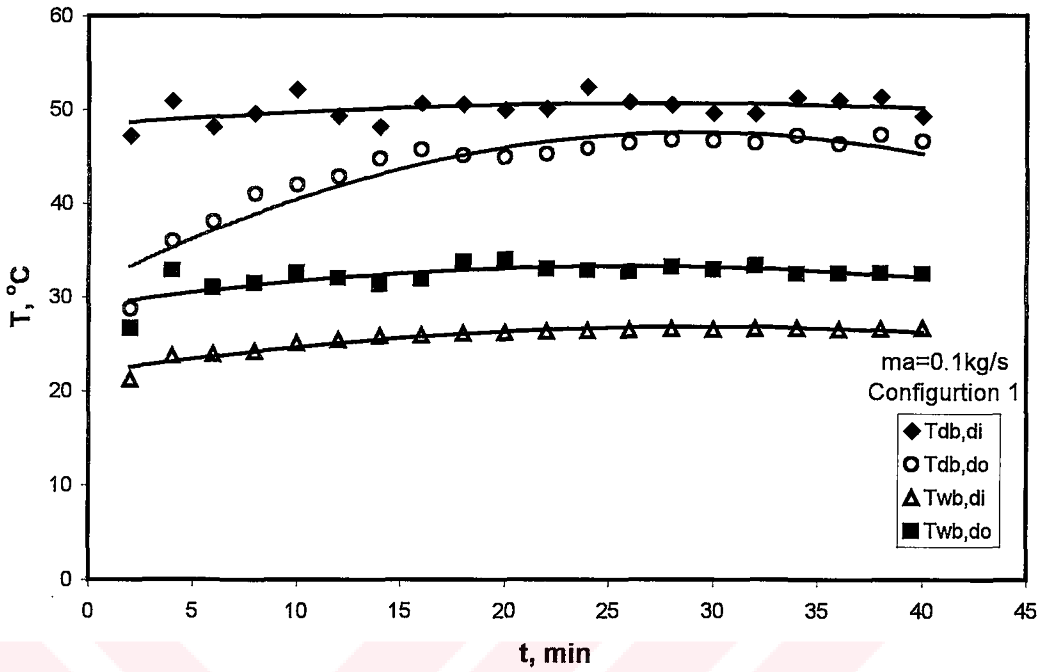

Figure 5.4.1 The variation T_{db} and T_{wb} at inlet and outlet sides of the bed with time at m_a=0.1kg/s in the bed for the configuration 1

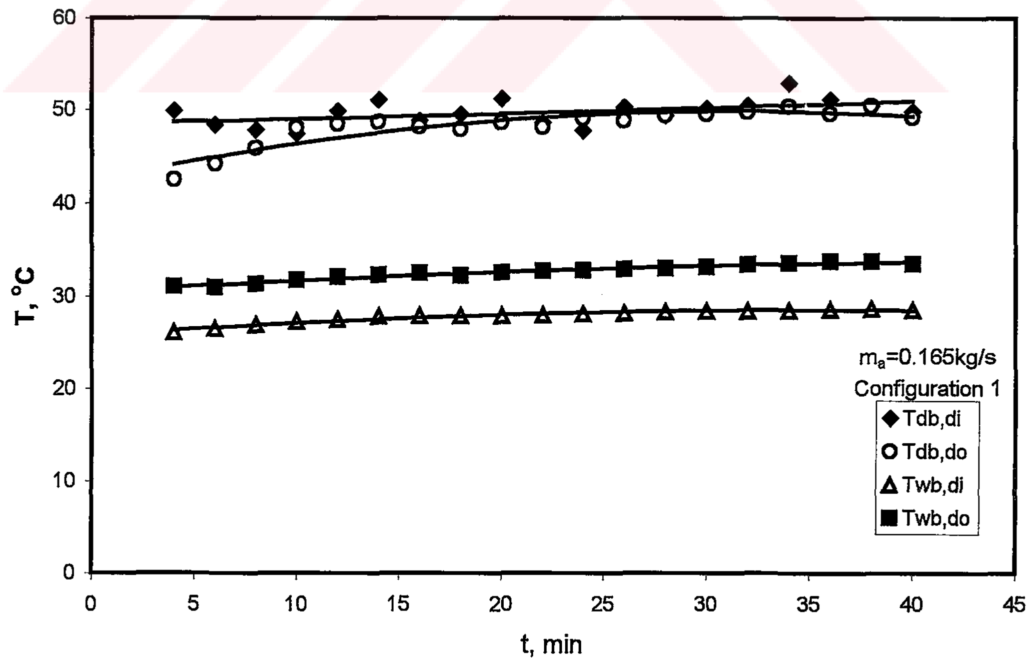

Figure 5.4.2 The variation T_{db} and T_{wb} at inlet and outlet sides of the bed with time at m_a=0.165kg/s in the bed for the configuration 1

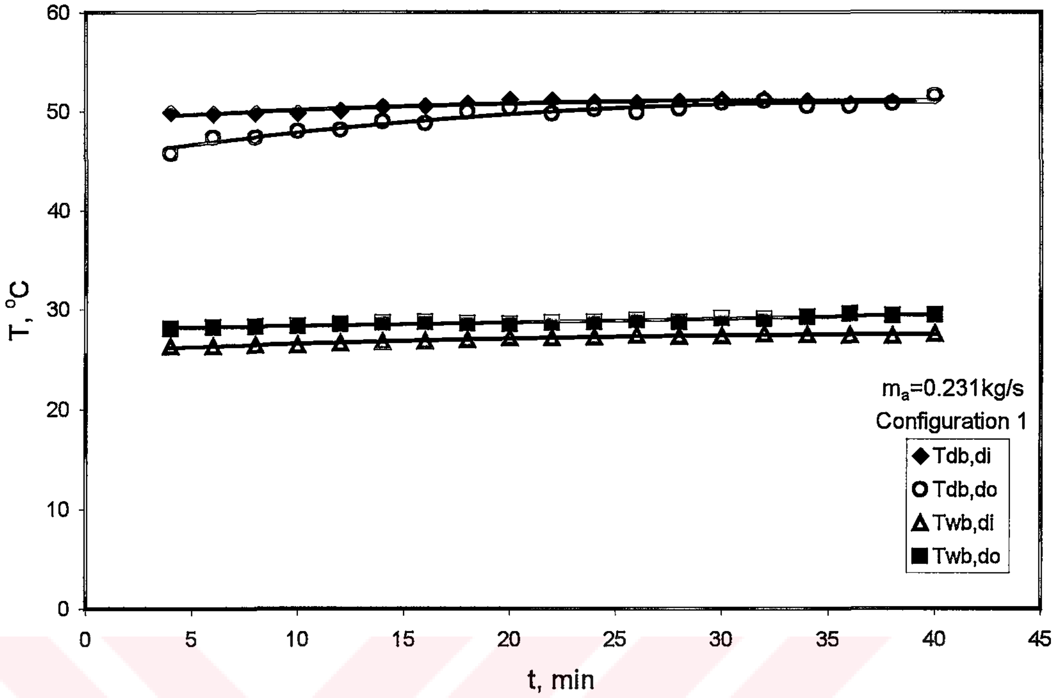

Figure 5.4.3 The variation T_{db} and T_{wb} at inlet and outlet sides of the bed with time at m_a=0.231kg/s in the bed for the configuration 1

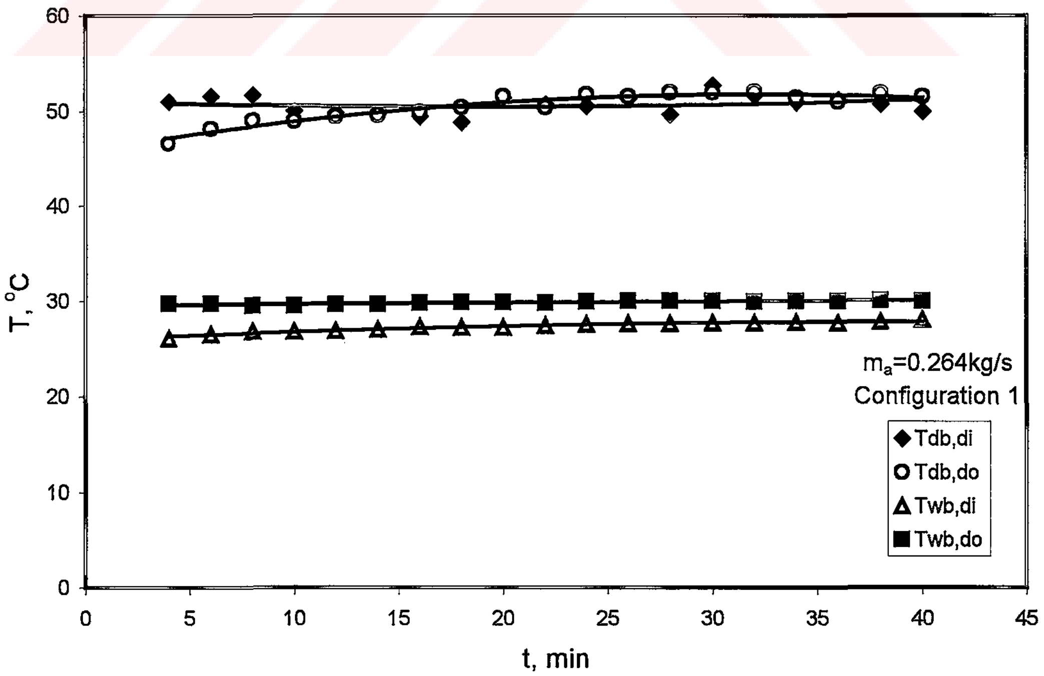

Figure 5.4.4 The variation T_{db} and T_{wb} at inlet and outlet sides of the bed with time at m_a=0.264kg/s in the bed for the configuration 1

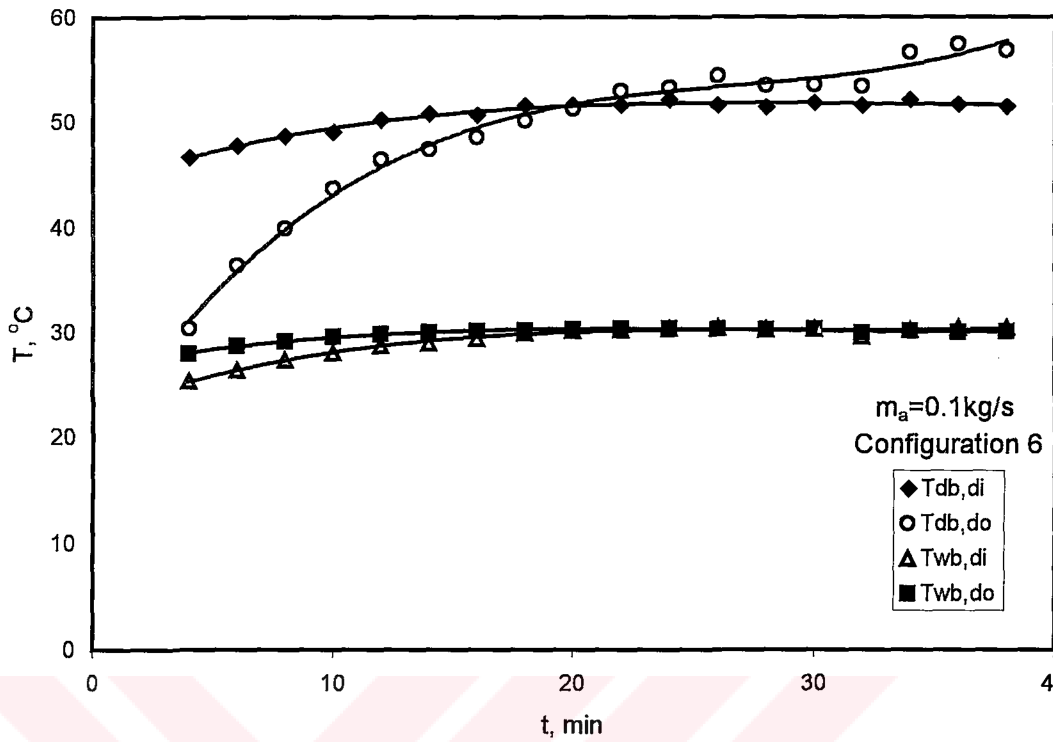

Figure 5.4.5 The variation T_{db} and T_{wb} at inlet and outlet sides of the bed with time at m_a=0.1kg/s in the bed for the configuration 6

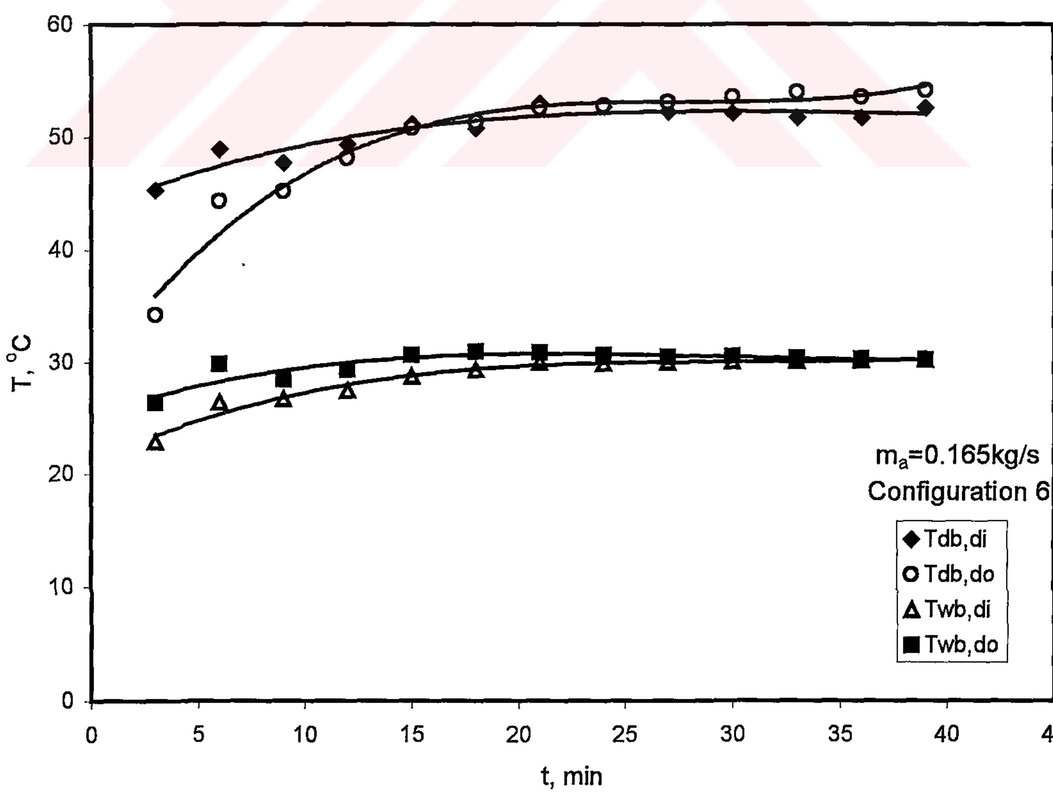

Figure 5.4.6 The variation T_{db} and T_{wb} at inlet and outlet sides of the bed with time at m_a=0.165kg/s in the bed for the configuration 6

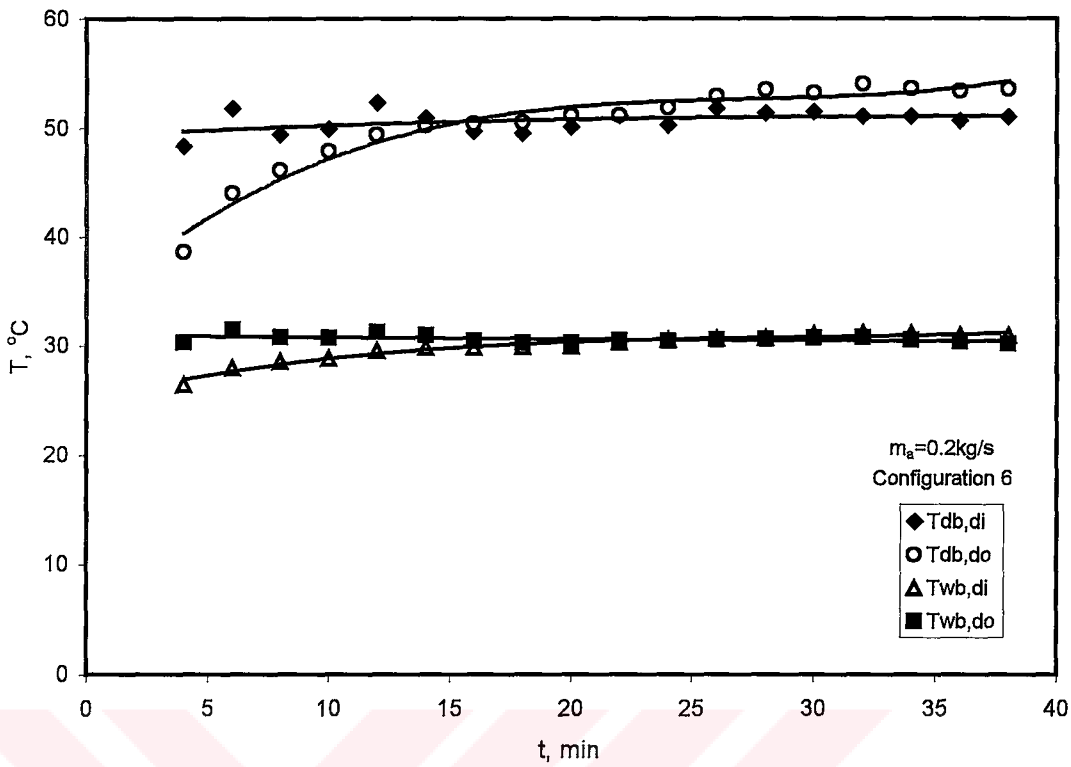

Figure 5.4.7 The variation T_{db} and T_{wb} at inlet and outlet sides of the bed with time at m_a=0.2kg/s in the bed for the configuration 6

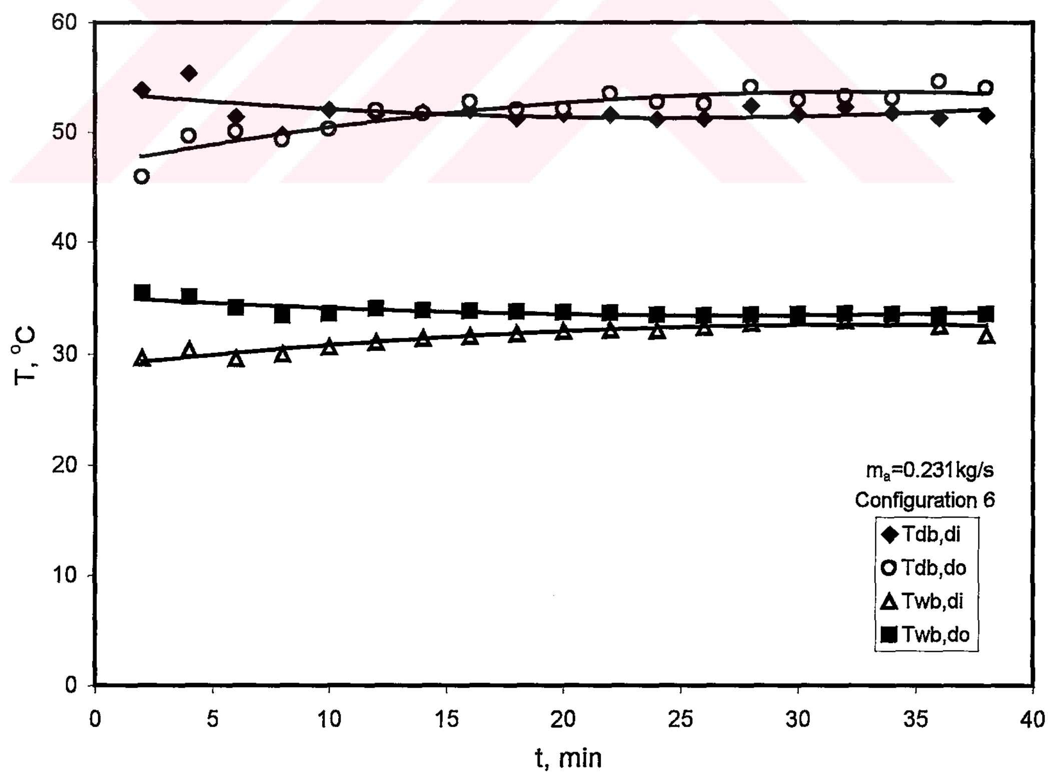

Figure 5.4.8 The variation T_{db} and T_{wb} at inlet and outlet sides of the bed with time at m_a=0.231kg/s in the bed for the configuration 6

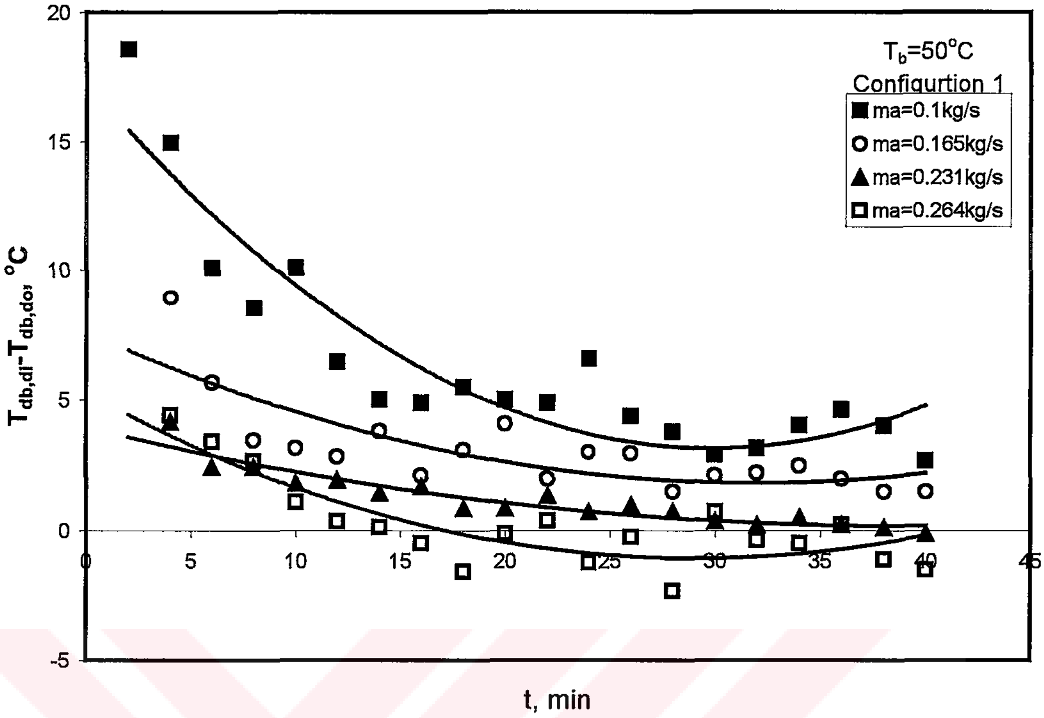

Figure 5.4.9 The variation of difference between T_{db} at inlet and outlet sides of the bed with time at the T_b=50°C for different m_a in the bed for the configuration 1

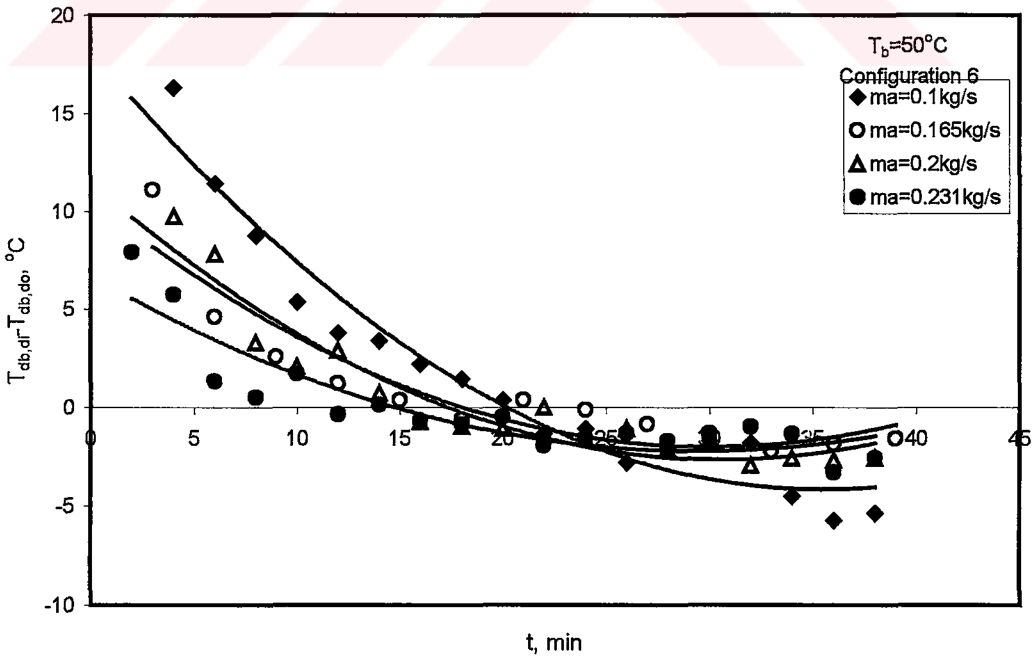

Figure 5.4.10 The variation of difference between T_{db} at inlet and outlet sides of the bed with time at the T_b=50°C for different m_a in the bed for the configuration 6

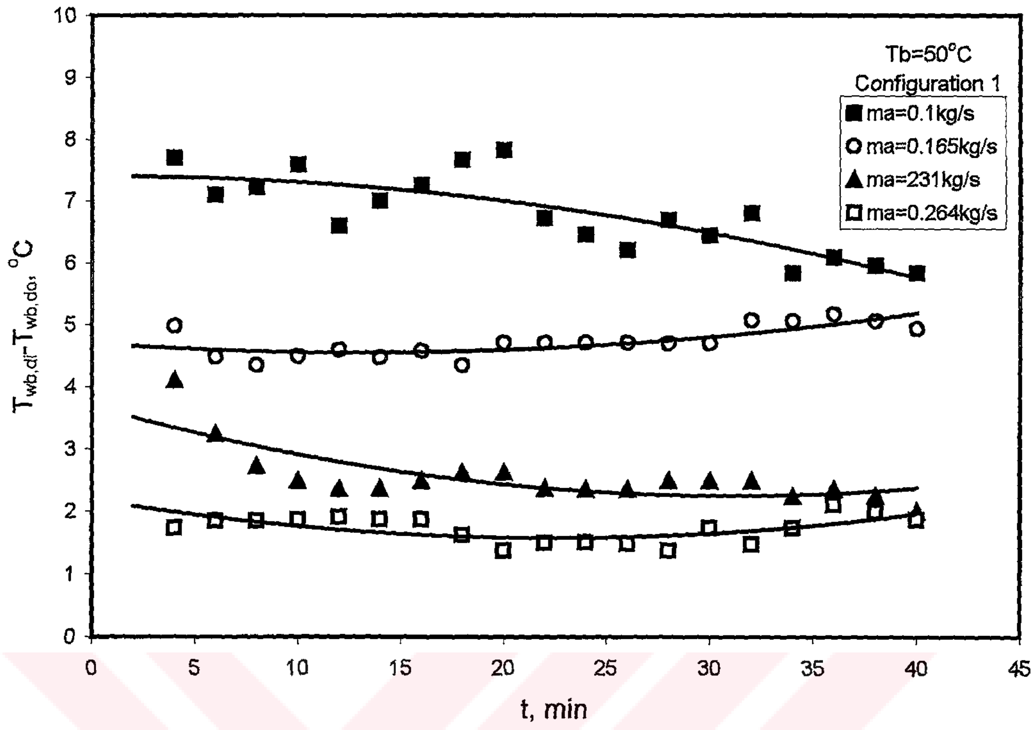

Figure 5.4.11 The variation of difference between T_{wb} at inlet and outlet sides of the bed with time at the T_b=50°C for different m_a in the bed for the configuration 1

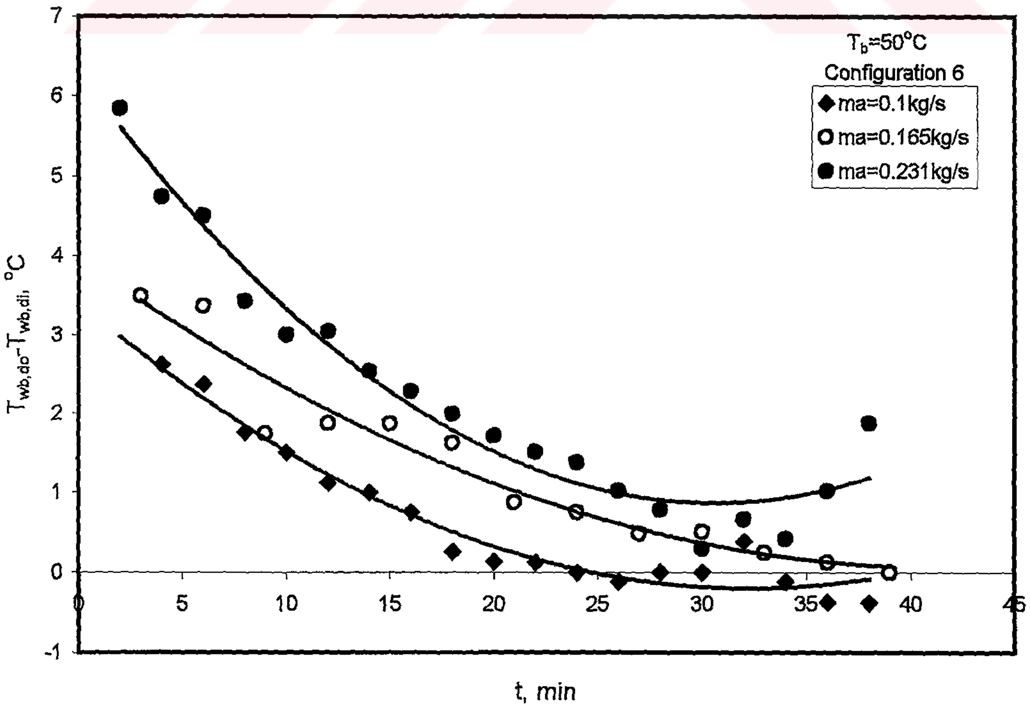

Figure 5.4.12 The variation of difference between T_{wb} at inlet and outlet sides of the bed with time at the T_b=50°C for different m_a in the bed for the configuration 6

The variations of MER with the drying time are plotted in the Figure 5.4.13 for the configuration 1 and in the Figure 5.4.14 for the configuration 6 at 4 different air mass flow rates in the bed and in the bed temperature of 50°C. The MER values are gradually decreasing with the drying time for either configuration as shown in the Figures 5.4.13 and 5.4.14. Furthermore, the higher air mass flow rates in the bed result the higher MER values for the either configuration. In order to see more clearly this result, the mean MER values during the drying test are plotted corresponding to the air mass flow rates for either configuration in the Figure 5.4.15, a less gradually increase in mean MER values with the increasing air mass flow rate in the bed are observed. The mean MER values for the configuration 6 are also higher than that of the configuration 1 for all tested air mass flow rates and the variations of mean MER values with the drying time are about linear for the configurations 1 and 6 and are about parallel to each other. These linear relations between the mean MER and the air mass flow rates in the bed are given in the following equations for the configurations 1 and 6 with the error margin of about ±5 percent and ±2.5 percent, respectively,

$$MER=0.0967m_a+0.1635 \quad \text{for the configuration 1} \qquad (5.4.1)$$

and

$$MER=0.1432m_a+0.1769 \quad \text{for the configuration 6} \qquad (5.4.2)$$

When compared these linear increases in MER with the increasing air mass flow rate and the increasing air dry bulb temperature in the bed, the increase in MER with the increasing air mass flow rate is less according to that of the increasing air dry bulb temperature as shown in the Figures 5.3.15 and 5.4.15. So, the variation of air dry bulb temperature in the bed has much important effect than that of the air mass flow rate in the bed in order to increase the MER of drying process.

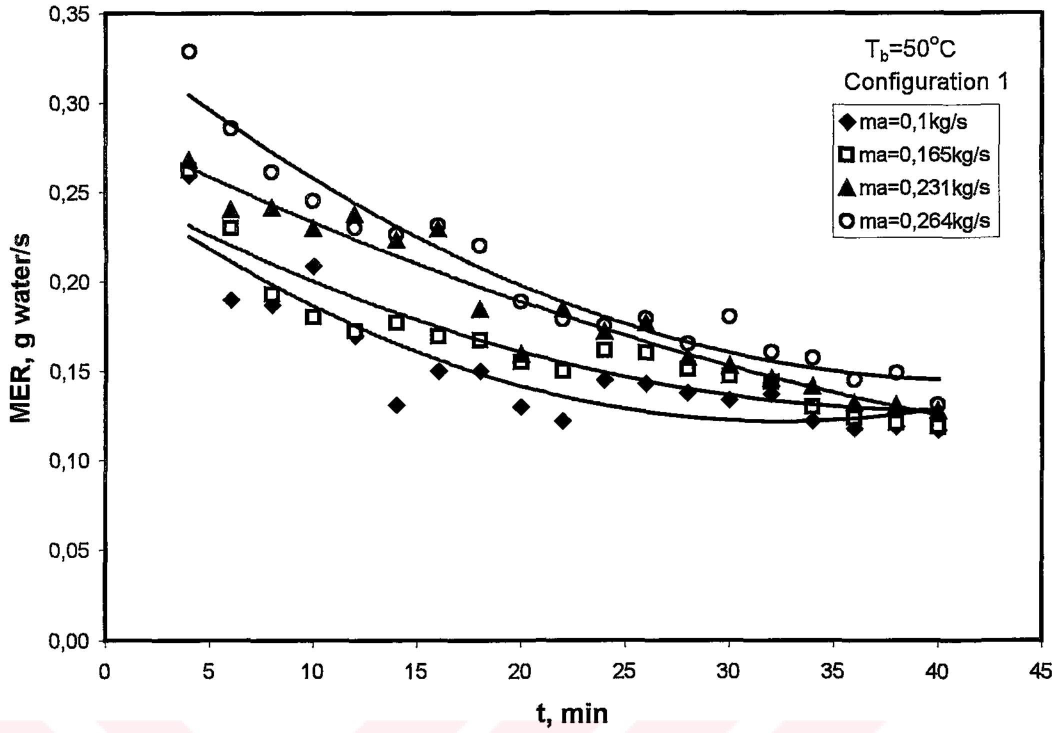

Figure 5.4.13 The variation of MER with time at T_b=50°C in the bed for the different m_a in the bed for the configuration 1

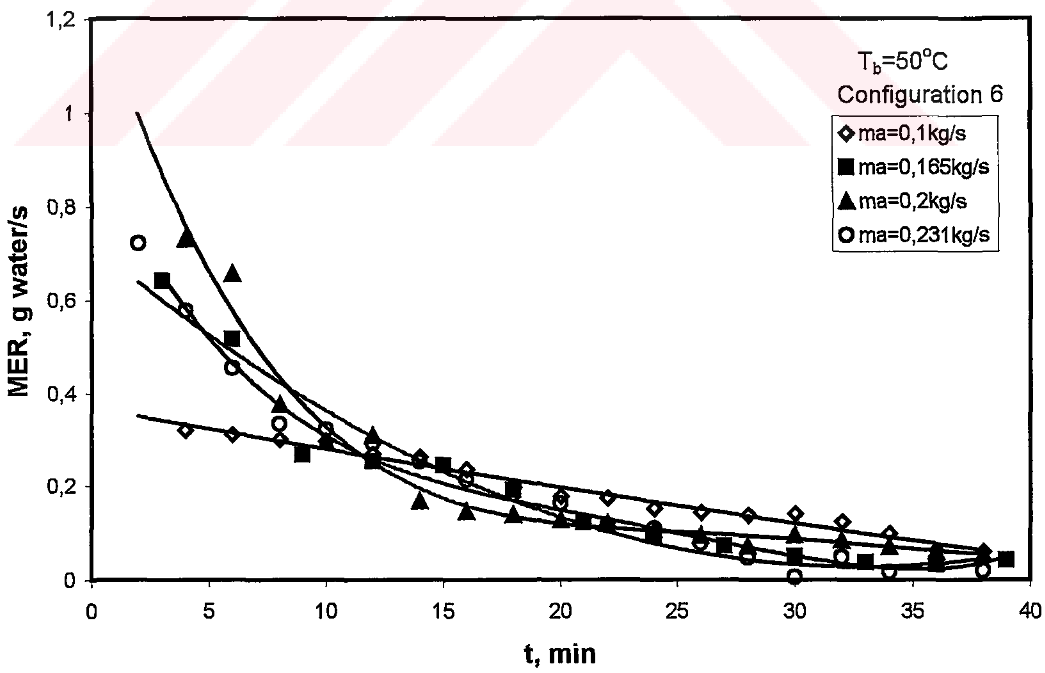

Figure 5.4.14 The variation of MER with time at T_b=50°C in the bed for the different m_a in the bed for the configuration 6

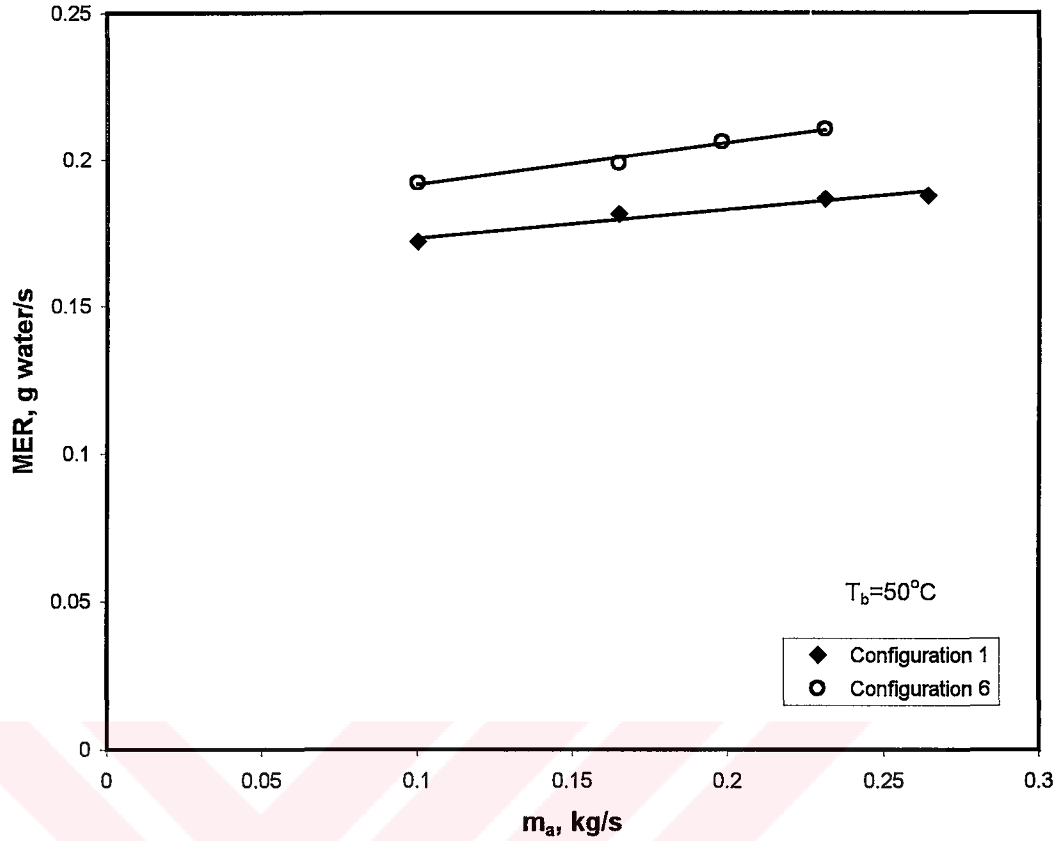

Figure 5.4.15 The variation of mean MER with m_a at T_b=50°C in the bed for the configurations 1 and 6

The variations of the SMER with the air mass flow rate in the bed are plotted in the Figure 5.4.16 for the configurations 1 and 6. The SMER is decreasing when the air mass flow rate in the bed is increasing for either configuration as shown in the Figure 5.4.16, and these decreases in the SMER with the increasing air mass flow rate are about linear. The cause of this result is that the necessary power consumed by the fan is increasing in order to supply the air at higher mass flow rates into the bed and the power consumed by the electrical heater is increasing in order to obtain the hot air flow in the bed at higher air mass flow rates. Also, the SMER values for the configurations 6 are higher than that of the configurations 1 for all tested air mass flow rates as shown in the Figure 5.4.16, and the variation of the SMER for either configuration are about parallel to each other. Also, the linear relations between the SMER and the air mass flow rates are given in the following equations for the configurations 1 and 6 with the error margin of about ±4 percent and ±2.4 percent, respectively,

$$SMER=-0.1125m_a+0.059 \quad \text{for the configuration 1} \qquad (5.4.3)$$

and

$$SMER=-0.1467m_a+0.078 \quad \text{for the configuration 6} \qquad (5.4.4)$$

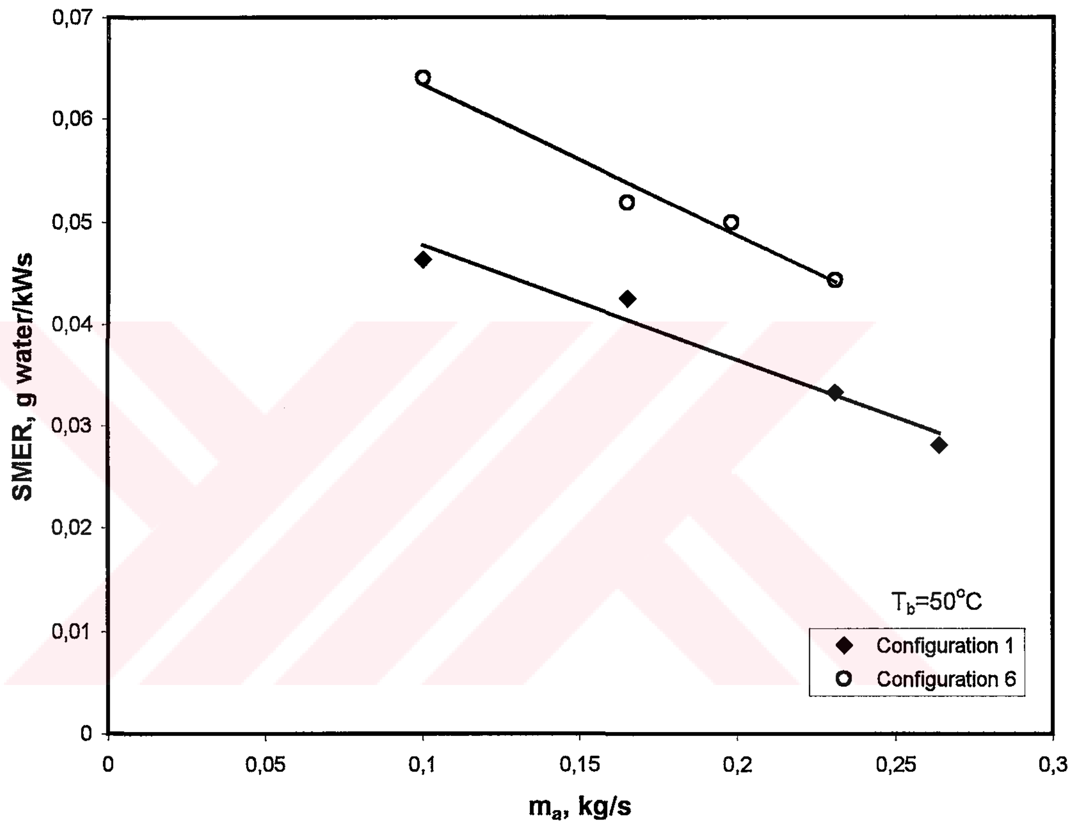

Figure 5.4.16 The variation of mean SMER with m_a at T_b=50°C in the bed for the configurations 1 and 6

The mean DE values during the drying test are plotted corresponding to the air mass flow rates in the bed in the Figure 5.4.17 for the configurations 1 and 6. The DE is decreasing when the air mass flow rate in the bed is increasing for either configuration as shown in the Figure 5.4.17. These variations of DE with the air mass flow rate are parabolic for either configuration and these parabolic relations between the DE and air mass flow rate are given in the following equations for the configurations 1 and 6 with the error margin of about ± 0.4 for either,

$$DE=-998.37m_a^2+222.65m_a+46.06 \quad \text{for the configuration 1} \qquad (5.4.5)$$

and

$$DE=-2135.6m_a^2+462m_a+52.3 \quad \text{for the configuration 6} \qquad (5.4.6)$$

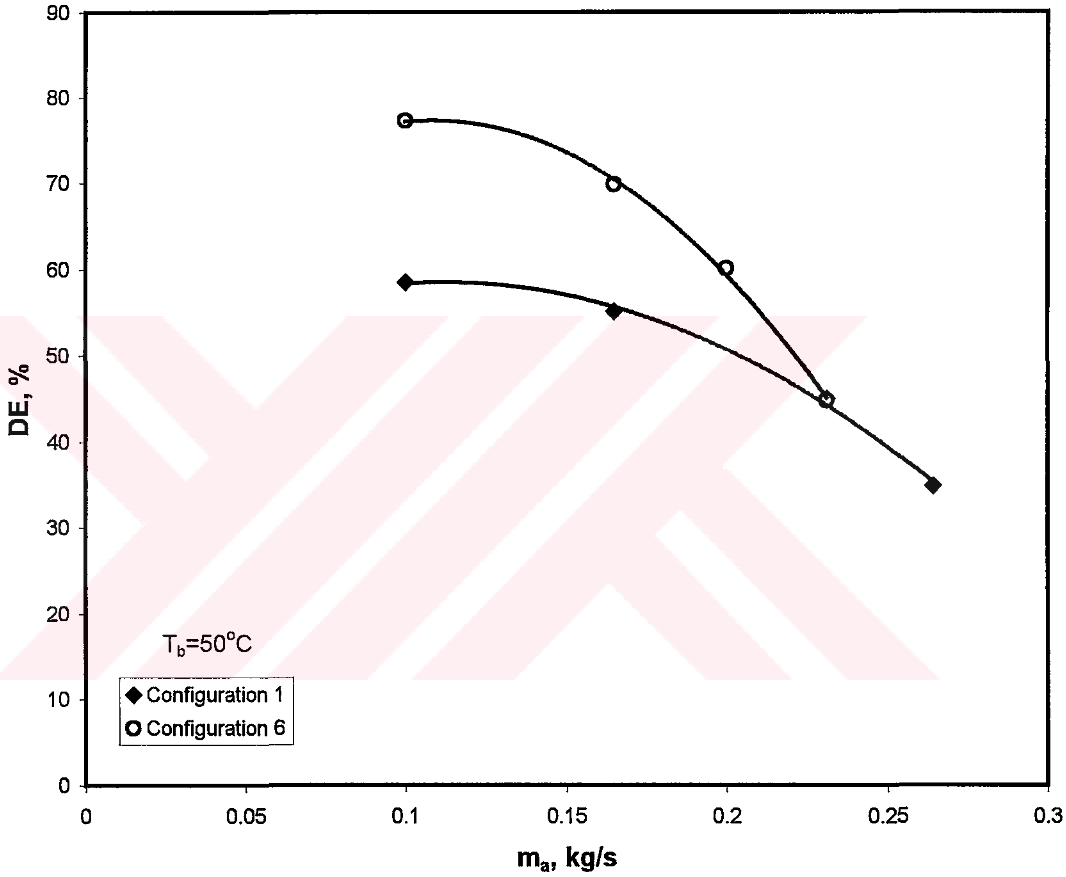

Figure 5.4.17 The variation of mean DE with the ma at T_b=50°C in the bed for the configurations 1 and 6

5.5 THE EXPERIMENTAL INVESTIGATIONS OF THE FLOW FIELD DEVELOPMENT IN THE BED

In the concept of investigation of the flow field in the bed, the axial air flow velocities in the empty bed, which any swirl generator is not placed in, were measured, and the axial and tangential velocity components of the swirling air flow in the bed, which the swirl generators are placed at upstream section of the bed, were measured at 3 different Re, 50000, 90000 and 125000, by traversing the three-tube pressure probe across the bed cross-section. In order to generate the swirling flow field in the bed, 13 different axial guide vane type swirl generators, which have different configurations, were used. The configuration types, codes and dimensions of tested swirl generators are given in the Table 3.2 in the section of 3.2.3.

Figure 5.5.1 shows the axial velocity distributions in the empty bed and the bed in which placed swirl generators, that is, in the non-swirling and swirling flow fields. The axial velocity measurements present the non-parabolic distribution in the empty bed, that is, the axial velocity distribution in the empty bed is remaining about constant across the cross section of the bed as shown in the Figure 5.5.1. In contrast, the swirl generators cause the parabolic axial velocity distributions. In other words, the swirl generators present that the axial velocity magnitudes decrease parabolically from the wall to the center axis of the bed as shown in the Figure 5.5.1. The axial velocity magnitudes in the bed, which swirl generators were placed in, are greater than that of the empty bed especially in the region near the bed wall, however, the axial velocity magnitudes in the swirling flow fields in the bed are less than that of the non-swirling flow in the bed in the core region near the center axis of the bed. Also, this decrease in the axial velocity magnitudes from the wall to the center of the bed in the swirling flow field increases with the increasing swirl number as shown in the Figure 5.5.1. When the axial velocity magnitudes are less gradually decreasing from the wall to the center of the bed in the swirling flow field, which has the lowest swirl number of 0.204, the axial velocity magnitudes are parabolically decreasing from the wall to the center axis of the bed in the swirling flows, which have higher swirl numbers. The flow is becoming stagnant near the center axis of the bed in the swirling flow field which has the swirl number of 0.48 and 0.637, and back flow is occurring in the region about the center axis of the bed in the swirling flow which has the highest swirl number of 0.637. When the little back flow is occurring exactly at the axis of the bed for the swirling flow field which has the swirl number of 0.48, the flow is becoming stagnant at the station of y=130mm in the swirling flow field which has the swirl number of 0.637, that is, the back flow is occurring in the core region which covers the region of r=20mm from the axis of the bed for the swirling flow field which has the highest swirl number of 0.637 as shown in the Figure 5.5.1. However, any back flow is not occurring in the swirling flow field which has lower swirl numbers, only the axial velocity magnitudes are decreasing towards to axis of the bed, that is, any slowness in the flow is observed from the wall to the axis of the bed at lower swirl numbers.

The Figure 5.5.2 represents the tangential velocity distributions in the swirling flow field in the bed. When there is no any tangential velocity components of the air flow in the non-swirling flow field in the bed, the tangential velocity magnitudes represent any distributions across the bed in the swirling flow field. The tangential velocity magnitudes are gradually increasing from the wall to the center axis of the bed, but at any station near the center axis of the bed the tangential velocity magnitudes are beginning to abruptly decrease and these decreases in the tangential velocity magnitudes near the center of the bed are approaching to zero at the center axis of the bed. In other words, there is less tangential flow in the region near the axis of the bed, in fact, it can be said that there is no any tangential flow in the center axis of the bed. This core region, which the tangential velocities decrease in, is less for the swirling flow field which has lower swirl numbers; and is large for the swirling flow field which has higher swirl numbers. That is, when the decrease in tangential velocity magnitudes towards to the axis of the bed is occurring at the station of y=125mm for S=0.637, it is occurring at the station of y=140mm for S=0.3 as shown in the Figure 5.5.2. Also, the higher tangential velocity magnitudes are observed for the swirling flow field which has higher swirl numbers as shown in the Figure 5.5.2. In other words, the tangential velocity magnitudes increase with the increasing swirl number.

The Figure 5.5.3 represents the variation of S with Re. It is observed that there is no any variation in swirl number magnitudes with the Re as shown in this figure.

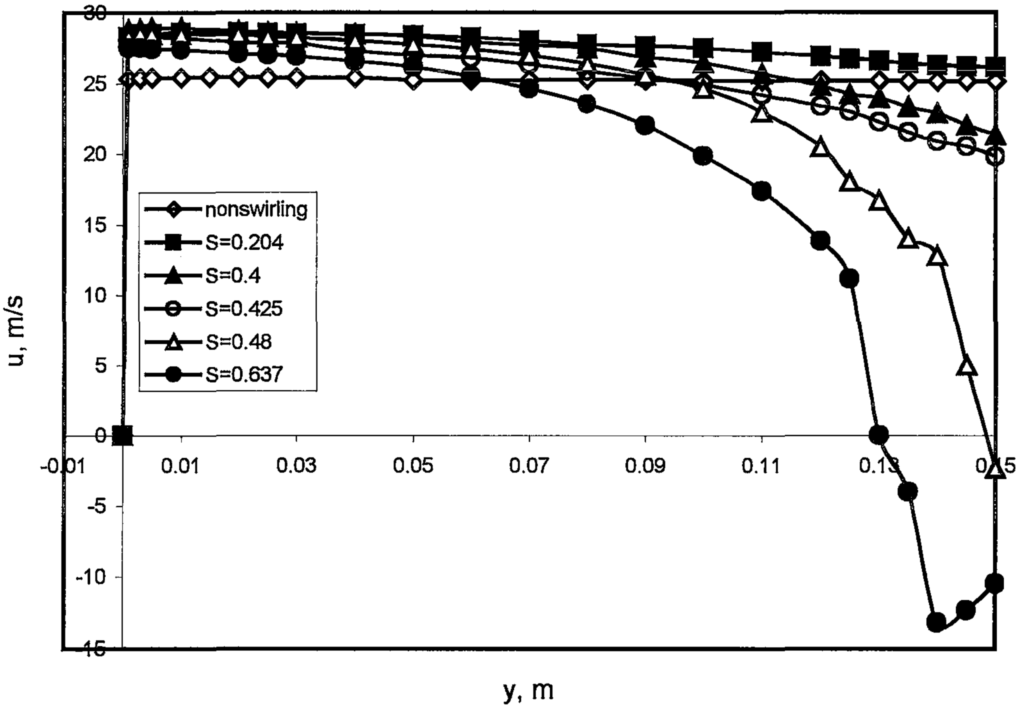

Figure 5.5.1 The axial air velocity distributions in the non-swirling and swirling flow fields in the bed

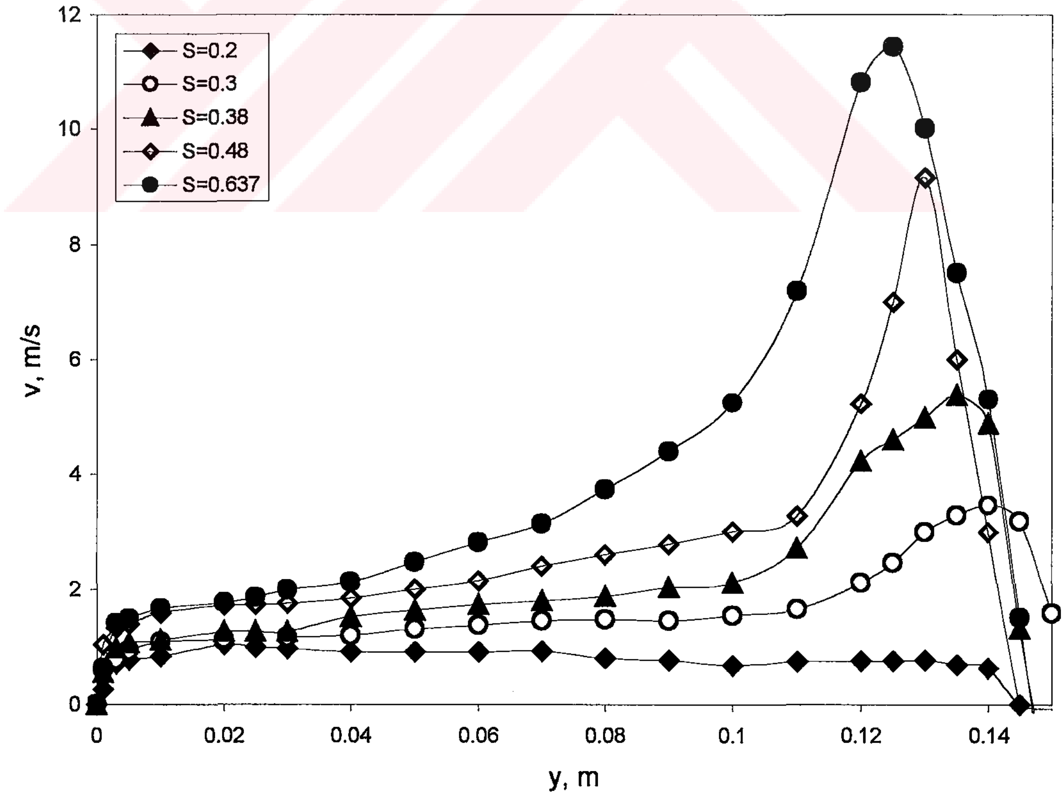

Figure 5.5.2 The tangential velocity distributions in the swirling flow field in the bed

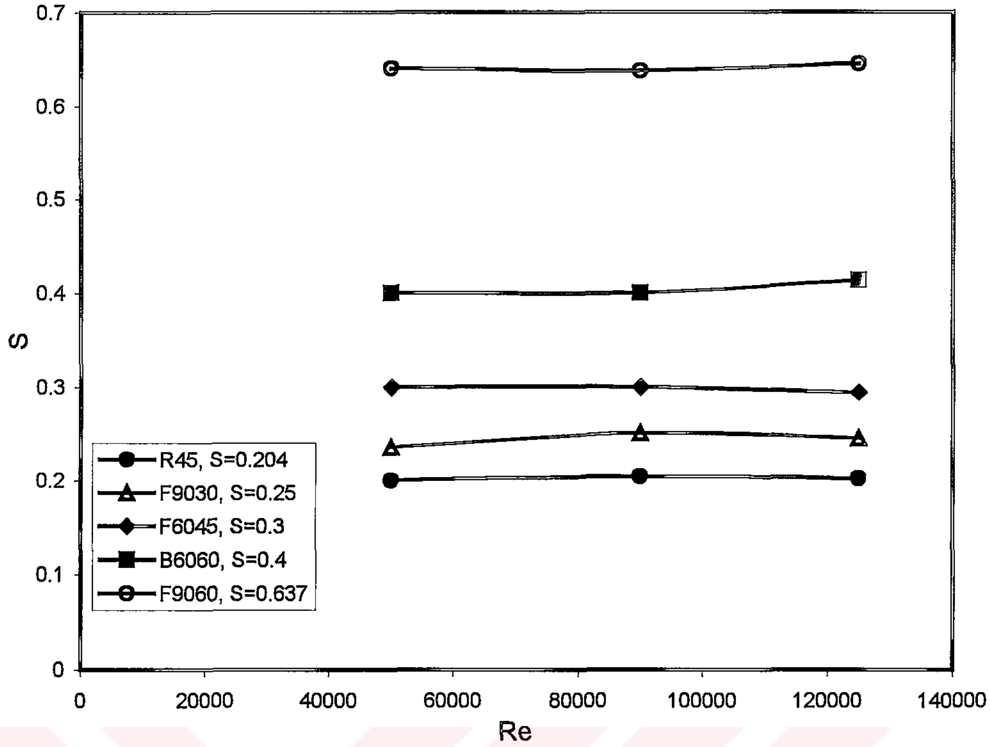

Figure 5.5.3 The variation of swirl numbers, S, with the Re

5.6 THE EFFECTS OF SWIRLING FLOW FIELD IN THE BED ON DRYING OF WHEAT GRAINS

At seven different swirl numbers, S, the drying tests were done in order to see the effect of swirling flow field in the bed for drying the wheat grains. Experiments were done at air dry bulb temperature of 50°C and mass flow rate of 0.231kg/s in the bed for the configuration 1 for all sets. The measured dry bulb and wet bulb temperatures at inlet and outlet sides of the bed during the drying test period of 40min are plotted in the Figures 5.6.1-5.6.7. The results observed from these figures are similar to the results observed in the configuration, bed temperature and mass flow rate experiments, which were previously explained. As shown in the Figures 5.6.1-5.6.7, the dry bulb temperatures at inlet and outlet sides of the bed are greater than that of the wet bulb temperatures at inlet and outlet sides of the bed for all sets. Also, when dry bulb temperatures at inlet side of the bed are greater than that of the outlet side of the bed, wet bulb temperatures at outlet side of the bed are greater than that of the inlet side of the bed during the test period for all sets. When the dry bulb temperatures at inlet side of the bed are remaining about constant in the range between ±2°C of bed temperature of 50°C, the dry bulb temperatures at outlet side of the bed are gradually increasing with the drying time and it is closing to the dry bulb temperatures at inlet side of the bed towards the end of the drying duration as shown in the Figures 5.6.1-5.6.7. In other words, the difference between the dry bulb temperature magnitudes at inlet and outlet sides of the bed are greater at the beginning of the drying test, and this difference is decreasing towards the end of the drying time, and towards the end of the drying time the difference between them is closing as shown in these figures. That is, a decrease in the difference between the dry bulb temperatures at inlet and outlet sides of the bed with drying time is observed for all tests. At the same time, this result is clearly shown in the Figure 5.6.8. Also, the differences between the dry bulb temperatures at inlet and outlet sides of the bed, which has the swirling flow field in, are compared with that of the non-swirling flow field by plotting the variation of dry bulb temperature difference between the inlet and outlet sides of the bed with the drying time in the Figure 5.6.8. The differences between the inlet and outlet sides of the bed for the swirling flow field are greater than that of the non-swirling flow field as shown in the Figure 5.6.8.

The wet bulb temperatures at inlet and outlet sides of the bed are exposing a less gradual variation during the drying time as shown in the Figures 5.6.1-5.6.7, and the wet bulb temperatures at outlet side of the bed are also greater than that of the inlet side of the bed. The wet bulb temperature differences between the outlet and inlet sides of the bed are plotted corresponding to the drying time in the Figure 5.6.9, and the differences between wet bulb temperatures at outlet and inlet sides of the bed, which has the swirling flow field in, are greater than that of the non-swirling flow field in the bed as shown in the Figure 5.6.9. At the same time, when this difference is about constant with the drying time for the non-swirling flow field in the bed, the differences between the wet bulb temperatures at outlet and inlet sides of the bed for the swirling flow field are decreasing with the drying time as shown in the Figure 5.6.9.

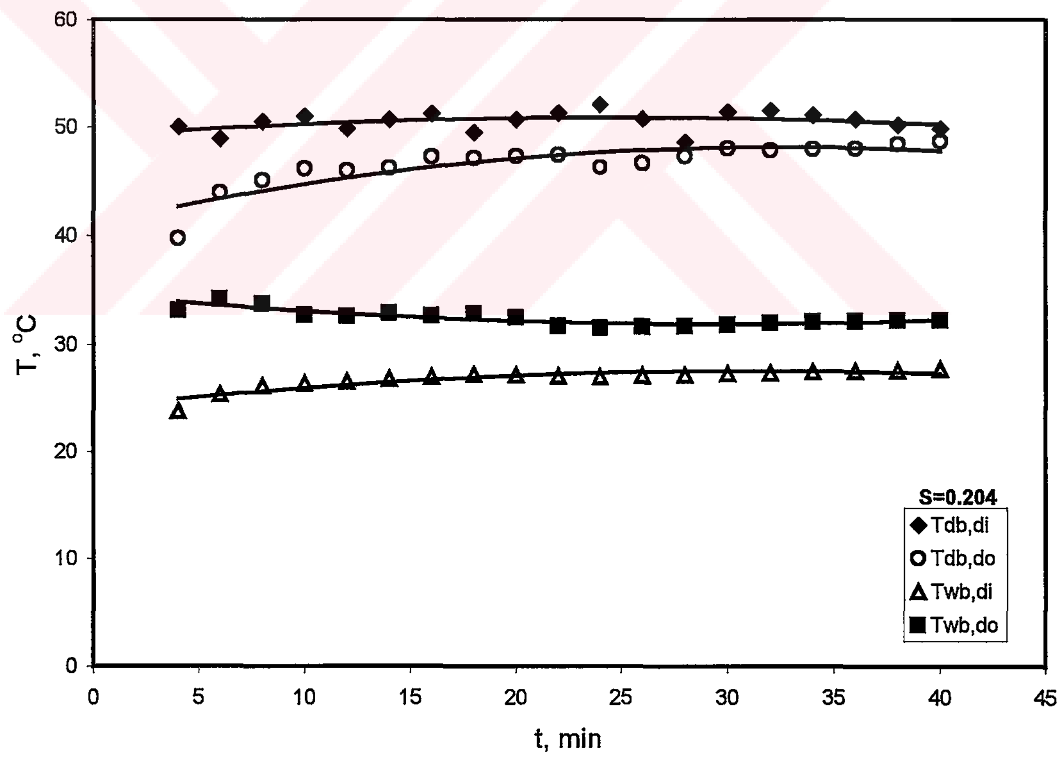

Figure 5.6.1 The variation of T_{db} and T_{wb} at inlet and outlet sides of the bed in the swirling flow field with S=0.204

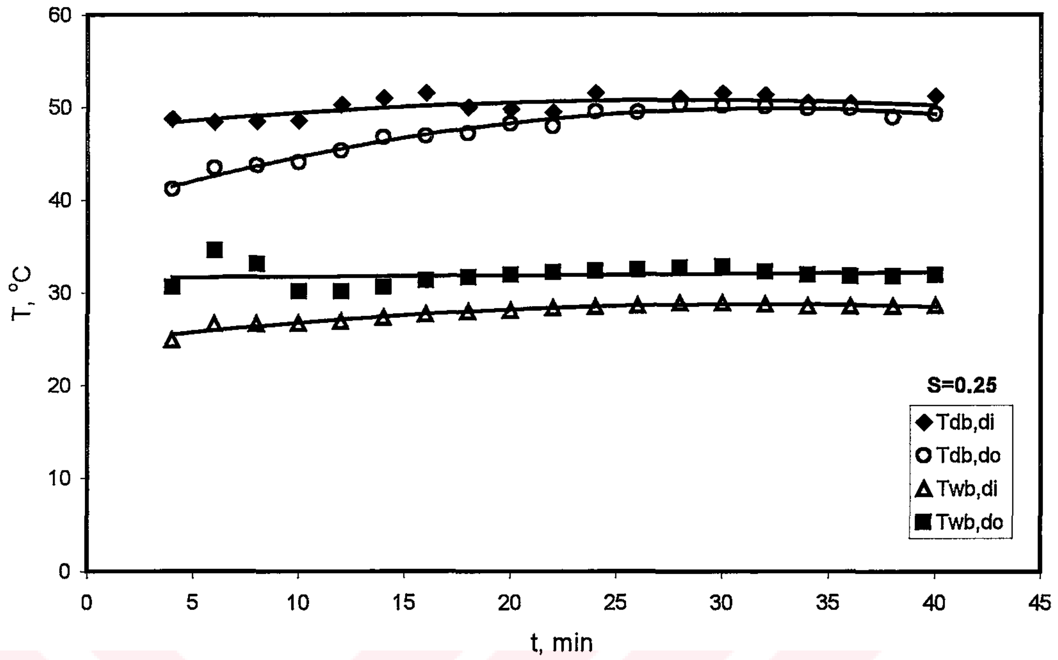

Figure 5.6.2 The variation of T_{db} and T_{wb} at inlet and outlet sides of the bed in the swirling flow field with S=0.25

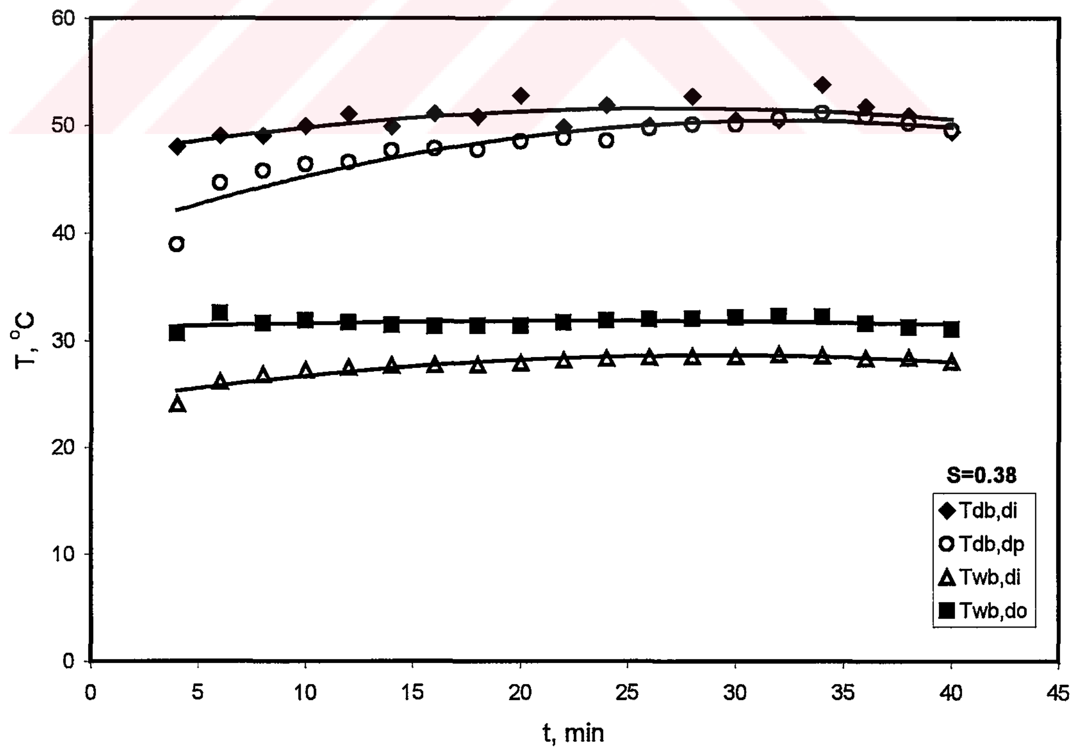

Figure 5.6.3 The variation of T_{db} and T_{wb} at inlet and outlet sides of the bed in the swirling flow field with S=0.38

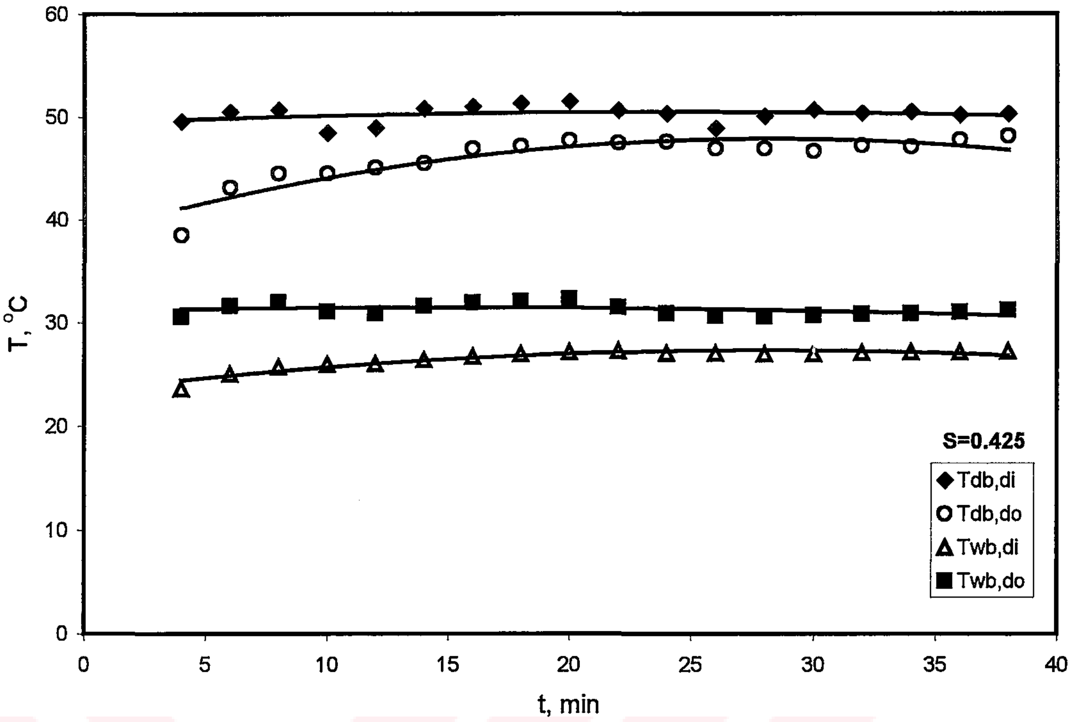

Figure 5.6.4 The variation of T_{db} and T_{wb} at inlet and outlet sides of the bed in the swirling flow field with S=0.425

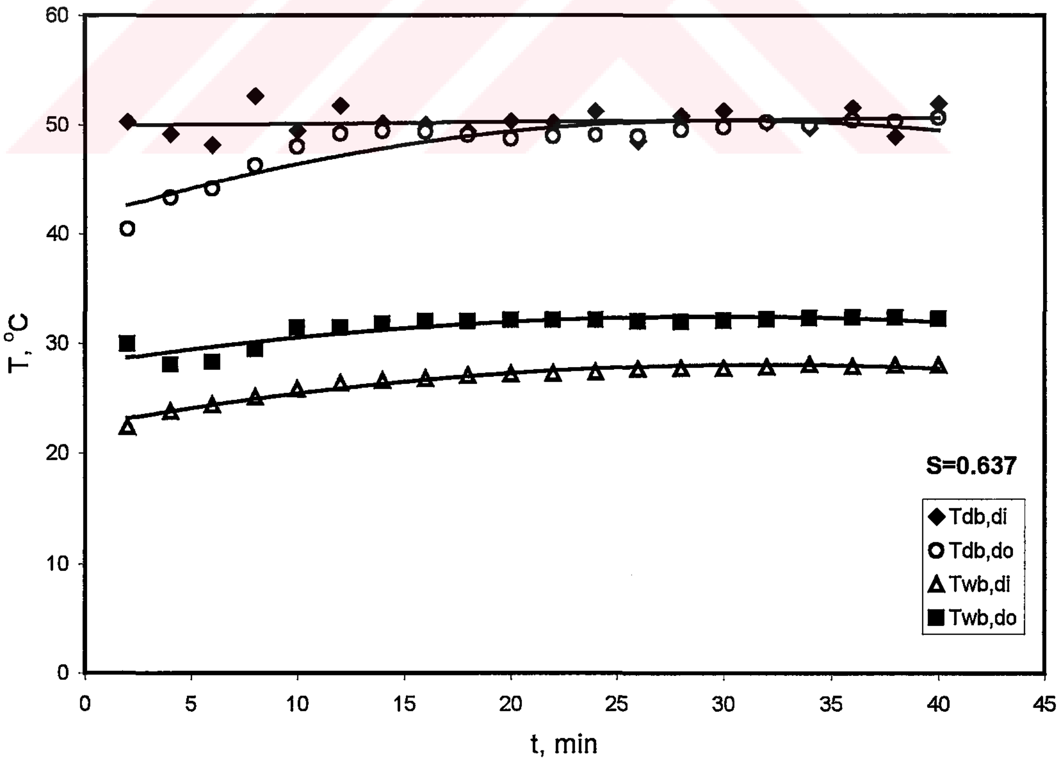

Figure 5.6.5 The variation of T_{db} and T_{wb} at inlet and outlet sides of the bed in the swirling flow field with S=0.637

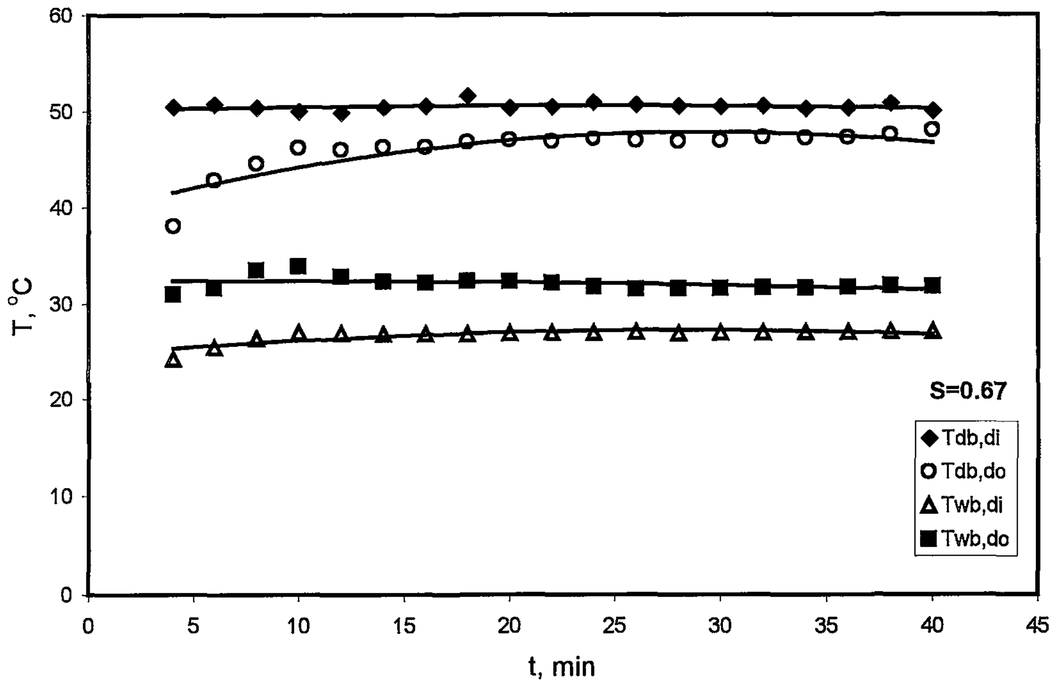

Figure 5.6.6 The variation of T_{db} and T_{wb} at inlet and outlet sides of the bed in the swirling flow field with S=0.67

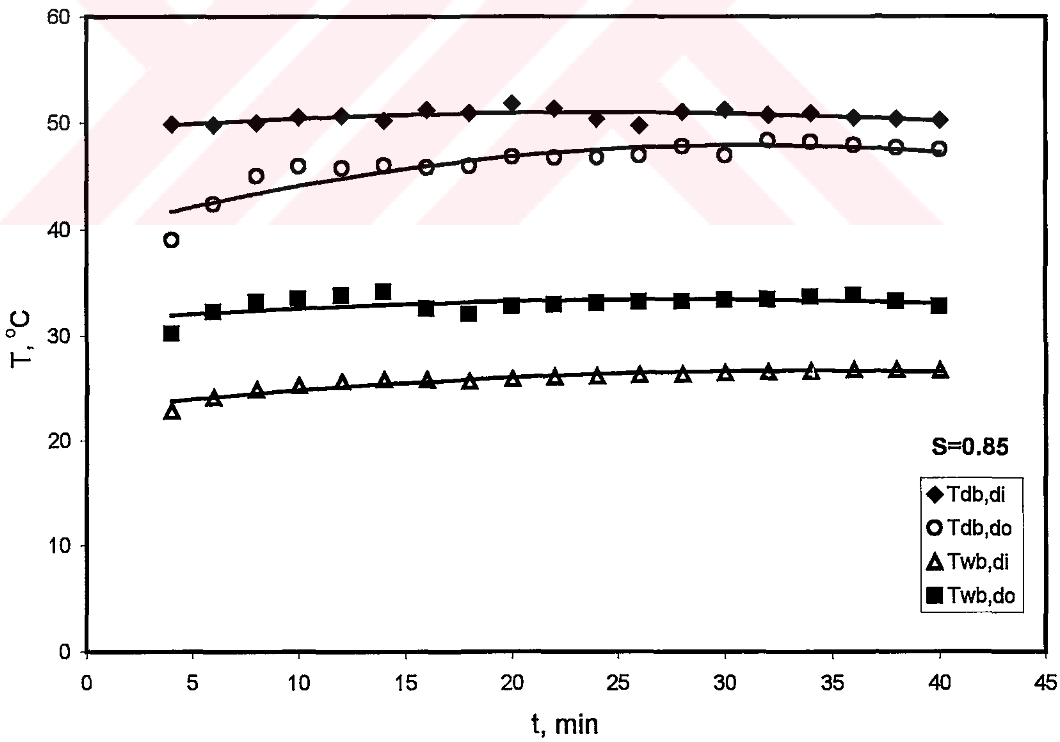

Figure 5.6.7 The variation of T_{db} and T_{wb} at inlet and outlet sides of the bed in the swirling flow field with S=0.85

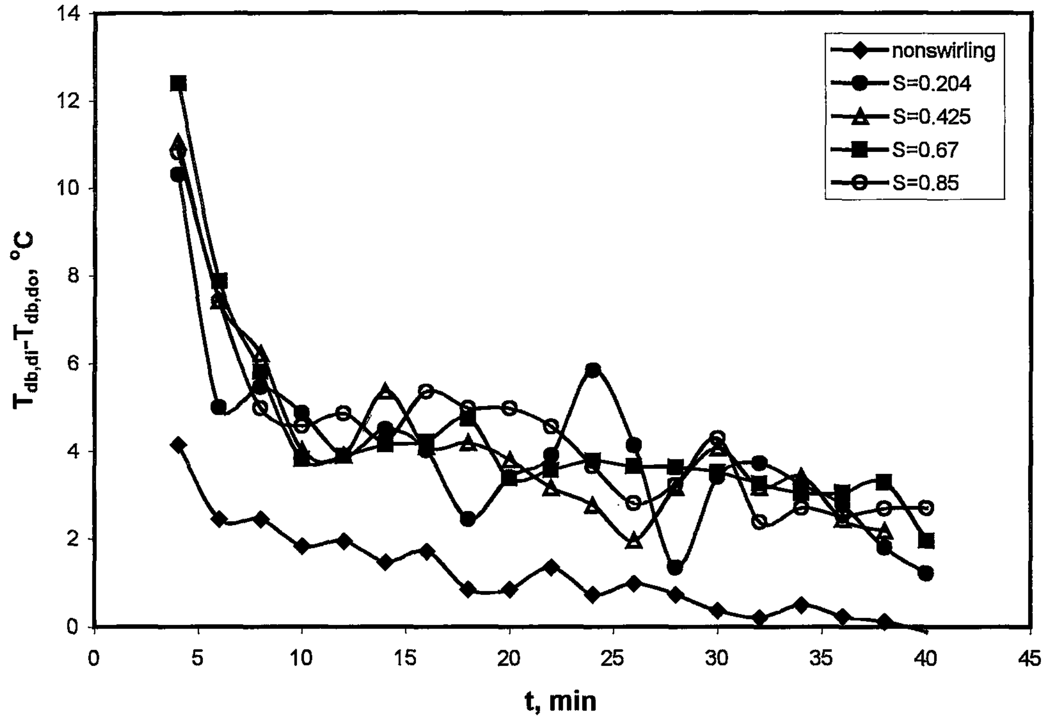

Figure 5.6.8 The variation of T_{db} differences between the inlet and outlet sides of the bed for non-swirling and swirling flow fields with drying time

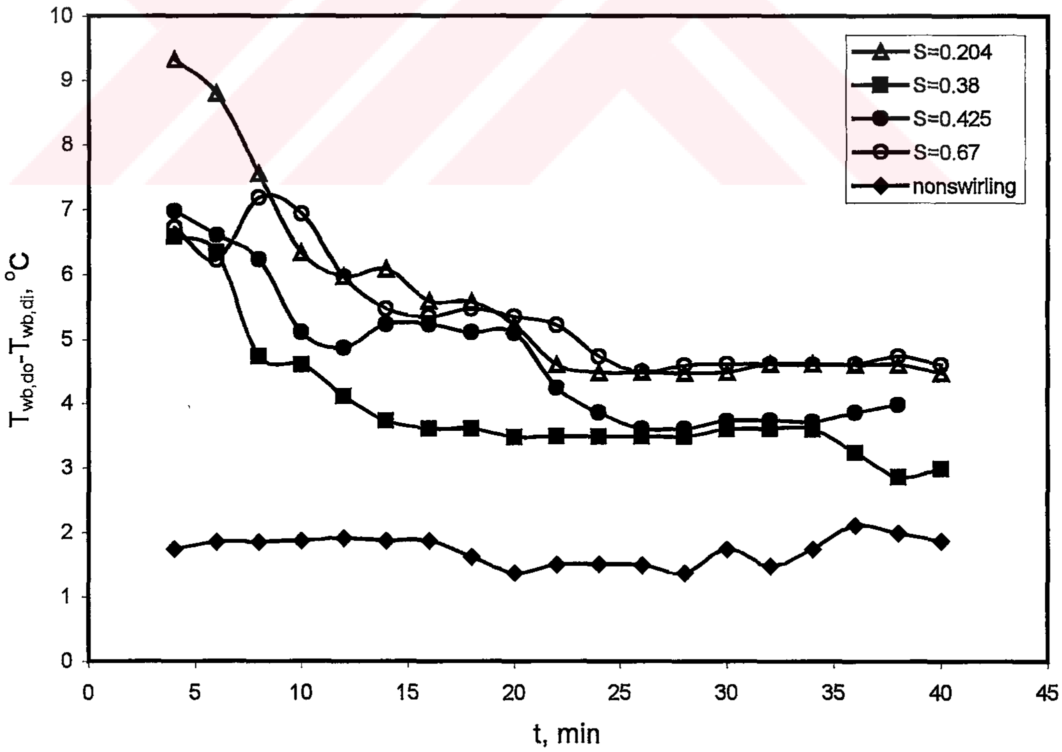

Figure 5.6.9 The variation of T_{wb} differences between the inlet and outlet sides of the bed for non-swirling and swirling flow fields with drying time

The variations of MER with drying time are plotted for both swirling and non-swirling flow fields in the bed in the Figure 5.6.10. The MER values are decreasing with the drying time for the non-swirling and the swirling flow fields as shown in this figure. The instant MER values are lying in the band which covers the MER values of 0.125-0.35g water/s. The higher S results the higher MER. In order to see more clearly the variation of MER with S, the mean MER values in the duration of drying are plotted corresponding to the swirl number, S, in the Figure 5.6.11. The exponential increase in the MER with the increasing S is observed in the Figure 5.6.11. This exponential relation between the MER and S is given in the following equation with an error margin of about 9 percent,

$$MER = 0.178^{0.242S} \tag{5.6.1}$$

Swirling flow field, which has the swirl number in the range of 0.2-0.85, increased the MER in the range of 5-25 percent. Therefore, the swirling flow field has an important effect in order to increase the drying rate.

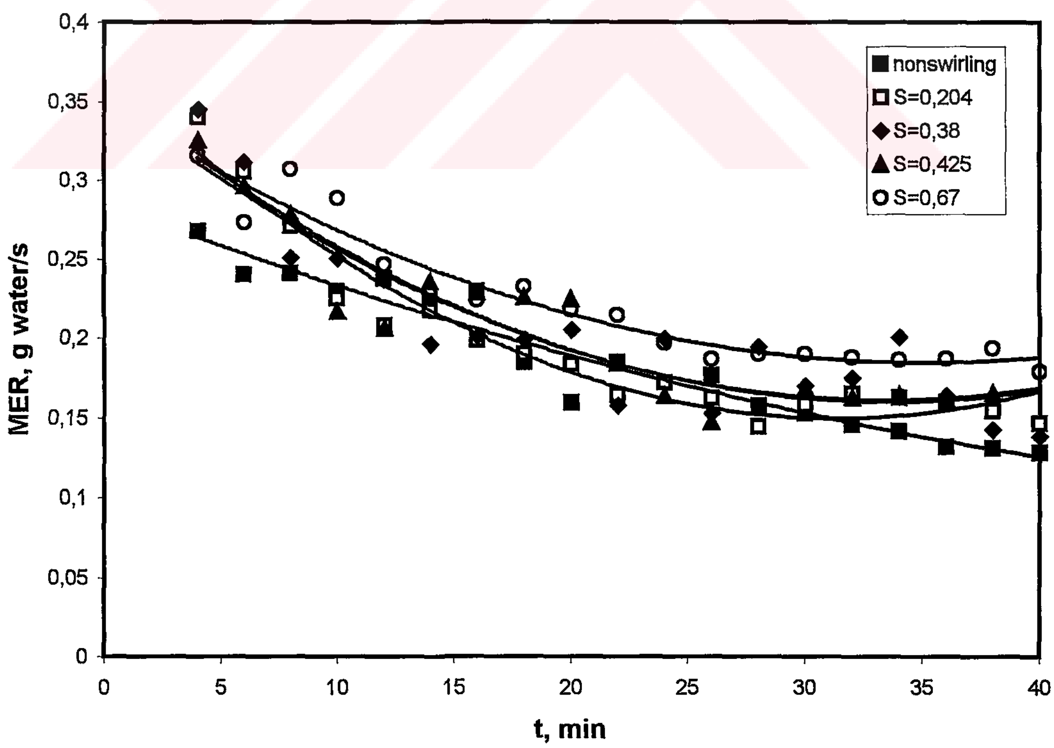

Figure 5.6.10 The variation of MER with drying time for swirling and non-swirling flow fields in the bed

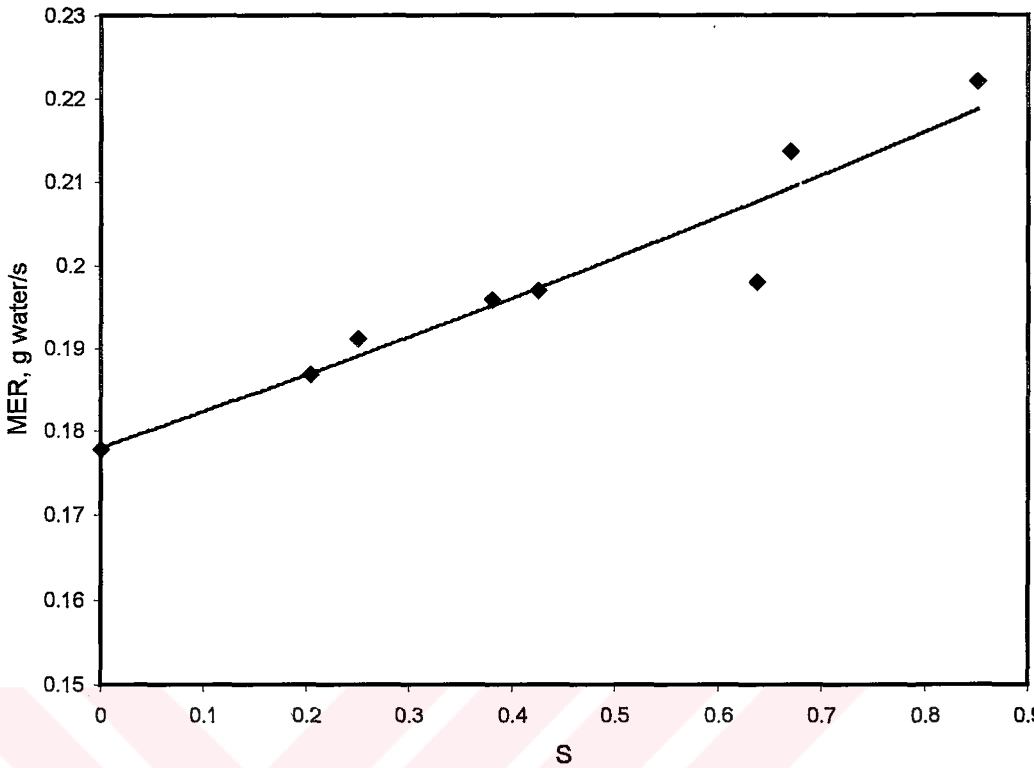

Figure 5.6.11 The variation of MER with S

The variation of SMER with the S is shown in the Figure 5.6.12. The all SMER values of the swirling flow field in the bed are greater than that of the non-swirling flow field in the bed, however, this increase in SMER for the swirling flow field is not continuing with the increasing S. The swirl generators with the radial vanes have greater SMER values when compared with that of the forward vanes. In other words, the higher camber angles give the higher SMER values since the radial vanes have higher camber angle, 180°, than that of the forward vanes with camber angle of 90°. The highest SMER value was obtained at S=0.425 when the radial type axial guide vanes which have the stagger angle of 60° was used as the swirl generator as shown in the Figure 5.6.12. For the swirl generators which have the forward vanes, the highest SMER value was obtained at S=0.637 when the forward type vanes which have stagger angle of 60° was used as shown in the Figure 5.6.12. The SMER is also based on the power consumed by the system as much as the MER. The highest SMER values for either radial and forward vanes are obtained when the vanes that have the stagger angle of 60° are used. For either radial and forward vanes the SMER values are increasing with the increasing S until the SMER values for the vanes that have stagger angle of 60^o, but the much increase in stagger angle decreases the SMER when the increase in S is continuing as shown in Figure 5.6.12. Thus, the swirl generators with forward and radial vanes that have the stagger angle of 60^o and higher stagger angles should be used because of these vanes give the higher MER values corresponding to higher S values, although, these give decreasing SMER values with the increasing S. The SMER is also based on the power consumed by the system as much as the MER. Thus, the SMER values are more affected from the configuration type of the swirl generators. The relations between the SMER and S are given by the following equations for forward curved vanes and radial vanes with an error margin of about 1 and 3, respectively,

$$\mathrm{SMER} = -0.0215S^2 + 0.0254S + 0.0482 \quad \text{for forward curved vanes} \qquad (5.6.2)$$

and

$$\mathrm{SMER} = -0.0528S^2 + 0.0526S + 0.0482 \quad \text{for radial vanes} \qquad (5.6.3)$$

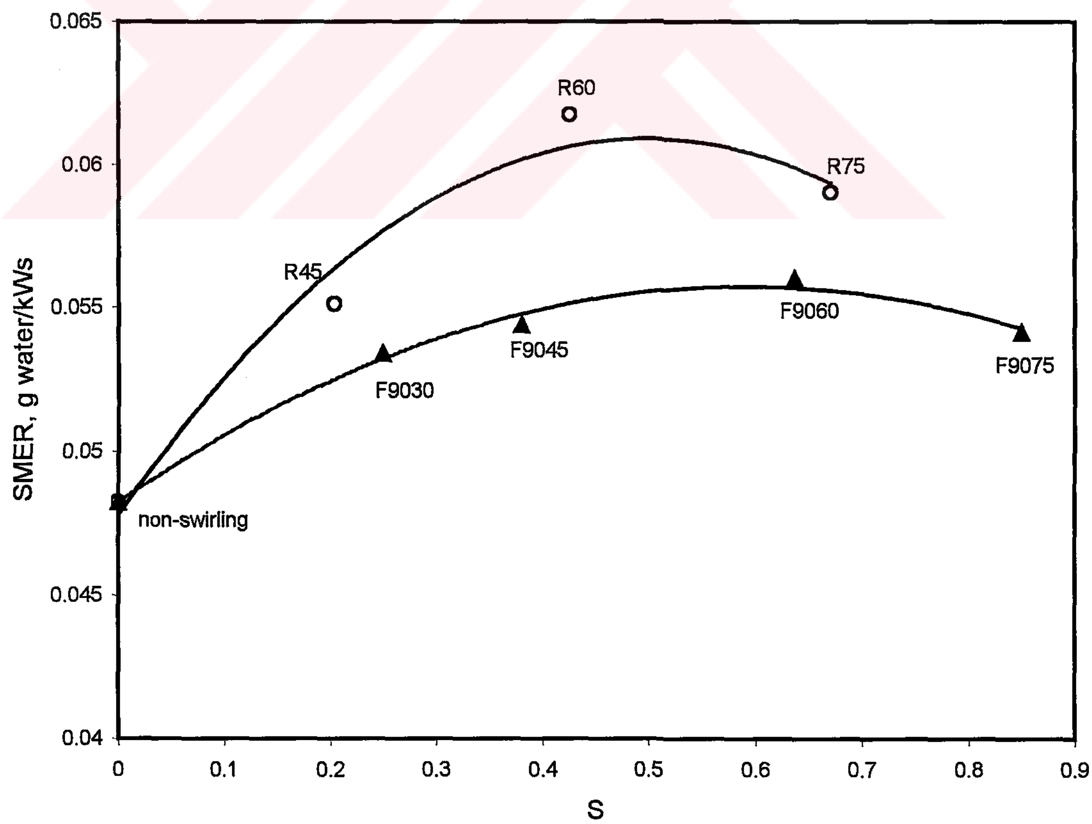

Figure 5.6.12 The variation of SMER with S

The variation of DE with the drying time is shown in the Figure 5.6.13 and as shown from this figure the DE values have the non-distinct changes with the time and some fluctuations. The DE values are lying in a band which has the range of about 25-70 percent. In order to see the clear variation of DE with the S, the mean DE values during the drying are plotted corresponding to the S in the Figure 5.6.14. The all DE values for the swirling flow field in the bed are greater than that of the non-swirling flow field in the bed as shown in the Figure 5.6.14 and the DE values for the swirling flow field are lying in the band which has the range of about 47-64 percent for the S values covered while the DE for non-swirling flow field was about 45 percent. But the any distinct variation of DE with the S were not observed as shown in the Figure 5.6.13. Also, the highest DE value is observed for the swirl generator which has the forward type axial guide vanes with the camber angle of 90° and the stagger angle of 75°.

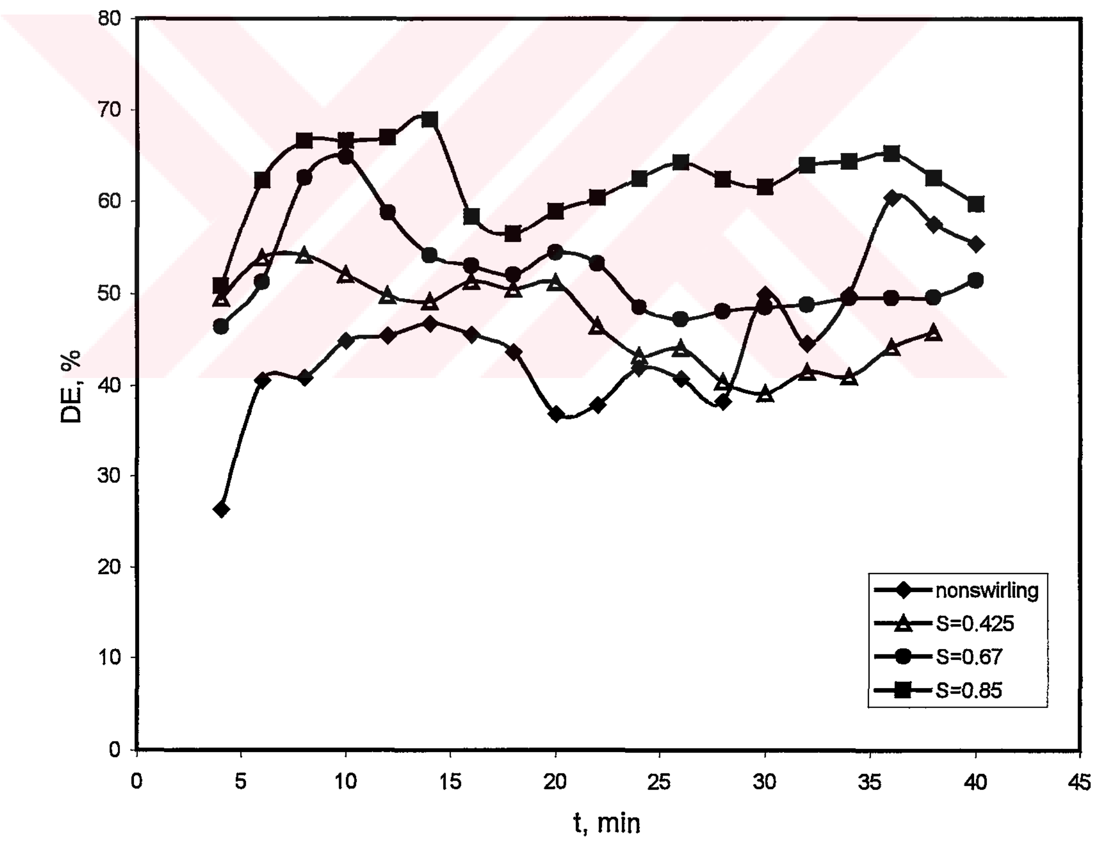

Figure 5.6.13 The variation of DE with drying time for the swirling and the non-swirling flow fields in the bed

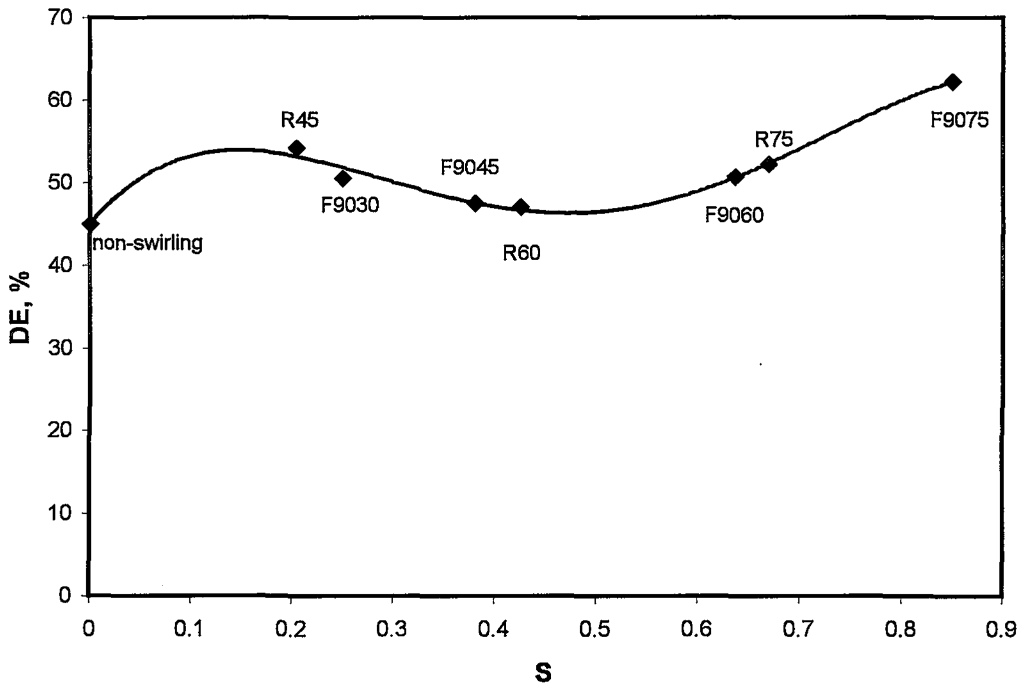

Figure 5.6.14 The variation of DE with S

5.7 COST ANALYSIS

In this section of the thesis, the cost rates were estimated and compared when the petroleum products and the direct electrical energy were used as energy supply in order to heat the drying air as being alternatives to heat pump.

For drying of 1 kg water, required energy is about 2470 kJ/kg, which is defined as latent heat of evaporation water. If this energy is used for drying of wheat grains, and if we know the initial moisture content and desired final moisture content of wheat grains to be absolutely dried, we can calculate the necessary heat capacity in order to dry the 1 kg of dry wheat at desired conditions. If the initial moisture content is 60 percent and the final moisture content is 9 percent in dry basis for the wheat grains, the moisture removal from the wheat is to be 51 percent or 0.51 kg water/1.6 kg wet wheat, that is, the amount of moisture removed from the wheat is to be 0.32 kg water/1kg dry wheat. If we take the weight of wet wheat as 1.6 kg and the drying test is applied during test period of 1 hour, the necessary moisture (water) extraction rate is to be 0.51 kg/h in the wet wheat. So, the necessary total heat capacity to dry the wet wheat grains can be calculated by multiplying the drying rate, which is defined as the moisture extraction rate, with the latent heat of vaporization for water as the following,

$$Q=MER*LHV=0.51\ kg/h*2470\ kJ/kg=1260\ kJ/h \quad (5.6.4)$$

where MER designates moisture extraction rate or drying rate, kg/h, and LHV designates the latent heat of vaporization of water, kJ/kg. That is, the necessary total heat capacity to dry the wheat grains is estimated as about 1260 kJ/h or 0.35 kW.

When the heat pump is used as an energy supply to heat the drying air, the compressor of the heat pump consumes 0.117 kW of energy if the coefficient of performance, COP, of the heat pump is taken to be 3 since the COP of heat pump used in this study is determined in the range of 2.84-3.35. And, if we assume the efficiency of the compressor as 70 percent, the electrical energy consumed by the compressor is estimated as 0.167 kW. The cost rate is also estimated as 0.0198 $/h while the unit price of the electrical energy is 0.119 $/kWh.

When the electrical energy is directly used to heat the drying air, the cost rate for the consumed electrical energy is estimated as 0.0417 $/h in order to supply the total necessary heat capacity of 0.35 kW for drying wet wheat grains of 1.6 kg in the test period of 1 hour at desired conditions while the unit price of the electrical energy is 0.119 $/kWh.

As the alternative energy supply, if the some petroleum products and electrical resistance heaters are used to heat the drying air, their cost rates are estimated by using the values of their energy contents and unit prices, which are listed in the below table. The cost rate for the petroleum products is estimated by,

$$Q=HHV*m*\eta_c \quad (5.6.5)$$

where HHV designates the higher heating value, kJ/kg

m designates the mass flow rate, kg/h for fuels

η_c designates the combustion efficiency of the systems and it was assumed as 70 percent for each conventional fuel burning systems.

Table 5.4 Cost rate analysis for some petroleum products

	Density, kg/m^3	HHV, kJ/kg	m, kg/h	The unit price, $/lt	Cost rate, $/h
Diesel fuel	830	45845	0.0393	1.03	0.0488
Fuel-oil RF1	879	43417	0.0415	0.63	0.0297
Fuel-oil RF4	940	43000	0.0418	0.35	0.0155
LPG	603	49592	0.0363	0.563	0.0339

As a result, the heat pump is more economic device when it is used as energy supply in any dryer unit when it is compared with the diesel, fuel-oil RF1, LPG and direct electrical energy. The lowest cost rate was obtained for the heat pump after that of the fuel-oil RF4 as shown in the above table. But, the fuel-oil RF4 emits harmful gases into the dryer since it contains the sulfur of amount of about 3.5 percent by weight. In contrast, the heat pump supplies clean air into the dryer. Thus, the heat pump is very health conscious system. When the cost rate of heat pump is compared with that of the direct electrical energy, it is shown that the heat pump is more economical at the range of about 110 percent as compared to the direct electrical energy.

5.8 CONCLUSION

The constructed system is an original and new contribution to the related literature, due to the introduction of heat pump to fluidized bed dryer and the swirling air flow in the bed for drying granular materials such as wheat. The heat pump dryer is a more complex system since the interaction of the two working fluids and the heat pump coupled with a dryer. The all components of the system are also dependent on each other. Any change in one component will inevitably influence the others. There are also many parameters and factors affecting the operating conditions and these factors are also more interactive each other. Thus, the experimental study on the heat pump dryer is more difficult.

In the available literature, heat pump was introduced to the different type dryers as generally batch type and continuous conveyor type. The heat pump dryers were generally used to dry wood, it was not previously used to dry granular materials such as wheat. At the same time, the heat pump was not previously coupled with the fluidized bed type dryers. The researchers, who previously studied on the heat pump dryers or fluidized bed dryers, investigated the dryer performance in the different conditions such as different materials, larger capacities, larger drying loads, longer drying times, different refrigerant working in the heat pump, different capacities and types in heat pump components and etc than the conditions and capacities that worked in this study. Therefore, the comparison of results obtained in this study with that of the studies in the available literature was to be more difficult.

General conclusions and discussions based on the conducted sets of experiments can be given in the followings:

The configuration 6, which has the closed cycle, has the highest MER, SMER and DE, and the second highest COP among the all tested configurations. When the configuration 5, which has the partially closed cycle, has the lowest MER and DE, and the second lowest SMER, the configuration 1, which has the completely open cycle, has the lowest SMER and COP, and the second lowest MER, and DE in the moderate range among the configurations tested in this study. Therefore, the worst performance is presented by the configurations 1 and 5. The configurations 3 and 4, which have the partially open and partially closed cycles, present the performance in the moderate range in MER, SMER and DE, but they only present the highest COP. Although the COP is not a critical factor for drying process since it is the indicator of heat pump performance. Thus, the closed system, configuration 6, is recommended as the best configuration.

Prasertsan et al. [8] observed that the open cycle where the air supply passes through a series of condenser, dryer and evaporator as the configuration 3 tested in this study seems to be the best configuration since it gives the highest SMER and MER, and also the closed cycle configuration either with or without evaporator bypass is not appropriate for the high drying rate process. But the closed cycles that tested by Prasertsan et al. [8] were different from the closed cycle tested in this study, the configuration 6. They discharged some part of the wet and hot air leaving from the dryer into the ambient before it enters into the evaporator and the other part of the exhaust air passes through the evaporator as different the configuration 6 tested in this study. The SMER of the close system analyzed by Zylla et al. [21] was higher than that of the open system as similar result observed in this study. The maximum MER and COP also resulted in the maximum SMER in their study. This case was also observed in this study. For the configuration 6 the highest MER and COP were also obtained at the highest SMER.

The MER and DE increase with the increasing air flow temperature in the drying medium while the SMER decreases with the increasing air flow temperature in the drying medium.

The increase in air mass flow rates in the drying medium causes the increase in the MER and decrease in the SMER and DE.

The increase in air flow temperature is more important than the increase in air mass flow rate in the drying medium in order to increase the dryer performance. In other words, air temperature for drying wheat grains in the bed has an important effect on drying rate, but mass flow rate or velocity of air has not played an important role on drying rate as much as the air temperature in the bed. This result was also observed by Hajidavalloo and Hamdullahpur [47], Dimattia et al. [50], Giner and Calvelo [51] and Syahrul et al. [48]. They presented that the effect of temperature is more critical than other parameters.

The swirling flow field enhances the dryer performance. The swirling flow field which has the swirl number in the range of 0.2-0.85 increases the MER in the range of 5-25 per cent and increases the SMER in the range of 12-28 per cent and increases the DE up to 38 per cent when it is compared with the non-swirling flow field in the bed. Thus, the swirling flow field accelerates the drying process, and so the drying time decreases and the drying rate increases. The enhancement of the heat transfer rates especially in the swirling pipe flows was fairly studied by many researchers, previously. But the effects of swirling flows on the drying process were not previously studied.

The COP for a well-designed heat pump is in the range of 2-4, with an average value of 3. The COP value of the heat pump that was used in this study was obtained as 3 on an average. That is, it was well-designed. The DE was obtained in the range of about 24-65 percent for the system experimentally investigated in this study. Prasertsan et al. [5] obtained the DE of a heat pump dryer that was used to dry banana and wood as in the range of 20-75 percent. The DE is also based on the drying load and the kind of drying material as much as the other parameters such as ambient and drying air temperatures, air mass flow rates and dryer type etc. The efficiency of dryer tested in this study was obtained in the moderate range corresponding to the available literature because of the wheat grains is a material which has a very low-mass diffusivity, high internal resistance to diffusion, and the load capacity of wheat grains in the dryer were very low in this study.

When the introduction of heat pump to the fluidized bed dryer is compared with the electrical heater as the heat supply of the dryer, it was observed that the heat pump usage is more economic at the rate of 110-151 per cent. While Prasertsan et al. [5] obtained that the energy costs for the heat pump dryer as about 0.39 \$/h for drying banana and wood, for the heat pump dryer used in this study it was obtained as about 0.0198 \$/h for drying wheat grains. That is, heat pump proved to be more efficient mechanism for drying than the pure resistive heating at any operating condition and it is more suitable for drying granular materials especially. In addition, heat pump dryer is an energy-efficient drying equipment because heat is also recoverable.

As a result, the main contributions of this thesis to the literature will be that the introduction of heat pump as energy supply into the fluidized bed type dryer which is used to dry granular materials and the effect of swirling flow field on the performance of fluidized bed type dryer.

CHAPTER 6

SUGGESTIONS FOR FUTURE WORK

The experimental set-up designed and constructed is very flexible and it enables for doing in a wide range of experiments with so many system design and operation parameters under control for future research on the manner. Some suggestions for the development of set-up and study concepts are outlined below:

1. The heat pump unit in the set–up can be connected to an air conditioned space
2. The different swirling flow generating techniques can be used to generate the swirling flow which has the different swirl number magnitudes
3. The different granular materials than the wheat can be used for drying
4. The heat pump components which have the different capacities can be used
5. The different working fluid in the heat pump can be used
6. The set-up can be re-configured by introducing the solar energy system to the fluidized bed dryer
7. Instead the fluidized bed dryer, a different dryer type can be coupled with the heat pump
8. The theoretical analysis can be applied to the whole system or can be applied separately to the each unit, fluidized bed dryer and heat pump
9. The second law analysis or exergy analysis can be theoretically applied to the system by using the measured data in the experiments
10. The void fraction effect for drying the granular materials can be experimentally investigated.

APPENDIX 1

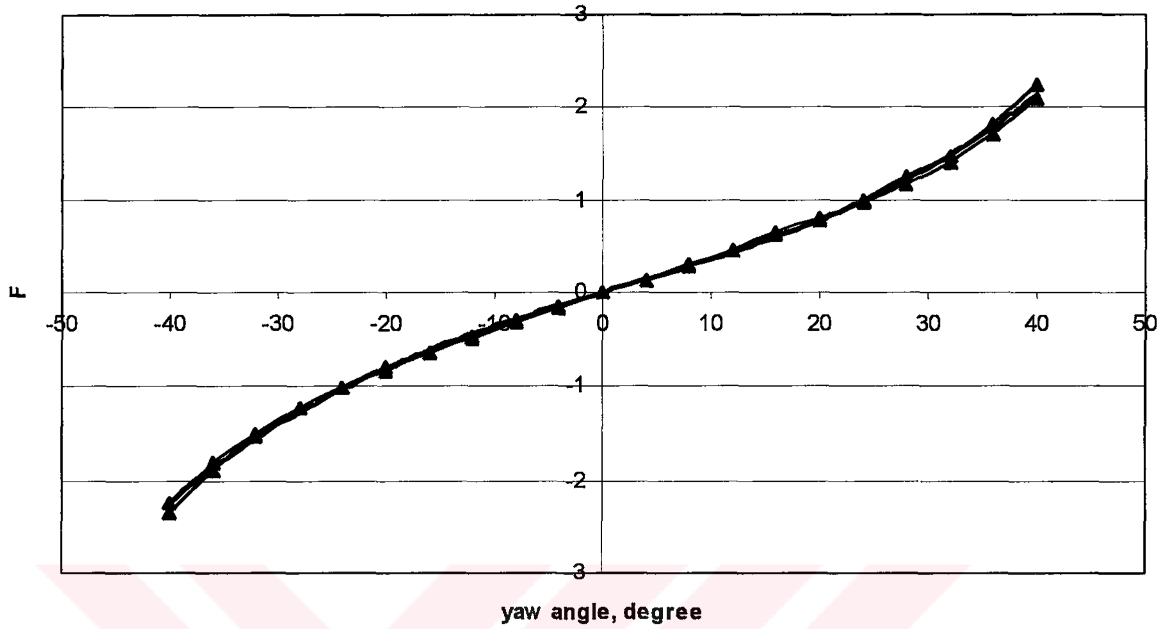

Figure 1. The calibration curve of F for 3-tube pressure probe

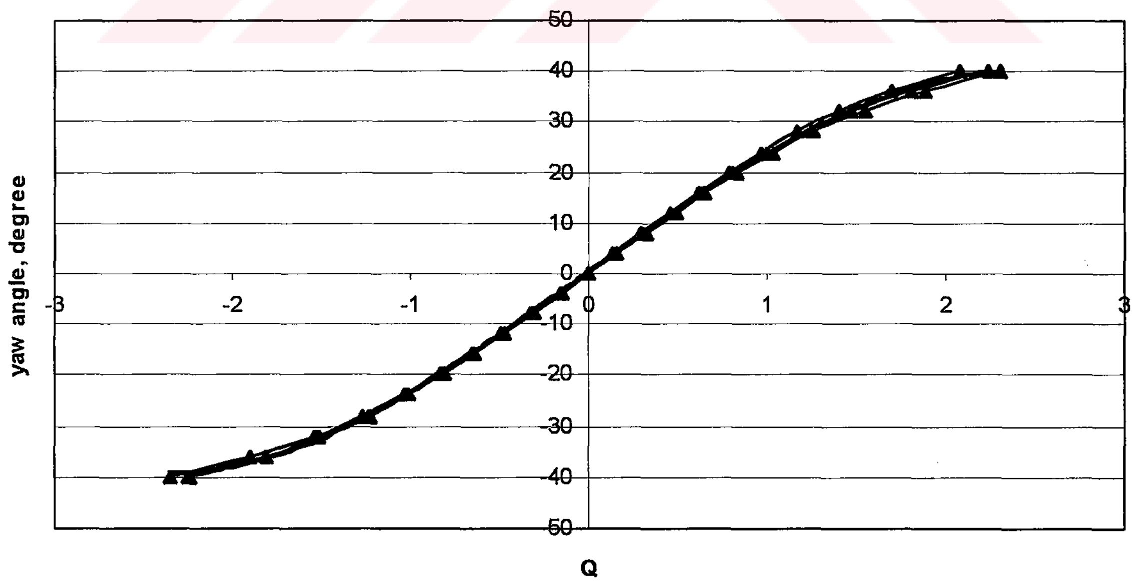

Figure 2. The calibration curve of Q for 3-tube pressure probe

APPENDIX 2

Correction Chart for The Head of Alcohol

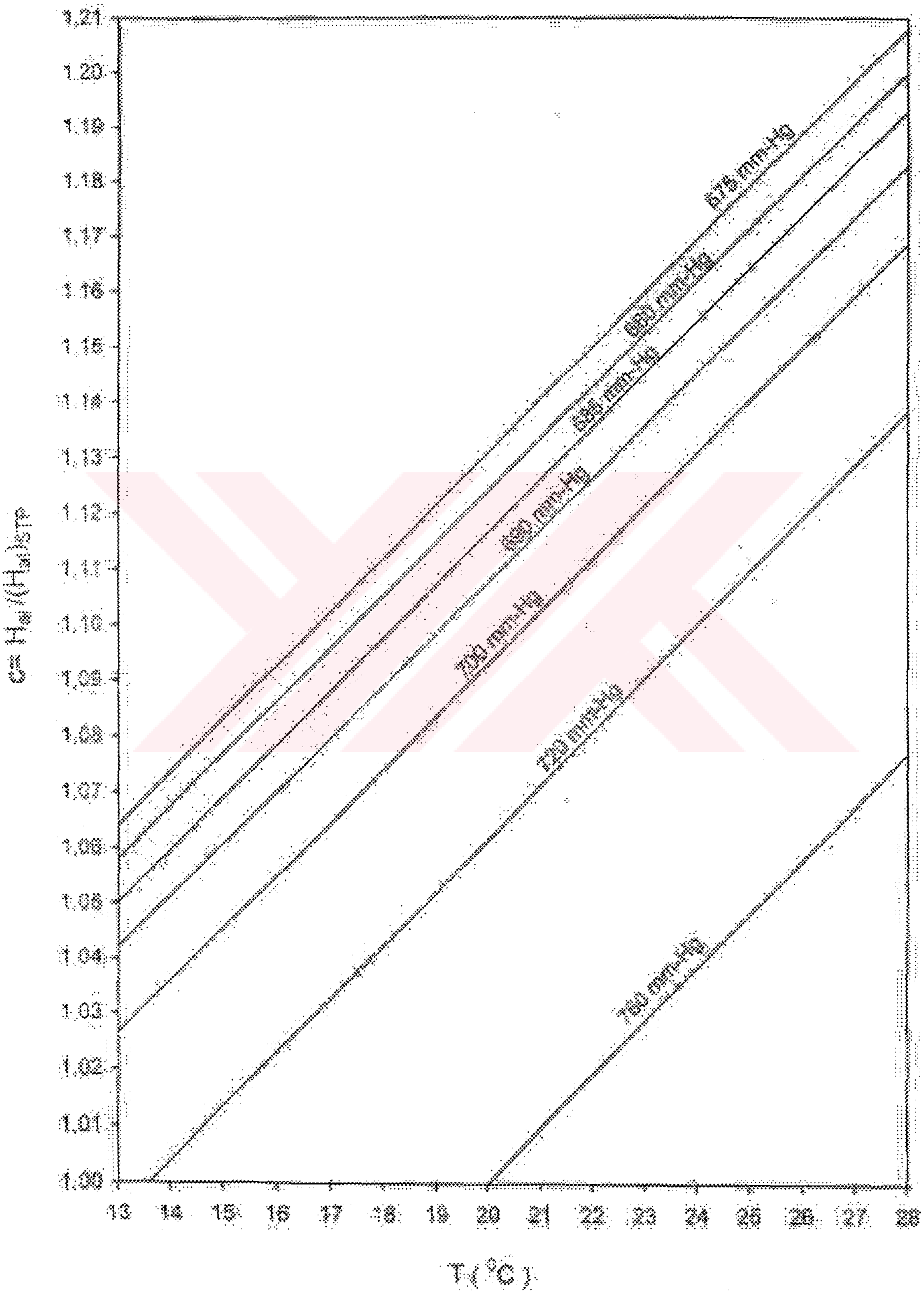

REFERENCES

1. Al-Mansour, F., and Tomsic, M. (1994). Heat Pumps in Industry. *Heat Recovery Systems and CHP*, **14**(1), 51-60

2. Lazzarin, R. M. (1995). Heat Pumps in Industry 2: Applications. *Heat Recovery Systems and CHP*, **15**(3), 305-317

3. Prasertsan, S., Saen-Saby, P., Prateepchaikul, G., and Ngamsritrakul, P. (1995). Factors Influencing Heat Pump Dryer Performance. *Proceedings of the 6th ASEAN Conference on Energy Techonology*, Bangkok, 371-379

4. Prasertsan, S., and Saen-Saby, P. (1998). Heat Pump Drying of Agricultural Materials. *Drying Technology*, **16**(1-2), 235-250

5. Prasertsan, S., Saen-Saby, P., Prateepchaikul, G., and Ngamsritrakul, P. (1996). Effects of Product Drying Rate and Ambient Condition on The Operating Modes of Heat Pump Dryer. *Drying'96-Proceedings of the 10th International Drying Symposium*, Krakow, Poland, A, 529-534

6. Prasertsan, S., and Saen-Saby, P. (1998). (Heat Pump Dryers: Research and Development Needs and Opportunities. *Drying Technology*, **16**(1-2), 251-270

7. Prasertsan, S., Saen-Saby, P., Ngamsritrakul, P., and Prateepchaikul, G. (1996). Heat Pump Dryer Part 1: Simulation of the Models. *International Journal of Energy Research*, **20**(12), 1067-1079

8. Prasertsan, S., Saen-Saby, P., Ngamsritrakul, P., and Prateepchaikul, G. (1997). Heat Pump Dryer Part 2: Results of the Simulation. *International Journal of Energy Research*, **21**(1), 1-20

9. Prasertsan, S., Saen-Saby, P., Ngamsritrakul, P., and Prateepchaikul, G. (1997). Heat Pump Dryer Part 3: Experimental Verification of the Simulation. *International Journal of Energy Research*, **21**, 707-722

10. Chou, S. K., Hawlader, M. N. A., Ho, J. C., Wijeysunder, N. E., and Rajasekar, S. (1994). Performance of a Heat Pump Assisted Dryer. *International Journal of Energy Research*, **18**(6), 605-622

11. Almedia, M. S. V., Gouveia, M. C., Zdebsky, S. R., and Parise, J. A. R. (1990). Performance Analysis of a Heat Pump Assisted Drying System. *International Journal of Energy Research*, **14**, 397-406

12. Carrington, C. G., and Bannister, P. (1996). An Emprical Model for a Heat Pump Dehumidifier Drier. *International Journal of Energy Research*, **20**, 853-869

13. Perera, C. O., and Rahman, M. S. (1997). Heat Pump Dehumidifier Drying of Food. *Trends in Food Science and Technology*, **8**, 75-79

14. Pendyala, V. R., Devotta, S., and Patwardhan, V. S. (1990). Heat Pump Assisted Dryer Part 1: Mathematical Model. *International Journal of Energy Research*, **14**, 479-492

15. Pendyala, V. R., Devotta, S., and Patwardhan, V. S. (1990). Heat Pump Assisted Dryer Part 2: Experimental Study. *International Journal of Energy Research*, **14**, 493-507

16. Jolly, P., Jia, X., and Clements, S. (1990). Heat Pump Assisted Continuous Drying Part 1: Simulation Model. *International Journal of Energy Research*, **14**, 757-770

17. Jia, X., Jolly, P., and Clements, S. (1990). Heat Pump Assisted Continuous Drying Part 2: Simulation Results. *International Journal of Energy Research*, **14**, 771-782

18. Clements, S., Jia, X., and Jolly, P. (1993). Experimental Verification of a Heat Pump Assisted Continuous Dryer Simulation Model. *International Journal of Energy Research*, **17**, 19-28

19. Toal, B. R., Morgan, R., and McMullan, J. T. (1988). Experimental Studies of Low Temperature Drying by Dehumidification. Part 1: Apparatus and Theory. *International Journal of Energy Research*, **12**, 299-314

20. Toal, B. R., Morgan, R., and McMullan, J. T. (1988). Experimental Studies of Low Temperature Drying by Dehumidification. Part 2: Experimental. *International Journal of Energy Research*, **12**, 315-344

21. Zyalla, R., Abbas, S. P., Tai, K. W., Devotta, S., Watson, F. A., and Holland F. A. (1982). The Potential for Heat Pumps in Drying and Dehumidification Systems, 1: Theoretical Considerations. *International Journal of Energy Research*, **6**, 305-322

22. Tai, K. W., Zyalla, R., Devotta, S., Diggory, P. J., Watson, F. A., and Holland F. A. (1982). The Potential for Heat Pumps in Drying and Dehumidification Systems 2: An Experimental Assessment of the Dehumidification Characteristics of a Heat Pump Dehumidification System Using R114. *International Journal of Energy Research*, **6**, 323-331

23. Tai, K. W., Zyalla, R., Devotta, S., Diggory, P. J., Watson, F. A., and Holland F. A. (1982). The Potential for Heat Pumps in Drying and Dehumidification Systems 3: An Experimental Assessment of the Dehumidification Characteristics of a Heat Pump Dehumidification System Using R114. *International Journal of Energy Research*, **6**, 333-340

24. Kiranoudis, C. T., Maroulis, Z. B., and Kouris, M. D. (1996). Design and Operation of Convective Industrial Dryers. *AIChE Journal*, **42**(11), 3030-3040

25. Baines, P. G., and Carrington, C. G. (1988). Analysis of Rankine Cycle Heat Pump Driers. *International Journal of Energy Research*, **12**, 495-510

26. Carrington, C. G., and Baines, P. G. (1988). Second Law Limits in Convective Heat Pump Driers. *International Journal of Energy Research*, **12**, 481-494

27. Tiwari, G. N., Singh, A. K., and Bhatia, P. S. (1994). Experimental Simulation of a Grain Drying System. *Energy Conversion and Management*, **35**(5), 453-458

28. Braven, K. D., Herold, K., Mei, V., O'Neal, D., and Penoncello, S. (1993). Improving Heat Pumps and Air Conditioning. *Mechanical Engineering*, **115**(9), 98-102

29. Wallin, E., Franck, P. A., and Berntsson, T. (1990). Heat Pumps in Industrial Processes-An Optimization Methodology. *Heat Recovery Systems and CHP*, **10**(4), 437-446

30. Poduval, A. M. K., and Murthy, S. S. (1992). Performance of a Dehumidifying Compression Heat Pump with Auxilary Heat Input. *Heat Recovery Systems and CHP*, **12**(3), 211-223

31. Manuel, S. V. A., Marcio, C. G., Suzana, R. Z., and Jose, A. R. P. (1990). Performance Analysis of Heat Pump Assisted Drying System. *Int. J. of Energy Research*, **14**(3), 397-406

32. Theerakulpisut, S. (1990). *Modeling heat pump grain drying system*, Ph.D. Thesis. Australia: University of Melbourne

33. Travis, D. P., Rohsenow, W. M., and Baron, A. B. (1973). Forced-convection condensation inside tubes: a heat transfer equation for condenser design. *ASHRAE Transactions*, **79**(1), 157-165

34. Threkeld, J. L. (1970). *Thermal Environmental Engineering*. (2nd ed.). Englewood Cliffs, NJ: Prentice-Hall.

35. Kays, W. M., and London, A. L. (1984). *Compact Heat Exchangers*. (3rd ed.). New York: McGraw-Hill.

36. Kreider, J. F., and Kreith, F. (1981). *Solar Energy Handbook*, New York: McGraw-Hill.

37. Incropera, F. P., and DeWitt, D. P. (1990). *Fundamentals of Heat and Mass Transfer*. (3rd ed.). New York: John Wiley & Sons.

38. Kusuda, T. (1965). *Calculation of the temperature of a flat-plate wet surface under adiabatic condition with respect to the Lewis relation, in humidity and moisture, in*

principles and methods of measuring humidity in gases, 1, New York (Cited in Threlkeld): R. E. Ruskin, Reinhold.

39. ASHRAE Handbook and Fundamentals. (1989). Refrigerant tables and charts. (SI ed.). *American Society of Heating, Refrigerating and Air-Conditioning Engineers*, Atlanta

40. Charters, W. W. S., and Aye, L. (1993). Modeling Heat Pump Grain Drying Systems. *AHTM Conference*, **31**, 1-6

41. Chou, S. K., Hawlader, M. N. A., Ho, J. C., and Chua, K. J. (1999). The Contact Factor for Dryer Performance and design. *International Journal of Energy Research*, **23**, 1277-1291

42. Baker, C. G. J. (1999). Predicting the energy consumption of continuous well-mixed fluidized bed dryers from drying kinetic data. *Drying Technology*, **17**(7-8), 1533-1555

43. Baker, C. G. J., Al-Roomi, Y. M., and Al-Sharrah, G. (2000). Optimal design of well-mixed fluidized bed dryers. *Drying Technology*, **18**(7), 1509-1555

44. Baker, C. G. J. (2000). The design and performance of continuous well-mixed fluidized bed dryers-an analytical approach. *Drying Technology*, **18**(10), 2327-2349

45. Hajidavaloo, E., and Hamdullahpur, F. (1999). Mathematical modeling of simultaneous heat and mass transfer in fluidized bed drying of large particles. *Transactions of the CSME*, **23**(1B), 129-145

46. Hajidavaloo, E., and Hamdullahpur, F. (2000). Thermal analysis of a fluidized bed drying process for crops. Part 1: Mathematical modeling. *International Journal of Energy Research*, **24**, 791-807

47. Hajidavaloo, E., and Hamdullahpur, F. (2000). Thermal analysis of a fluidized bed drying process for crops. Part 2: Experimental results. *International Journal of Energy Research*, **24**, 809-820

48. Syahrul, S., Hamdullahpur, F, and Dincer, I. (2002). Energy analysis in fluidized-bed drying of large wet particles. *International Journal of Energy Research*, **26**, 507-525

49. Chandran, A. N., Subba Rao, S., and Varma, Y. B. G. (1990). Fluidized bed drying of solids. *AIChE Journal*, **36**(1), 29-38

50. DiMattia, D. G., Amyotte, P. R., and Hamdullahpur, F. (1996). Fluidized bed drying of large particles. *Transactions of the ASAE*, **39**(5), 1745-1750

51. Giner, S. A., and Calvelo, A. (1987). Modeling of wheat drying in fluidized beds. *Journal of Food Science*, **52**, 1358-1363

52. Fyhr, C. and Kemp, I. C. (1999). Mathematical modeling of batch and continuous well-mixed fluidized bed dryers. *Chemical Engineering and Processing*, **38**, 11-18

53. Sivashanmugam, P., and Sundaram, S. (1999). Hydrodynamics of annular circulating fluidized bed drier. *Powder Technology*, **103**, 165-168

54. Soponronnarit, S., Swasdisevi, T., Wetchacama, S., and Wutiwiwatchai, W. (2001). Fluidized bed drying of soybeans. *Journal of Stored Products Research*, **37**, 133-151

55. Aly, A. S., and Fathalah, K. A. (1999). A three-phase model of a batch fluidized bed. *Heat and Mass Transfer*, **34**, 405-412

56. Becker, H. A. (1959). A study of diffusion in solids of arbitrary shape, with application to the drying of the wheat kernel. *Journal of Applied Polymer Science*, **1**, 212-226

57. Kazarian, E. A., and Hall, C. W. (1965). Thermal properties of grain. *Transactions of the ASAE*, **8**, 33-37

58. Henderson, S. M. (1952). A basic concept of equilibrium moisture. *Agricultural Engineering*, **33**, 29-32

59. Fortes, M., Okos, M. R., and Barrett, J. R. (1981). Heat and mass transfer analysis pf intra-kernel wheat drying and rewetting. *Journal of Agricultural Engineering Research*, 26, 109-125

60. Brooker, D. B., Bakker, A. F. W., and Hall, C. W. (1974). *Drying Cereal Grain*. The AVI Publishing Company.

61. Luikov, A. V. (1966). *Heat and mass transfer in capillary porous bodies*. London: Pergamon Press.

62. Howard, J. R. (1989). *Fluidized bed technology*. New York: Adam Hilger.

63. Bejan, A. (1993). *Heat transfer*. New York: Wiley.

64. Watano, S., Yeh, N., and Miyanami, K. (1998). Drying of granules in agitation fluidized bed. *Journal of Chemical Engineering of Japan*, **31**(6), 908-913

65. Abid, M., Gibert, R., and Laguerie, C. (1990). An experimental and theoretical analysis of the mechanisms of heat and mass transfer during the drying of corn grains in a fluidized bed. *International Chemical Engineering*, **30**(4), 632-642

66. Thomas, P. P., and Varma, Y. B. G. (1992). Fluidized bed drying of granular food materials. *Powder Technology*, **69**, 213-222

67. Christie, I., Ganser, G. H., and Wilder, J. W. (1998). Numerical solution of a two-dimensional fluidized bed model. *International Journal for Numerical Methods in Fluids*, **28**, 381-394

68. Palancz, B. (1983). A mathematical model for continuous fluidized bed drying. *Chemical Engineering Science*, **38**(7), 1045-1059

69. Hoebink, J. H. B. J., and Rietema, K. (1980a). Drying granular solids in a fluidized bed-1: Description on basis of mass and heat transfer coefficients. *Chemical Engineering Science*, **35**, 2135-2140

70. Hoebink, J. H. B. J., and Rietema, K. (1980b). Drying granular solids in a fluidized bed-2: The influence of diffusion limitation on the gas-solid contacting around bubbles. *Chemical Engineering Science*, **35**, 2257-2265

71. Sazhin, V. B., Oygenblik, A. A., Dorokhov, I. N., and Kafarov, V. V. (1986). A mathematical model of fluidized-bed drying of granular solids. *Heat Transfer-Soviet Research*, **18**(2), 71-80

72. Srinivasa, K. C., Subba, R. S., and Varma, Y. B. G. (1994). A kinetic model for drying of solids in batch fluidized beds. *Industrial Engineering of Chemical Research*, **33**, 363-370

73. Bahu, R. E. Fluidized bed dryers. *Industrial Drying of Foods*, 65-89

74. Chase, G. G. *Solid Notes, 3-5*. The University of Akron.

75. Dimattia, D. G., Amyotte, P. R., and Hamdullahpur, F. (1996). Slugging Characteristics of group D particles in fluidized beds. *The Canadian Journal of Chemical Engineering*, **75**, 452-459

76. Reay, D., and Allen, R. W. K. (1982). *Drying in Fluidization*. London: Academic Press.

77. Reay, D., and Allen, R. W. K. (1982). Predicting the performance of a continuous well-mixed fluid bed dryer from batch tests. *In Proc. 3rd Int. Drying Symp., Birmingham, England*, **2**, 130-140

78. Keey, R. B. (1992). *Drying of loose and particulate materials*. New York: Hemisphere Publishing Corporation

79. Krischer, O., and Kast, W. (1978). *The Scientific Fundamentals of Drying Technology*. Berlin: Springer-Verlag

80. Leuckel, W. (1968). The aerodynamics of swirling flows. *Rev. Gen. Thermique*, **7**, 1367-1383

81. Hay, N., and West, P. D. (1975). Heat transfer in free swirling flow in a pipe. *Journal of Heat Transfer*, **97**, 411-416

82. Algifri, A. H., Bhardwaj, R. K., and Rao, Y. V. N. (1988). Heat transfer in turbulent decaying swirl flow in a circular pipe. *International Journal of Heat and Mass Transfer*, **31**, 1563-1568

83. Ito, S., Ogawa, K., and Kuroda, C. (1980). Turbulent swirling flow in a circular pipe. *Journal of Chemical Engineering of Japan*, **13**, 6-9

84. Thorsen, R., and Landis, F. (1968). Friction and heat transfer characteristics in turbulent swirl flow subjected to large transverse temperature gradients. *Journal of Heat Transfer*, 87-97

85. Kitoh, O. (1991). Experimental study of turbulent swirling flow in a straight pipe. *Journal of Fluid Mechanics*, **225**, 445-479

86. Tiwari, G. N., Singh, A. K., and Bhatia, P. S., (1994). Experimental Simulation of a Grain Drying System. *Energy Conversion and Management*, **35**, 453-458

87. Threkeld, J. L. (1970). *Thermal Environmental Engineering*. (2nd ed.). Englewood Cliffs, NJ: Prentice-Hall

88. Incropera, F. P. and DeWitt, D. P. (1990). *Fundamentals of Heat and Mass Transfer*. (3rd ed.). New York: John Wiley & Sons

89. Çarpınlıoğlu M. Ö., and Özbey M. (1997). A calibration method for 3-tube pressure probes. *Turk Journal of Engineering and Environmental Sciences*, **21**, 239-243

90. BS 1042, Part 2A. (1973). *British Standard Methods for the Measurement of Fluid Flow in Pipes*. British Standard Institution

91. Vanecek, V., Markvart, M., and Drbohlav, R. (1966). *Fluidized bed drying*. London: Leonard Hill Books

92. Simmonds, W. H. C., Ward, G. T., and McEwen, E. (1953). The drying of wheat grain. Part 1: The mechanism of drying. *Transactions of Institutional Chemical Engineers*, **32**, 265-278

93. Uçkan, G., and Ülkü, S. (1986). Drying of corn grain in a batch fluidized bed drier. *Drying of Solids: Recent Developments* (Mujumdar, A.S. ed.). New York: Wiley

94. Zahed, A. H., Zhu, J. X., and Grace, J. R. (1995). Modeling and simulation of batch and continuous fluidized bed dryers. *Drying Technology*, **13**(12), 1-28

95. Alvarez, P., and Shene, C. (1996). Experimental study of the heat and mass transfer in a fluidized bed dryer. *Drying Technology*, **14**(3-4), 701-718

96. Theologos, K. N., Maroulis, Z. B., and Markatos, N. C. (1997). Simulation of transport dynamics in fluidized-bed dryers. *Drying Technology*, **15**(5), 1265-1291

97. Maroulis, Z. B., Kremalis, C., and Kritikos, T. (1996). A learning process simulator for fluidized bed dryers, application to bentonite. *Drying Technology*, **13**(8-9), 1763-1788

98. van Ballegooijen, W. G. E., van Loon, A. M., and van der Zanden. A. (1997). Modelling diffusion-limited drying behavior in a batch fluidized bed dryer. *Drying Technology*, **15**(34), 1837-1855

99. Geldart, D. (1973). Types of gas fluidization. *Powder Technology*, **7**, 285-292

100. Geldart, D. (1986). *Gas fluidization technology*. New York: Wiley

101. Reay, D., and Allen, R. W. K. (1982). Predicting the performance of a continuous well-mixed fluidized bed dryer from batch tests. *Proc. 3rd International Drying Sempozium*. Birmingham, England, **2**, 130-140

102. Reay, D., and Baker, C. G. J. (1983). *Drying in fluidization.* (2nd ed.). London: Akademic Press

103. McKenzie, K. A., and Bahu, R. E. (1991). *Material model for fluidized bed drying.* Drying 91. (Mujumdar, A.S. ed.). Amsterdam: Elsevier Science Publication, 130-141

104. Keey, R. B. (1992). *Drying of loose and particulate materials.* New York: Hemisphere Publishing Corporation, 232-235

105. Krischer, O., and Kast, W. (1978). *The scientific fundamentals of drying technology.* (3rd ed.). Berlin: Springer-Verlag, 305-339

106. DiMattia, D. G. (1993). *Onset of slugging in fluidized bed drying of large particles.* M.Sc. Thesis. Halifax, Canada: Technical University of Nova Scotia

107. Hendeson, S. M. (1952). A basic concepy of equilibrium moisture. *Agricultural Engineering*, **33**, 29-32

108. Fortes, M., Okos, M. R. and Barnett, J. R. (1981). Heat and mass transfer analysis of intra-kernel wheat drying and rewetting. *Journal of Agricultural Engineering Research*, **26**, 109-125

109. Smithberg, E. and Landis, F. (1964). Friction and forced convection heat transfer characteristics in tubes with twisted tape swirl generators. *Journal of Heat Transfer*, **86**(1), 39-49

110. Junkhan, G. H., Bergles, A. E., Nirmalan, V. and Ravigururajan, T. (1985). Investigation of turbulators for fire tube boilers. *Transactions of the ASME*, **107**, 354-360

111. Hong, S. W. and Bergles, A. E. (1976). Augmentation of laminar flow heat transfer in tubes by means of twisted tape inserts. *Journal of Heat Transfer*, **98**, 251-256

112. Sethumadhavan, R. and Raja Rao, M. (1982). Turbulent flow heat transfer and fluid friction in helical wire coil inserted tubes. *International Journal of Heat and Mass Transfer*, **26**(12), 1833-1845

113. Kumar, P. and Judd, R. L. (1970). Heat transfer with coiled wire turbulence promoters. *The Canadian Journal of Chemical Engineering*, **48**, 378-383

114. Uttarwar, S. B. and Raja Rao, M. (1985). Augmentation of laminar flow heat transfer in tubes by means of wire coil inserts. *Transactions of the ASME*, **107**, 930-935

115. Ito, S., Ogawa, K. and Kuroda, C. (1980). Turbulent swirling flow in a circular pipe. *Journal of Chemical Engineering of Japan*, **13**(1), 6-9

116. Hay, N. and West, P. D. (1975). Heat transfer in free swirling flow in a pipe. *Journal of Heat Transfer*, **18**, 411-416

117. Algifri, A. H., Bhardwaj, R. K. and Rao, Y. V. N. (1987). Heat transfer in turbulent decaying swirl flow in a circular pipe. *International Journal of Heat Transfer*, **31**(8), 1563-1568

118. Sheen, H. J., Chen, W. J., Jeng, S. Y. and Huang, T. L. (1996). Correlation of swirl number for a radial type swirl generator. *Experimental Thermal and Fluid Science*, **12**, 444-451

119. Kitoh, O. (1991). Experimental study of turbulent swirling flow in a straight pipe. *Journal of Fluid Mechanics*, **225**, 445-479

120. Lopina, R. F. and Bergles, A. E. (1969). Heat transfer and pressure drop in tape generated swirl flow of single phase water. *Transactions of the ASME*, **19**, 434-442

121. Thorsen, R. and Landis, F. (1968). Friction and heat transfer characteristics in turbulent swirl flow subjected to large transverse temperature gradients. *Journal of Heat Transfer*, **90**, 87-98

122. Yılmaz, M., Çomaklı, Ö. and Yapıcı, S. (1999). Enhancement of heat transfer by turbulent decaying swirl flow. *Energy Conversion and Management*, **40**, 1365-1376

123. Yılmaz, M., Çomaklı, Ö., Yapıcı, S. and Şara, O. N. (2002). Heat transfer and friction characteristics in decaying swirl flow generated by different radial guide vane swirl generators. *Energy Conversion and Management*, accepted in 21 January 2002

124. Bali, T. (1998). Modelling of heat transfer and fluid flow for decaying swirl flow in a circular pipe. *Int. Comm. Heat and Mass Transfer*, **25**(3), 349-358

125. Bali, T. and Ayhan, T. (1999). Experimental investigation of propeller type swirl generator for a circular pipe flow. *Int. Comm. Heat and Mass Transfer*, **26**(1), 13-22

126. Özbey, M. (1997). *Effects of turbulators on flow development and heat transfer in pipe flows*. M. Sc. Thesis. University of Gaziantep, Turkey

127. ASHRAE. (1981). *Fundamentals Handbook, American Society of Heating Refrigeration and Air Conditioning Engineers*, Atlanta

128. Leuckel, W. (1968). The aerodynamics of swirling flows. *Rev. Gen. Thermique*, **7**, 1367-1383.

CURRICULUM VITAE

The author was born in Samsun in 1972. He has finished the high school in Samsun in 1989 and entered the Mechanical Engineering Department of Gaziantep University in 1989. He has been graduated as a mechanical engineer in 1994. He started to work as a research assistant in the same department while has continued the M. Sc. Program. He received his M. Sc. Degree in mechanical engineering in 1997.

He has been married and has a daughter named Ecenur.